3D Structuration Techniques of LTCC for Microsystems Applications

THÈSE N^{O} 4772 (2010)

PRÉSENTÉE LE 27 AOÛT 2010
À LA FACULTÉ SCIENCES ET TECHNIQUES DE L'INGÉNIEUR
LABORATOIRE DE PRODUCTION MICROTECHNIQUE 2
PROGRAMME DOCTORAL EN SYSTÈMES DE PRODUCTION ET ROBOTIQUE

ÉCOLE POLYTECHNIQUE FÉDÉRALE DE LAUSANNE

POUR L'OBTENTION DU GRADE DE DOCTEUR ÈS SCIENCES

PAR

Yannick FOURNIER

acceptée sur proposition du jury:

Prof. M.-O. Hongler, président du jury
Prof. P. Ryser, directeur de thèse
Prof. J. Binder, rapporteur
Prof. M. Hrovat, rapporteur
Prof. P. Muralt, rapporteur

ÉCOLE POLYTECHNIQUE
FÉDÉRALE DE LAUSANNE
Suisse
2010

A Mira, dont l'affection et la vitalité sans pareilles
furent une aide inestimable chaque jour de ce périple

A mes parents, pour leur amour et leur soutien inconditionnels

Nothing great in the world has ever
been accomplished without passion.

Georg Wilhelm Friedrich Hegel,
1770-1831

Résumé

Cette thèse présente de nouvelles techniques de structuration 3D pour une technologie céramique relativement nouvelle appelée LTCC, qui signifie *Céramique Co-cuite à Basse Température* en français. Il s'agit d'un matériau développé à l'origine pour l'industrie de l'encapsulation microélectronique ; ses stabilités chimique et thermique le prédisposent aux applications militaires et à l'industrie automobile, telles que les électroniques de gestion moteur et les antennes Wi-Fi (fréquences giga hertziennes). Cependant, ces dernières années ont vu un intérêt croissant pour la recherche en microsystèmes céramiques : la microfluidique, l'encapsulation, les MEMS (microsystèmes électromécaniques) et les capteurs. Positionnée au croisement de la technologie classique des couches épaisses sur substrat en alumine et des céramiques à haute température, cette nouvelle sorte de céramique facilement structurable comble un trou dimensionnel et technologique entre les microsystèmes en silicium et les "macro microsystèmes" classiques, de sorte qu'il est maintenant possible de structurer des micro dispositifs de taille entre 150 µm et 150 mm. En effet, la technologie LTCC permet l'impression de conducteurs et autres encres de 30 µm à plusieurs mm, la structuration de 150 µm à 150 mm, et des structures suspendues avec des écartements de seulement 30 µm grâce aux matériaux sacrificiels. Les capteurs et leur encapsulation sont maintenant réunis dans ce qu'on pourrait appeler une "encapsulation fonctionnelle".

Les contributions de cette thèse portent à la fois sur nos apports technologiques, et sur les capteurs et dispositifs microfluidiques novateurs créés en utilisant les méthodes que nous avons développées. Ces réalisations n'auraient pas été possibles avec les techniques de lamination et cuisson standard utilisées jusqu'à présent. En somme, nous permettons de contourner les problèmes liés à la circuiterie microfluidique : en l'occurrence, le contrôle des dimensions cuites finales, la difficulté de produire des cavités et des structures ouvertes avec les délaminations de couches afférentes, et l'absence de "mode d'emploi" pour l'industrialisation de dispositifs fluidiques. Les accomplissements de ma recherche peuvent être résumés ainsi :

- Le contrôle des dimensions finales est maîtrisé après étude de l'influence des paramètres de lamination, prouvant qu'ils ont un impact considérable. Il est maintenant possible d'avoir un jeu de règles de conception pour un matériau donné, en déviant des recommandations des fournisseurs pour la fabrication de structures fragiles nécessitant une lamination réduite.
- Une nouvelle technique de lamination a été mise au point, permettant l'assemblage de circuits microfluidiques complexes qui ne supporteraient normalement pas une lamination

standard. La méthode est basée sur des sous-laminations partielles pseudo-isostatiques, avec l'aide d'un caoutchouc contraint, subséquemment consolidées par une lamination uniaxiale standard. Le conflit entre des couches bien liées et une géométrie finale acceptable est grandement atténué.

- Nous avons formulé une nouvelle classe de Matériaux Sacrificiels Volumiques (SVM) permettant la fabrication de structures ouvertes sur LTCC *et* sur substrats en alumine standard ; il s'agit en fait d'encres sérigraphiables préparées en mélangeant ensemble des composés minéraux, une phase vitreuse et des liants organiques expérimentaux. C'est une amélioration appréciable par rapport aux SVM pour LTCC existants, limités aux structures fermées telles que les membranes fines.
- Un multicapteur de diagnostic innovant, de classe industrielle et potentiellement à bas coût, a été développé pour l'industrie pneumatique, permettant la mesure de la pression, du débit et de la température d'air comprimé. Le dispositif est entièrement monté par brasage tendre sur une plateforme électro-fluidique, le rendant *de facto* lui-même un vrai *composant SMD électro-fluidique*. Il comprend en plus sa propre électronique SMD intégrée, et grâce aux techniques d'assemblage hybride standard, se passe de fils et de tuyauterie externes – cette prouesse n'avait encore jamais été réalisée. Cela ouvre la voie au diagnostic *in situ* de systèmes industriels par l'usage de capteurs intégrés à bas coût qui fournissent des signaux directement conditionnés.

En plus des développements susmentionnés, nous proposons une revue extensive des Matériaux Sacrificiels Volumiques existants, et nous présentons de nombreuses applications du LTCC aux capteurs et aux microsystèmes, comme des capteurs de microforce capacitifs, un microréacteur chimique et des micropropulseurs.

En conclusion, le LTCC est une technologie adaptée à la production industrielle de capteurs et dispositifs microfluidiques : les étapes de fabrication sont toutes industrialisables, avec une transition aisée du prototypage à la production en série. Néanmoins, la structuration de canaux, cavités et membranes obéit à des lois complexes ; il n'est pas encore possible de choisir avec précision les bons paramètres de fabrication sans test préalable. En conséquence, une ingénierie minutieuse et la maîtrise du savoir-faire de toute la chaîne de fabrication sont encore nécessaires pour produire des circuits électro-fluidiques en LTCC, en contraste avec les techniques plus anciennes comme les couches épaisses sur alumine et les circuits imprimés en FR-4.

Nonobstant son manque de maturité, la encore jeune technologie LTCC est prometteuse à la fois dans les domaines de la microélectronique et de la microfluidique. Les ingénieurs ont une meilleure compréhension des possibilités de structuration, des implications de la lamination, et des problèmes les plus courants ; ils ont maintenant tous les outils en main pour créer des circuits microfluidiques complexes.

Mots-clés : LTCC (Céramique Co-cuite à basse température), Techniques de structuration 3D, Matériaux Sacrificiels Volumiques (SVM), Lamination, Dispositifs microfluidiques SMD, Capteur intégré multifonctions SMD.

Abstract

This thesis aimed at developing new 3D structuration techniques for a relatively recent new ceramic technology called LTCC, which stands for *Low Temperature, Co-fired Ceramic*. It is a material originally developed for the microelectronic packaging industry; its chemical and thermal stabilities make it suitable to military-grade and automotive applications, such as car ignition systems and Wi-Fi antennae (GHz frequencies). In recent years however, the research in ceramic microsystems has seen a growing interest for microfluidics, packaging, MEMS and sensors. Positioned at the crossing of classical thick-film technology on alumina substrate and of high temperature ceramics, this new kind of easily structurable ceramic is filling the technological and dimensional gap between microsystems in Silicon and classical "macro microsystems", in the sense that we can now structure microdevices in the range from 150 µm to 150 mm. In effect, LTCC technology allows printing conductors and other inks from 30 µm to many mm, structuration from 150 µm to 150 mm, and suspended structures with gaps down to 30 µm thanks to sacrificial materials. Sensors and their packaging are now merged in what we can call "functional packaging".

The contributions of this thesis lie both in the technological aspects we brought, and in the innovative microfluidic sensors and devices created using our developed methods. These realizations would not have been possible with the standard lamination and firing techniques used so far. Hence, we allow circumventing the problems related to microfluidics circuitry: for instance, the difficulty to control final fired dimensions, the burden to produce cavities or open structures and the associated delaminations of tapes, and the absence of "recipe" for the industrialization of fluidic devices. The achievements of the presented research can be summarized as follows:

- The control of final dimensions is mastered after having studied the influence of lamination parameters, proving they have a considerable impact. It is now possible to have a set of design rules for a given material, deviating from suppliers' recommendations for the manufacture of slender structures requiring reduced lamination.
- A new lamination method was set up, permitting the assembly of complex microfluidic circuits that would normally not sustain standard lamination. The method is based on partial pseudo-isostatic sub-laminations, with the help of a constrained rubber, subsequently consolidated together with a final standard uniaxial lamination. The conflict between well bonded tapes and acceptable output geometry is greatly attenuated.

- We achieved the formulation of a new class of Sacrificial Volume Materials (SVM) to allow the fabrication of open structures on LTCC *and* on standard alumina substrates; these are indeed screen-printable inks made by mixing together mineral compounds, a glassy phase and experimental organic binders. This is an appreciable improvement over the so-far existing SVMs for LTCC, limited to closed structures such as thin membranes.
- An innovative industrial-grade potentially low-cost diagnostics multisensor for the pneumatic industry was developed, allowing the measurement of compressed air pressure, flow and temperature. The device is entirely mounted by soldering onto an electro-fluidic platform, *de facto* making it a true *electro-fluidic SMD component* in itself. It comprises additionally its own integrated SMD electronics, and thanks to standard hybrid assembly techniques, gets rid of external wires and tubings – this prowess was never achieved before. This opens the way for *in situ* diagnostics of industrial systems through the use of low-cost integrated sensors that directly output conditioned signals.

In addition to the abovementioned developments, we propose an extensive review of existing Sacrificial Volume Materials, and we present numerous applications of LTCC to sensors and microsystems, such as capacitive microforce sensors, a chemical microreactor and microthrusters.

In conclusion, LTCC is a technology adapted to the industrial production of microfluidic sensors and devices: the fabrication steps are all industrializable, with an easy transition from prototyping to mass production. Nonetheless, the structuration of channels, cavities and membranes obey complex rules; it is for the moment not yet possible to choose with accuracy the right manufacturing parameters without testing. Consequently, thorough engineering and mastering of the know-how of the whole manufacturing process is still necessary to produce efficient LTCC electro-fluidic circuits, in contrast with older techniques such as classical thick-film technology on alumina substrates or PCBs in FR-4.
Notwithstanding its lack of maturity, the still young LTCC technology is promising in both the microelectronics and microfluidics domains. Engineers have a better understanding of the structuration possibilities, of the implications of lamination, and of the most common problems; they have now all the tools in hand to create complex microfluidics circuits.

Key words: LTCC Low Temperature, Co-fired Ceramic, New 3D structuration techniques, Sacrificial Volume Materials, Lamination, SMD microfluidic devices, Integrated SMD multifunction sensor for pressure, flow and temperature.

Acknowledgements

Although a Ph.D. thesis is expected to be a personal accomplishment, it is often successful through a fruitful teamwork - and it was the case. I had the chance to meet and interact with really great and highly motivated people in the lab and at EPFL - something that keeps you enthusiastic to go to work everyday, even when experiments do not go the way you want :).

My first thanks go to my thesis director, Prof. Peter Ryser, who gave me both freedom and support to pursue my project, as well as responsibilities such as for equipment and safety. I am particularly indebted for his phone call of summer 2004, during which he proposed me to carry out a Ph.D. thesis in his laboratory; the road was long, but worth the reward!

I make a point in heartily thanking my supervisor and group leader Dr. Thomas Maeder for his unconditional support during all these years, his more than relevant scientific advices and constructive criticisms, and the thorough revision of my work, for which I owe him my deepest gratitude. Thomas is one of the brightest minds I have ever met, and I will keep excellent memories of our endless conversations and other common perfectionistic fine-tunings - from software codes to academic compositions, via ceramic artwork.

I am also indebted to Prof. Jacques Jacot and Prof. Theo Lasser, who both gave me the opportunity to study at EPFL back in 2000; since then, they have never stopped sharing their precious experience and advices with me on topics covering way beyond professional matters.

Regarding my thesis committee, I would like to thank Prof. Josef Binder, Prof. Marko Hrovat and Prof. Paul Muralt for their participation, as well as for the reviewing of my manuscript and their productive remarks. Similarly, I owe warm thanks to Prof. Max-Olivier Hongler, who accepted to be the president of the jury.

Many people have contributed to the success of this thesis; however, the most important cooperation was with Dr. Frank Seigneur, with whom we have produced many complex LTCC circuits and exchanged invaluable experience, both from personal and professional aspects through our numerous travels together. Many technical realizations would not have been possible without the help of Misters Timothée Haller, Matthias Garcin, Igor Saglini, Stanislas Wuilloud, Nicolas Dumontier, Giancarlo Corradini, as well as the mechanics and technicians of the ATPR, ATSE & ACI / ACORT workshops. Thanks also to the safety board of the STI Faculty for our meetings, which, I believe, were successful in avoiding some potential disasters: Misters Patrick Pugeaud, Marc Salle, Patrick Charpilloz and Joseph Guzzardi.

I wish to express my gratitude to several former students, some of whom have become friends or colleagues: Raphaël Willigens, Simon Wiedmer, Olivier Thommen, Pierre-Antoine Thivolle, Olivier Triverio, Nicolas Craquelin, Sandra Giudice, Jaya Thakur, Aurélie Barras, Grégoire Boutinard Rouelle and many others, whose work had a significant impact on the sensors and tools presented in this thesis.

The following colleagues occupy a special place in my heart for their true friendship and their indefectible support: Mesdames Nathalie Serra, Caroline Jacq and Karine Genoud, as well as Mr. Giuseppe Zamuner. It is very gratifying to know you can rely on friends in bad moments. Our secretaries and former apprentices, Mesdames Karine Genoud, Diane Morier-Genoud & Morgane Katz, deserve a standing ovation for their wonderful work and their efficiency, always of good mood. I would like to especially congratulate Karine for keeping "l'esprit LPM" throughout the years, i.e. by perpetuating traditions and cementing our heteroclite laboratory.

Thanks also to my office mates: Hansu Birol, Niki Johner, Damien Sonney, and Fabrizio Vecchio for their pleasant cooperation and funny conversations; this is extended to the whole LPM laboratory for good laughs and cheerful "wild" aperos: Lucas, Antoine, David, Simon, Mathieu, Zoltan, Mario, Pierre, Fabien, Stephan, Jonas, Julien, Ludovic, Christophe, Nicolas, Fabrizio, Conor, Bo, et al.

On a more spiritual level, special thanks to Dr. Jelena Godjevac and Mr. Louis-Séverin Bieri for their general advices on Ph.D. theses and encouragements. Louis also significantly contributed to the Design of Experiments study discussed in this thesis, along with Dr. Mario Bellino, Prof. Pierre Lambert (ULB) and Dr. Jean-Marie Fürbringer.

I would not like to forget my friends from neighboring laboratories (ASL, LIS, LMIS, LOB...), with whom we: a) organized several robotic contests, b) attended countless "movienights", c) created AéroPoly (EPFL's aeronautical association), or d) ran hundreds of kilometers in surrounding woods. Hence, thanks to Jean-Christophe, Antoine, Markus, Francesco, Nicolas, Milena, Samantha, Sylvain, Sebi, Gaëlle, Donovan, Adrian, Pablo, Kai, Christophe, Fabien, Sanna and all others! These were incredible associative and social experiences.

Finally, I will not have enough words to express my gratitude towards my beloved family, in particular my parents Jacques & Anne-Marie for their unconditional support of all kinds, their patience and their wise guidance, as well as Diane & Nataël for their delicious family meals. I cannot wait to tell you at the public defense all the things you awaited to understand :). Last but not least, my deepest and warmest thanks go to Mira, who has always believed in me; her endless support, commitment, joy and humor illuminated every day of this thesis (and countless sleepless nights at work!).

THANKS EVERYONE FOR THESE TREMENDOUS 10 YEARS AT EPFL,
OF WHICH 6 AT THE LPM!

Yannick Fournier
Lausanne, August 2010

Contents

Chapter 1

Introduction

This thesis aims at developing new 3D structuration techniques for Low Temperature Co-fired Ceramic (LTCC), in order to allow the design of microfluidic sensors and devices, which is not possible with standard lamination and firing techniques used so far by the pure electronics industry. This introduction briefly explains the LTCC system, compares it with other manufacturing techniques, and describes the problems related to microfluidics circuitry. We then expose the red thread of the presented research: the control of fired dimensions through the influence of lamination parameters, the development of a new class of sacrificial materials to allow the fabrication of open structures, and the creation of an industrial-grade low-cost multisensor for the pneumatic industry.

1.1 The LTCC ceramic – from electronics to microfluidics

In recent years, the research in ceramic microsystems has seen a growing interest, in particular for microfluidics, packaging, M(O)EMS (Micro(-opto-)electromechanical systems) and sensors. Positioned at the crossing of standard thick-film technology on alumina substrate and of high temperature ceramics, a new kind of easily structurable ceramic has emerged these last twenty years, called *LTCC*. LTCC stands for *Low Temperature Co-fired Ceramic*; it is also known as GreenTape™ (brand name from DuPont™) in its unfired form. It is a material originally developed for the microelectronic packaging industry; in particular, the telecommunication sector has focused on obtaining reliable dielectric substrates, where electrical signals could move fast and undistorted at high frequencies through the high-density wiring network in a reduced component volume that enables integration of passive elements (see an example on Figure 1.1). Its chemical and thermal stabilities make it suitable to military-grade and automotive applications, such as car ignition systems and Wi-Fi antennae (frequencies $>$ GHz) [1].

Featuring an outstanding combination of properties, the LTCC has seen this last decade developments beyond pure electronics, in the fields of sensors, microfluidics and biomedical applications [4, 5]. Our laboratory [6] being active in the development of ceramic sensors, sensor integration & packaging and in their industrialization, it was natural to orientate our

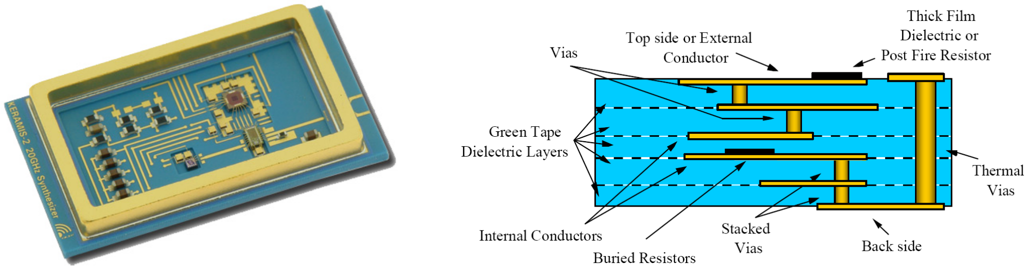

(a) Synthesizer 20 GHz KERAMIS-2 for Satellite Communications from IMST [2].

(b) Schematic cross-section of LTCC circuit depicting interconnect technology [3].

Fig. 1.1: Examples of purely electronic LTCC circuits.

research towards a technology enabling the design of sensors tailored for the industry. Therefore, LTCC was chosen as thesis subject by Dr. Hansu Birol, materials scientist who oriented his research [7] on the interactions of LTCC with co-fired printed materials, and on the development of carbon sacrificial layers for enabling the structuration of closed cavities such as thin membranes. The field of research around LTCC turned out to be immensely vast, but mature enough to allow the development of industrial devices - or at least to try to. Hence, as a microengineer specialized in techniques of production, robotics and industrialization, I decided to pursue the research with another orientation: the design of sensors manufacturable with industry-compatible techniques, in particular for the pneumatic industry. Consequently, LTCC is the material selected for the fabrication of nearly all the devices presented in this thesis – except some related work based on "classical" thick-film technology on alumina substrates, its ancestor and nonetheless cousin.

1.1.1 General properties

The LTCC system is basically thick-film ceramic sheets (LTCC tapes of raw thickness from 50 to 600 µm), which serve as dielectric layer and are co- and post-fired with thick-film pastes. The great advantage of the sheets is that they can be structured very easily in the raw (unfired) form: by punching or laser cutting, thus allowing three-dimensional structures like channels, membranes, vias, and holes. The sheets are individually screen printed, then stacked and laminated before the firing (up to 850-920 °C for 2 to 8 h). The sintering occurs at temperatures above 700 °C and induces a shrinkage from 0 to 18 % in the sheet plane (X-Y direction), and from 15 to 44 % in Z (thickness) [3, 8–16]. Figure 1.2 shows an example of fluidic circuit at various stages of manufacturing: after laser cutting, during stacking, after lamination, after post-screen printing and at the final stage after SMD components soldering.

A fired LTCC module is hermetic, can be used at high temperatures (up to 600 °C) and in harsh environments. LTCC can be both fired only once (co-firing) and refired (post-firing), but the sintering occurs only the first time, so there are practically no dimensional changes on secondary firings. The term *low temperature* indicates the usability of high conductivity metals with low melting point such as silver, gold and copper, in addition to platinum and palladium.

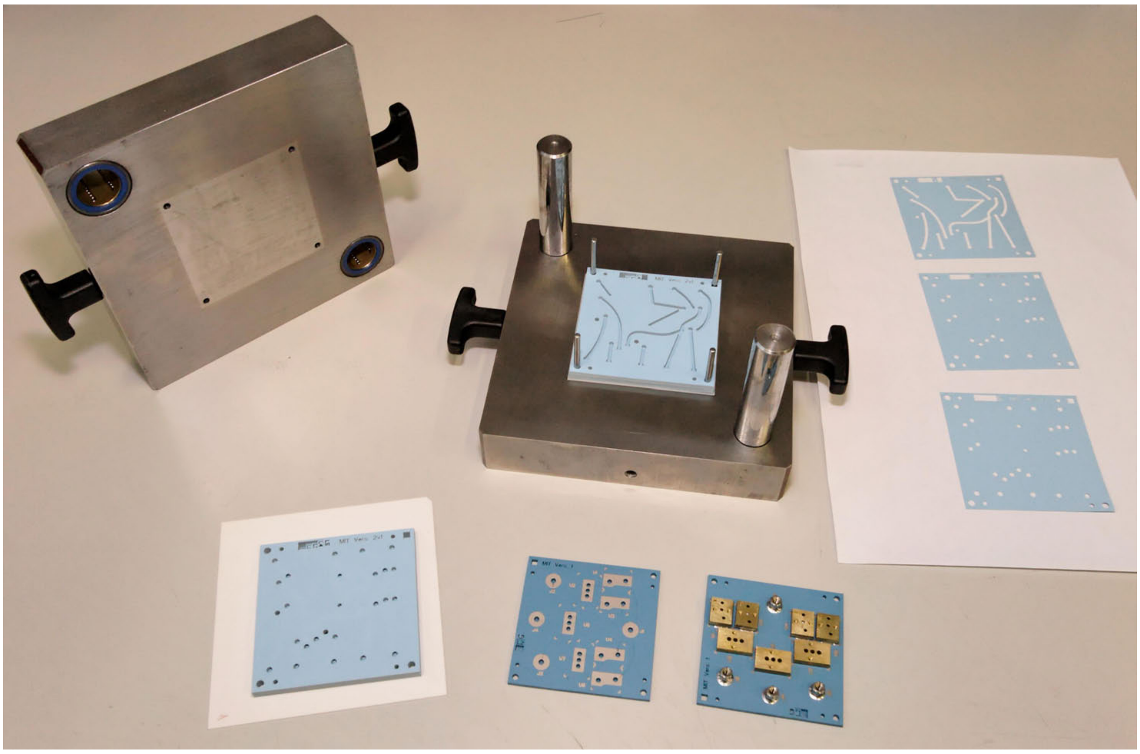

Fig. 1.2: LTCC fluidic circuit at various stages of manufacturing: green, laser cut (*right*), stacked on alignment fixture before lamination (*center*), laminated (*bottom left*), fired and post-metallized (*bottom center*) and mounted with soldered metallic components (*bottom right*).

To the contrary, the related HTTC (High Temperature Co-fired Ceramic) technology requires refractory metals (W, Mo) with lower conductivity, as it is processed at 1400-1600 °C.
The manufacturing of LTCC requires numerous steps; however all of them are simple and allow for easy intermediate inspection, thus decreasing the risk of malfunction in mass production. In summary, the resulting substrate is versatile and presents outstanding properties, among which:

- Good short-term chemical resistance to strong acids and bases [17–19];
- Very good thermal stability, and good thermal conductivity;
- Very low dielectric losses at high-frequencies, high breakdown voltage;
- Multilayered circuit with integrated resistors, capacitors, inductances;
- Multiple possibilities of cavities: unfilled cuts or with sacrificial material (graphite + mineral);
- Good solderability and bondability with the help of appropriate metallization; well gluable too.
- Use of noble metals (Au, Pt, Ag, Pd, Cu) possible, thanks to low firing temperature (< 920 °C).
- Batch production suitable for both prototyping and mass production without notable adaptation.

1.1.2 Filling a technological gap

Sensors and microsystems have seen continuous miniaturization these last four decades, and two categories have emerged, depending on the manufacturing techniques employed and their sizes:

- MEMS (Microelectromechanical systems), made up of components between 1 to 100 µm in size; the devices generally range in size from 20 µm to a millimetre, and the materials involved are mostly silicon, polymers and metals [20].
- "Macro microsystems", made of metallic, plastic, ceramic, composite and MEMS components between 500 µm to 20 mm in size, yielding devices ranging from 1 mm to 100 mm.

There was a gap between the two categories in the sense that technologies that cover the range gap from 100 µm to 500 µm have somewhat been missing - until the arrival of LTCC. The LTCC technology allows printing conductors and other inks from 30 µm to many mm, structuration from 150 µm to 150 mm, and suspended structures with gaps down to 30 µm thanks to sacrificial materials. It offers the advantage to have almost similar processing conditions for prototyping or mass production. Furthermore, it gives possibility to integrate MEMS, thanks to many assembly techniques available: by soldering, gluing (DIE attach), wirebonding, etc.

1.1.3 Comparison with concurrent methods

There are several other techniques in competition with LTCC for microfluidic applications. Some are dedicated to prototyping only, or the opposite: only for mass production. Some allow structuring only fluidic channels without integration of electric layers or passives. Some are for liquid fluidic only (no gas), and others limited in temperature.

HTCC HTCC (High Temperature Co-fired Ceramic), whose tape material is based on alumina, requires firing at ca. 1500 °C in H_2:H_2O atmosphere with Mo- or W-based conductors [21] and does not feature a set of functional materials as extensive as the LTCC, which is compatible with noble metals. For instance, the refractory metals of HTCC (Mo and W) have a lower conductivity than the Au, Ag, Pd, Pt or Cu of LTCC. Historically HTCC is an older technology, but it evolved modestly compared with LTCC. The processing of LTCC is very similar to that of HTCC, with more accessible firing conditions. The main raw material used in LTCC fabrication is the unfired "green" tape, e.g. glass-ceramic dielectric powder joined by an organic binder [21]. In this state, the material can be easily shaped and patterned by mechanical and laser cutting. LTCC combines the inherently multilayer capability of HTCC technology with the processing advantages of "classical" thick-film technology, i.e. the use of Ag- and Au-based conductors, and firing in a standard air atmosphere below 950 °C [11]. As a reminder, the melting points of Au and Ag are at 960 °C and 1100 °C respectively [1]. Furthermore, passive elements such as resistors, capacitors and inductors may be easily embedded using special thick-film and/or tape materials [22]. In contrast, these features are not available on HTCC.
One of the most famous custom HTCC ceramic packaging supplier is KYOCERA.

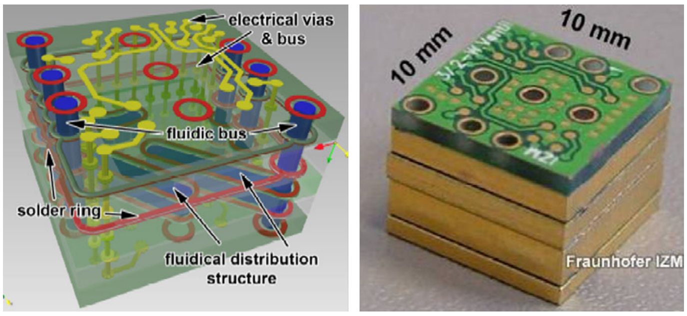

Fig. 1.3: Stacked fluidic mini-PCB of the Fraunhofer IZM in Berlin, demonstrator of the Match-X technology [23].

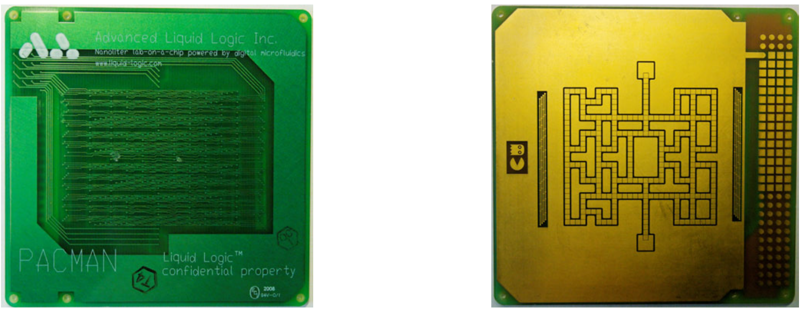

(a) Front view.

(b) Rear view, with electrical contacts.

Fig. 1.4: Fluidic PCB from Advanced Liquid Logic enabling "Digital Microfluidics" [24].

PCB (FR-4 or PTFE) Using classical PCB (Printed Circuit Board, made of FR-4, glass-reinforced epoxy laminate sheets) to make fluidic circuits has been demonstrated by the Fraunhofer IZM ("Match-X" technology) in 2004 [23], as depicted on Figure 1.3. FR-4 is a sophisticated and well-established substrate technology with low initial and production costs, but we have (to our knowledge) not seen further use of it except in custom applications. For GHz-range applications, special boards are often made of PTFE (polytetrafluoroethylene), fiberglass and ceramic; the article [1] of Kulke gives an interesting comparison between LTCC and PCB/PTFE. Although PCBs are cheaper to make simple electric circuits, the main drawbacks of using PCB compared with ceramics are:

- Maximum service temperature of 150 °C (standard materials);
- Difficulty of machining for fluidics (milling FR-4 yields an important tool wear due to the fiberglass reinforcement);
- It suffers from high dielectric losses in high frequencies;
- The technology does not offer hermeticity because of the organic matrix.

Another technology has been developed by a company founded in 2004 named Advanced Liquid Logic [24], which is now commercializing PCBs designed for "Digital Microfluidics";

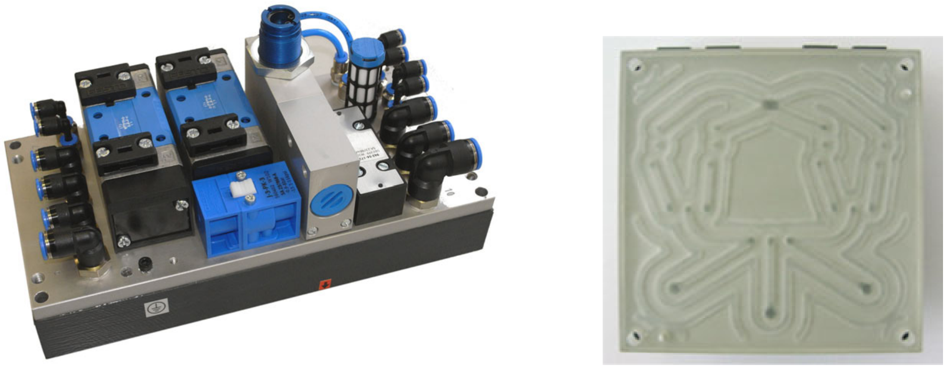

(a) FESTO's new integrated multi-layer duct plate technology provides the pneumatic logic and control functions for OYSTAR AEROFILL's latest-generation machines [28].

(b) Prototype in epoxy resin, seen from below. Source: FESTO-PNEUMOTECH [29].

Fig. 1.5: Examples of FESTO's fluidic platforms made in aluminium and epoxy resin/polyurethane.

this allows only for moving liquids electrostatically and cannot be applied to gasses. An example is presented on Figure 1.4.

SLS (Selective Laser Sintering) Selective Laser Sintering is an additive manufacturing technique that uses a high power laser (for example, a carbon dioxide laser) to fuse small particles of plastic, metal (Direct Metal Laser Sintering), ceramic, or glass powders into a mass representing a desired 3-dimensional object. It is a prototyping method only: it is a slow method, allows only piece by piece prototyping, is more suitable for forms than for circuits and overall it yields porous pieces.

Alumina + classical thick-films LTCC has for ancestor the classical thick-film technologies, usually with alumina or AlN as substrate. As it is a mono-substrate technology, the making of fluidic circuits requires assembling the substrates by sealing [25] (with the notable exception of micro-fluidic channels demonstrated in section 4.2.2).
The multilayer circuits may be manufactured by screen printing, but this is a sequential process, hence less advantageous for numerous layers [26, 27].

Aluminium and epoxy resin/polyurethane To make purely fluidic circuits, there is a basic method involving a platform made of an aluminium lid (contening the fluidic openings) covering a matrix of channels initially made in transparent epoxy resin. It allows for easy processing and prototyping, as the channels can be observed from below (Figure 1.5b). For mass production, the epoxy is then advantageously replaced by polyurethane, as depicted in Figure 1.5a by a commercial application of FESTO for a manufacturer of aerosol filling and closing equipment.

Silicon As explained in subsection 1.1.2, Silicon MEMS technology is not a direct competitor to LTCC - instead, they must be used in complement to each other. The partial overlap is

because Silicon devices aim at structural dimensions from micrometric up to 50 µm to 2 mm, while the LTCC aims are from 0.1 mm and above.
LTCC is an elegant hermetic packaging solution for MEMS (integrated by die attach and wirebonding), along with the integration of passives. The major drawbacks of Silicon devices are their manufacturing conditions: an expensive clean room is absolutely necessary, in which heavy and complicated processes are performed. Reviews of microfluidic MEMS and integration with LTCC can be found in [30–33].

1.1.4 LTCC tapes suppliers and types of inks

Several studies and theses have been devoted to the material compositions of the various LTCC tapes and their influence on sintering [34–39]; we will therefore not cover this topic. We propose however in Appendix section D.1 a listing of the tape suppliers, of the worldwide foundries, and of the type of inks.

1.2 Domain retained for the thesis

1.2.1 Description of problems

From the above we understand that LTCC is an ideal technology to design electro-fluidic circuits in ceramic; it is suitable to harsh environments, ensures a good hermeticity, and benefits from multiple ways of assembly (by gluing, soldering, glass sealing, wirebonding etc.) for external components such as fluidic fittings, electrical connectors, SMD components or mechanical inserts. So, what are the problems preventing a circuit designer from using LTCC as an end-user technology, in the same way an electrical engineer would use standard PCB in FR-4 to make electric circuits? Is it possible to manufacture microfluidic devices and sensors with industrial techniques? In what directions should research be led to help reach these aims? The answers are of course multiple.

Shrinkage First, the tape materials endure a relatively important volume shrinkage upon sintering (around 40 % (Figure 1.6a), either a combination of X, Y and Z for standard LTCC or only in Z for “zero-shrinkage” LTCC) that is largely dependent on both the pre-firing (i.e. lamination) and firing conditions, on the type of tape (Figure 1.6b), on the type and quantity of co-fired functional inks, and that is often inhomogeneous. This yields unpredictable results of the final output geometry not only in size, but also in shape; an inhomogeneous shrinkage inevitably induces deformations.
This effect is worsened by the geometric ratio between height and width of a structure, which has a non-negligible influence on the quality of the output. It is easy to imagine that relatively high and narrow structures protruding out of a large surface will be in conflict with each other first during the lamination, and then during the firing. Therefore, deformations such as warping, sagging, cushion, cracks or tearing are frequent, as depicted on Figure 1.7. The presented structures are a good example that LTCC does not always turn out like imagined with the 3D

CAD software: the uniaxial lamination of structures with high aspect ratio at reduced pressure leads to such unpredictable results.
Consequently, it would be very beneficial to know how lamination influences the shrinkage, and what kind of structure geometries are manufacturable or not. We will expose in chapter 3 our study with Design of Experiments of potentially influential lamination parameters: pressure, temperature, duration and the number of layers. It is also important to mention that we will only study unconstrained (free) sintering (UCS, standard shrinking tapes) and self-constrained sintering (SCS, for "zero-shrinkage" tapes), and not the other forms of constrained sintering (PAS and PLAS, see Figure 3.1 on page 52).

Channels and closed cavities Second, the core definition of microfluidics is to implement bridges, channels and closed cavities in a circuit, which are often crossing each other. For instance, such bridging elements may act as low mass carriers for resistive temperature sensors or heater elements combined in complex sensor systems like calorimetric or anemometric flow sensors (see section 5.3). Unfortunately, if one tries to simply cut inner tapes, stack, laminate and fire according to manufacturers' recommendations, he will be rewarded with a bad surprise. This will always be the case for isostatic lamination, but the result is not necessarily better for unixaxial lamination (see Figure 3.2a on page 54). In effect, high differences in lamination pressure along the sample geometry lead to inhomogeneous densification effects inside LTCC structures embedded in cavities, causing delamination, distortion, sagging and even crack formation at unconstrained sintering [40, 41]; Figure 1.8 attests of such failed attempts.
So, what can be intended to solve this problem? Apart from using sacrificial inserts (see below), the crushing of channels suggests reducing lamination, i.e. pressure, temperature, and/or duration. This is what was tried, yielding unsuccessful results as depicted with a crossing of fluidic channels on 1.9b, showing evidence of sagging and delamination after firing, because the bridging element might not be exposed to any pressure at all during lamination. The problem was not resolved but just shifted: the cavities presented less sagging but more delaminations, as well as an even greater shrinkage (up to 14 %).
Therefore, research is required to improve the quality of tape bonding while reducing the lamination. We propose a new method of tape assembly based on partial, reduced pseudo-isostatic sub-laminations with the help of a constrained rubber, which are consolidated together with a final standard uniaxial lamination.

Sacrificial inserts One demonstrated solution to ensure deformation-free structures is the usage of sacrificial inserts, also called Sacrificial Volume Materials (SVM). So far, only carbon sacrificial paste was successfully used on standard LTCC, and only for closed cavities; open structures such as cantilevers cannot benefit from the SVM support during the firing, as the carbon paste burns before the end of the sintering. Furthermore, the use of SVM that survive the firing (for instance, mineral pastes) was not yet possible on LTCC due to a shrinkage mismatch between the tape and the paste; Figure 1.10, and Figure 4.9 on page 107 can testify of failed attempts of using, on DUPONT 951 LTCC, mineral pastes suitable to alumina substrates (of course non-shrinking).

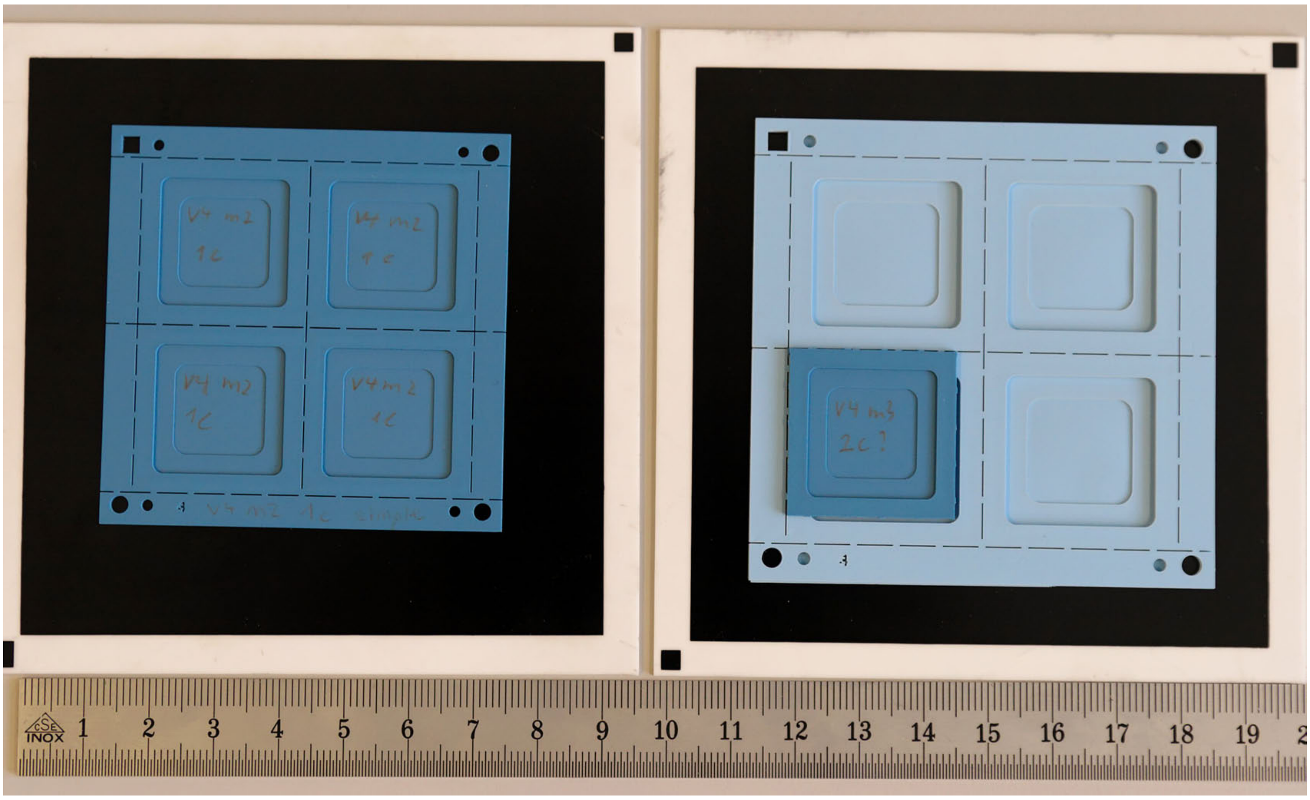

(a) Comparison of dimensions and color between a fired (*left*) and a green circuit DP951 (*right*). The ruler is in cm.

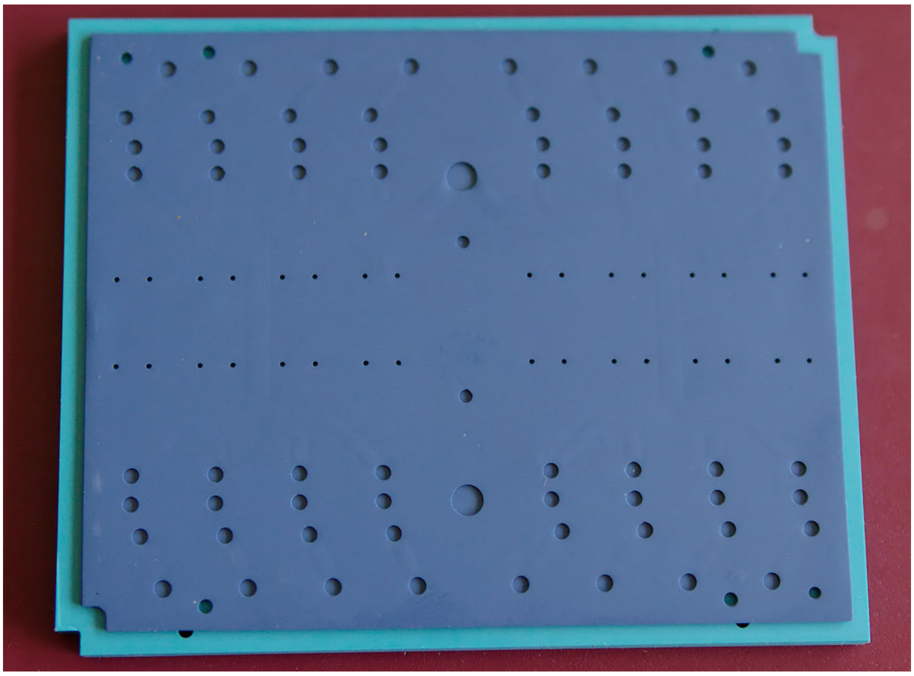

(b) Well visible difference of shrinkage of the same circuit made in two different LTCC tapes: DuPont 951 (bottom) and Heraeus CT700 (top). The dimensions of the DP are around 93×76 mm.

Fig. 1.6: Examples of circuits showing evidence of the shrinkage of standard LTCC, as well as variations between tapes.

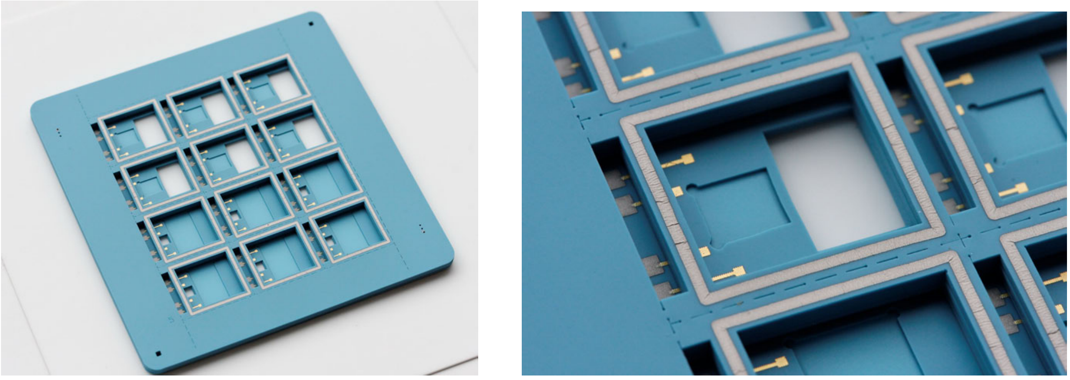

(a) Global circuit, production in batch of two sub-parts.

(b) Close-up on a sub-part. The cracks in the Ag:Pd screen-printed solder pad frame are due to improper processing.

Fig. 1.7: LTCC structures with a large height-width ratio, presenting geometric deformations due to shrinkage conflicts. This example confirms that uniaxial lamination of structures with high aspect ratio at reduced pressure leads to unpredictable results. Courtesy of FRANÇOIS GILLARD from the EPFL-LPM.

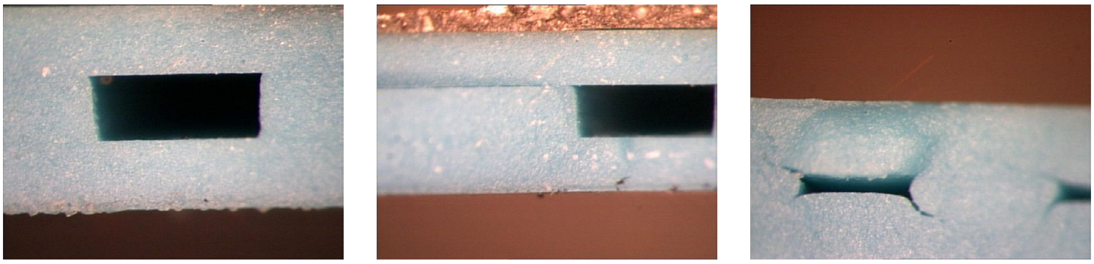

(a) Laminated at 20 bar, with good bonding of tapes at the edges (by chance).

(b) Laminated at 20 bar, with delaminations of tapes.

(c) Laminated at 206 bar: crushing of channels.

Fig. 1.8: 0.5 mm wide channels of three-layer 254 µm DP951 LTCC circuits laminated at 70 °C for 10 min but at different pressures, depicting the influence of lamination pressure on the output quality of unfilled cavities. For reference, DUPONT recommends laminating at 206 bar (3000 psi) at 70 °C for 10 min.

There is definitely room for improvement in this field: hence, we present the development of Mineral Sacrificial Pastes (MSP) adapted to standard LTCC, but also to “zero-shrinkage” tapes (HERAEUS HERALOCK) and to classical hybrid substrates.

Industrialization Many LTCC sensors developed with microfluidics R&D techniques are promising, but how many are apt to industrialization? Usually only the healthiest prototypes are presented in publications, but the techniques have a low global yield. In effect, taking into account all the defective production during screen printing and firing, the intrinsic variability of the processes, and the indispensable (mostly kept secret) know-how of the operators, it is often premature to declare a technique ready for industrialization. This leads to the following question:

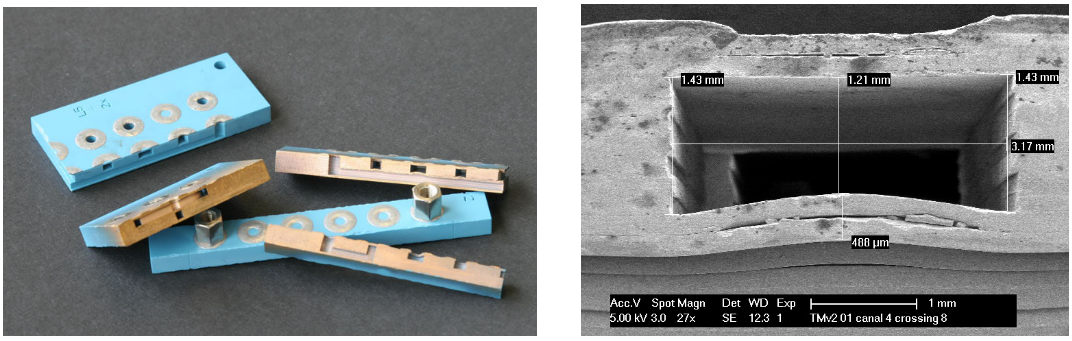

(a) Circuit after diamond saw cutting and flash gold deposition to allow further observation with SEM.

(b) SEM cross section of a 3 mm×1.47 mm, 7-layer LTCC channel crossing another channel at 90°. The dark stains are finger prints; the sample had not been polished after cutting.

Fig. 1.9: LTCC test fluidic circuit with multiple channels crossing each other, showing sagging and delamination after firing due to a reduced (hence poor) lamination (at 25 °C - 160 bar - 10 min). The fluidic connections are ensured by soldered nickeled-brass M3 nuts.

Fig. 1.10: Photo showing failed attempts of using our best mineral sacrificial paste formulated *for alumina* with DP951 LTCC. The tapes, initially flat, suffered from substantial deformations and cracks, due to the shrinkage mismatch. To give an idea of the scale, the underlying alumina substrate measures 4"×4".

Is LTCC a technology mature enough to allow mass production of microfluidic sensors compatible with classical assembly techniques and manufacturing standards?

By classical assembly techniques we mean soldering, gluing, wirebonding; for instance, is it possible to reliably solder fluidic interconnections on LTCC sensors? Can we ensure an acceptable reproducibility of the manufacturing process and hence the produced devices? What about the long-term degradation of the ceramic properties and of the screen-printed passives like heaters? These questions were clearly not answered sastifactorily at the beginning of this thesis.

Thanks to the cooperation with an industrial partner active in the pneumatic field, we decided to develop an industrial-grade LTCC multisensor oriented for diagnostics. The goal is to measure *in situ* compressed air pressure, flow and temperature, and to condition the output signals with integrated electronics. Furthermore, we want to avoid as much as possible external wires and fluidic tubing: the aim is to provide an SMD sensor that can be put in place, soldered and directly working, thus employing industrial assembly techniques. In a general manner, the techniques developed in this thesis have been elaborated while keeping in mind industrialization as much as we could.

Limits of LTCC technology Although this is not a "problem", we do not know yet the limits of LTCC structuration. Being a relatively new technology, many ways and ideas have not yet been explored. Student projects usually involve developing a sensor for a particular application, and are thus a good opportunity to test new techniques at low cost; however, new ideas usually occur unpredictably. Therefore, we expect some testing to be done "on-the-fly".

1.2.2 Summary of chosen orientations

My research plan can be split into two main parts:

1. The scientific study of poorly understood phenomena and the enhancement of LTCC materials from a technological aspect.
2. The creation of LTCC devices and sensors, with the first part providing the necessary tools for the second.

To summarize, the thesis "red thread" and the corresponding selected approaches can be written as:

1. **To ensure circuit fired dimensions through the control of lamination parameters:** With a scientific-based approach, by using specific mathematical tools such as Design of Experiments, to determine which are the most influential parameters that govern the LTCC tape shrinkage and draw a model to better predict it.
2. **To permit the assembly of complex microfluidic circuits that would normally not sustain standard lamination:** With the setup of a new lamination method, based on partial pseudo-isostatic sub-laminations with the help of a constrained rubber at a reduced set of parameters, subsquently consolidated together with a final standard uniaxial (metal) lamination.
3. **To allow new structuration techniques with the development of mineral sacrificial materials:** Our strategy, in order to allow the creation of open structures such as cantilever beams, is to explore a chemically-enabled solution by preparing and testing new paste compositions based on the latest state-of-the-art attempts, which will be dissolved by weak acids after firing. This will leave a gap, thus revealing the open structure.
4. **To develop new LTCC sensors assembled with industrial techniques:** In particular, through the thorough technical development of a fully functional low-cost integrated multisensor with a direct industrial application (diagnostic for compressed air

installations), with the use of standard hybrid assembly techniques to prove its feasibility in an industrially-compatible environment.

1.3 Structure of the thesis

The thesis is divided in the following chapters:

- We present in chapter 2 the equipment necessary to produce the presented LTCC circuits and the associated know-how.
- In chapter 3, we focus on the lamination, a critical step in LTCC manufacturing; it describes standard issues, techniques and equipment developed during this thesis as well as the latest state-of-the-art lamination techniques. It also presents a systematic study of lamination parameters on firing shrinkage.
- Mineral sacrificial materials allowing structuration of open structures both in classical thick-film technology and in LTCC are developed in chapter 4, after an extensive review of existing methods; a direct application to microforce sensors is proposed.
- Various sensor applications are disclosed in chapter 5, among which an integrated multi-sensor.
- A general discussion with conclusions and perspectives are gathered in chapter 6, and the latest innovations are sketched out in section 6.2.
- Finally, appendixes give complementary information, especially the glossary of Appendix E that lists all LTCC-specific vocabulary terms. Readers foreign to Hybrid Technology are invited to browse it before further reading.

This document is voluntarily written with some redundancy, with the idea to avoid requiring the reader to read it entirely when only one part is of interest. Extensive use of internal and external hyperlinks was also made, which is very convenient for the electronic version[1].

---

[1] The PDF is accessible on http://library.epfl.ch/en/theses/?nr=4772.

Chapter 2

LTCC technology: useful know-how

This chapter describes the manufacturing steps of the microfluidic LTCC circuits presented in this thesis from the engineering point of view, in order to point out where special attention is needed. It is logically organized according to the manufacturing order, i.e. first the layout rules, second the processing steps, then the assembly techniques, followed by how to detect defects in fired structures. The lamination step however is just overviewed; it is the subject of chapter 3.

Key words: Layout rules, CAD oftwares, Equipement used, Processing issues, Defects detection.

2.1 Design and layout

2.1.1 Design software packages

People new to hybrid circuitry will usually start with simple designs of low complexity. After the impossible to circumvent paper & pencil first draft, the beginner will generally draw his circuit with widely-used layout softwares, or mechanical CAD[1] softwares such as PTC® PRO/ENGINEER and DASSAULT SYSTÈMES SOLIDWORKS®. Although these softwares allow drawing the tape borders and cavities, they lack the electrical verification capability (usually refered as DRC, *Design Rule Check*). They also often cannot output in the necessary file formats required by the tape cutting machines (typically DRILL data for a puncher, and AutoCAD DXF or HPGL[2] for a laser), nor in the file formats used for creating the screen printing masks (typically GERBER RS-274-X used by many photoplotters). Moreover, compensating for the firing shrinkage is usually a problem, and must be carried out in an external software; to correct a mistake, everything must be done again. As such, the workflow can be long and painful.

---

[1] Computer-Aided Design

[2] HEWLETT-PACKARD Graphics Language

The "make-do with what's at hand" solutions Some leading thick-film research groups have replied to my survey about their software use; most were seeking for a specific software solution too, and were using the following softwares as temporary solutions, or for a part of the workflow only:

- AUTODESK® AUTOCAD (can output DXF)
- CORELDRAW from COREL® (for outputting masks)
- CAM350® from DOWNSTREAM TECHNOLOGIES (to convert DXF to GERBER and DRILL)
- CAHL[3], rather simple and outdated now

Teams designing PCBs or purely (non-shrinking) hybrid alumina-substrate circuits are usually employing widely-used PCB design softwares, such as:

- ALTIUM DESIGNER from ALTIUM (formerly PROTEL INTERNATIONAL)
- BOARD STATION XE from MENTOR GRAPHICS®

These softwares are very good at designing circuitry, but lack hybrid- and LTCC-specific modules, which are very convenient for controlling the shrinkage variations, for managing the multiple layers, for implementing thick-films resistors, etc. In our laboratory, at the time of PROTEL, we had to use ADOBE® ILLUSTRATOR® to compensate for the shrinkage, before re-importing into PROTEL to get a DXF output; a very tedious process.

Software requirements for designing LTCC Here is a summary of what a CAD software needs to provide to allow designing complex microfluidic LTCC circuits:

- Support for multilayered substrates and multilayered screen printings on each substrate, both mechanically and electrically;
- Electrical schematics (necessary for complex circuits);
- Easy control of various X-Y asymmetric shrinkages;
- Possibility to output both co-fired (unshrinked) and post-fired (shrinked) drawings;
- Possibility to implement and calculate custom thick-film resistors;
- Electrical and mechanical verification through Design Rule Check;
- Librairies for standard and custom-made components;
- Output of drawings in the most frequent formats such as DXF, HPGL, DRILL-MILL, GERBER, SMD Pick-and-Place;
- 3D visualization is a great plus to avoid potential conflicts;
- Thermal simulations for power sensitive applications.

---

[3] COMPUTER AIDED HYBRID LAYOUT SOFTWARE, available together with the book *Thick Film Technology and Applications*, M. HASKARD, KEG Pitt, Electrochemical Publications, 1997 and referenced in [42]

A solution: a software tailor-made for LTCC As the complexity of our circuits increased constantly (overall the electrical part), acquiring a dedicated software became a necessity. To our knowledge, only one LTCC & thick films design software was available on the market in 2006 at the time of our market research: HYDE[4] from DURST CAD [43]. It allows designing standard thick-films circuits with one substrate (e.g. alumina) or multilayered LTCC circuits (up to 50 tapes with 100 layers each are supported). HYDE is layer-oriented, customizable with macros, and comes with many optional modules (thermal simulation, file input/output formats, 3D viewer etc.). Among other features, HYDE accepts the integration of dice in cavities, their linking with wire bonding, the implentation of vias accross multiple layers, and top + bottom wiring. Furthermore, the software easily allows for X-Y anisotropic shrinkage compensation[5]. This effect can either be controlled by software, or by alternate stacking of the tapes (0° - 90° - 0°...). This latter solution is not always applicable, as it shifts the problem toward elliptic or stairs-like vias and cavities (see section 3.3.3), and is partially effective for circuits with odd tape numbers. Some drawbacks[6] reside in its austere GUI[7], in repetitive tasks, and in the absence of user-setting retention for some features.

The acquisition of a specific software was even justified for one particular project [44–46] (see also section 3.3), of which the goal was the hermetic packaging of a MOEMS that involved 10 LTCC layers (of which 7 electrical) and 400 connections, all linked with wire bonding, vias and a bottom BGA[8] connector. To confort this assertion, the 2D screenshot of Figure 2.1a testifies how much a screen can be cluttered when all electrical layers are made visible; a 3D view can be seen on Figure 2.1b.
Another example is proposed on Figure 2.2, this time for an electro-fluidic platform whose purpose is the interconnection of electrovalves. This circuit will be shown at later stages of processing throughout the chapter and in section 3.3.3 and section 3.4.2 too.

The workflow starts by designing the electrical connections in the SCHEMATIC module; the footprint of components is selected at this stage. Then the *layout package* gets imported in the HYBRID module, where the components are physically placed on the tapes, the cavities and conductor tracks are drawed, and the vias are placed. The remaining *air wires* between pads show the not-yet-connected conductor tracks, and aid the user in avoiding shortcircuits or unconnected pins. To help uncluterring the screen, visual filters based on the layers to be displayed are created. After careful verification of the mechanical and electrical layout (the *design rules check*), the different files necessary for fabricating a circuit are output:

- HPGL or DXF files for laser cutting, one for each tape;
- DRILL-MILL files for via punching or CNC-milling;
- SMD Pick and Place files for the automatic placement of SMD components;
- GERBER files, one for each layout of screen mesh to be screen printed.

---

[4] HYbrid DEsign
[5] See in chapter 3 on page 51.
[6] Tested with version 12; as of 2010, version 13 is available.
[7] Graphical User Interface
[8] Ball Grid Array

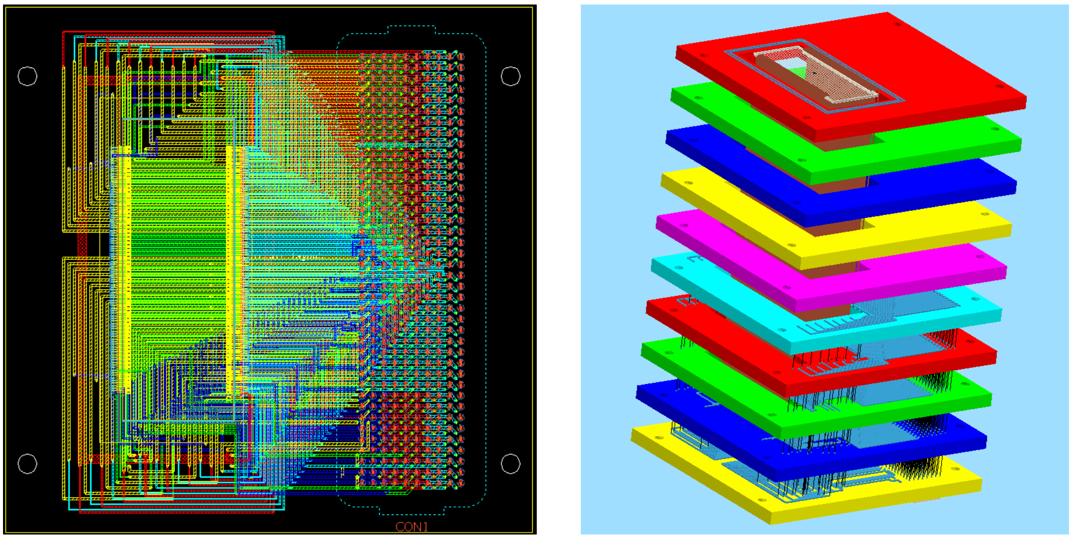

(a) 2D view with all electrical layers visible.

(b) 3D exploded view.

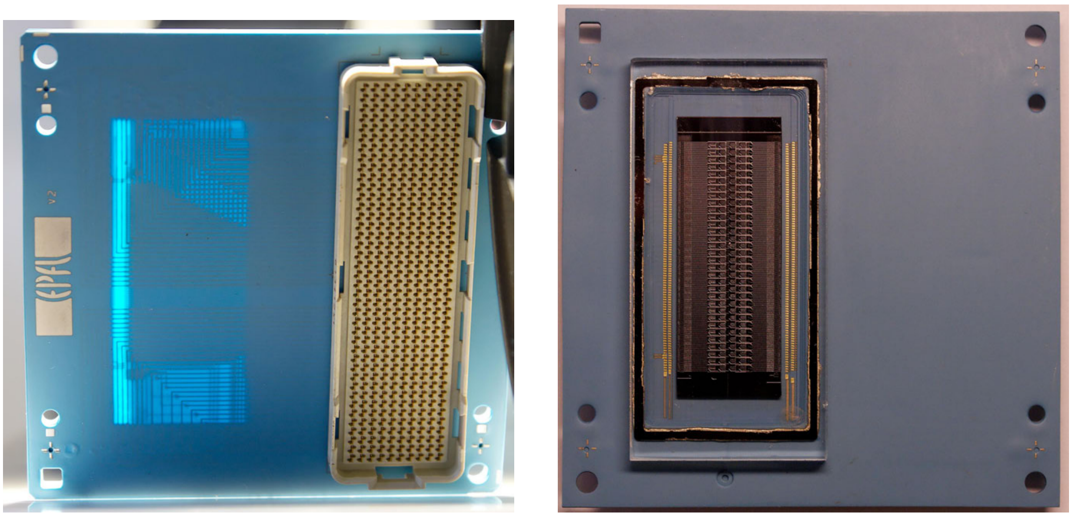

(c) Fabricated circuit seen in transparency from below; the complex electric lines are well visible.

(d) Fabricated circuit seen from top, with the window ensuring hermetic packaging soldered.

Fig. 2.1: *Top*: screenshots made with the HYDE software enhanced with LTCC and 3D modules, depicting a complex electrical design: a 10-layer circuit for the packaging of an optical MEMS, described in [45, 46]. *Bottom*: the corresponding fabricated circuit.

Competitors Since 2006, competitors upgraded their products, but we have not tested them. CAD DESIGN SOFTWARE proposes CDS[9] for Hybrid / MCM[10] / LTCC. Shrinkage control is now a lot easier in ALTIUM than in PROTEL; however, there is still no LTCC-specific module available to our knowledge.

---

[9] Circuit Design Software

[10] Multi-Chip Module

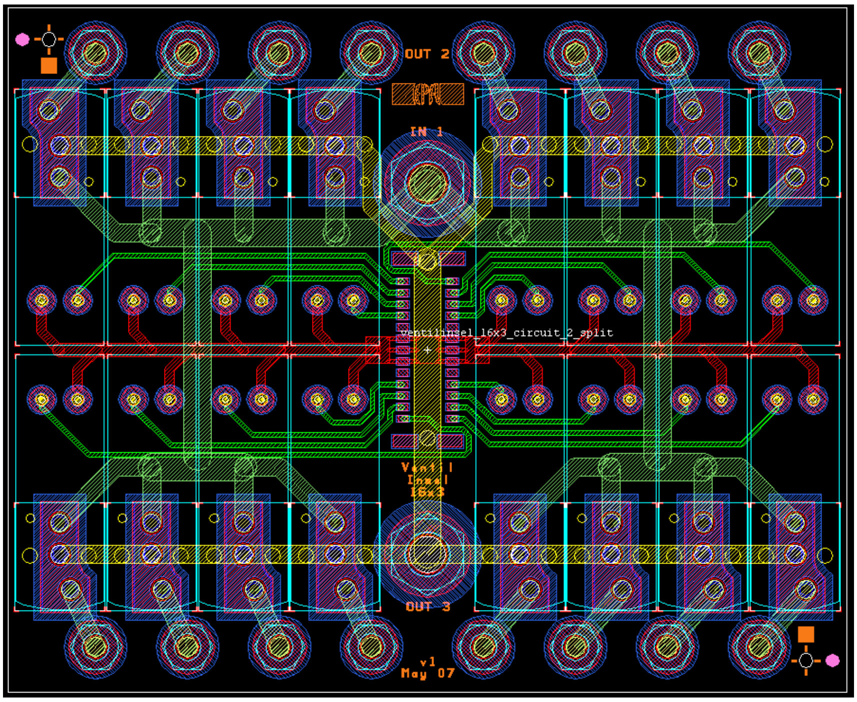

Fig. 2.2: Schematic top view of an electro-fluidic platform whose purpose is the interconnection of electrovalves, and which will be presented at later stages of processing later. Channels are in dark green and yellow; electrical lines in light green and red, solder pads in violet and solder in dark blue.

2.1.2 Design rules

Distances and dimensions of features In practice, the design rules differ little from the theory. Please refer to the design guides [9, 10, 12, 47] for more information.

Paste and tape compatibilities Although LTCC suppliers provide charts of their pastes assortment, determining the compatibilities between pastes, or the right tape-paste combination is often an issue. The reasons are many:

- Insufficient testing from the manufacturer;
- Erroneous or evasive datasheets;
- Absence of standardization in the LTCC industry;
- Retention of information due to military / business confidentiality constraints;
- Novelty of some LTCC systems;
- Numerous possibilities of combinations, leading to difficult predictions.

General rules of thumb apply well in the majority of cases, but experiments revealed unforeseen usages, such as the DP5092D and 5093D PTC resistor post-fire pastes for alumina system yielding better results on LTCC than on alumina [48]. The other issues we have encountered are gathered in Appendix section D.3 on page 243.

2.2 Manufacturing steps of an LTCC circuit

The LTCC process flow is a concept easy to understand, though complex due to numerous steps; it is also iterative and varies upon the equipment employed. Flow charts are abundant in literature; the design guides [9, 10] and the thesis [49] of Dr. Hansu Birol cover the subject in detail. Horvath wrote in 2008 an interesting summary of LTCC manufacture operations in [50].

The purpose of this section is not to give a general overview and not to list all possible variants, but to describe the particularities necessary to manufacture the circuits presented in this thesis. Thus, only the equipment that was used in our laboratory is presented in this section. The process flow of operations carried out in our laboratory when manufacturing circuits is nonetheless partially displayed Figure 2.3: post-firing operations are not shown.

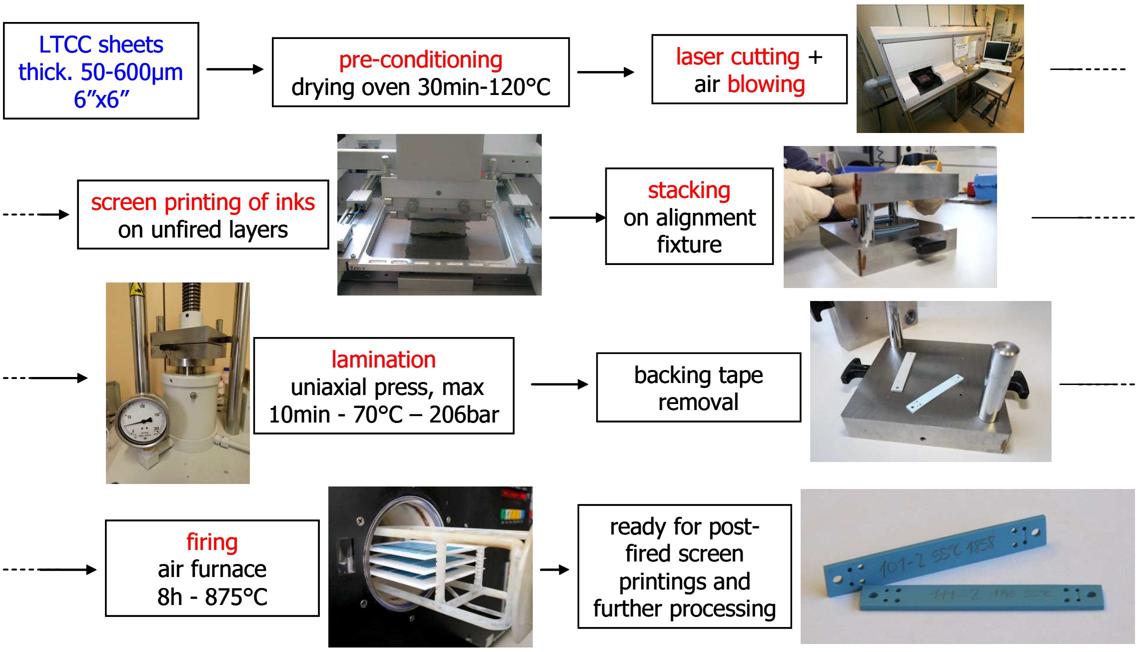

Fig. 2.3: Part of the experimental LTCC manufacture process flow in our laboratory.

2.2.1 Slitting & blanking: pre-cutting operations

Let's first explain this title with two definitions:

Slitting	is a process of cutting coils to specified widths along the length of the coil.
Blanking	is a process of cutting coils into square and rectangular shapes with close tolerances.

LTCC is usually delivered in rolls or in square sheets. Rolls need to be cut at the desired dimensions, while square sheets (6″×6″) do not need to be cut and can be directly deposited on alumina substrates for further processing.

Removal of the backing tape At this stage, it is in absolute not necessary to remove the backing tape (a Mylar carrier for DuPont 951 [9] and Heraeus HL2000 [15], as shown on Figure 3.14c on page 72, or similar polyester for Ferro A6 [12]), as it helps maintaining lateral dimensions during screen printing. This requires nevertheless compatible punchers and cutting tools, as well as special vacuum stones to carefuly remove the backing tape just before the stacking. Our IR Nd:YAG laser is not appropriate for cutting the Mylar, because the polyester melts or burns badly and tends to stick to the LTCC. Thus, our machinery forces us to remove the backing tape. For DP951, which comes in 6"×6" square sheets, this is done by hand by gently ripping a corner, and then by pulling apart the Mylar from the tape in one swift movement, immediately followed by laying the tape on a clean alumina substrate; an easy task for 254 µm and 165 µm thick tapes, average for 114 µm and clearly requiring experience for 50 µm. Evidently the tapes must always be pulled and not pushed after the Mylar removal. For Heraeus tapes, which come in rolls and must be slitted and blanked, a scalpel is first slid along a side of the tape to help release the backing tape; the procedure is afterward the same as for DuPont with a difficulty comparable to the 50 or 114 µm. In all cases, the backing tape is stored in a safe place to be reused as anti-dust cover or protection during lamination.

It is worth mentionning that pyrolyzable backing tapes are suggested in a technical disclosure of 2001 by Motorola [51]. The goal is to eliminate the tape removal step; for this purpose a tape material that has a pyrolysis profile that matches the ceramic firing profile and leaves minimal ash must be selected. A variety of tape materials were evaluated for process suitability including polyethylene, cellulose, and polyester based tapes. Optimal results in terms of residual ash and firing profile were obtained with polyester tape containing acrylate adhesive.
As claimed in the document, minimal residual ash content is required to maintain solderability of components, in the case metallized solder pads are screen printed. Nevertheless, we have never encountered this method in literature elsewhere.

2.2.2 Preconditioning

Preconditioning is useful to relieve the stress induced by the removal of the backing tape. It consists in heating LTCC tapes in an oven to allow levelling by relaxation of internal stresses without too much drying. The oven temperature for stabilization is between 80 °C for Heraeus tapes and 120 °C for DuPont 951, and the duration is between 15 min (HL2000) and 30 min (DP951).

2.2.3 Laser cutting

LTCC prototyping is conveniently done by laser cutting as it requires almost no preparation, but overall it is very easy to make small design changes on-the-fly and between iterations. The main drawback is the generation of dust (LTCC particles) and the operation time that ranges from 3 to 20 min per tape, depending on the type of LTCC used; in effect, with our laser the cutting speed varies from 0.7 to 10 mm/s (see Appendix section D.2).
Our laser cutting machine is indeed an industrial trimming laser machine model LS9000 from

(a) The whole laser machine.

(b) Galvo-mirrors (top), sensor probe (center) and X-Y table (bottom).

Fig. 2.4: Our laser cutting & trimming machine LS9000 from LS Laser Systems [52].

LS Laser Systems [52], used for the passive and active trimming of thick-film resistors. The laser source LS-520G is a Nd:YAG with Q-switch, with a wavelength $\lambda = 1064$ nm; the max output power is 3 W in monomode "TEM00", and the spot size is around 50 µm. In practice the achieved cutting width depends on the combination of type of tape, output power, cutting speed, pulse frequency, etc.: a high power at slow pace on a thin tape yields a cutting width of 100 µm or more.
Lasers in UV wavelength are known to exhibit a smaller spot size, but tests demonstrated that the right wavelength is function of the tape (see section 6.2.3).

For mass production, punching would be the best choice: no dimensional variations between center and edges, no dust generated, very short cycle duration (a few seconds), to the detriment of expensive punching tools impossible to modify on-the-fly.

Peculiarities of laser machines using a galvo-mirror beam deflection system B. Balluch & W. Smetana studied in [40, 41] the optimization of laser parameters to counteract the disadvantage of laser cutting machines using a galvo-mirror beam deflection system. Compared to static laser beam systems incorporating movable X/Y-supports, galvo-mirrors induce an angle to the beam upon striking the tape surface; the problem lies in the cutting edges that are inclined increasingly, the more the beam is deflected from the perpendicular center position. Additionally, the laser beam may run slightly out of focus for greater deflection angles.
Instead of lasering their CeramTec GC tapes in one pass (yielding for instance a 35 µm-wide test cut), they obtained much better results with repeated laser cutting cycles with decreased pulse energy; four passes yielded a fine cut line only 14 µm wide.
We also observed a similar effect when cutting small holes in large tapes; for very sensitive

Fig. 2.5: Screen printing operation: *(a)* AUREL 900T machine with cameras for optical alignment [54]; *(b)* Fresh screen printing of a DP7484 Pd/Ag metallization for solder pads on a large CERAMTEC GC electro-fluidic platform. Note the custom "cradle" of alumina blocks to accommodate the important circuit thickness to the printing squeegee.

applications, we had no other choice but to split the tape layout in multiple tiles to reduce the maximum angle of deflection of our galvo-mirror, thus reducing the associated errors.

2.2.4 Screen printing

Screen printing is impossible to circumvent when processing LTCC. The operation is very similar to those used for hybrid circuits in classical thick-film technology on alumina substrates, except that printing on unfired tapes requires a table with a porous vacuum stone to hold the tape. An important technical know-how is paramount for printing fine features correctly, and as it is often specific to the machine employed, it is beyond the scope of this document. The reader can refer to the report of HORVATH [50] for an interesting description of issues encountered in screen printing operations on LTCC, and to the thesis of Dr. SONIA VIONNET-MENOT [53] for an extensive description about the rheology of thick-film pastes.

For our printing operations we used two machines commonly found in the industry: the AUREL 900T from AUREL AUTOMATION [54] (see Figure 2.5), and the EKRA E1 from ASYS (formerly EKRA) [55].

After printing, the inks are allowed to settle 5 min at room temperature, then dried in a ventilated oven at 80 to 120 °C for 3 to 10 min. This allows solvents to evaporate before the next screen printing operation (on unfired LTCC), or before firing in a belt oven (for post-firings), see subsection 2.2.8.

Effect of drying cycles on green tapes M. RICHTARSIC et al. from LOCKHEED MARTIN studied in 1998 [56] the effect of drying cycles on the *green state shrinkage* (i.e. leading to errors on screen printing, stacking and lamination). They concluded that *excluding preconditioning, the most important consideration to controlling prelamination registration mismatch in LTCC is to duplicate the number of dry cycles per each sheet in the book; this rule applies regardless to* *the amount of metal conductor printed on a sheet*. From our own experience the more screen printing operations a tape undergoes, the more important the difference in size will be with the tapes that are not printed. A difference of 0.1 mm (over 65 mm) is often encountered upon stacking (for instance for the integrated multisensor of section 5.3). This leads to a dilemma: either non-printed tapes should "suffer" equivalent drying cycles to follow the size modification of printed tapes (at the risk of excessive drying and subsequent lower quality bonding of tapes during sintering), or tapes should be individually cut in accordance to their future processing (along with screen meshes varying in size accordingly). This latter option complicates the process and increases the risk of errors, overall when a screen is planned for several tapes (vias for example).

2.2.5 Stacking with special equipment

Stacking is a delicate operation; the tapes are fragile, overall when they have been screen printed and dried several times. They must be the less possible manually handled; in an R&D laboratory though, it is impossible to automate the whole manufacture process. However, it is not only important that the tapes must be correctly stacked, but also that the whole stack be correctly placed in the lamination press – our first experiences with LTCC stacks freely laid between metal plates yielded trapezoidal circuit shapes because of the pressing inhomogeneities (see section 3.2). We have thus developed specific equipment over the years to get serious and reproducible results.

Alignment fixture with pins Originally, we were manually stacking the tapes with manual and optical alignment; to allow the stack to be transferred on the lamination press, we tacked tape corners with a drop of IPA (isopropylic alcohol) to ensure a minimum cohesion. The process was cumbersome and not reproducible.
We knew other research teams who were using fixed pin alignment fixture; before we fabricated our own equipment however, they advised us to design an apparatus with mobile pins: after experience they remarked that the tapes get deformed at pins locations during lamination. Such a classical alignment fixture with fixed pins is visible on page 4 of the excellent review [5]. Therefore, we designed an alignment fixture with mobile pins compatible with our lamination press; we made it thick and heavy, in order to keep a flat shape and retain heat during lamination. The apparatus, made of the $\mathrm{K107/1.2436}$ tool steel, is presented on Figure 2.6. Originally the whole fixture was placed in a drying oven to laminate at temperatures above ambient, but the operation was cumbersome; we thus later added thick-film heaters and temperature regulation electronics (Figure 2.6b), yielding a truly temperature-controlled lamination fixture.

Semi-automated optical alignment and stacking machine Over the time, the stacking of tapes on pins proved to be difficult for thin tapes (e.g. 50 µm) and for large circuits, because of the natural sagging of the center. This resulted in deformed tapes, so we slightly increased their registration holes: this lead to a lower stacking precision. It was thus necessary to design a semi-automated optical alignment machine with a vacuum system, depicted on Figure 2.7.

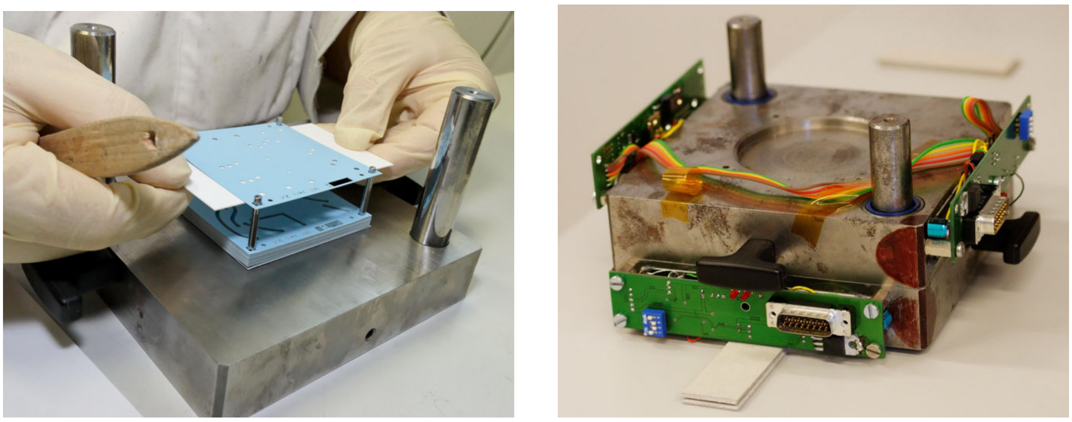

(a) LTCC being stacked with pins on early version of fixture without heating.

(b) Fitted with thick-film heaters and their control electronics.

Fig. 2.6: LTCC alignment fixture in early and current versions.

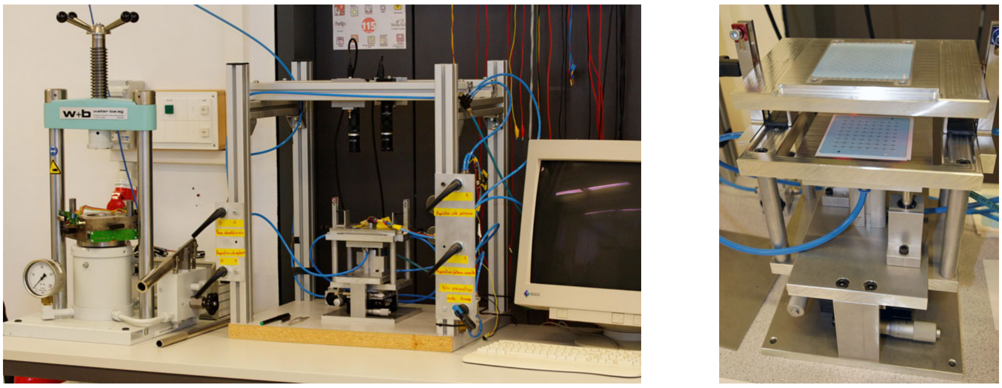

(a) **(b)**

Fig. 2.7: Experimental semi-automated optical alignment and stacking machine specially developed to handle fragile tapes. *(a)* Machine placed right of our uniaxial lamination press. *(b)* Close-up on tape stacking with mobile vacuum plate (top) and translating stack plate (bottom) mounted on precision X-Y-θ table.

This was carried out during the 2008 master project of Sandra Giudice [57], based on similar equipment developed at the University of Oulu, Finland. The appartus features a mobile vacuum plate and a translating stack plate mounted on precision X-Y-θ table. It is fully compatible with our developed pseudo-isostatic lamination technique (see section 3.3), and also permits the deposition of materials to improve the lamination quality (see section 3.4) just before the stacking.

2.2.6 Lamination

Lamination is a critical step in the LTCC process flow, and is the subject of ongoing research and developments. Hence, this step is covered extensively in chapter 3; please refer to section 3.3 for a description of the necessary equipment and for a discussion of the lamination parameters. Here is nevertheless a short description adapted from the excellent website http://www.ltcc.de of the IMST [2].
There are two possibilities of laminating the tapes in the process of LTCC production:

- The first one is uniaxial lamination; the tapes are pressed between heated plates at 70 °C, 200 bar for 10 min (typical values for DP951). As advised by DuPont, this method requires a 180° rotation after half the time, in order to compensate for the differences of X- and Y- shrinkage (we have however compensated for this in our layout software). The uniaxial lamination can cause problems with cavities/windows, and it yields higher shrinking tolerances than the isostatic lamination. The main problem comes from the flowing of the tape, which results in high shrinkage tolerances (especially at the edge of the part) during the firing and varying thickness of single parts of each layer; it causes serious problems to high frequency electronics, which rely on tight geometric tolerances for proper functionning.
- The second way is to use an isostatic press. The stacked tapes are vacuum packaged in a foil and pressed in hot water (temperature and time are just the same like using the uniaxial press); this method is however inappropriate for the lamination of unfilled cavities, and suffers from longer process times. In effect, these are mainly the high temperature inertia of the press; some take hours to reach the desired temperature. It is problematic for prototyping only; in mass production, the press would be at constant temperature.

2.2.7 Firing

The firing of our LTCC circuits takes place in a controlled box air furnace from ATV Technologie, model PEO 601 [58], shown on Figure 2.8. The machine features 6 IR lamps, can reach 1'000 °C and provides two gas flow inlets allowing a controlled atmosphere; it can be programmed through an external computer.

The firing profiles we use last from 6 to 8 h (see Appendix A); they were inspired from those encountered in literature or advised by manufacturers (in particular from [9, 11] for DP951), with the following particularities:

- For the burnout of the organics between 200 °C and 500 °C, we first ramp up to 350 °C at ca. 3 K/min, followed by a very slow ramp up to 450 °C, lasting between 2 to 4 hours, depending on the quantity of LTCC to fire. This is used instead of a prolonged dwell around 440 °C, known as the temperature of organics burnout of DuPont 951, in order to cover the whole spectrum and also to be compatible with tapes from other suppliers and with our SVMs.

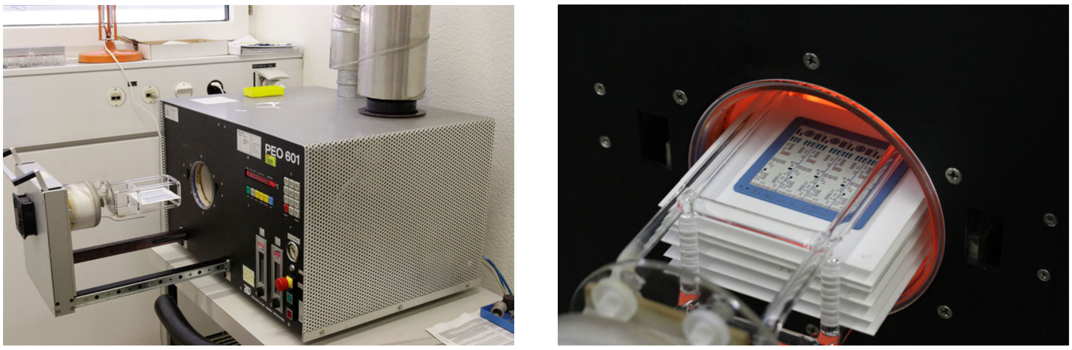

(a) Global view, door open. The oven can be directly programmed or controlled by a PC.

(b) Detail of substrate carrier heavily loaded, with door partially open and lamps in function.

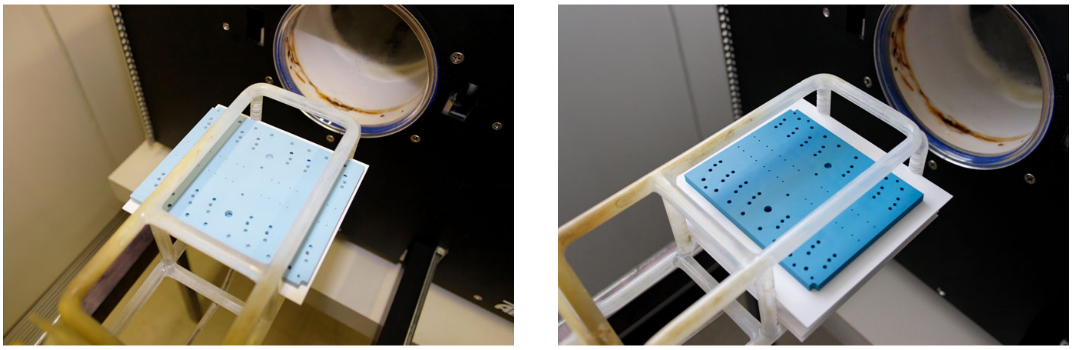

(c) Example of LTCC circuit of very large dimensions (110×90×5.6 mm, 22 tapes), before firing.

(d) Circuit of (c), after firing. Note the change of color and the subsequent shrinkage.

Fig. 2.8: ATV PEO 601 lamp air furnace [58] used to fire LTCC circuits.

- The sintering begins around 700 °C and ends between 850 °C and 900 °C, depending on the tape and the ramp. These rates, selected in the suitable range for the tape, are usually between 1.5 and 10 K/min. This is followed by a 30 min-dwell at peak temperature, which allows large circuits to reach an homogenous temperature during 15 to 20 min.
- In practice, we observed in our oven up to 20 K of difference between the desired temperature profile and the actual temperature inside the furnace, measured by external thermocouples at the peak of firing; we thus selected 896 °C to ensure we reach 875 °C (for DP951). The possible overtemperature resulting from this increase has no effect on the quality of bonding or on the shrinkage, at least for DP951.
- The circuits (especially important for the small ones or for large single tapes) are surrounded by small alumina pieces, as pictured on Figure 3.8. This is to prevent the pieces from falling down the substrate carrier during the firing; this happened more than once at the beginning, probably due to the combination of combustion gas exiting the tapes (creating an air cushion) and a slightly non-horizontal substrate carrier.

2.2.8 Post-firing operations

Post-firing operations are usually iterations of previous operations but with conditions similar to standard hybrid technology, because the LTCC tape has already shrunk and is very stable upon next re-firings. Screen printing, drying, and re-firing are the typical operations for adding classical pastes such as conductors, resistors and overglazes. The oven used for refiring is a 6-zone belt air furnace, model of 1998 2K6-78C52-6AN, from SierraTherm [59] pictured on Figure 2.9; only the peak firing temperature varies depending on the paste:

- between 500 and 510 °C for overglaze DP QQ550;
- between 580 and 625 °C for overglaze ESL G-481;
- around 850 °C for nearly all other pastes.

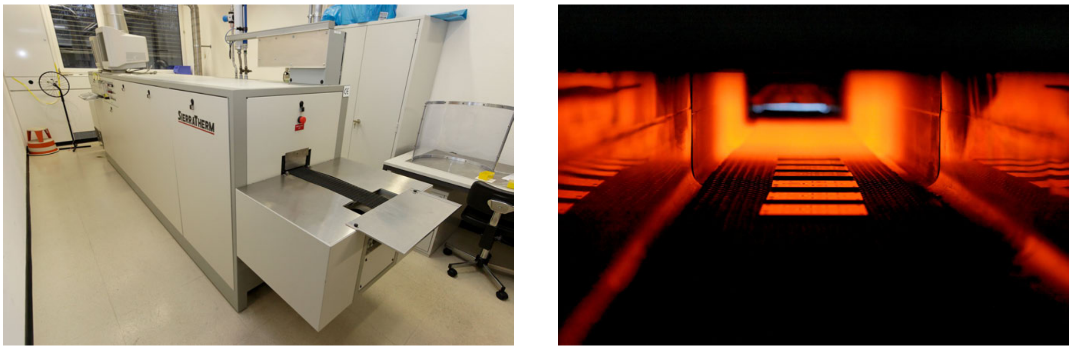

(a) Photo of the exit side of furnace; the black belt leads fired pieces on the metallic receptacle.

(b) Inside of furnace chamber with LTCC circuits leaving the hottest zone (~850 °C). The depicted firing concerns a post-fired Ag:Pd metallization suitable for soldering.

Fig. 2.9: SierraTherm 6-zone belt air furnace used for post-firings and standard hybrid firings.

Soldering

For solder pastes, which can be deposited by syringe dispensing or screen printing with a coarse screen mesh (80 meshes / 100 µm), there is no drying step: to the contrary, the elements to be soldered must be put in place without delay to avoid letting the solder dry too much. In effect, the drying diminishes the retention of tack, which is necessary to "stick" the components to the substrate between mounting and reflow; it can hence degrade the wettabilty upon reflow. The oven used for reflow operations in our lab are of two types:

Classical reflow oven, heating by radiation A standard reflow oven from Essemtec (Figure 2.10), with lamps heating from above. The maximum reachable temperature being below 220 °C, lead-free pastes with a higher melting point such as Sn-Ag-Cu cannot be processed in this oven; we were forced to acquire the next oven upon entry in force of the ROHS (Restriction of Hazardous Substances) directive in 2006.

Fig. 2.10: ESSEMTEC classical reflow oven; heating by radiation.

Controlled atmosphere oven, heating by conduction This oven, model SRO 702 from ATV [58], can reach 450 °C with heating rates of up to 100 K/min. The chamber may be evacuated and/or flushed with nitrogen or forming gas (N_2-H_2 95 %-5 %). The forming gas is used as a reducing agent for high-temperature soldering ($>$ 250 °C), to reduce surface oxides and thus allow soldering without the use of liquid flux. The heating principle is by conduction on an anodized aluminium plate heated by quartz lamps from below.

This oven (Figure 2.11) allows a better control of the process parameters than the classical reflow oven, but its cooling rate is lower. To ensure a void-free solder joint, the degassing of flux and bubbles through a vacuum step is mandatory; a validated firing sequence (see graph in Appendix section A.2 on page 218) is given hereafter:

1. Purge of the chamber with N_2 by succesive vacuum and N_2 injection;
2. Heating ramp at 90 K/min to the first dwell, slightly below the melting point to ensure temperature uniformity in the circuit.
3. Second heating ramp up to 10-20 °C above the melting point, and holding for 30 to 60 s to ensure all solder locations have correctly melted.
4. The vacuum pump valve is opened while N_2 is flowing: the solder begins degassing (it boils clearly), and the heat conduction is maintained as the pressure drops only to a few millibars. The N_2 is then closed: the vacuum (and thus boiling) is maximum, and heat conduction drops to a minimum as the thin layer of nitrogen between the aluminium plate and the LTCC circuit vanishes.
5. Vacuum is stopped, the N_2 valve is reopened and the heating lamps are shut off in order to gently start the cooling, which is then reinforced by injecting additional N_2.

2.2.9 Singulation

We singulate our circuits most of the time after firing by manual breaking along stamp-like pre-cuts (see right Figure 1.6a on page 23); this however yields blunt edges (Figure 5.21).

When precise, nicely cut borders are desired, diamond saw dicing is used. The process is unfortunately very slow (4 to 8 hours per circuit in some cases) and the cutting tools wear

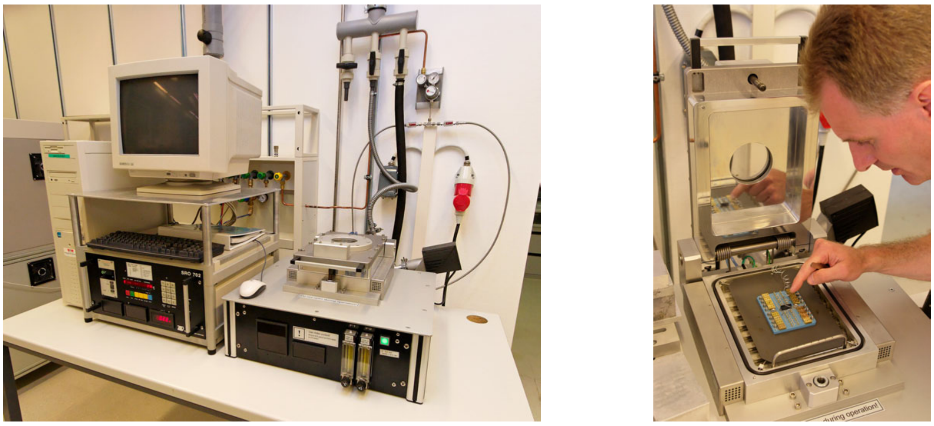

(a) Overview of computer, control unit, heating chamber and gas tubings (nitrogen N_2, Forming gas N_2-H_2, exhausts).

(b) Operator applying control thermocouple on LTCC circuit prior to soldering.

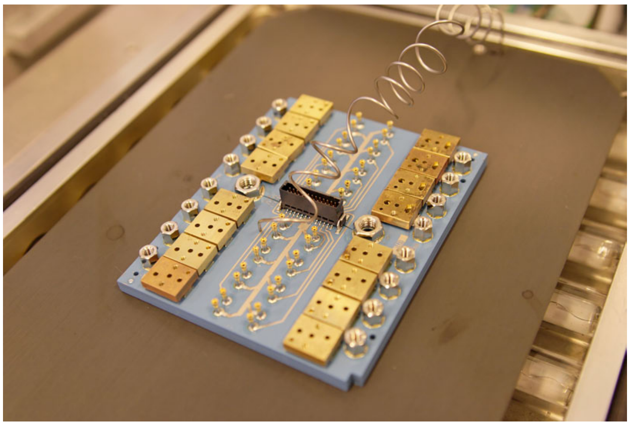

(c) Detail of heating plate and lamps prior to soldering of the biggest LTCC circuit ever produced in our laboratory (depicted unfired on Figure 2.8c): 22 tapes of DP951-254 µm, fired dimensions 93×76×4.6 mm, mass 112 g.

Fig. 2.11: ATV SRO 702 controlled atmosphere oven; heating by conduction.

rapidly, when they do not break in the middle of a cut. The machine is also limited to circuits not higher than 2.5 mm.

We also tested singulation by laser cutting with mitigated results:

- Before firing: the cutting is slow and generates a lot of dust; the efficiency decreases greatly for circuits thicker than 1 mm, for the laser gets out of focus.
- After firing: the process is slow and the laser strongly affects the LTCC surface; this must be reserved to the surgical cutting of fine structures such as cantilevers or sacrificial nipples. The same restriction applies to thick circuits.

2.3 Assembly techniques

Several assembly techniques are available for the assembly of components onto LTCC circuits, or of LTCC circuits onto larger devices.

Soft soldering We successfully tested soft soldering of standard SMD components onto LTCC circuits, but also fluidic fittings such as M3 or M5 nuts in nickeled brass, or brass adapters (see section 5.8). Various solder pastes were used: Sn-Bi (melting point around 140 °C), Sn-Pb (m.p. ~179 °C), and Sn-Ag-Cu (m.p. > 220 °C). The integrated multisensor of section 5.3 shows evidence that it is possible to reliably solder a whole LTCC circuit onto a fluidic PCB.
Müller studied in detail in [60] the soldering of Kovar frames onto LTCC for hermetic ceramic microwave packages for space applications.

Laser soldering A thesis was carried out at the EPFL-LPM by Dr. Frank Seigneur on the hermetic packaging of microsystems; in particular, he studied extensively the soldering of transparent windows by laser [46, 61]. This is the method used for the packaging of a MOEMS, as displayed on Figure 2.1).

Wire bonding Wire bonding is the primary method of making interconnections between an integrated circuit (IC) and a printed circuit board (PCB) during semiconductor device fabrication. Ball bonding usually is restricted to gold and copper wire and usually requires heat. Wedge bonding can use either gold or aluminum wire, with only the gold wire requiring heat. In either type of wire bonding, the wire is attached at both ends using some combination of heat, pressure, and ultrasonic energy to make a weld.
We tested with success ball wire bonding on LTCC for the same project as described above, shown on Figure 2.12.

Gluing Gluing was tested with success with various types of cyanoacrylates and epoxies; please refer to the Master project reports [62, 63] for more information.

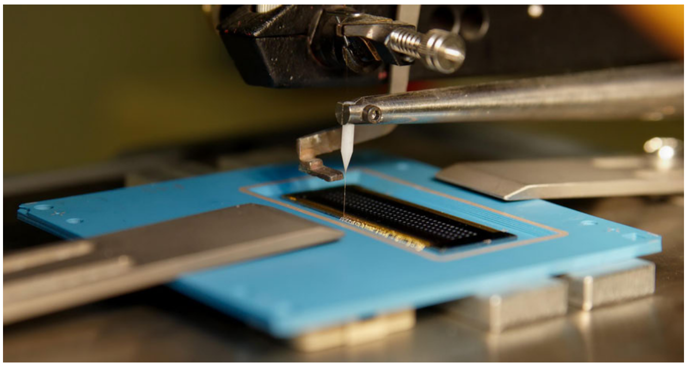

Fig. 2.12: Ball wirebonding of a MOEMS onto an hermetic LTCC substrate.

Polymer fittings Fittings made with tubes wrapped in a modified polymer, indeed Grafted Maleic Anhydride Polyethylene, were tested with success by WILLIGENS for our microreactor (see Figure 5.38 in section 5.5). They survived without problem many hours of operation with NaOH and HCl.

Glass sealing Sealing glass can be used to bond LTCC to ceramic or metals; overglaze pastes can also be used for this operation, which requires a temperature of 500 to 600 °C (see Appendix D).

2.4 Detection of defects

ZERNA, OPPERMANN et al. describe in [64, 65] methods for the observation of defects in fired LTCC circuits, among which ultrasonic and X-ray microscopies. They studied especially the assembly of SMD components on substrates, such as BGA solder joints or glued dices, but did not cover defects of LTCC such as delaminations. They note that no better non-destructive methods are known today.

Ultrasonic echography

This method has a lateral resolution ranging from 70 to 700 µm, depending on the transducer frequency (from 230 to 10 MHz respectively), for a maximum penetration depth of 3 mm. Delaminations and similar defects in LTCC are in the range of 0.5 to 10 µm, and usually not directly under the surface; the method is thus only applicable to global imagery of assemblies, and not suitable to assess the quality of tape bonding.

X-ray CT scanner

X-ray microscopy with CT (computer tomography) scanners has seen increased used these last years in the microelectronics industry. These scanner featured resolutions of 10 to 20 µm some years ago; for instance, we had the opportunity in 2006 to submit a fluidic circuit (one of the kind presented in section 5.8) to PHOENIX¦X-RAY SYSTEMS + SERVICES GMBH in Germany for testing purposes. It was interesting to see the fluidic channels and the conductor tracks in 3D, but unfortunately the delaminations were too small to be seen. The whole scanning process took hours, and the aspect ratio of our fluidic circuits was not optimal for CT scanners: as the source & detector rotate around the sample, the detector can only approach the LTCC surface when it is facing an edge: when scanning a face, the distance is at least equal to the half of the largest circuit dimension; this yields inhomogeneous images. Therefore, the method was not further investigated to detect delaminations; we were forced to continue with the destructive method used so far: SEM (Scanning Electron Microscope) imagery, which requires diamond saw cutting, polishing and flash gold deposition.
Nevertheless, X-ray scanners achieve today resolutions of 1 µm: that revives the interest for LTCC structures.

Analysis of defects in LTCC magnetic sensor with buried coils In a joint effort with our Plasma Physics Research department (EPFL-CRPP) on the magnetic diagnostic set for the European project ITER[11], we developed LTCC magnetic sensors (see Figure 2.13) with up to 10 layers of buried coils (20 turns each). As we suffered from a low fabrication output, we decided to investigate if tracks or vias had been cut at some point in the stack. An X-ray CT scanner[12] for in-vivo observation of rats was just installed at the EPFL-LBO (Laboratory of Biomechanical Orthopedics), so it was a good opportunity to test X-ray microscopy again: this time the tracks to observe were 200 µm wide. We give here a summary of our observations; the complete pictures can be found in my report [66], and more information on the magnetic sensor has been published in collaboration with Testa et al. from the EPFL-CRPP in [67, 68].

The instrument allows scanning objects on 360° with an X-ray source outputting up to 120 kV and 80 µA (max 10 W), with different filters for a better differentiation between object and carrier. We used the Aluminium 1.0 mm filter. The main selectable parameters are: resolution 9, 18 or 35 µm; scanning rotation on 180° or 360°; averaging steps (for noise reduction) between 1 and 10. Of course, they directly influence the scanning duration, generated data size and reconstruction (post-processing) duration. To give an idea, a scan of a single coil (in two steps because of its length) takes 0:33 h at 18 µm, 180° and 2 averaging steps, and generates 4.5 GB of raw data; switching to 9 µm jumps the scanning time to 2 h.
After numerous attempts, we determined that a resolution of 35 µm was not enough for our fine tracks; 18 µm is good, and 9 µm is unnecessarily fine. Rotation on 180° instead of 360° is enough, and more than two averaging steps does not improve the quality.
Furthermore, reconstructing 3D data from the succession of raw 2D scans did not bring additional information worth spending time and resources. The reason lied in the flat shape of our samples: had the LTCC samples been spherical, it would have been much easier for reconstruction. When the scanner source irradiates the LTCC on the edge, almost no X-ray go through the 30 mm of matter and the result is a black image, thus yielding bad results in the reconstructed 3D model.

Figure 2.14 shows the cross section of a sensor with 8 layers and 10 turns; the stacks of vias are well visible, as well as the "ghostly" appearance of tracks in the middle of the piece, due to the X-ray absorption.

Figure 2.15 presents a defective coil with 2 layers and 20 turns. Many pseudo-defects are visible, but a zoom on the region marked by in red unveils the most possible cause of failure: a metallized hair trapped during stacking or screen printing, interrupting a track. Similar observations and other defects were noted on other sensors.

In conclusion, the 3D X-ray scanning helped in determining the possible causes of problems leading to signal interruption in our defective LTCC samples. However, the features of the scanner could not be fully exploited, because of the relatively dense matter of LTCC coils, and because of the flat shape of the samples. The document [66] discusses the possible causes of defects and proposes corrections.

---

[11] International Thermonuclear Experimental Reactor

[12] MicroCT X-ray scanner SkyScan1076.

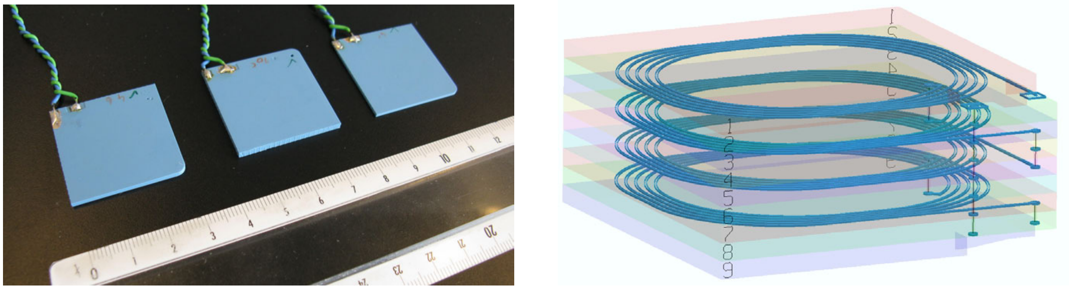

(a) (b)

Fig. 2.13: LTCC magnetic sensors specially designed for the ITER project. *(a)* Three sensors variants, from left to right: 5 turns/4 layers, 20T/10L, 5T/4L. Ruler in cm. *(b)* 3D semi-transparent view of a sensor with 5 turns per layer and 4 layers of coils.

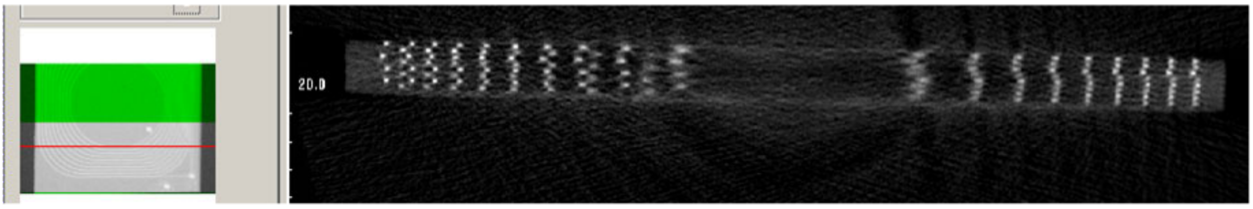

Fig. 2.14: X-ray cross section of a sensor with 8 layers and 10 turns: note the stacks of vias, well visible, and the "ghostly" appearance of tracks in the middle of the piece, due to the X-ray absorption.

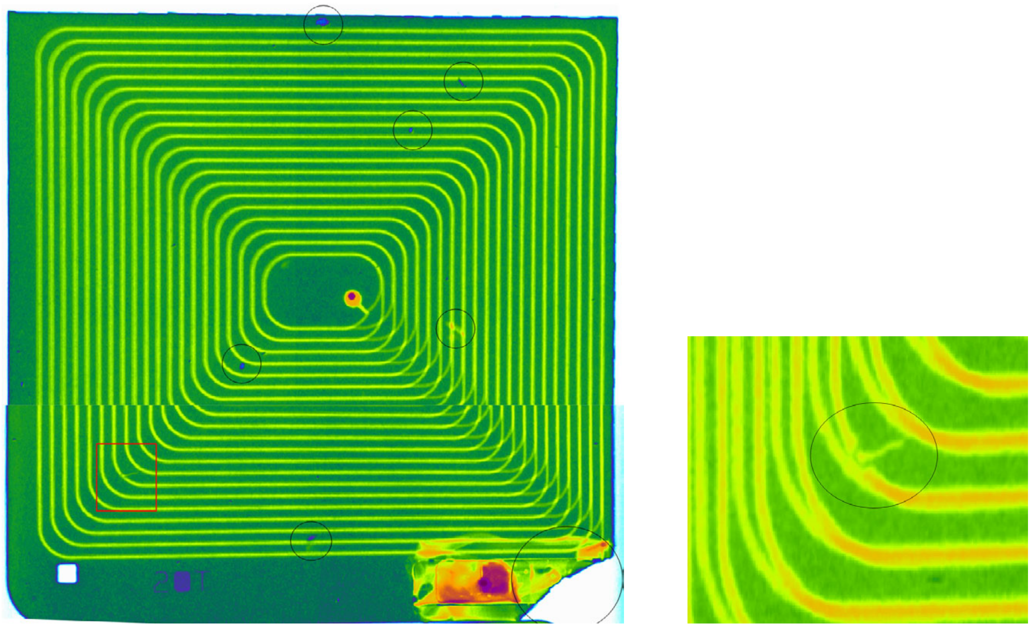

(a) (b)

Fig. 2.15: X-ray scans of defective coil with 2 layers and 20 turns. Many pseudo-defects are visible: blue spots are indeed dead pixels of the scanner detector. The orange stains short-circuiting two tracks represent post-fired paste deposited to connect the two vias stacks; the inner tracks are not affected. The connection pad was broken after determination of open-circuit. *(a)* Reconstructed top view; *(b)* Zoom on red square, unveiling a possible cause of failure: a metallized hair trapped during stacking or screen printing, interrupting a track.

2.5 Conclusion

The manufacturing of microfluidic devices in LTCC is an iterative succession of steps that are, for most of them, already industrialized, and the prototyping fabrication steps differ little fundamentally from those used in mass production. For instance, mechanical punching can be used instead of laser cutting, as it is the case already for vias of the electronics industry. Nonetheless, the fabrication of channels, cavities and membranes obey rules that are dependent on the circuit geometry, on the type of LTCC tape, on the amount and type of inks screen printed, on the manufacturing equipment (see chapter 3); it is for the moment not yet possible to predict with accuracy how to laminate a circuit in order to ensure the right output geometry and a correct bonding of tapes at the same time – at least not before a few iterations of testing. Consequently, thorough engineering and mastering of the know-how of the whole manufacturing process is still necessary to produce efficient LTCC circuits, to the contrary of older techniques such as classical thick-films on alumina substrates or PCBs in FR-4. For instance, with the increasing complexity of our circuits it was necessary to design and build specific equipment such as a semi-automated optical alignment machine and a heated lamination fixture.

The facilities necessary for their fabrication require a moderate investment, in regard to the silicon MEMS industry (see below); a semi-clean room is sufficient for LTCC. For instance, the cost to get similar equipment as in our laboratory is in the order of 1 million € (without taking into account the building and infrastructures such as oven exhaust ventilation); for mass production, this would maybe be two to three times higher.

The succession of operations allows for easy visual or optical inspections at all intermediate steps, at least before the firing; it yields the possibility to remove individual defective tapes, thus avoiding unnecessary costs. After firing, except for cases involving strong circuit deformations, other inspection methods such as X-ray scans or ultrasonic echographies are necessary to assess the quality of internal ceramic structures or of dense solder joints such as BGA arrays.
In contrast, the manufacturing of silicon devices requires much more expensive facilities and a more strict clean room environment. It is also much more difficult to inspect wafers at intermediate steps; many MEMS are tested only at final steps of fabrication, thus yielding proportionally more defective devices.

Chapter 3

Lamination: issues and solutions

All things are difficult before they
are easy.

Thomas Fuller, 1608-1661

LTCC has attracted considerable interest as a material for sensors and microfluidic circuits, for which dimensional accuracy and physical integrity of cavities are essential. Unfortunately, classical lamination techniques employed for electronics only prevent the manufacturing of closed cavities. This chapter describes standard issues (section 3.1), as well as the techniques and equipment developed during this thesis to circumvent this problem (section 3.3); for instance, a pseudo-isostatic lamination technique with the use of a constrained rubber coupled to partial sub-laminations.

Another important issue is the irregular shrinkage behavior of LTCC tapes, which must hence be taken into account when designing devices. Nevertheless, the shrinkage observed in practice can be different than that given by the manufacturers; we have thus analyzed[1] *and modeled with Design of Experiments (DoE) the shrinkage of* DuPont 951AX *LTCC foils (section 3.2). Unlike most past studies [37–39, 70], which concentrated on firing conditions or paste compositions, only the influence of the most obvious lamination parameters is characterized here. A linear model is proposed and the relative importance of the parameters discussed. The most important (lamination pressure and temperature) play a non-negligible role (up to 1 % of linear dimension) on shrinkage for a given firing profile. As expected, the more pre-densification the LTCC receives during lamination, the less it shrinks during firing.*

Other innovative lamination techniques are then discussed (section 3.4), such as Cold Low Pressure Lamination (CLPL) with adhesives, Cold Chemical Lamination (CCL) with solvents, or lamination with sacrificial inserts.

Key words: Partial and pseudo-isostatic laminations, Shrinkage modeling, Unconstrained sintering, Design of Experiments.

---

[1] *Adapted from the paper [69] presented at the* 4th *European Microelectronics and Packaging Symposium - IMAPS 2006, Terme Čatež (Slovenia):* Y. Fournier, L.S. Bieri, T. Maeder, *and* P. Ryser, Influence of lamination parameters on LTCC shrinkage under unconstrained sintering, *pp. 165-170 of Proceedings*

3.1 Introduction

Lamination and sintering are two critical operations impossible to circumvent when manufacturing LTCC. They are usually performed in two separate, sequential steps: the lamination and the air firing (called unconstrained sintering), but techniques and equipment exist for carrying out the two steps during the same operation, called constrained sintering. Hintz et al. made a classification of these methods, depicted on Figure 3.1.

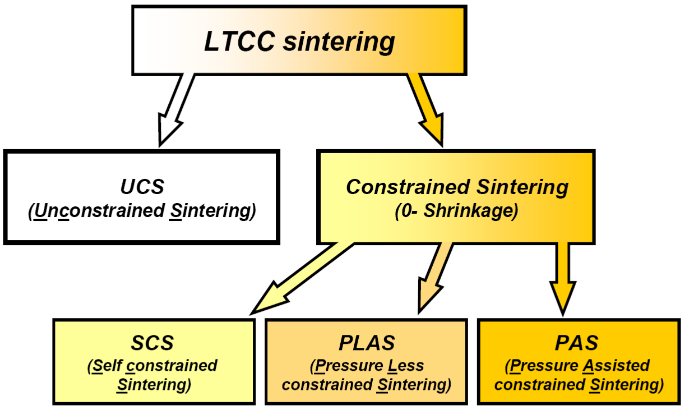

Fig. 3.1: Chart of the different sintering methods; adapted from Hintz & Thust [71].

Free sintering is the mostly used method for the production of LTCC substrates, also called the "Unconstrained Sintering" (UCS) method. The most prominent disadvantage of this inexpensive LTCC sintering process is the shrinkage of tiles in all directions with relative high tolerances of up to ±0.5 %. The typically achieved ±0.2 % for X- and Y-direction still causes problems for device mounting and requires post processing to provide acceptable catch pad tolerance. Additionally, module warping caused by TCE mismatch of conductor inks leads to more problems at assembly; the relative high lamination pressure often generates deformation of cavities and holes. On the opposite, constrained sintering essentially almost eliminates the X/Y-shrinkage, and shifts all the shrinkage in the Z- direction. Three constrained sintering processes are known [71]:

- the Self Constrained Sintering (SCS);
- the Pressure Less Assisted constrained Sintering (PLAS);
- the Pressure Assisted constrained Sintering (PAS).

Besides the costs of additional release tapes and their removal after sintering (for PLAS and PAS), the installation of a special hot pressure-sintering furnace has to be considered. Table 3.1 lists the advantages (+) and disadvantages (-) and some technical characteristics of all methods but the SCS. The SCS profile is very similar to the one of UCS, except for the shrinkage which is close to the one of PLAS/PAS (given at 0.20 % ± 0.04 % in X-Y and from 32 % to 44 % in Z for HL2000 [15]), and for the lamination pressure which is half of UCS with 1500 psi.

The main disadvantage of the PLAS/PAS, regarding the application of LTCC to microfluidics, is the impossibility to produce unfilled cavities and fine structures: they would get irremediably

Table 3.1: Advantages and disadvantages of different LTCC lamination and sintering processes: UCS (Unconstrained sintering), Pressure-Assisted constrained Sintering (PAS) and Pressure-Less Assisted constrained Sintering (PLAS); table compiled by M. Hintz & H. Thust from TU Ilmenau in 2002 [72]. Note that the SCS (Self-Constrained Sintering) was not available at the time.

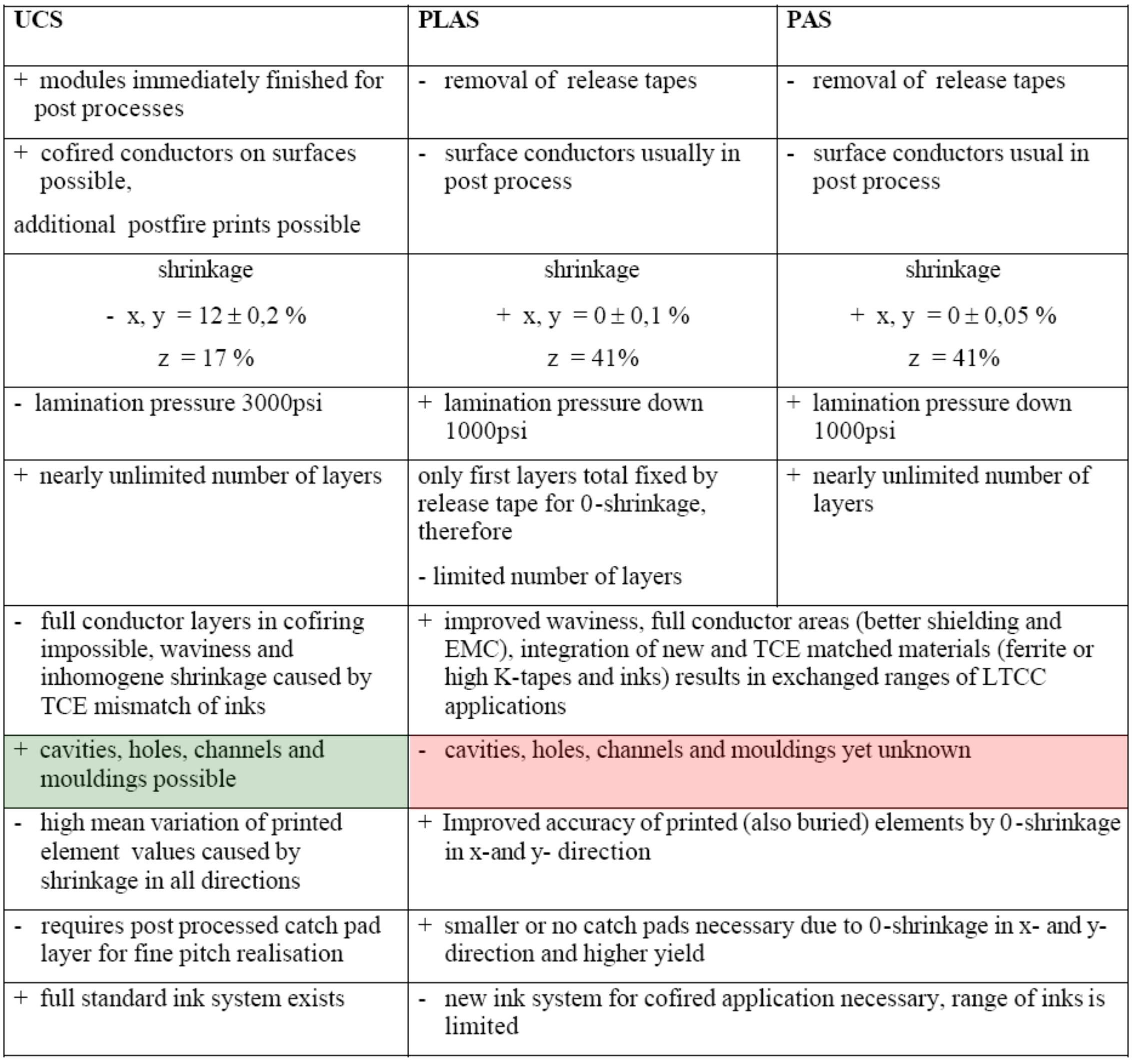

UCS	PLAS	PAS
+ modules immediately finished for post processes	- removal of release tapes	- removal of release tapes
+ cofired conductors on surfaces possible, additional postfire prints possible	- surface conductors usually in post process	- surface conductors usual in post process
shrinkage - x, y = 12 ± 0,2 % z = 17 %	shrinkage + x, y = 0 ± 0,1 % z = 41%	shrinkage + x, y = 0 ± 0,05 % z = 41%
- lamination pressure 3000psi	+ lamination pressure down 1000psi	+ lamination pressure down 1000psi
+ nearly unlimited number of layers	only first layers total fixed by release tape for 0-shrinkage, therefore - limited number of layers	+ nearly unlimited number of layers
- full conductor layers in cofiring impossible, waviness and inhomogene shrinkage caused by TCE mismatch of inks	+ improved waviness, full conductor areas (better shielding and EMC), integration of new and TCE matched materials (ferrite or high K-tapes and inks) results in exchanged ranges of LTCC applications	
+ cavities, holes, channels and mouldings possible	- cavities, holes, channels and mouldings yet unknown	
- high mean variation of printed element values caused by shrinkage in all directions	+ Improved accuracy of printed (also buried) elements by 0-shrinkage in x-and y- direction	
- requires post processed catch pad layer for fine pitch realisation	+ smaller or no catch pads necessary due to 0-shrinkage in x- and y-direction and higher yield	
+ full standard ink system exists	- new ink system for cofired application necessary, range of inks is limited	

crushed (see Figure 1.8 on page 24). From an industrial point of view, it is also not favorable, because the green laminates have to be stacked together with sacrificial tapes and porous plates placed in a unixaxial ram; special, expensive sintering equipment is necessary. Thus, **the topics covered in this thesis encompass only unconstrained sintering and self-constrained sintering (i.e. Heraeus HeraLock) processed with unixaxial lamination.**

Occuring at the beginning of the unconstrained sintering process, the thermo-compressive lamination is typically performed at temperatures between 25 and 80 °C and attached pressures of 8 to 150 MPa hold for 3 to 10 min. These parameters have to be optimized depending on the binder system used. At contact points between two green tapes, the polymer chains of each tape diffuse into each other (Figure 3.2b). The occurring mass flow moves and rearranges

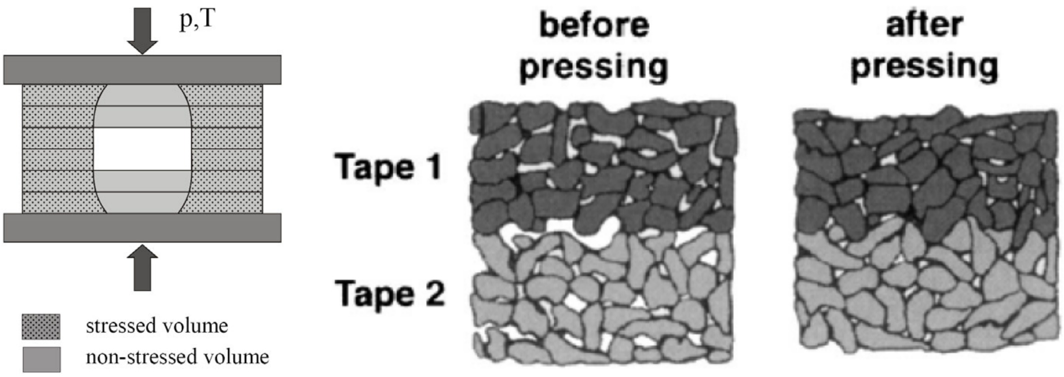

(a) Source:ROOSEN [73]. **(b)** Source:PIWONSKI [74].

Fig. 3.2: Schematic representations of effects occuring during lamination with thermo-compression. *(a)* Inhomogeneous pressure distribution during uniaxial thermo-compression of a 6-layered LTCC structure with a central buried cavity. *(b)* Cross-section representating grains of LTCC tapes interpenetrating upon lamination (HELLEBRAND's model).

the particles in the interface of the two adjacent green tapes. The interpenetration of the particles in both non-fired tapes and the adhesion of the binders of both tapes allows to achieve a defect-free junction between the tapes after sintering (when done properly), in which the former interface cannot be detected anymore. Compared with the green tapes density, the density of the laminate is increased by thermo-compression [73].

Manufacturing issues in microfluidics and with sensors

LTCC technology, originally intended for high-density, high-frequency and automotive circuits, is attracting more and more interest in other applications such as sensor technology and microfluidics. Unfortunately these new applications come up against new problems; while dimensional accuracy was not an issue for early low-integrated purely electronic circuits, it may be critical for the latest high-density and fine pitch circuits. Similarly, sensors and microfluidic circuits that directly use LTCC require accurate control of their absolute dimensions for proper functioning. The main issues of LTCC free-sintering are discussed next.

First, for all LTCC applications manufactured with UCS or SCS, the main issue is the shrinkage upon sintering: in X-Y (planar) axis, it ranges from 0.2 % to 0.5 % for near “zero-shrinkage” tapes, and from 10 % to 15 % for "standard" tapes. However, the effects of deviating from the standard parameters during lamination are not formally known; the LTCC tape suppliers provide little information about this. For instance, a different shrinkage than the values provided in datasheets is often encountered (typically 13.0 % instead of 12.5 % [1, 75]), despite carefully following the manufacturing guidelines.
Beside, it would also be interesting to know the effect of lamination duration on shrinkage and on quality of tape interpenetration; most suppliers advise a lamination cycle of 10 minutes, and shortening this process could be beneficial for mass production.

(a) SEM fluidic circuit cross-section along a channel (reconstructed from five images). The circuit was laminated 10 min at 70 °C - 200 bar and does not show delaminations at this location, despite the presence of a crossing of channels.

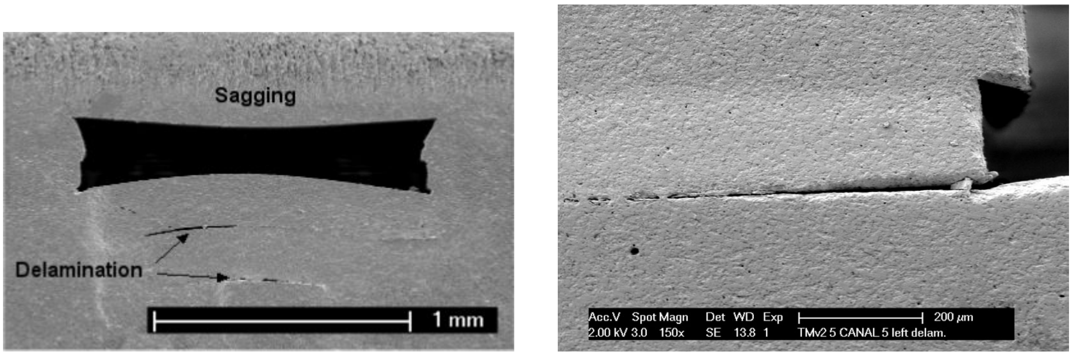

(b) SEM cross section of a $1{\times}0.42$ mm, 2-layer channel showing sagging and delaminations, despite being from the same circuit as (*a*).

(c) SEM picture showing a delamination between LTCC layers in a cavity corner. The lamination was 160 bar for 10 min at 25 °C.

Fig. 3.3: Examples of DP951 LTCC cavities, sometimes suffering from defects issued from poor laminations. Sagging is due to lamination or glass softening during LTCC sintering; delaminations are due to poorly transmitted lamination pressure. From a common work with Dr. Hansu Birol.

Second, all circuits involving empty cavities face a real dilemma: the sagging of the walls (bridge effect) and delaminations between layers. As can be seen on Figure 3.3b channels get crushed during lamination (even with a vertical uniaxial press) because there is nothing to sustain the forces acting on the walls (Figure 3.2a), and the recommended temperature (70 °C) softens the LTCC. Moreover, the lower stresses around cavities result in poor lamination, local variations of shrinkage and delaminations in the adjacent layers as well as in the corners of cavities (Figure 3.3c).

The crushing of channels suggests reducing the lamination pressure, which we tried by pressing at 20 bar instead of 206; this resulted in very poor tape bonding, i.e. strong delaminations, showed on Figure 3.4.

Thus, choosing the right parameters for processing microfluidic circuits and predicting their final dimensions with good accuracy is difficult, and it is critical to take into account the impact of shrinkage variations on design considerations.

In section 3.2 we study the influence on shrinkage of the pre-firing parameters, i.e. most obviously the lamination: its temperature, duration, pressure, as well as the number of LTCC layers. For this purpose, experiments on test samples are conducted using Design of Experiments (DoE) with a minimized number of runs, in order to directly obtain an evaluation of the importance of all parameters, their mutual interactions, as well as the quality of measurements.

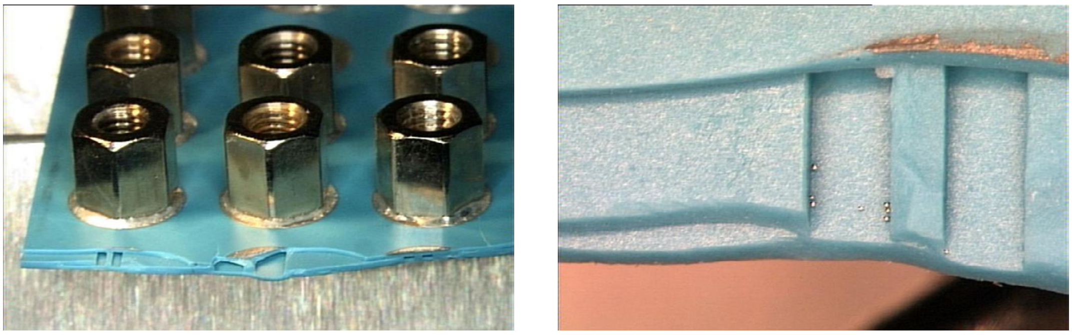

(a) Large view with soldered M3 nuts as fittings. Channels widths/spacings are from left to right: 0.5/0.3 mm, 1.5/0.7 mm, 0.5/0.4 mm.

(b) Close-up view of the left pair of 0.5/0.3 mm channels.

Fig. 3.4: Early test of LTCC fluidic circuit made of three DP951 tapes laminated at 70 °C but at reduced pressure (20 bar instead of 206) to avoid the crushing of channels. Pairs of channels were tested with various channel and interstice widths. This example perfectly depicts delaminations between tapes due to a poor lamination.

The first set of experiments shows obviously that some parameters can be neglected, and we consequently propose a simplified linear model.

The section 3.3 is dedicated to the lamination technique we developed, involving pseudo-isostatic laminations with the help of a constrained rubber and multiple-steps sub-laminations. We pass in review innovative lamination techniques in section 3.4, along with the problem of cavity integrity.

3.2 Influence of lamination parameters on firing shrinkage

3.2.1 Introduction: issues and state of the art

The reasons that motivated this study were exposed in the chapter's introduction; we begin therefore directly with the core of the problem.
At the time of the experiments, we were using DuPont GreenTape™ 951AX LTCC 6"×6" 254 µm-thick foils to manufacture 50×50 mm fluidic circuits assembled from up to 22 layers, and containing channels up to 3 mm wide, without co-firing screen printed films. The shrinkage of the tape is given by the manufacturer according to Table 3.2. Upon delivery of an LTCC lot, its X-Y shrinkage is certified to 0.1 %, for example at 12.5 %; from batch to batch the shrinkage can vary from 12.4 to 13.0 %. For coarse fluidic applications this is acceptable, but for circuits with fine screen printing or sensitive mechanical structures this is problematic (for instance the LTCC version of the MilliNewton microforce sensor developed at EPFL-LPM, described in Appendix section B.3), so circuit raw dimensions must be adapted frequently.

Table 3.2: Shrinkage of DuPont GreenTape™ 951 LTCC tape system as given by the manufacturer for various sintering methods. [3, 9]

Direction of shrinkage / Shrinkage performance	Free-sintered [%]	Pressure Less Assisted Sintering (PLAS) [%]	Pressure Assisted Sintering (PAS) [%]
X - Y	12.7 ± 0.3	0.20 ± 0.05	< 0.05 ± 0.02
Z	15.0 ± 0.5	40.0 ± 0.5	40.0 ± 0.5

Our setup and process used for this study are described later (see section 3.2.2). The main manufacturing problems we are facing are the following:

1) When following the manufacturers processing guidelines for lamination (70 °C – 200 bar – 10 min), the shrinkage is different from predicted and presents up to 3 % of anisotropy. We observe shrinkage greater than 13 %, instead of less than 13 %; however we slightly deviated from guidelines by using a uniaxial lamination press instead of an isostatic one. As a reminder, shrinkage for standard commercial tapes (under unconstrained sintering and not "zero-shrinkage") is in the range from 9.3 % to 15.3 % in X-Y with variations of up to ± 0.3 %, and in Z (along the lamination axis) from 10.5 % to 24 % with variations up to ± 1.5 % (from datasheets [9, 10, 12, 13]).
2) For unfilled channels with a height/width ratio lower than 1, those more than 1 mm wide get irremediably crushed with the same set of lamination parameters. The top and bottom layer are either touching each other, or suffer from tearing. Narrower channels are usually not subject to sagging, but can still suffer from delaminations (see section 1.2.1 and section 3.1 above).
3) Apart from using sacrificial carbon inserts, the crushing of channels suggests reducing lamination, i.e. pressure, temperature, and/or duration. This is what was tried, yielding

> unsuccessful results as depicted with a crossing of fluidic channels on 1.9b on page 25, showing evidence of sagging and delamination after firing. The problem was not resolved but just shifted: the cavities presented less sagging but more delaminations, as well as an even greater shrinkage (up to 14 %). This latter point is not surprising; our former experiments proved that such reduced lamination conditions lead to less pre-densification of LTCC, resulting in a correspondingly higher firing shrinkage [76, 77].

State of the art The shrinkage behavior of ceramics depends on many parameters, including particle size, shape distribution, as well as size and mass of the package laminate. Most of the past studies are oriented on paste composition, thick-film compatibility, firing profiles, constrained sintering or visco-elastic modelling focussing on the molecular level. A good example is the thesis of A. MOHANRAM [39], who also covered the defects during co-firing in [38], and studied the camber deformation with his colleague LEE [37]. V. SUNAPPAN et al. addressed the quality of tape in function of the setter type, of the placement in furnace, and of the profile and furnace used [70].

We learned, after carrying out our experiences, that LAUTZENHISER et al. had worked in 2002 with the HERAEUS HL2000 tape to design a microwave module; they studied in [78] the shrinkage of HL2000, in particular the influence of various firing profile variations, as well as the effect of casting variations of the tape made with different organic binder contents and casting parameters. Their measurements showed little variation of fired dimensions; the observed X-Y shrinkage was between 0.10 % and 0.18 %. They also tested the effect of time at peak during the firing on Z-shrinkage; they concluded that there is no significant change between a firing peak of 30 min and 3 h: the found a Z-shrinkage of ~29.3 % from loose sheets, and of ~22.6 % from laminate.
Therefore, they concluded that the way the green HL2000 tape is handled *may be* more important than firing variations in their effect on fired dimensions; by handling they meant manipulations during lamination, and manipulations between the lamination and firing steps. Surprisingly, they did not vary the lamination parameters accordingly, but used for all their tests a standard isostatic lamination with 15 min at 75 °C at a pressure of 4500 psi (310 bar). They tested however the effect of single or double lamination on the fired thickness and found a slight increase of Z-shrinkage for the double lamination; again, it led to the conclusion that green-handling variations *may be* a more important source of variations on HERALOCK shrinkage than small firing profile changes. This chapter will prove that this hypothesis is right, for the tape DUPONT 951 at least.

Nevertheless, little if any studies discuss the effects of lamination from a circuit manufacturer's point-of-view. Indeed, from our knowledge from literature, most experiments are run with the lamination parameters recommended by the tape supplier, or with slightly diverging "home recipes", but there are no indications about the consequences of significantly deviating from these recommendations. The suppliers themselves encourage the user to experiment at their own risk [3].
Therefore, before investigating new techniques to improve the integrity of the channels, it was favored to determine the influence of lamination parameters on X-Y shrinkage. Shrinkage in Z is

less problematic, because it does not cause misalignment issues upon further processing such as screen printing. The Z-shrinkage will occur whatever the type of LTCC used ("zero-shrinkage" or not), because a loss of volume is inevitable with the matter densification upon sintering; in the case of "zero-shrinkage" tapes, all the volume loss is encountered in Z.

Parameters influencing LTCC shrinkage The parameters that can possibly influence the LTCC shrinkage are numerous. The Table 3.3 is a probably non-exhaustive list, in the manufacturing chronological order. In this list, some items are difficult to vary (furnace type or lamination press per example), or would require very long processing time between two iterations (e.g. length of firing profile). Thus, only the most obvious parameters involved at the lamination stage were retained for this study, for uniaxial lamination only.

Table 3.3: List of parameters and operations that can possibly influence the LTCC shrinkage, with subsequent explanation.

Parameter / Operation	Reasons
Aaging of LTCC sheets	age, atmosphere humidity and temperature
Method of removing Mylar® backing tape	by hand or with a vacuum setter; before of after blanking.
Preconditioning	before or after blanking; temperature, duration.
Cutting method	by laser or punching.
Type of protective tape (for lamination)	MYLAR, TEDLAR, polyethylene; new or reused sheets, etc.
Layer stacking method	alternated or not *[a]; numbers of layers.
Lamination technique	type of press (uniaxial or isostatic); pressure + its rate of (de)application; temperature; duration.
Interval of time between operations	between lasering and screen printing; between screen printing and firing, etc.
Firing method	belt or box furnace; type of setter *[b]; profile for burnout/sintering (ramps, peak T); position in the furnace.
Type and flow of firing gas	air, N_2, H_2, formingas N_2-H_2, etc.

*[a] LTCC sheets have an orientation because they are tape cast.

*[b] SUNAPPAN et al. have observed dependence for peak temperature [70].

3.2.2 Experimental

Design of Experiments plan Due to the long firing profile (eight hours) and the number of parameters involved, it was decided to concentrate on only four parameters for the DoE plan:

- the number of LTCC layers (n)
- the lamination pressure (p)
- the lamination temperature (T)
- the lamination duration (t)

It was also decided to measure the samples dimensions at three distinct states:

state A:	lasered green tape
state B:	laminated stack
state C:	fired circuit

to observe two effects:

1) expansion AB, due to lamination,
2) shrinkage BC, due to firing.

The measurement at state A is a necessary step, because the laser was found to exhibit some variability in the cutting dimensions. The Design of Experiments plan chosen is a Linear Full Factorial Design with central point. However quadratic terms cannot be added, for the factorial design does not allow it. The central point will just allow verifying the "lack of fit". The orthogonality does not need to be verified because this plan is orthogonal by definition [79].

Discussion of the selected parameters The parameters of the experiment were varied according to Table 3.4. The reasons are as follows:

Table 3.4: Experiment parameters of first DoE plan, with the achievable precision of our system.

Parameter	T	t	p	n
Position	[°C]	[min]	[bar]	[layer]
min	25 ± 1	05 ± 0.1	080 ± 7	3
central	40 ± 1	15 ± 0.1	190 ± 7	6
max	55 ± 1	25 ± 0.1	300 ± 7	9
DUPONT recommendations	70	10	206	≥ 8

- *Temperature (T):* too low (ambient) and the layers interpenetrate badly. Too high (> 70 °C) and the LTCC softens so much that it creeps, and the channels get crushed during lamination. Note that our max T reaches 55 °C only, instead of the recommended 70°C. This is because we first tried at 70 °C and 300 bar, and our test samples were so damaged that they were barely measurable.

- *Duration (t):* time is potentially less important than the other parameters. DuPont recommends 10 min, but we found advices from 5 to 15 min in the literature without any explanation. We decided to start the timer once the pressure reached the desired value (p hold for the first 2 min, see on page 71).
- *Pressure (p):* from our first experiences, this parameter seemed to play the most important role on shrinkage and lamination quality. Too low ($<$ 80 bar) results in bad lamination. Too high ($>$ 200-300 bar) and channels get crushed. If p is applied unequally, a trapezoidal deformation or general curvature of the fired samples is generated, despite no visible indices after lamination. Therefore a high-quality alignment fixture is paramount.
- *Number of layers (n):* due to the inhomogeneity of LTCC sheets (in thickness with the grain orientations, and in X-Y with the tape casting [5,36,80]), the number of layers could influence the shrinkage by friction against the alumina substrate during firing. Circuits with cavities require at least three layers (unless using sacrificial pastes); below that number, warpage is prone to occur (see an example of single layers fired on Figure 4.27a on page 138)
  A meaningful parameter could be the height/width ratio of the stack; it was not tested in this study, however.

Based on previous observations and expected materials behavior, the parameter dependencies are expected to be:

1) For lateral expansion by lamination: increase with T, p, t;
2) For shrinkage by firing: decrease with increasing T, p, t;
3) The effects for n are less straightforward: although we can reasonably expect a greater lateral expansion upon lamination for a bigger n, it is not clear what repercussions this can have on shrinkage.

LTCC test samples Test samples of 72×10 mm have been designed to allow four optical distance measurements per piece: two for length (X1, X2) and two for width (Y1, Y2), thanks to Ø 2.5 mm circular through holes (Figure 3.5). It is done with the help of a vision system by means of a blob detection algorithm that allows precise determination of the center of each hole.

In raw dimensions, X1 = X2 = 50 mm and Y1 = Y2 = 5 mm. The Y measurements are for anisotropy determination; priority is given to X. To minimize distortions, the pin alignment holes are placed at the extremities of the samples. To ensure that channels would not be crushed by the test conditions, two simple 1.5 mm-wide channels are placed between the measurement and the alignment holes; it is then easy to verify their integrity already after the lamination (Figure 3.6).

Two samples are prepared for each set of parameters, one on each array of pins. This is due to our alignment fixture, which requires an even number of samples to balance the load upon pressing (Figure 3.7). Up to five pairs of samples can be laminated simultaneously, thanks to intermediate metal plates.

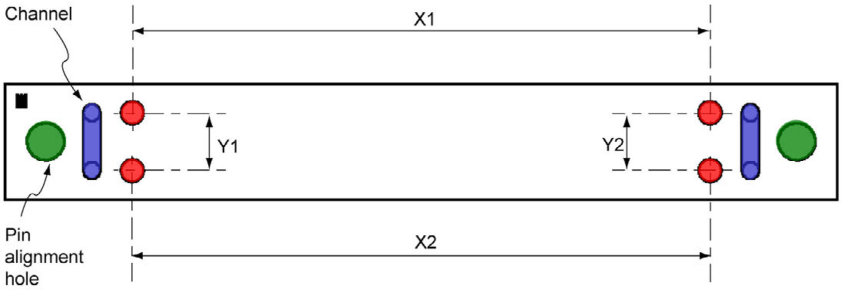

Fig. 3.5: "X-ray" sketch of LTCC test samples, showing from outside to inside: the two pin alignment holes (green), the two channels (blue), and the two pairs of optical measurement holes (red). The latter allow two length measurements (X1, X2) and two width measurements (Y1, Y2).

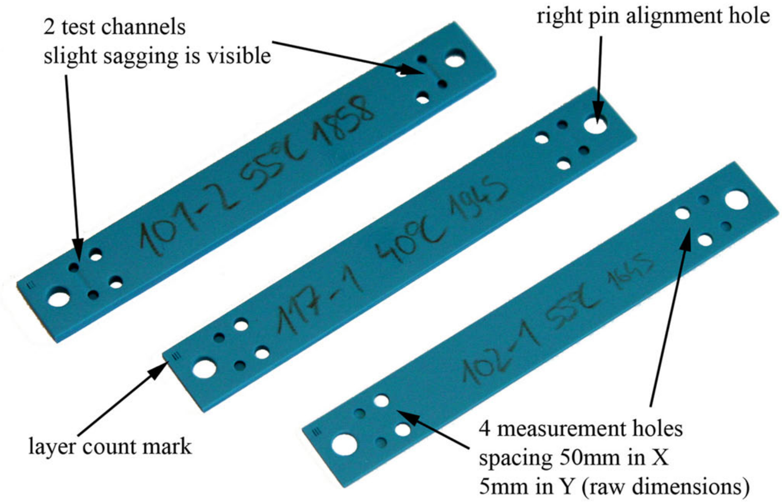

Fig. 3.6: LTCC test samples used for DoE experiments. From left to right: samples made of 9, 6 and 3 stacked layers.

Experimental setup A package of LTCC tape DuPont 951AX containing one hundred 6"×6" sheets has been used for the experiments; its shrinkage was rated at 12.7 %. The pack had been opened for 3 months and was kept in ambient conditions (23-25 °C, 40-50 % RH) in its plastic bag. All experiments were carried out during the same day (from preconditioning to firing).

Each sheet had its Mylar backing tape removed, and was immediately put on alumina substrates in a drying oven at 120 °C for 30 min for preconditioning. Then, the structuration was done by laser (see subsection 2.2.3) with the sheet orientation mark pointing down. The dust generated by the cutting was removed by air blowing and a soft brush. For the state A, top layers were measured with the camera of the laser system. The vision system has a measurement repeatability of $\sigma_{\text{measure}} = 3\,\mu\text{m}$, i.e. 0.006 % over 50 mm (calculated from initial tests and the system resolution).

The home-made alignment fixture (Figure 3.7) was pre-heated in a drying oven set at 25 °C, 42 °C or 58 °C to reach respectively 25 °C, 40 °C or 55 °C on the LTCC, accounting for a slight cooling during manual stacking and lamination.

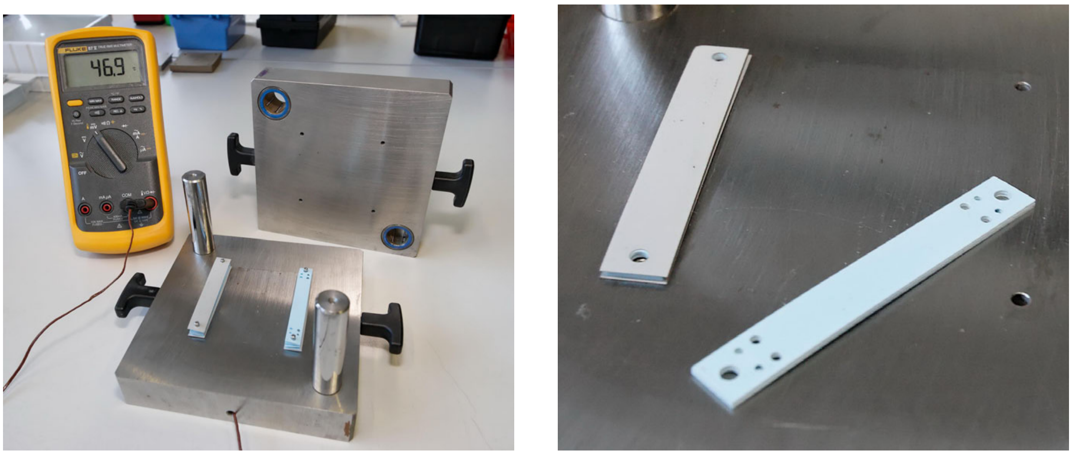

(a) Collated and stacked on pins of alignment fixture.

(b) Just after lamination (*left*) and removal of release tape (*right*).

Fig. 3.7: Test samples before and after lamination. The release tape used was DP TEDLAR (visible on the left sample).

Collating and stacking occurred as fast as possible to limit cooling. The release tape used to prevent LTCC from sticking to metal plates was DUPONT TEDLAR[2] . The same TEDLAR layers were reused many times, as they did not suffer much from deformations.
To allow LTCC reaching the desired temperature T, the whole stacked alignment fixture was placed again in the pre-heated drying oven for 5 to 10 min. After removal of the mobile pins, it was placed in a uniaxial press on 3 mm-thick rubber discs acting as buffers against pressure imbalances and heat losses[3]. The pressure was gradually increased until reaching the nominal value ± 7 bar, then the timer was started and the pressure manually maintained for 2 min before releasing the press lever. Due to the creep response of rubber, the pressure then slightly decreased (Figure 2.6b on page 39).

After lamination, the TEDLAR release tape was promptly removed and the second measurement was carried out. Test samples were subsequently laid on 0.6 mm-thick, 96 % alumina substrates, and loosely surrounded by small alumina pieces (explanation in subsection 2.2.7) before being fired at the end of the day. The repartition of the samples on the substrates was pseudo-random (vertically spread over the substrate carrier floors, and alternated left-right).

The firing occurred in an IR lamp heated quartz tube furnace (PEO-601 from ATV TECH [58], see subsection 2.2.7) under an air flow of 400 l/h during all the process. The firing steps are described in Appendix Table A.1 on page 217.
Note the slight discrepancies between the oven and the actual LTCC temperature. We ran numerous tests with three thermocouples to verify the inside temperature, one on each substrate, in contact with a sample. We observed up to 7 K difference between the outer and inner floors during the burnout dwell, and only 3 K during the sintering (Figure 3.8).

---

[2] This sheet material has since been removed from the DUPONT assortment.

[3] We have since given up using rubber discs, as the pressure loss was too important.

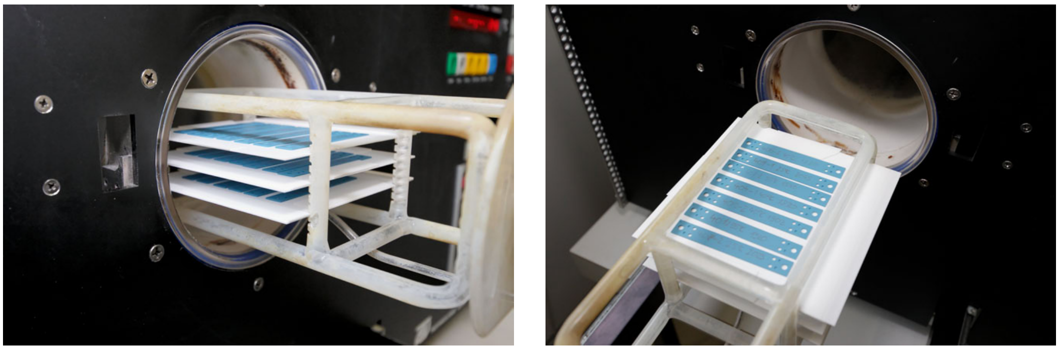

Fig. 3.8: Fired test samples loaded on three alumina setters exiting the ATV PEO 601 lamp furnace [58] on the quartz substrate carrier. Note the hardly-visible small alumina blocks (broken substrates indeed) surrounding the LTCC samples to avoid them falling down during the burnout.

After sintering, the oven was naturally cooled until reaching 400 °C, whereupon an additional air flow of 2000 l/h accelerated cooling down; at this stage the cooling rate should play no role in the quality of the samples. The samples were then optically measured one last time.

Hypotheses The following assumptions have been made:

- LTCC aging plays no role on shrinkage.
- LTCC sheets were of identical properties.
- Reusing TEDLAR release tapes plays no role.
- Firing profile is slow and long enough to ensure good organics burnout and sintering homogeneity for all the samples.
- Slight differences of temperature inside the oven are negligible, and firing runs are always similar.

Initial experiments with DuPont 951 Initially it was planned to analyze the two sub-models ABx and BCx (i.e. for lamination and for firing regarding the length), but the lamination process (ABx) yielded so variable results that no relevant information could be extracted. This can be explained because the increase of length on ABx is of the order of 0.10 % to 0.20 % – that is, between 0.04 and 0.10 mm, which is low in regard to the measurement system. On the contrary, the BCx sub-model is nearly identical to the ACx model, so we concentrated on the latter. The measurements results have been processed using complete model matrices with interactions.

Figure 3.9 presents the parameters influence in regard to the constant part (which is 13.48 % of shrinkage, i.e. 6.74 mm); the lamination parameters have relatively little influence. p is the most important one (-3.2 %), followed by T (-1.8 %), and the interaction $T \cdot p$ (-0.7 %). Surprisingly t and n do not play a big role, with -0.2 % each (the interaction $T \cdot t$ is even greater with +0.3 %). All other interactions are smaller.

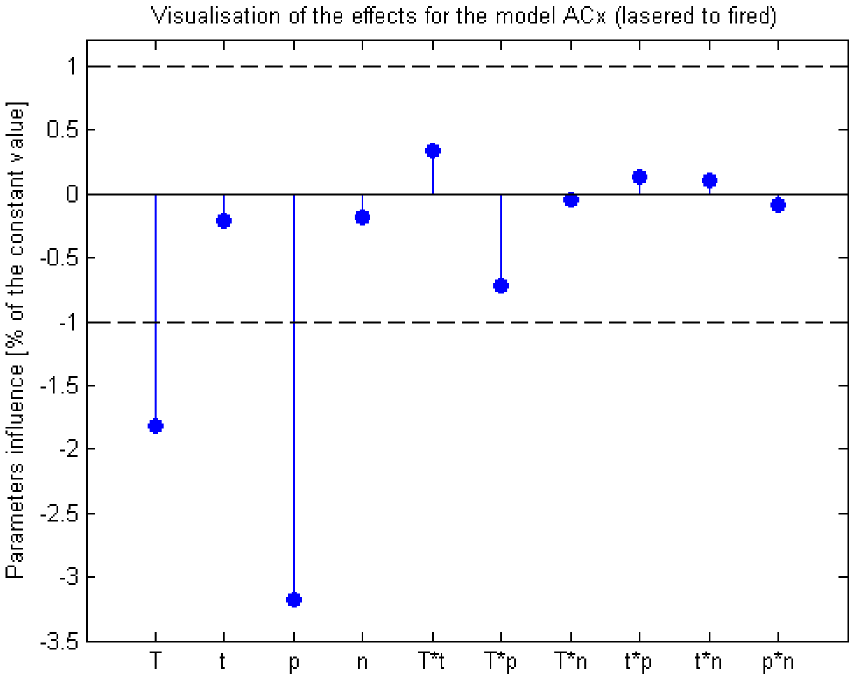

Fig. 3.9: Influence of the different parameters and their interactions for the shrinkage model ACx (from lasered state A to fired state C, in length), relatively to the constant shrinkage part of 13.48 %: lamination temperature T, pressure p, duration t, and number of tape layers of the stack n.

It is interesting to note that the influence of n on the whole shrinkage ACx only comes from expansion by lamination (ABx), because n has an effect of nearly zero on the firing (BCx, not displayed). This can be explained because the lamination is prone to be influenced by the height-width ratio, where the height is directly linked to n: the friction of layers in contact with the lamination fixture must be taken into account, with regard to the deformation of the stack during the lamination. By analogy with modeling clay that would spread upon hard pressing, LTCC presents a similar visco-plastic behavior to a lower extent. To the contrary, layers see almost no friction during sintering (the molecules of the green ceramic have interpenetrated and densified during the lamination).

These initial results confirm our expectations: more pre-densification provided during lamination lessens the shrinkage upon firing. They also suggest that simplifications in the ACx model can be done. Thus, we decided to retain only the effects greater than the dashed lines (threshold at 1 %) on Figure 3.9, i.e. T and p, and to redo the experiments but with more points.

Second experiments with DuPont 951 To test the reproducibility of the initial experiments, a second run was conducted four months later with a second package of LTCC (shrinkage rated at 12.5 %, package opened four months before). This time only T and p were varied, with $t\,[\text{min}] = 5$, n [layer] $= 3$ and more intermediate points: $T\,[°\text{C}] = [25; 40; 55]$, $p\,[\text{bar}] = [80;\ 190;\ 300]$. In DoE this is a composite design with $N = 2$.

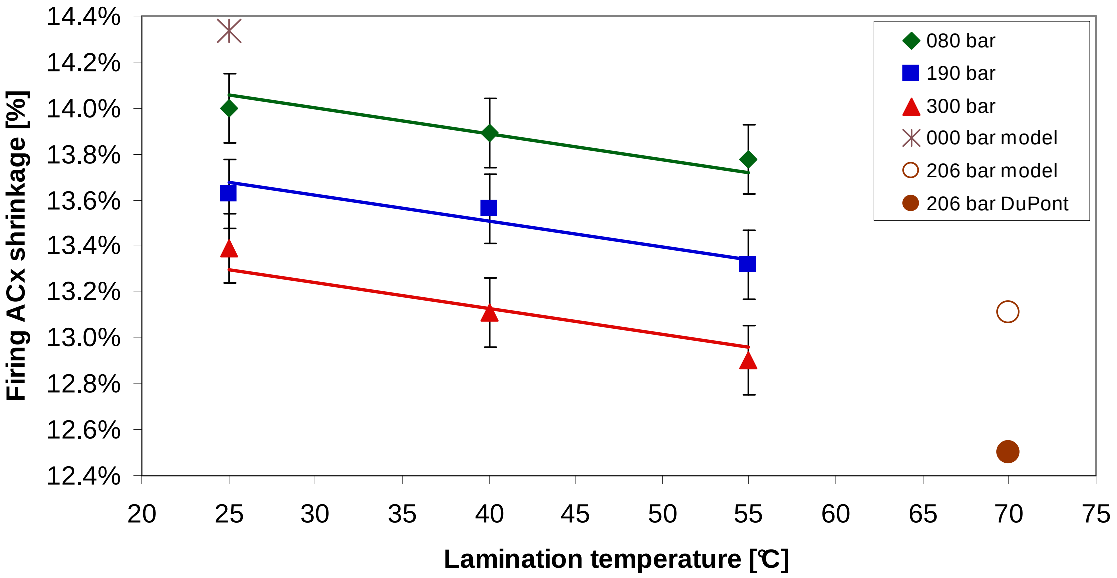

Fig. 3.10: Experiments of ACx shrinkage (from lasered to fired state) in function of lamination temperature T and pressure p, as well as model (continuous lines). Theoretical values calculated from our model are also given for 25 °C-0 bar and 70 °C-206 bar to compare with the value given by DuPont. Measurements error bars represent $1\,\sigma$.

The results are presented in Figure 3.10. This time, the pressure p has an influence that amounts to -$2.38\,\%$ of the mean shrinkage (central point), and -$1.3\,\%$ for T. The shrinkage is presented as a function of lamination temperature for three lamination pressures. Up to three experiments were conducted for each point of the graph, and the measurements error bars displayed represent 1 σ (standard deviation) of the process variability ($0.15\,\%$).

It is worth taking into consideration that the variability between two experiments of same parameters is two to five times larger than the variability between the two samples of a single experiment (fired at the same time). This is because the former contains the operator variability, as well as the LTCC inhomogeneities if the samples belonged to different sheets of tape.

3.2.3 Model of shrinkage for DuPont 951

Despite some overlapping of the error bars on Figure 3.10, it is clear that there is a distinct dependency of the shrinkage on temperature T and pressure p. It ranges from 13 % to 14 %, which is not negligible. A linear regression has been performed; our model of shrinkage is displayed on Figure 3.10 by three lines, one for each lamination pressure. After de-normalization and rearrangement, its equation is Equation 3.1, for the temperature rise ΔT relative to ambient conditions (298 K) and the pressure p:

$$f_{AC_x}\,[\%] = f_{AC_0} \cdot \left(1 - \frac{\Delta T}{\Delta T^*} - \frac{p}{p^*}\right) \quad \text{where} \quad \begin{array}{ll} f_{AC_0} & = 14.34\,\% \\ \Delta T^* & = 1'270\,\mathrm{K} \\ p^* & = 4'160\,\mathrm{bar} \end{array} \tag{3.1}$$

The linear model fits the points of the graph well. We have also accomplished an ANOVA analysis to assert the pertinence of our model: its Fisher P-factor[4] amounts to $3.0 \cdot 10^{-12}$, and its coefficient of determination $R^2 = 0.999985$. However, the R^2 is of little significance in our case, because our constant value is much larger than the half-effects and biases the result.
The parameters have also been scrutinized individually: the P-factor for $T = 5.8 \cdot 10^{-4}$, and for p it is $6.1 \cdot 10^{-6}$, which is very good. We also tried a model that includes the interaction $T \cdot p$ (as it was the third most important on Figure 3.9), but the P-factor of $T \cdot p$ was 0.63, which indicates a large uncertainty on this parameter.

It is interesting to compare our model with the data from DuPont for our lot of LTCC (12.5 % of shrinkage): with $T = 70$ °C and $p = 206$ bar we find a shrinkage of 13.11 % instead of 12.5 % as specified (also shown on Figure 3.10). Whereas this seems to confirm that the shrinkage is larger than proclaimed, we must be careful in applying our model beyond our maximum temperature, as the binder properties become nonlinear; our initial tests at 70 °C/300 bar completely crushed the sample. DuPont recommends $t = 10$ min while we used 5 min, but as we have seen it plays no appreciable role on shrinkage.

Regarding the X-Y anisotropy, Figure 3.11 regroups all second experiments. As a general rule a linear tendency is observed, albeit with a rather high scatter in the low shrinkage area. Especially, the points for 55 °C/300 bar present more dispersion than the others. Nevertheless, a linear regression has been drawn (with intercept set at zero), of which the equation is: $S_Y \approx 0.95 \cdot S_X$, with a sigma of 1.55 %.
However the coefficient of determination R^2 for this model is not satisfactory (0.78), due to the significant measurement dispersion in Y and likely onset of nonlinear behavior at high pressure and temperature (corresponding to the low-shrinkage range). More careful experiments should be done to refine it, notably by measuring the Y-shrinkage over the same distance as in X.

3.2.4 Conclusion of this study

The goal of this study was to analyze and model with *Design of Experiments* the shrinkage of DuPont GreenTape™ 951AX LTCC foils in function of lamination parameters. All the steps of our process are presented in detail. Taking into account that the usual LTCC shrinkage repeatability is around 0.2 – 0.3 %, our process seems to be under control with a shrinkage variability of 0.15 % (1 σ).
Our main suspicion is confirmed: globally, the lamination plays a non-negligible role on the shrinkage of LTCC under unconstrained sintering. In spite of this, we conclude from our experiments that the number of LTCC layers (n) and the duration of lamination (t) can be neglected to predict the shrinkage; only lamination pressure (p) and temperature (T) are retained for our linear model. Its Fischer P-factor amounts to $3.0 \cdot 10^{-12}$, which proves that the model fits the reality very well. As expected, the more pre-densification the LTCC undergoes during lamination, the less it shrinks during firing. It is also worth pointing out that the influence of lamination is of much higher importance (up to 2 %) than the intrinsic variations from batches to batches (± 0.3 %).

---

[4] The Fisher P-factor should ideally tend towards zero.

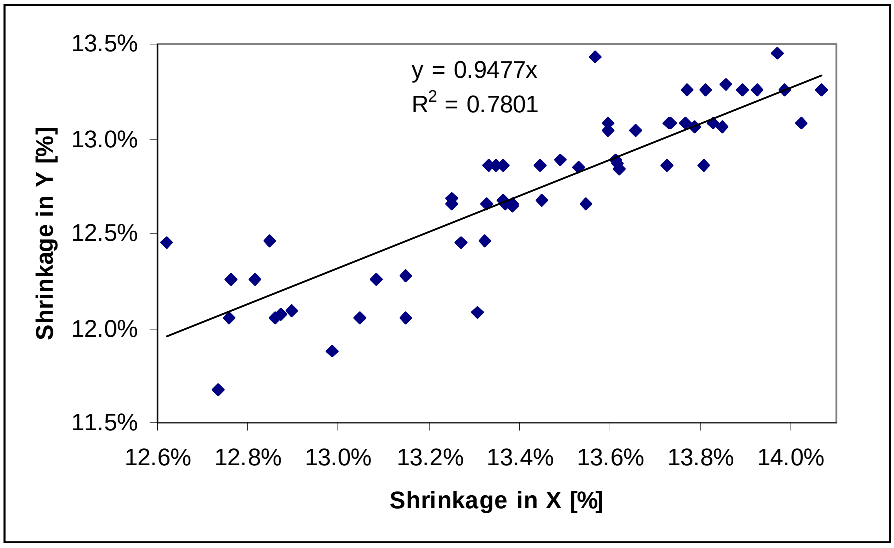

Fig. 3.11: Measurements of AC shrinkage (from lasered state to fired state) in X and Y to estimate anisotropy. A linear tendency is observed.

For the LTCC batch tested, in relation of the mean shrinkage, we found that p has a relative influence of -2.38 %, and -1.3 % for T; this translates into a change of -0.38 % and -0.17 % of the absolute shrinkage values. Our model of shrinkage applied to manufacturer's conditions is larger than what DuPont claims (13.11 % instead of 12.5 %), and more coherent with values encountered in literature [1, 75]. This result confirms our expectations, but we must stay careful: above 55 °C the properties of the tape organic binder are expected to become nonlinear; furthermore, the second set of experiments was run with a lamination duration t of 5 min, while DuPont recommends 10 min.

Such a model could be useful to define a standard of shrinkage prediction that manufacturers should provide with each batch delivered. It allows laminating under a broader set of conditions, instead of the one recommended by the manufacturer. Unfortunately, this proposal received no support from manufacturers[5], who, for obscure reasons, are reluctant to establishing standards for LTCC.

In practice, when tight tolerances are required on final dimensions, it is necessary to run a simplified version of the DoE test presented to qualify the LTCC batch in use. For co-firing operations, it is decisive to bring subtle variations to the shrinkage model used for the laser cutting (which is then different than the one employed for screen mask generation), to take into account the optical aberrations of the laser collimation. However, for projects including more co-firing than post-firing and where dimensions are of low importance, variations between batches play a secondary role and the same set of shrinkage values can be used between batches.

Ways to explore Although the shrinkage is now better understood, integrity of cavities is still unsatisfying and the whole process is still long. Therefore we want to investigate new

---

[5] I personally proposed to open the discussion during a special session of the IMAPS 2008 CICMT in Munich, without success.

methods of lamination, as covered next in section 3.3 and in section 3.4.
Regarding the optimization of the firing profile to obtain shorter times and a better circuit integrity, it should be done only at the industrialization stage of a product development, as the mass/volume of a circuit and the loading of the oven are closely related; it is worth reminding however that for thick circuits, the longest part of the firing profile is the organics burnout.

This study can be completed by carrying out more experiments and integrating the following parameters in the DoE plan:

- To test the effect on Z-shrinkage, Z measurements can easily be introduced [78].
- The number of tapes n, although not having much effect on shrinkage, greatly influences the integrity of structures with cavities depending on their height/width ratio.
- To test the influence of firing conditions, sintering with or without top cover plates (porous or not) and/or setter tapes can be introduced (see section 6.2.5 on page 215).
- Last but not least, the shrinkage studied in this chapter applies only to LTCC that is not screen printed: the influence of thick-film pastes is not negligible, and can sometimes surpass the influence of pressure and temperature, as discussed on page 165. To test the effect of screen-printed inks, the type of paste and percent of surface covered for specific test patterns would be interesting parameters, but complicates the model because it depends on interactions between materials. A. ROOSEN et. al 2004 have studied the shrinkage as a function of temperature of blank LTCC tapes and of pure metal paste films with an optical dilatometer in [81]; they showed that metal pastes, even those recommended for the investigated LTCC tape, are not very well adapted. This led to sintering homogeneities that resulted in warpage, camber or even cracking.

3.3 Developed lamination technique

From our early experiments it was clear that a solution had to be sought for the lamination of microfluidic circuits, to ensure good tapes bonding while reducing the lamination pressure and temperature. After numerous attempts involving several compliant materials and multiple lamination steps, we ended with an elegant solution applicable to both open and closed structures: the use of constrained rubber to emulate a pseudo-isostatic lamination, coupled with partial sub-laminations of sensitive structures. The two elements of the method are decribed next; they involve using our experimental alignment and heating fixture described in subsection 2.2.5 on page 38.
Nonetheless, we still use standard uniaxial lamination between metal plates for circuits that do not contain cavities or that are tolerant regarding the quality of lamination.

3.3.1 Pseudo-isostatic lamination with rubber

This element of the solution is issued from a common work with my colleagues Dr. Frank Seigneur and my supervisor Dr. Thomas Maeder. The underlying idea behind the use of rubber onto a flat metal plate is to allow the lamination of open structures that are flat on one side (in contact with the metal), but with relief on the other (in contact with the rubber), which is possible thanks to the visco-elastic deformation of rubber. An example is shown on Figure 3.12; the project is described in detail by Seigneur in [45]. By extension, this method is applicable to closed structures by repeating partial pseudo-isostatic laminations onto sub-parts of the structures, which, taken individually, form open structures with semi-relief (see later in subsection 3.3.2).

Our early first tests were made using an unconstrained 12 mm-thick, 81×86 mm square rubber plate (Figure 3.15), positioned over the LTCC stack between the metal plates of the lamination press. A Tedlar or Mylar sheet protected the LTCC from the rubber and the press (Figure 3.14c). The result was not reproducible; deformation of the laminated LTCC stack occurred. When the rubber was compressed, its size in X and Y increased to an important

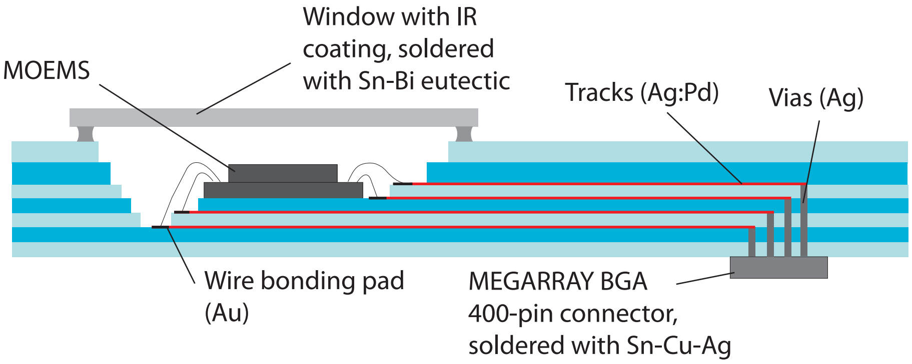

Fig. 3.12: Schematic cross-section of an LTCC circuit we produced with Dr. Frank Seigneur for the hermetic packaging of a MOEMS chip; the disposition in “stairs” of the wire bonding pads required the use of our constrained rubber lamination fixture. Adapted from [45, 46].

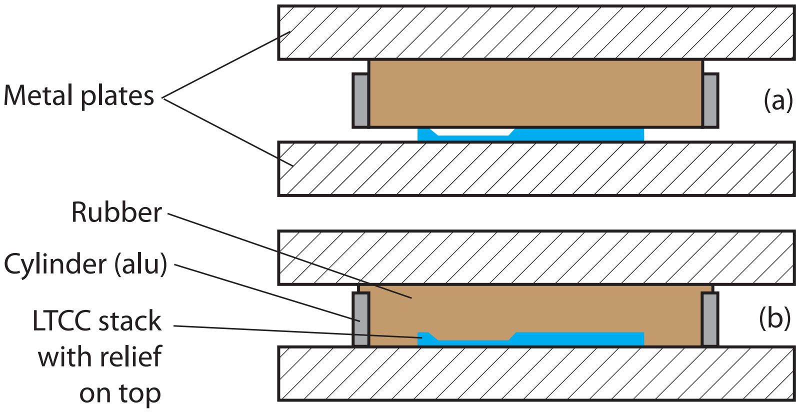

Fig. 3.13: Schematic cross-section of our constrained rubber lamination fixture. (*a*) Just before pressing; (*b*) Stack under pressure, rubber deformed on top only. Adapted from [45, 46].

extent (~ 20 %), applying forces that deformed the LTCC stack.
To prevent this, a thicker rubber plate (17 mm thick) was employed and constrained within a circular aluminum tube (see Figure 3.13 and Figure 3.14a) of 120 mm of internal diameter. The height of the rubber plate was slightly greater than the tube (2 to 3 mm), allowing the rubber to be compressed by the lamination press (Figure 3.14b); in this way, the deformation in X-Y was minimal. For projects similar to the MOEMS packaging presented above, and to further improve the homogeneity of the pressure, a small rubber piece was cut to the size of the cavity and inserted before lamination. When the depth of the cavity is too high, we switch to multiple sub-laminations: first the tapes that form the "height" of the cavity with metal, then the cavity bottom with rubber, and finally the assembly of both with metal.

Choice of release tape As stated above, we initially tested MYLAR and TEDLAR as release tapes. These sheets turned out to be too rigid and were corrugated after lamination, diminishing the effect of rubber (thus lowering lamination) in bottom of cavities, as can be seen on Figure 3.15. The advantage of MYLAR is its almost free availability, as it is the backing tape of DUPONT 951 tapes, but it is also electrostatic and thus attracts a lot of dust and hairs. For the TEDLAR, which we got in sample sheets from DUPONT but whose production was later stopped, its advantages were its strong mechanical stability, its absence of electrostaticity and its easiness to cut by laser.
We then got the idea to use a solid gel between the rubber and the LTCC, in order to apply pressure more uniformly, but this was not eventually tested for practical reasons. Instead we employed commonly available food wrapping low-density polyethylene (LDPE, see Figure 3.14a), which is around 30 to 40 µm thick and presents very advantageous plastic properties, at the expense of an important electrostaticity that translates into difficult manipulations. The PE is of course single-use too, but its cost is negligible and we obtained very satisfying results with it.

On the rate of lamination pressure application removal To our knowledge, the rate at which the lamination pressure is applied, and even more important, at which it is removed, is a topic that is never discussed in literature, but of paramount importance. This parameter has a

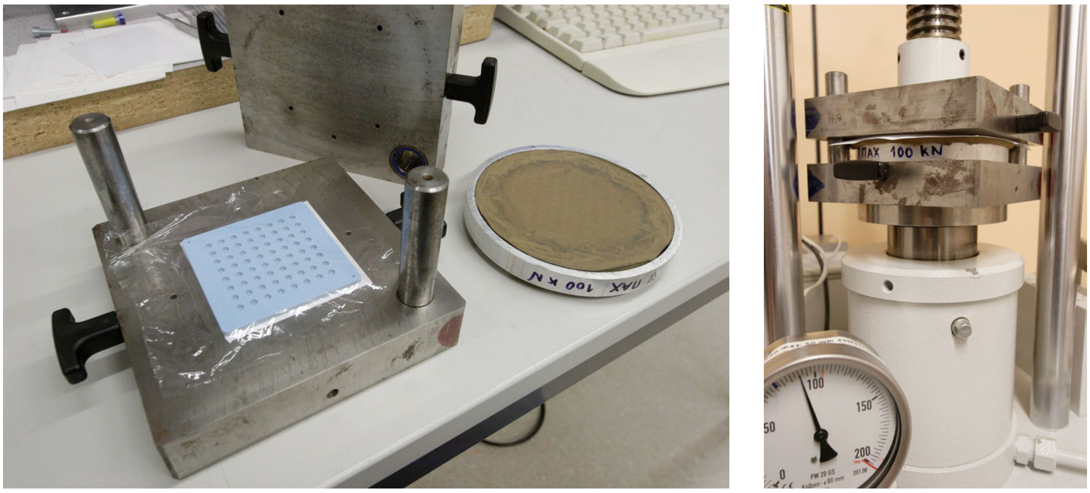

(a) Lamination stack just before assembly and pressing (upper MYLAR sheet protecting the rubber not shown, see (b)).

(b) Stack mounted on unixaxial press, reading 90 kN.

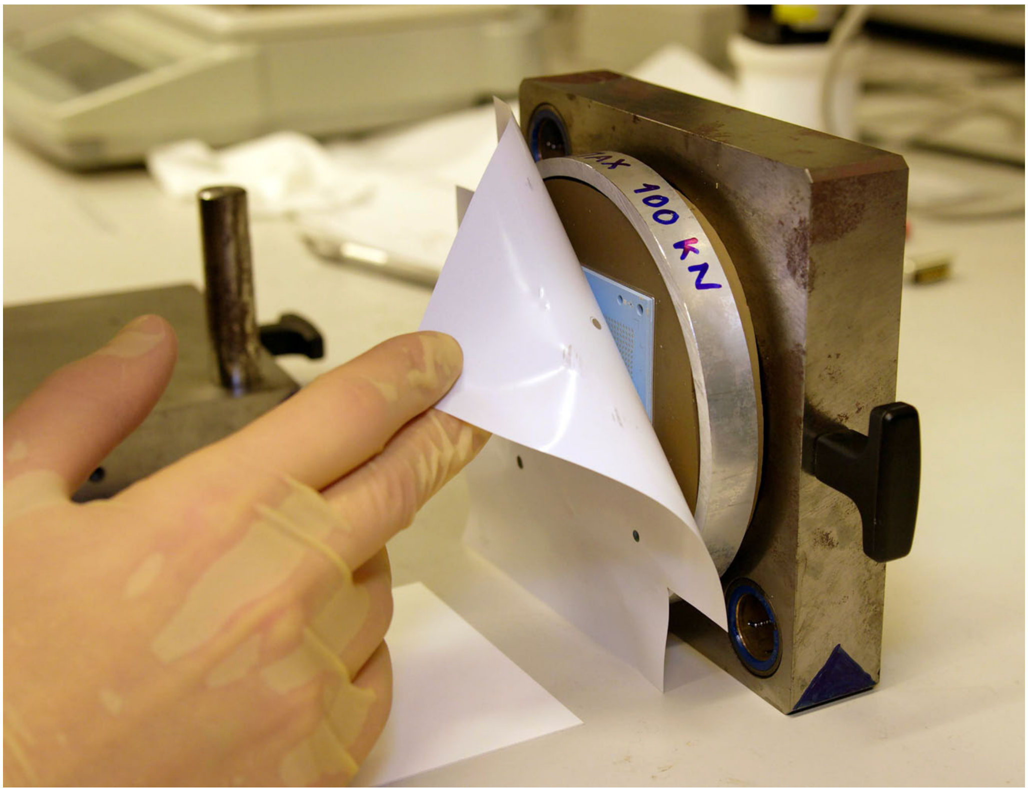

(c) Removal of the sheet protecting the LTCC just after lamination. Note the early configuration; we have later introduced the use of a PE (instead of MYLAR) protective sheet between the LTCC circuit and the rubber, to prevent parasitic sticking (see (a)).

Fig. 3.14: Experimental lamination fixture with constrained rubber.

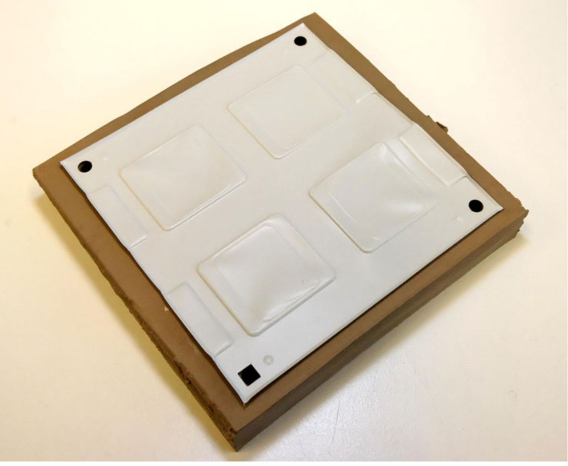

Fig. 3.15: Early test of pseudo-isostatic lamination with square rubber and TEDLAR as release tape, which could only be used once due to corrugation and provoked a diminished lamination of lower cavities because of its too high thickness and rigidity.

low influence on the structural integrity following lamination for standard isostatic lamination (because the displacement is low and homogeneous), and often goes unnoticed for unaxial lamination of structures with low aspect ratio. For pseudo-isostatic lamination, however, a fast decrease of pressure at the end of the lamination inevitably leads to warping and creasing, due to the non-linear visco-elastic behavior of rubber. Indeed, when we manually decrease the hydraulic pressure of our uniaxial press from 100 kN (corresponding to 90 bar for our 120 mm-diameter rubber), the displacement of rubber is maximum in the last 10 kN, and we decrease the rate from max 5 kN/s to ~1 kN/s in order to avoid friction between LTCC and rubber. To assess this effect, we tried once opening the pressure release screw violently: the LTCC structure was unusable.

The same reflection can be made for the application of pressure: we have always observed the greatest care in our work. Nevertheless this is less problematic in our case, as our press is actuated by hand with a lever, which drastically limits the rate of application but forces a stair-like curve. There is also the question of maintaining the pressure throughout the duration or not: in effect, the creep with rubber is much higher than for metal unixaxial lamination, and the pressure decreases up to 10-15 % after 10 min. In the early times of our testing we maintained the pressure at least 2 min, but it increased the variability of the process, so we stopped doing so.

Possible improvement In its current form, the contrained rubber solution is insatisfactory. Due to the relatively low wall thickness of our aluminium cylinder constraining the rubber, we decided by prudence to limit the press force usage to 100 kN, which translates into 90 bar (9 MPa) for a 120 mm diameter surface. Altough not always a problem (see subsection 3.3.3 below), it is sometimes desirable to laminate at higher pressure (i.e. 206 bar) with rubber. A simple solution would be to machine a stronger constraining frame in steel – the same wall thickness would be sufficient, for a two to three times higher strength. The height of rubber extending above the frame can also be slightly reduced, as the upper part of the rubber suffers

from strong deformations and wears rapidly – 1 mm should be appropriate.
Another improvement would be the use of a slim-like gel, which would remove the need to place custom inserts in deep or high aspect ratio cavities.

3.3.2 Partial sub-laminations

To compensate for the necessary reduction of lamination pressure and temperature to create fragile structures, we have developed a lamination technique alternating between a pseudo-isostatic lamination with the help of a constrained rubber, coupled to a classical uniaxial lamination between two metal plates. It requires the introduction of partial laminations that preserve crushable sub-parts from the pseudo-isostatic lamination while ensuring a good tape bonding at locations where pressure would have been zero with a pure uniaxial lamination. This multiple-step lamination process is then always ended by a final metal lamination to join sub-parts together.
One drawback of the method is the partial loss of the "drum-skin effect", which is very advantageous to manufacture membranes with standard shrinking LTCC due to the near absence of lamination of the suspended portion. For instance the DP951 benefits from this effect, while it is almost inexistent for HERALOCK. When a membrane must be fabricated by pseudo-isostatic sub-lamination, care must be taken not to laminate too much to ensure a minimum of tensile stress upon firing (we have demonstrated in section 3.2 that the higher the lamination, the lower the shrinkage).

Procedure For a complex structure such as the multisensor involving sandwiched suspended bridges in a buried channel (described in section 5.3, with tapes listed in section 5.3.3 on page 161), the procedure is listed next. The lamination parameters are grouped at the end: pressure in [bar], temperature in [°C] and duration in [min].

1) Rubber lamination of tapes T4, T5 and T5b forming the bottom lid, with MYLAR and PE sheets (90-46-10);
2) Metal lamination of tapes T3 and T3b forming the central sandwich bridges with thermistors (100-40-10);
3) Rubber lamination of tapes T2 and T1 (inverted of course, so that the top of T1 is on the metal side), forming the top lid, and to ensure a good lamination of the ground plane located on the bottom of tape 1 (90-46-10);
4) Metal lamination of the whole stack with MYLAR sheets only (80-25-10).

Unfortunately, we never eventually conducted SEM analyses to assess the increased quality of tape bonding of the method, but we are intimately convinced of its virtues through other observations, among which the excellent resistance to overpressure of our pressure sensor prototypes (see in Appendix section C.1 on page 234).

The procedure requires a careful mastering of the processing conditions, as the deviation of lamination pressure between the sub-parts causes stresses later upon firing due to differences in shrinkage. This might sound naive, but the operator's training is of outmost importance, and from my experience the technological know-how is often underestimated and neglected by more "academic" scientists. This might also be the reason why other research groups gave up employing this method. In effect, although we got this idea without prior knowledge of their work, we later learned of failed attempts and abandonment of this method from discussions with teams of the UNIVERSITY OF OULU (Finland) and of Germany, principally because of the difficulty to apply the same pressure to the different sub-parts, which led to cracks upon firing. There are only few publications that relate this method: a journal article from THELEMANN, THUST and HINTZ in 2002 [82], a patent from PLESKACH in 2003 [83], and the recent research from MALECHA, JURKÓW and GOLONKA from Poland [84, 85] (see section 3.4).

Manipulation trick In some special cases, a soft sub-lamination is performed only to allow two tapes to be manipulated together. For instance, when laser cutting or screen printing must be done by alignment in transparence through thin tapes, a quick lamination at 20 bar, at ambient temperature and for 2 to 3 min is sufficient. This is for example necessary to structure large holes in thin tapes that are screen printed with large surface of ink, potentially sticking to the screen mesh after passage of the squeegee: it is preferable to first screen print the tape, and then to laser cut the large holes, so that the tape is not weakened beforehand.

3.3.3 General lamination parameters

For sub-laminations

In section 3.3.1 we exposed the current limitation of our pseudo-isostatic lamination apparatus to 90 bar. Although this might sound as a limitation compared with the 206 bar/3000 psi recommended by DUPONT (while HERAEUS advises 103 bar/1500 psi), it is not always desired to laminate pseudo-isostatically at higher pressures. When it is performed for sub-laminations in particular, we want to avoid "flattening" the tapes surfaces too much (cf. Figure 3.2b), in order to guarantee that the final metal lamination will still allow the sub-laminated parts to interpenetrate each other. As such, 80 to 90 bar for sub-laminations and 80 to 160 bar for the final metal lamination proved to be a good order of magnitude.
The same applies to duration: sub-laminations are done for 3 to 5 min, rarely 10 min, but the final lamination lasts always 10 min at least. For the temperature however, it is sometimes preferable to use a higher temperature (40 to 50 °C) for sub-laminations of heavily screen-printed tapes such as ground planes (to ensure a good bonding of LTCC between the metal grid) than for the final metal lamination (25 to 40 °C), because of the risk of general collapse.

It is however worth mentioning that laminations cannot be added serially in a linear way to obtain a similar result: one lamination of 200 bar is not equal to two of 100 bar executed in a row. The pre-densification process is complex and non-linear.

For normal one-step laminations

It is impossible to give numbers valid as a general rule, as each circuit is different in geometry, in screen printing and in type of tape. Based on our experience, we can however draw some guidelines. For the sake of readability, the parameters are grouped and abbreviated as follows: pressure in [bar], temperature in [°C] and duration in [min], e.g. 80-25-10 translates into 80 bar at 25 °C for 10 min.

DuPont 951 We have tested various kinds of circuits; the parameters depends on the presence of cavities:

- For plain LTCC without cavities, there is no problem to laminate at 206-70-10 as recommended.
- With the introduction of narrow channels one- or two-layer high, of aspect ratio not more than twice large as high, the temperature must be reduced to ~40 °C to avoid collapsing the cavities; reducing the pressure to 160 bar might also be necessary.
- For complex fluidic circuits (channels more than 6 layers high, two “floors” of channels) the temperature must be reduced to ambient temperature or to 30 °C, and the pressure reduced to 190 bar or less. It is however better to perform sub-laminations, or to use other laminations techniques such as Cold Chemical Lamination (see subsection 3.4.2). A good example is presented on Figure 3.16: on the left the circuit was laminated with Terpineol at 190 bar for 5 min at 40 °C, yielding a disastrous output; on the right it was laminated with Terpineol too, but only at 10 bar for 1 min at 25 °C, keeping a good shape. Please refer to section 3.4.2 for the Terpineol application.

Heraeus CT700, Ceramtec GC Our experience is unfortunately very limited with standard shrinking tapes of other suppliers than DUPONT. We have tested two of them, and here are their lamination recommendations:

- HERAEUS recommends laminating the CT700 [14] at 240 to 270 bar, during 5 to 10 min at 60 to 80 °C; the expected shrinkage is given at 14.4 % in X-Y, and at 14.9 % in Z.
- For the GC, CERAMTEC recommends a pressure of 50 to 130 bar, during 0.5 to 3 min, and at 30 to 80 °C [8]; the expected shrinkage is given at 21.0 % in X, at 21.4% in Y, and at 18.0 % in Z with ± 0.5 % each time.

When manufacturing the large electro-fluidic platform presented in Figure 2.2, we tried three tapes for comparison: the DP951, the HERAEUS CT700 and the CERAMTEC GC, as depicted on Figure 3.17a. It was *a posteriori* not a good idea to conduct tests on so large circuits, as we got mitigated results, and we could not afford experimentating more due to various constraints. Anyway, here is the outcome:

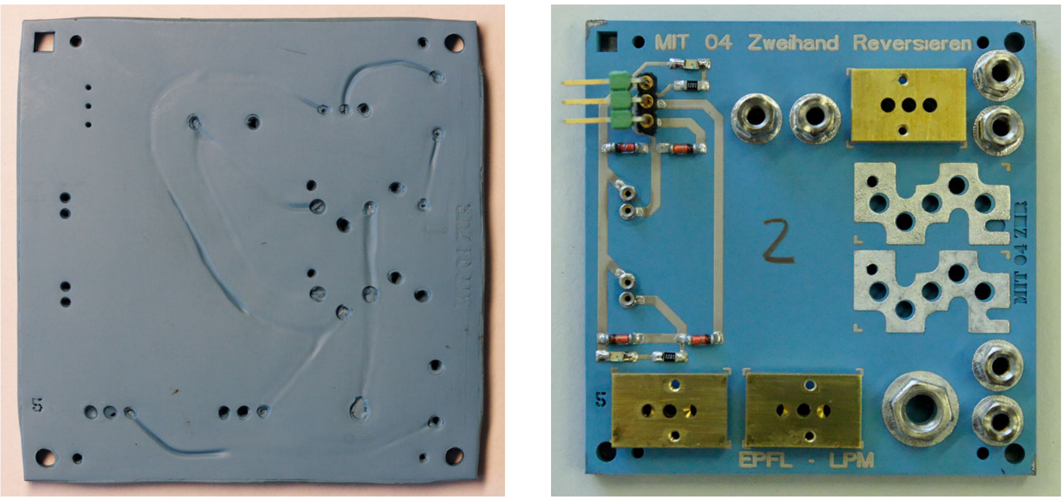

(a) Lamination with Terpineol at 190 bar for 5 min at 40 °C.

(b) Lamination with Terpineol at 10 bar for 1 min at 25 °C.

Fig. 3.16: The same electro-fluidic circuit shown (*a*) crushed due to excessive lamination, just after firing, and (*b*) healthy, after mounting of SMD components but two for demonstration purpose.

- The 254 µm DP circuits were the first to be tested (laminated at 80 to 90 bar, at 25 °C, for 10 to 15 min). All 22-layer circuits suffered from tearing in the center between the two main orifices, at the location of the central buried channel (Figure 3.17c). We suspect the tearing to be caused by the too important difference of shrinkage between bulk zones and suspended structures (above and below channels); although it is usually not a problem, the large size may be in cause.
- The 320 µm CT700 tape was tested in second, first with three tests of three-layer circuits laminated at 25, 65 and 83 °C, from 160 to 190 bar for 10 min to assess the tape shrinkage (see one of them on Figure 1.6b on page 23). The outcome was correct even at 83 °C, so we decided to stack the eighteen layers and to laminate at 190 bar and 85 °C for 10 min. Nonetheless, what would have been correct for three layers turned to disaster for eighteen layers, as testifies Figure 3.17b. Unfortunately, we had no more ressources to run another test with a reduced lamination.
- The 600 µm[6] CeramTec circuit was fabricated last. Not willing to reiterate the same mistake, the circuit was laminated at 58 °C, with a pressure that first rose to 80 bar for only 15 s, and that was then decreased to 50 bar for 15 more seconds; it was fired with a top alumina plate, and the output is excellent. This is the only CeramTec circuit we have ever fabricated, though; the screen printing of solder pads can be seen on Figure 2.5b on page 37.
  Note on Figure 3.17a that the external dimensions were slightly reduced, compared with the circuit in DuPont, to accommodate the larger shrinkage and hence the maximal manufacturing dimensions of our installations.

---

[6] The standard thickness is 360 µm, but we got a special delivery directly from the supplier.

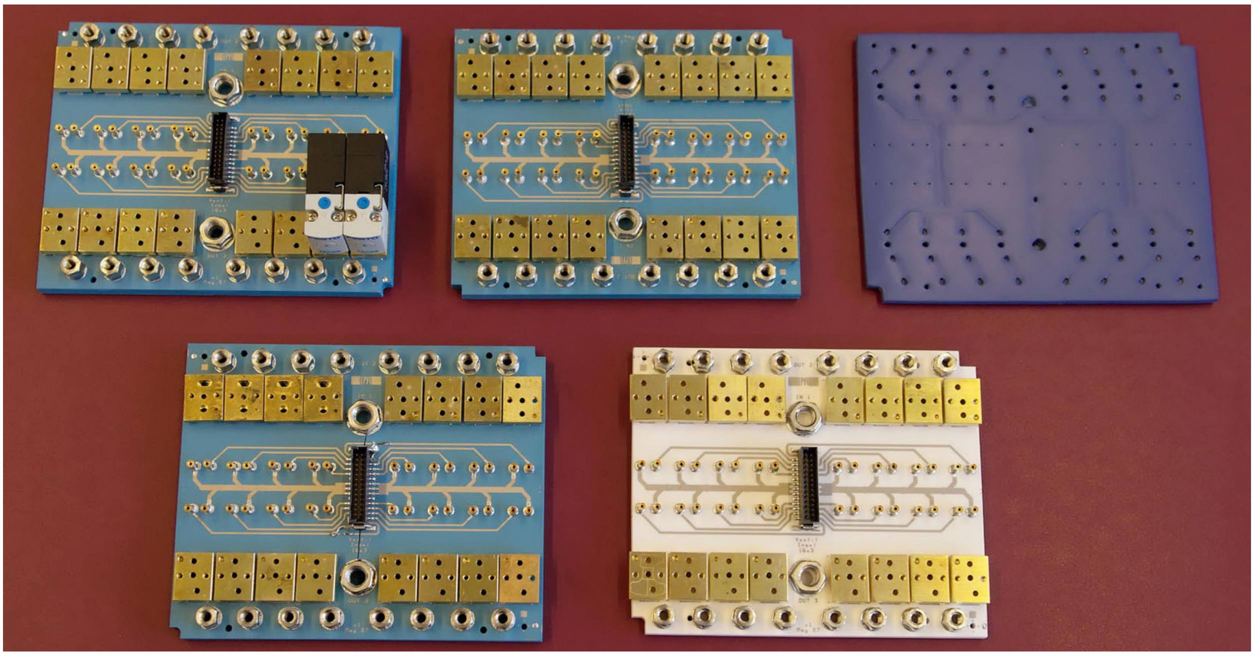

(a) Three DP951 (blue), one CT700 (violet) and one GC (white). The DP suffered from tearing in the center; the CT700 was crushed at lamination; the CeramTec was the only one fired correctly.

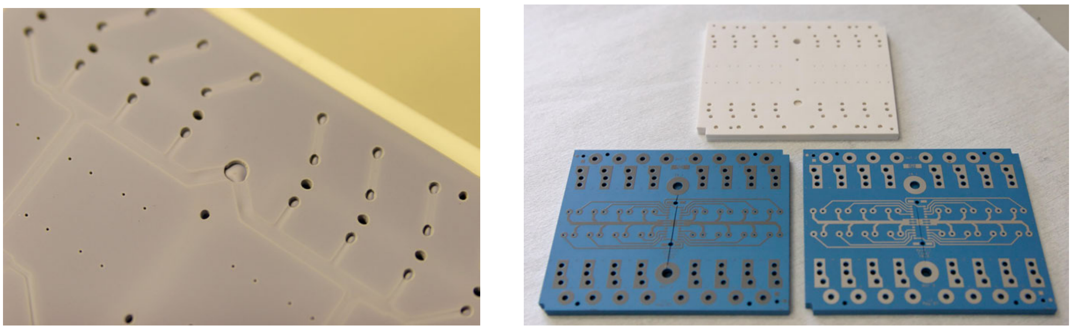

(b) Detail of the CT700 just after lamination: its structure collapsed.

(c) Fired circuits: one DP951 with fresh DP7484 Pd/Ag metallization screen printed (*bottom left*), one DP951 with the same post-fired metallization (*bottom right*) and one virgin GC (top): the DP suffered from tearing, the GC is intact.

Fig. 3.17: Large electro-fluidic platforms manufactured in three LTCC tapes: DP951, Heraeus CT700 and CeramTec GC. The twenty-two 254 µm DP tapes were laminated at 80 to 90 bar at 25 °C for 10 to 15 min, the eighteen 320 µm CT700 tapes at 190 bar-85 °C-10 min, and the nine 600 µm CeramTec tapes at ~65 bar-58 °C-0.5 min. The fired dimensions are around 93×76×4.6 mm.

Heraeus HeraLock HL800 & HL2000 No large fluidic circuits were fabricated with these special tapes. However, some testing could be done during the fabrication of the prototypes of capacitive force and flow sensors (see Appendix section C.2). Here are the supplier's recommendations:

- For HL2000: isostatically at 103 bar, 75 °C and 1.5 min.
- For HL800: isostatically at 210 bar, 70 °C and 4 min (plus 3 min of pre-heating).

We tested structures in HL2000 such as suspended bridges (Figure 3.18a) laminated with metal in one time at 160 bar, 55 °C, for 10 min, but it resulted in strongly ondulated bridges. For comparison, we got perfect similar structures in DP951 laminated once at 160-25-10 and in two times at 115-55-10.
We also tested lamination of thermal bridges over sacrificial paste (cf. subsection 4.6.2), for which the choice of lamination is crucial: lamination with rubber yields deformations at hinges (Figure 3.18c), while lamination with metal gives a nice output (Figure 3.18d).

Regarding HL800, we have so far experienced bad results, both with and without screen printings: the tape has tendency to self warpage, as Figure 3.18b can attest. This relatively new tape (2008) needs either a minimum number of layers (around ten I would say) to be "flat" after firing, or maybe more development from its supplier.

Miscellaneous

180° rotation half-way through Regarding the claim from DuPont [3, 11] that "a 180° rotation of the lamination die is required after the first 5 minute time period", I tried it at the very beginning of my laminations tests five years ago, but without noticing any benefit. This might make sense in the case the lamination fixture applies pressure inhomogeneously, but if it requires opening the whole fixture and manipulating the tapes (with all the risks of damage associated), the disadvantages exceed the hoped-for advantages; furthermore, it increases the process variability.

Alternate stacking DuPont, Heraeus and others [5, 14] also advise to stack tapes in alternate 90° orientation in order to compensate for the anisotropic X-Y shrinkage, with regard to the tape cast orientation that is indicated on each green sheet. We used this technique for our early tests, but concluded it was easier to compensate for the shrinkage in the CAD software. It is not only cumbersome to keep track of each tape orientation for circuits with a high number of tapes, but the asymmetric behavior is reported on the wall quality of large circular holes drilled in the LTCC, as Figure 3.19a can attest. This effect is apparently amplified upon lamination under high pressures: compare the straight walls of Figure 3.19b (laminated <20-25-10) and the irregular walls of Figure 3.19c (laminated 160-25-10). The problem is not simple, because the geometry of the walls is also determined:

- By the laser cutting profile; see the studies of Balluch & Smetana [40, 41];

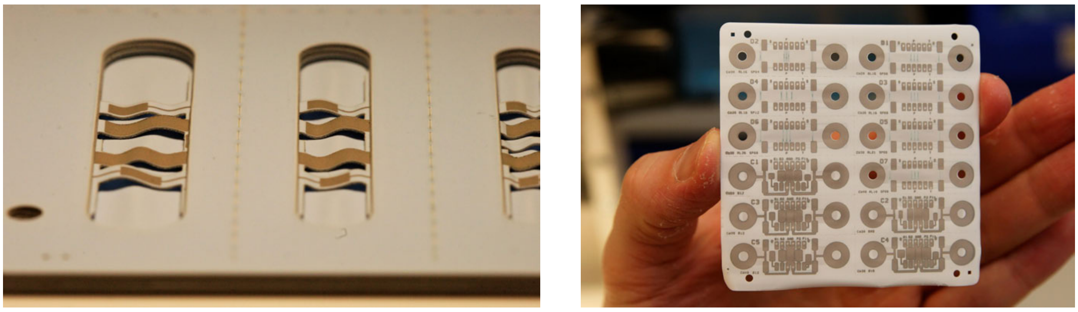

(a) Suspended capacitive bridges in HL2000 deformed after one lamination at 160 bar, 55 °C, 10 min.

(b) HL800 circuit deformed after firing; the single metal lamination was at 160 bar, 25 °C, 10 min.

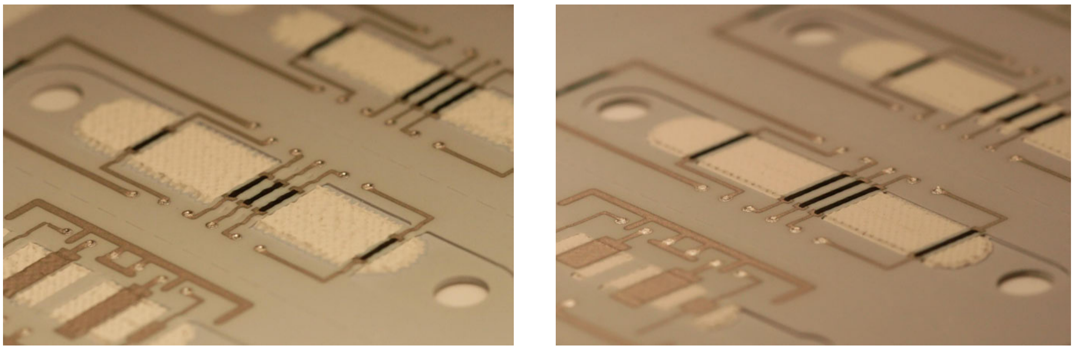

(c) Suspended HL2000 thermal bridges after rubber sub-lamination over sacrificial layer: structures are deformed.

(d) Same as *(c)* but with metal sub-lamination: structures are intact.

Fig. 3.18: Tests with Heraeus HL2000 and HL800.

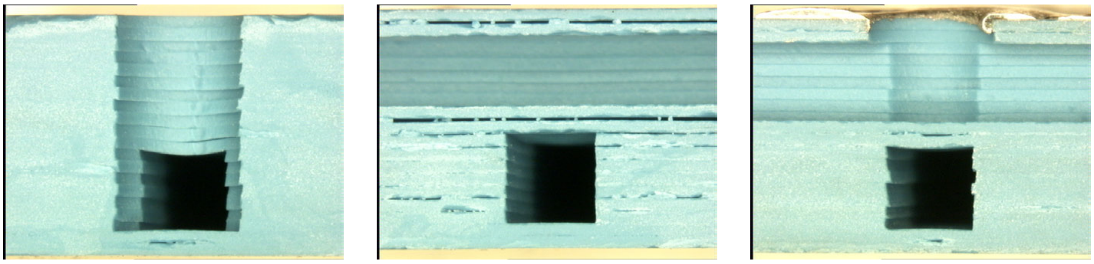

(a) Irregular walls of an 18-layer well; laminated at <20-25-10.

(b) Regular walls at a crossings of channels, due to loss of pressure; laminated at <20-25-10.

(c) Irregular walls of a similar crossings of channels; laminated at 160-25-10.

Fig. 3.19: Test fluidic channels fabricated with alternated (0°-90°-0°) tape stacking; the wall geometry is dependent of the asymmetric shrinkage and of the lamination pressure. The parameters are pressure [bar], temperature [°C] and duration [min].

- By the type of sintering (constrained or not): see the studies of Lee & Mohanram [37], and of Hintz & Thust [71, 72, 86].

3.4 Other innovative lamination techniques

The limitations in circuit design and geometries induced by the side effects of thermo-compressive lamination have generated research in this field for over a decade (Piwonski & Roosen worked on [74] in 1998 already). The main orientations taken so far were:

- Cold Low Pressure Lamination (CLPL), with adhesives that bind the tapes together;
- Cold Chemical Lamination (CCL), with solvents that slightly dissolve the tape surfaces;
- Lamination with inserts that are removed before or after firing.

The frontier between the first two orientations is not always evident, as we will see below. The next subsections review the methods in detail.

For reasons already exposed, we will not cover the Pressure-Assisted constrained Sintering (PAS) and the Pressure-Less Assisted constrained Sintering (PLAS) techniques. However, the latest state-of-the-art techniques can be found in section 6.2; for instance, the injection of sacrificial materials after lamination is discussed on page 208.

3.4.1 Cold Low Pressure Lamination (CLPL) with adhesives

Method of Roosen: specific double-sided adhesive As reported by Andreas Roosen from Erlangen University in 2005 in [73], Cold Low Pressure Lamination (CLPL) is a lamination technique to join ceramic green tapes in ceramic multilayer device processing. In contrast to the common thermo-compression method, CLPL is based on gluing the green tapes together at room temperature under low pressures (see Figure 3.20). During binder burnout and co-firing of the glued, laminated structures, a complete joining between the initial green tapes occurs. By this technique, non-metallized and metallized tapes can be joined, leading to a homogeneous body. The conventional thermo-compression method operates at temperatures above the glass transformation point of the binder system under an applied pressure; this causes a mass flow, which is critical in case of laminating sophisticated, complex structures. To the contrary, during CLPL no mass flow is generated, thus deformations during the lamination step are reduced. CLPL has a high potential for the lamination of fine, undercut and complex 3D structures with small lines and spaces of metallization and/or small cavities and micro channels.

The method was experimented by Roosen on DP951 LTCC with a specific double-sided adhesive tape of 12 µm thickness that was coated on both sides by a polyacrylate-based adhesive layer. Surprisingly, he did not give precise indications of his lamination conditions in [73], despite a thorough thermo-gravimetric analysis afterwards; we just know that it was done "at room temperatures at very low pressures". However, from another publication [87] we understand that the pressure is in the range "of a few MPa", i.e. circa 5 MPa[7].

After the burnout of the binder at further temperature increase, the adhesive tape melts,

---

[7] A previous publication with Dulce Couto from Bosch GmbH in 2004 [88] stated that "lamination was carried out by thrust[ing] the tapes forward through two laminating rollers [...] that moved with a rate of 0.3 m/min and exerted a pressure of approximately 0.05 kg/mm^2", which must be mistakenly underestimated by a factor of 10, as it would yield 0.5 MPa instead of or 5 MPa.

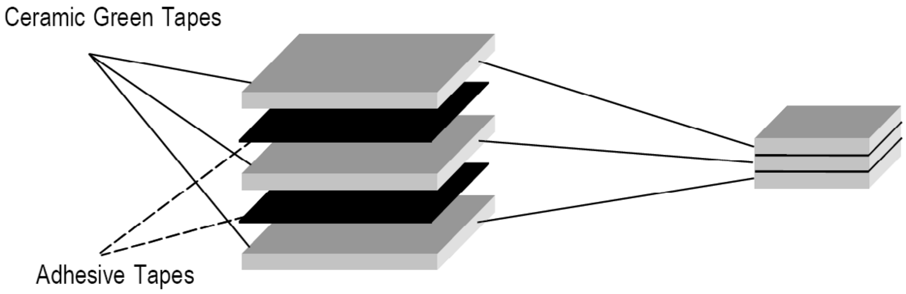

Fig. 3.20: Cold Low Pressure Lamination (CLPL) of ceramic green tapes [73].

which results in the formation of capillary forces in the porous tape. These forces drag the tape together and join them. We must point out that for laminates over 6 layers, defect-free structures were obtained only if the cavities were "open", i.e. with contact to the atmosphere. Closed cavities suffered from strong warpage effects and crack formation due to the gas pressure generated by the organics decomposition (defects were present at 270 °C already).

To summarize the advantages of the technique (from [73]):

- The method is carried out at room temperature and low pressures;
- No waiting period to reach a homogeneous temperature profile in the stack is necessary;
- There is no uncontrolled mass flow;
- It is suitable to build up fine structures or spatially complex 3D structures;
- It works also with green tapes from water based binder system;
- It is suitable for continuous manufacturing processes;
- It requires low investments costs.

Its main drawback is that it is not suitable for closed cavities, as the defects originating from the organics decomposition occur well before the sintering (at 270 °C already). To overcome these problems, we learn from [85] that Roosen et al. developed an upgraded version of the CLPL method [89]. The adhesive layer gluing the tapes was screen printed on the LTCC substrates using an acrylate-based liquid adhesive[8]. Therefore, the double-sided adhesive tape was replaced by a single material film; the frontier with chemical lamination is indeed fuzzy. It provided several advantages, for instance metalized tapes could be processed. However, the lamination had to be carried out in a clean room, because the adhesive liquid was extremely dust sensitive. The next adhesive-based method was also presented by Roosen et al. [90]. The adhesive film was applied to the green tape surface by a transfer tape consisting of an adhesive layer on a release liner. This method also allowed the processing of metalized tapes, while not being dust sensitive.

---

[8] Composition of 2-ethylhexyl acrylate and acrylic acid at a mass ratio of 90:10 to 99.5:0.5, 98:2 in particular.

3.4.2 Cold Chemical Lamination (CCL) based on solvents

Method of Suppakarn: poly(propylene glycol) PPG Nitinat Suppakarn et al. published in 2001 in [91] about solvent lamination of *alumina green tapes* that was readily accomplished using a mixture of ethanol, toluene, and poly(propylene glycol) (PPG). After lamination, the PPG is clearly present as a discrete film at the interface between the laminated tapes, and direct particle-particle contact does not, in general, exist across the joined surfaces. This condition, however, does not generate delamination during firing. Instead, stacks of green tapes laminated using this mixture routinely sinter to full density and no evidence of original joint persists through the firing process. PPG slowly diffuses through the organic binder film at room temperature; the PPG diffusion rapidly increases as the temperature is increased to 80 °C. The key to the efficiency of adhesives during green tape lamination is mutual solubility of the nonvolatile component of the glue and the base polymeric binder.
For LTCC it would be necessary to replace the solvents by more adequate ones; from our experiences, anything not too strong (for instance not toluene) that does not attack the tape too much would be suitable, such as alcohols possibly additioned with water. To be deposited as a film PPG would be appropriate, but a compound more solid at ambient temperature is preferable.

Methods based on honey: Da Rocha and Baker Zaira Mendes Da Rocha, Mário Ricardo Gongora Rubio et al. reported in 2004 [92] about having developed a new lamination method that use organic fluid as gluing agents: natural honey, and honey components: glucose, fructose, maltose, sucrose, as well as some polyester resins. In all cases, a good lamination was achieved, an no interface between layers could be observed.
They wrote that: *Compared with the CLPL method introduced by Roosen* (see subsection 3.4.1 above), *lamination using fluids allows selective deposition using available continuous manufacturing process equipement as well as faster process development and lower investment costs. Advantages of lamination using organic fluids can be summarized as follows:*

- *Excellent gluing function and easy tape alignment at room temperature due to their high viscosity;*
- *Low temperature and pressure process;*
- *No pressure gradients in LTCC laminate;*
- *Easy method of deposition, allowing lamination of complex shapes and non-uniform surfaces;*
- *Sintering temperature profile with high heating rate compared with CLPL method;*
- *Organic fluid deposition can be realized by dipping, screen printing or dispensing techniques.*

An application of this method can be found in 2007 with Amanda Baker, Michael Lanagan et al. who used a mix of honey and water to achieve cold, low-pressure lamination. Here is a summary of their processing, adapted from [93]: the goal was to co-fire high and low permittivity materials to build, by careful selection of materials and Finite Difference Time Domain modeling, miniaturized patch antennas that are 80 % smaller than conventional patch antennas. The host dielectric substrate block was fabricated from 50 layers of DP951 LTCC. To build up thickness, several layers of the LTCC were first isostatically laminated at 70 °C, 3000 psi for 10 min (DUPONT recommendations); the resulting 1 mm thick LTCC stacks were then punched to open area for plug insertion, and DP6145 silver paste was screen printed for internal and ground plane metallization. Each punched LTCC stack was painted with a honey/water 75/25 mixture and placed on an alignement fixture. The honey mixture acted as glue between the LTCC layers and eliminated the need of further lamination steps that often result in the distortion and smashing of the soft ceramic devices [92]. The circuits were then imbricated and fired with a standard firing profile with a peak at 850 °C and a dwell of 30 min.

Method based on Terpineol In 2006-2007 in our laboratory, we tried to deposit Terpineol on the surface of each tape during stacking (Figure 3.21), with the help of a spongy roll (see Figure 3.21a and section 3.3.3 above). We had chosen Terpineol as it is proportionally one of the most important compound of the organic binder of the DP951 system (tapes and inks), and a relatively benign solvent (it is present naturally in pines). It was indeed selected after rapid trials on leftover tape after we had eliminated other common solvents such as:

- Aceton instantaneously dissolved the tape;
- Isopropanol was not as strong as aceton, had a lower gluing effect than Terpineol, but prevents detaching tapes (in case of error) even in small quantities;
- DI water was ineffective on DP951: green tapes turned out to be rather hydrophobic;
- Saliva was interesting as it presented the gluing properties of isopropanol and the reversibility of water. It spread rapidly on the tape surface, but was not too much absorbed. The problem however lied in the production of sufficient and reproducible quantities for obvious reasons;
- Human sweat was envisaged but could not be tested, for similar reasons as saliva.

I must point out that these trials took place one year before my supervisor T. MAEDER undertook intensive research on solvents, reported in [94]. We have since not re-attempted the deposition technique with the spongy roll, as it is not well reproducible. Using a grooved cylinder (like those used for wetting stamps) could be an interesting solution, as the quantity of deposited solvent is controlled by the depth of grooves.

A problem often identified with application of compounds for CPL / CLPL is the difficulty in applying sufficiently thin layers in a controlled manner; this issue is especially acute when using thin tapes, e.g. less than 100 µm. An elegant solution would be a screen-printable paste comprising low-volatility active compounds (solvents, plasticizers, soft polymers), diluted in a temporary solvent that evaporates quickly upon oven drying. This would allow precisely controlled deposition of small amounts of compounds to locally soften / glue the tapes.

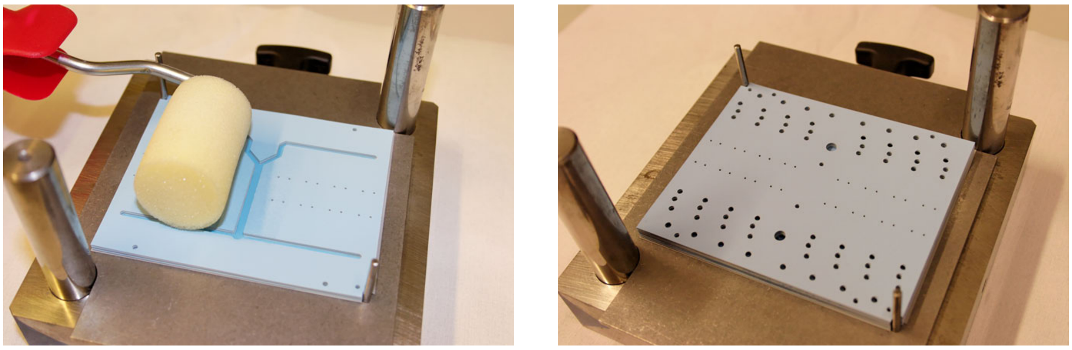

(a) Application of Terpineol tape by tape by spongy roll (depicted for lower channels).

(b) Picture of top layer with circular openings.

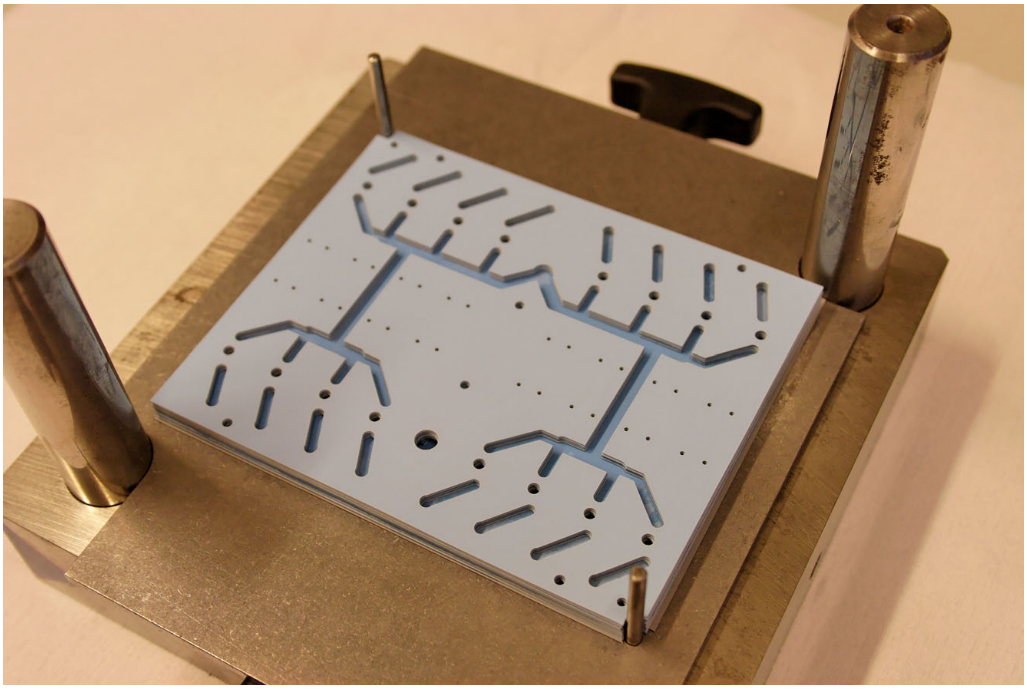

(c) Picture of the upper channels.

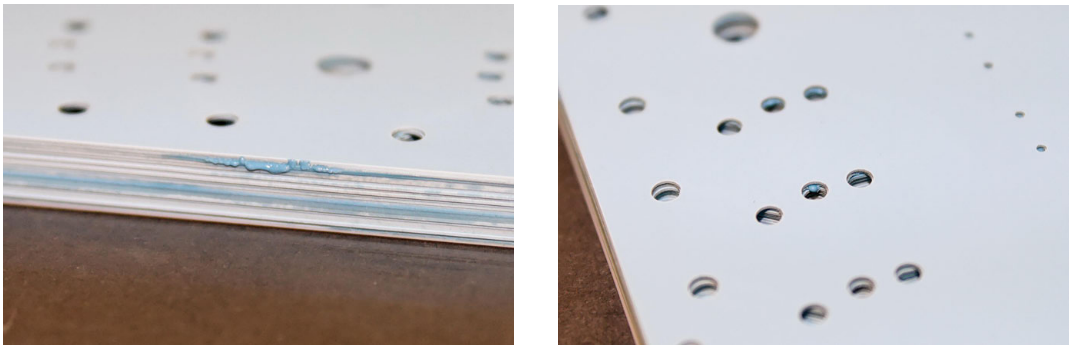

(d) Dissolved LTCC tape oozing out of lateral side.

(e) Dissolved LTCC tape oozing out of top opening.

Fig. 3.21: Failed attempt of using Terpineol as LTCC tape surface softener to improve bonding quality. The Terpineol was deposited in excessive quantity: right after the lamination, we see evidence of dissolved LTCC tape oozing out of layer boundaries. The LTCC circuit global green dimensions are 108×88×5.6 mm (made of 22 tapes of $\mathrm{DP951}$-254 µm).

Method of Jurków & Golonka, based on commercial thinner DOMINIK JURKÓW, a PhD student of a team led by Prof. LESZEK GOLONKA of WROCŁAW UNIVERSITY OF TECHNOLOGY, Poland, experimented since 2008 a method where a commercial thinner is screen printed on the green tape surface, or applied using a paint brush. The CCL method is well documented in [95, 96], which we will summarize here:

The tapes are first covered by a film of special liquid; a screen of 450 to 500 meshes is used. Various types of DP thinners and acetone were analyzed to ensure good bonding quality of the tapes, and DUPONT thinner 4553 was one of the best.

The ceramics are then put in a stack and laminated at low pressure, below 0.5 MPa. The method was tested successfully on lead-free ESL 41020 tape [95], on DP951AT (114 µm) [96] as well as on DP943, HERAEUS HL800 & HL2000 [85]. The structures were then sintered according to the manufacturers specifications; for the DP951 it was at 875 °C peak temperature during 15 min, for a total firing cycle of 90 min [96] (which is relatively short).

To attest the quality of their innovation, they produced a flow sensor both by traditional thermo-compressive lamination and by CCL. The cross-section of the thermo-compressed flow sensor is presented in Figure 3.22b; the delaminations visible are caused by the process pressure and temperature being too low. However, the sagging rate of the bridge, an effect of the pressure and temperature being too high, is significant. The bonding quality and the bridge geometry may be improved by using sacrificial materials (fugitive phase) intended to disappear during a cofiring process, but an influence of the fugitive phase on the electrical properties of screen-printed passives has to be analyzed.

The cross-section of the CCL module is shown in Figure 3.22b. The bridge is not deformed and its sagging rate is very low. The lamination quality is at the same level as in the thermo-compressed modules.

Nonetheless, the wall geometry of the channel is weak, because of tapes displacement. This problem is less prone to occur with the thermo-compressive method, as the position of each layer can be corrected during the stacking process; to the opposite, with the CCL method the green tapes are bonded immediately during stacking. The problem may be reduced by using more stable locating tape pins than in their setup; for instance, our optical alignment fixture (section 2.2.5 on page 38) would be quite appropriate for this task.

An application manufactured with the help of CCL is proposed in [97] with a three-element gas flow sensor in LTCC. For a more complete review of the CCL methods, please consult [85]; the CCL method is also compared with the next method: lamination with sacrificial inserts.

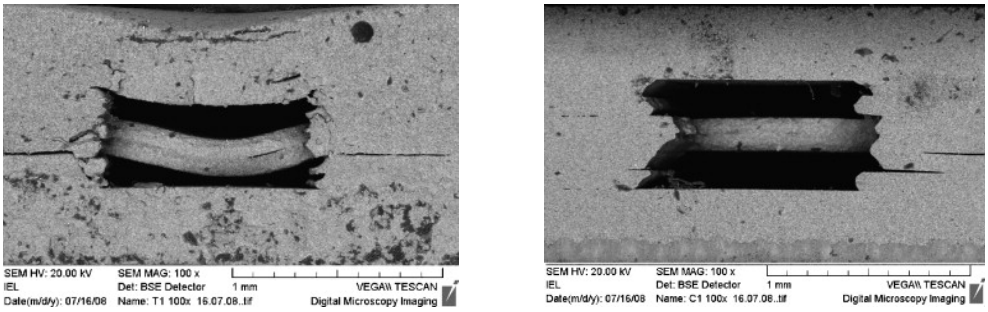

(a) LTCC tapes bonded by the thermo-compression method; bridge deformed.

(b) LTCC tapes bonded by the CCL method; the bridge is intact.

Fig. 3.22: Comparison of two lamination methods experimented by Jurków & Golonka: SEM photos of the cross-sections of a flow sensor manufactured with the two methods. Note the weak channel walls geometry, due to a bad alignment method and/or fixture. [96]

3.4.3 Lamination with sacrificial inserts

Lamination with carbon sacrificial layers This subject involves the use of sacrificial carbon tapes or pastes that act as solid inserts, thus forcing the LTCC tape to follow their shape upon lamination. They then decompose into CO_2 upon firing, at temperatures close to the LTCC sintering. Please refer to section 4.2.2 on page 100 and to Figure 4.4a for an extensive description.

Lamination with cetyl alcohol (method of Malecha) Karol Malecha, another PhD student of L. Golonka, was the first to use cetyl alcohol as a sacrificial insert that would allow lamination of cavities without reducing the pressure. [84, 85, 98, 99]. The main objective of his work was to present a simple and repeatable method for realization of microfluidic channels in "zero-shrinkage" HL2000 LTCC ceramics; the method is based on a two-step lamination process:
After laser cutting, the ceramics tape layers are stacked together in the proper order, placed between two cover plates and initially laminated using an isostatic press with a pressure of 10 bar. The process of filling the channels with cetyl alcohol consisted of two steps (see Figure 3.23). First, an organic insert was milled and heated above its melting point (49 °C). Second, liquid cetyl alcohol was poured into channel. After the filling process, all structures were laminated a second time with a standard pressure of 100 bar. Next all the LTCC modules were fired according to modified two-step firing profile in air, with a peak temperature of 850 °C. The burnout cycle was modified with an additional holding at 200 °C and a slower ramp rate to 450 °C to insure complete burnout of organic inserts.

This sacrificial volume material (SVM) is applicable to unfired LTCC to help keeping the right shape during the lamination, but it can be used as a filling material only (and not used an insert), to fill cavities obtained by prelamination.
The method was also put in application by Horváth in 2009 with mitigated results, as reported in [100]: *[...] Blistering is caused by the SVM occasionally creeping between tape*

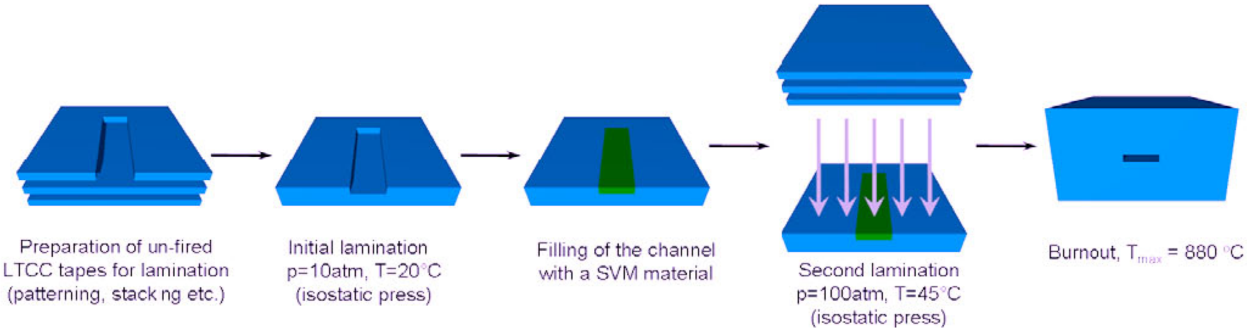

Fig. 3.23: Cetyl alcohol used as poured SVM material in pre-formed cavities: flow-chart of the "define and fill" process of Malecha and Golonka from Wrocław University of Technology [85].

layer gaps. Application of adhesives permitted a further reduction of pressure by suppression of SVM-creeping. These precautions helped to minimize geometry deformation during the fabrication process.

Interestingly, Malecha, Jurków and Golonka published together in [85] a comparison of their two lamination methods, i.e. with solvent or SVM; the influence of the lamination method on the spatial structures' quality was investigated:

- The method based upon two-step lamination with the use of sacrificial materials exhibits lower rates of delamination and better channel geometry quality than those obtained with the standard thermo-compression method; the organic inserts have considerably lowered sagging and contraction of the three-dimensional structures during the lamination and firing processes. With respect to results of the combined TGA/DTA/DTG analyses, the burnout process was modified, i.e. with an additional holding at 200 °C and a slower ramp rate to 880 °C, to insure complete burnout of the fugitive materials.
- The CCL process reduces deformation of spatial structures in comparison with the standard thermo-compression method. However, the bonding between individual LTCC tape layers is weaker for the CCL method than for the standard lamination process. Further research will encompass the search for a better solvent for improvement of the bonding strength between "zero-shrinkage" HL800 LTCC tapes.

Lamination with sublimable compounds Although it has not yet been tested on LTCC, the use of sublimable compounds that evaporate around 150 °C [101] is a promising solution that combines the advantage of the cetyl alcohol (neat decomposition) and of screen printing: the special compounds are formulated in inks, and not poured like the cetyl alcohol. Please refer to section 4.2.2 on page 99 for more information.

3.5 Conclusion

This chapter demonstrated that the lamination parameters play a paramount role on the firing shrinkage, and subsequently on the fired dimensions of LTCC circuits. The stake is not only the control of final dimensions, but also the possibility or not to produce cavities due to a general collapse of structures under a too elevated lamination pressure and/or temperature, inherently to the visco-plastic behavior of green tapes.

Regarding the influence on shrinkage of lamination parameters, which were for our study kept in a limited temperature range (25 to 55 °C) known not to provoke the collapse of structures of the studied design, we could determine with Design of Experiments a simple linear model for the DuPont 951 in function of temperature and pressure; the number of layers and the lamination duration were the two other parameters retained for the study, but they turned out to have a negligible impact *on shrinkage*. However, they certainly play a role on the type of structures possible to obtain and on the quality of bonding of tapes upon sintering, which were not studied.

Our linear model must nevertheless be applied with caution, because we deviate from the manufacturer's recommendations, and we expect the visco-plastic behavior of green tapes to become non-linear above 55 °C. We also expect tapes from other manufacturers to exhibit the same general tendency of presenting a lower shrinkage after an increased lamination (and *vice versa*), but the dependence on pressure and temperature is probably different because of other (secret) organic binders employed. For instance, we know that the DP951 tape is based on acrylate polymers (PEMA/PMMA) [102], while others are based on PVA or PVB (HL2000 supposedly [88, 103, 104]).

Therefore, this study should be seen as a motivation to further study the influence of lamination, and is a call to LTCC suppliers to conduct similar experiments in order to adopt a standard shrinkage measurment technique. I am convinced that the future of LTCC structuring for microfluidics involves reduction of lamination pressure and/or temperature, and if end-users could dispose from models to better predict the shrinkage of their circuits, it would be a great leap forward for the community.

To compensate for the reduction of lamination pressure and temperature necessary to create fragile structures, we have developed a lamination technique mixing pseudo-isostatic laminations with the help of a constrained rubber, and a classical uniaxial lamination between two metal plates. It requires the introduction of partial laminations that preserve crushable sub-parts from the pseudo-isostatic lamination, while ensuring a good tape bonding at locations where pressure would have been zero with a purely uniaxial lamination. This multiple-step lamination process is ended by a final metal lamination to join sub-parts together. The procedure requires a careful mastering of the processing conditions, as the deviation of lamination pressure between the sub-parts causes, later upon firing, stresses that can be fatal to the circuit due to an excessive difference of shrinkage.

Regarding the lamination parameters adopted to fabricate our circuits, we discussed in detail how the temperature, pressure and duration must be reduced depending on the type of circuit (with channels or not, with screen printings, in function of the tape etc.).

We also reviewed the latest innovative lamination techniques, among which Cold Chemical Lamination (CCL) based on solvents, Cold Low Pressure Lamination (CLPL) based on adhesives, and the use of sacrificial inserts, the frontier being often fuzzy with the evolution of methods. We suggest diluting the active compounds for CCL / CLPL (plasticizers, soft polymers, etc.) in a solvent, to allow controlled application of small amounts by screen printing.

Chapter 4

Mineral sacrificial compositions

In this chapter[1]*, the subject of LTCC structuration with sacrificial volume materials (SVM) is approached, with particular attention to mineral-based sacrificial materials. While carbon-based sacrificial materials are recommended for closed structures such as thin membranes or narrow channels typically found in microreactors and/or mixers, they are not suitable, in standard oxidizing firing atmosphere, for open structures like cantilevers or bridges, because they completely burn away before the end of the sintering, leading to the potential collapse of the suspended structure. Our approach for manufacturing open structures in LTCC lies in the use of sacrificial volume materials that survive the firing step, yet cause the least possible side effects (e.g. deformations or chemical reactions); the materials that survive firing temperatures of 900 °C and that can then easily be removed are conveniently found in mineral oxides. Early tests on* GreenTape 951 *LTCC revealed a strong shrinkage mismatch between the mineral paste and the tape, as well as an important porosity; therefore, we oriented our research in two phases to treat problems successively: first by developing pastes for standard hybrid alumina to get rid of the shrinkage issue (section 4.3), and then by migrating them toward LTCC (section 4.4). In this work, we demonstate that it is possible to use mineral pastes on DP951 LTCC that can either be screen printed as inserts or fill cavities, are easily removable with diluted weak acids, and that cause almost no deformations to nearby structures. A comparative review of existing methods is following the introduction, and direct sensor applications are proposed after the experimental part. The latest improvements of SVM, notably those compatible with "zero-shrinkage" tapes, are proposed last (section 4.6).*

Key words: Sacrificial Volume Materials (SVM) for alumina and LTCC, Mineral paste, Free-standing structures, Capacitive sensors.

---

[1] *Adapted from the conference paper [105], presented at 16th European Microelectronics and Packaging Conference - IMAPS 2007, Oulu (Finland):* Y. Fournier, S. Wiedmer, T. Maeder, *and* P. Ryser, Capacitive micro force sensors manufactured with mineral sacrificial layers, *pp. 298-303 of Proceedings, as well as from the paper [106], presented at 5th European Microelectronics and Packaging Symposium - IMAPS CICMT 2008, Munich (Germany):* Y. Fournier, O. Triverio, T. Maeder, *and* P. Ryser, LTCC free-standing structures with mineral sacrificial paste, *pp. 11-18 (TA12) of Proceedings.*

4.1 Introduction

The second approach undertaken in this thesis to open the way for new structuring possibilities is the use of sacrificial volume materials (SVM). The idea is to allow the LTCC to keep its shape throughout the firing process, whereas buried cavities or open structures normally suffer from sagging or distortions. The goal sought by using SVM is usually twofold:

1) To ensure support for overlying structures *during lamination,* hence to avoid deformations before firing;
2) To ensure support for overlying structures *during sintering*, hence to avoid deformations during firing.

Some techniques cover only the first goal, while others cover both. Our retained technique encompasses *mineral* materials that survive firing and are dissolved by weak acids, thus fullfilling both goals; although the idea of SVM is not new [5, 107–111], it was *not yet successfully* applied to unconstrained free-sintering LTCC in a mineral form before [112, 113]. The closed structures such as thin membranes can be processed with fugitive phases techniques from Dr. HANSU BIROL (see state of the art further for carbon sacrificial layers); the new technique presented is more suitable for open structures, especially cantilevers.

The present study of sacrificial materials was indeed split into two distinct phases; it was decided after we ran early tests of mineral sacrificial pastes on GREENTAPE 951 LTCC that revealed a strong shrinkage mismatch between the mineral paste and the tape, as well as an important porosity (similar results are displayed on Figure 1.10 on page 25). Therefore, we oriented our research into two phases to treat problems successively: a first phase to develop pastes for standard hybrid alumina (to get rid of the shrinkage issue) and for experimenting dissolution techniques, and a second phase for migrating the mineral paste onto LTCC.
The first phase was carried out in the frame of a semester project [114], of which the goal was to develop a prototype of microforce sensor (force range µN. . . mN). Instead of the traditional piezoresistive strain sensing through thick-film resistors used for higher forces, a more effective principle is used: measurement of beam displacement rather than strain (see explanation on page 223). A design of a cantilever sensor with capacitive electrodes, optionally coupled with an active electrostatic force cancellation to achieve higher sensitivity, is proposed and discussed. The structuration of the device is achieved in alumina with thick-films and mineral sacrificial layers (MSL); the resulting sensor properties are promising and open the way for improvements. The composition and dissolution of the sacrificial paste is of high importance, and is the cornerstone of the presented study.

In the second phase of this study, the mineral sacrificial pastes (MSP) previously developed for standard thick-film technology (alumina substrates) were adapted to LTCC in order to make a capacitive anemometer. Application of MSP materials on free-sintering (unconstrained and not "zero-shrinkage") LTCC is challenging: shrinkage must be matched to that of the LTCC in order to avoid excessive deformation, or sufficiently compliant materials must be used. Here, different MSP materials / materials systems are described, evaluated and compared with their (standard) thick-film counterparts, with respect to their ability to form deformation-free intricate micromechanical structures and their release (by oxidation and chemical dissolution) characteristics. Finally, by using the more successful MSP materials, an application is proposed with a capacitive microforce sensor serving as anemometer for an indoor slow flyer, which was the subject of a subsequent semester project [115].

This chapter continues as follows: first a classification of the various existing SVM pertaining to LTCC is proposed, completed by a state of the art. The two phases of the study (SVM for alumina, then LTCC) come afterward. The sensor applications are grouped at the end of the chapter; for reading consistency, the developments of sacrificial materials are separated from the sensors' performance analyses.

4.2 State of the art of sacrificial volume materials

4.2.1 Classification of methods and discussion

Structuration through sacrificial layers removed at the end of processing is standard in micromachined silicon MEMS, but is more seldom used in thick-film and LTCC technology; carbon-based fugitive phases are often encountered for LTCC [108, 113, 116], however they all disappear during firing before (or during) the ceramic sintering. In recent years various new methods have been explored by scientific teams doing research in thick films, but not all are suitable to free-sintering LTCC. As a beginning, we propose to review the background of existing SVM methods[2] and to discuss their applicability to LTCC. Figure 4.1 is a synoptic representation of Sacrificial Volume Materials classified first in function of the removal occurrence, and second in function of the chemical compound; Table 4.1 completes the information with mechanical and chemical characteristics. In both the chart and the table, the institutions, lead researchers and years of first publication are mentioned for each method. We would like however to point out that SVM systems involve complex interactions and are mostly application- or circuit-specific, therefore no classification could pretend being exhaustive and able to present a simple overview of the field. We classified the SVM in three main categories:

a) those that disappear well before sintering;

b) those that burn during sintering;

c) those that survive sintering and are removed or dissolved afterwards.

a) SVM disappearing well before sintering The first category is useful only when lamination is critical, but is of no help for the sintering: this is the case for instance for closed cavities or buried channels: they get crushed during pseudo-isostatic and isostatic lamination (see section 3.3) if left unfilled, but can benefit from the "drum-skin effect" upon sintering

---

[2] It covers, to our knowledge, almost all of them, except the latest involving polymers injected after lamination, method tested by Balluch & Smetana and discussed in section 6.2.3 on page 208.

Table 4.1: Comparison of Sacrificial Volume Materials (SVM) classified in Figure 4.1 in function of the removal occurrence, and second in function of the chemical compound. For each method the institution, lead researchers and year of first publication are mentioned. **This is pseudo-shrinkage: the SVM does not sinter, but "shrinks" by partially disappearing.

SVM type	Sublimable compounds	Cetyl alcohol	Graphite (air)	Graphite (N_2)	Al_2O_3 SPS
Institution	EPFL	Wrocław University of Technology, Poland	Sandia National Labs + EPFL	Bosch	Sandia National Labs
Lead researchers	Serra	Golonka, Malecha & Jurków	Peterson + Birol	Stecher	Peterson
First time published	2009	2007	2003 + 2005	1983	2005
Mechanical support during sintering	N	N	Y / N	Y	Y
Cohesion during/after sintering	N	N	None	N	N
SVM shrinkage during sintering	N/A	N/A	Disappears	N	N
Removal	Auto	Auto	Auto	Post-oxidation	Mechanical
Reactivity during sintering	None	None	(Reducing)	Reducing	Very low
Compatibility w/ closed cavities	Y	Y	Y (possible gas evolution)	N	N

SVM type	SrCO3	CaCO3 + C	MO + glassy binder	CaB_2O_4	Au
Institution	Univ. de Bordeaux 1, France	EPFL	EPFL	EPFL	CMC Electronics Cincinnati
Lead researchers	Ginet & Lucat	Fournier	Fournier + Maeder	Maeder	Sippola
First time published	2007	2008	2007 + 2009	2009	2004
Mechanical support during sintering	Y	Y	Y	Y	Y
Cohesion during/after sintering	N	N	Y	Y	Y
SVM shrinkage during sintering	N	Y (see caption**)	Y/N	Y	Y
Removal	Mechanical, weak acid	Mechanical, weak acid	Acid	Weak acid	KI
Reactivity during sintering	Very low	Low	Variable	High	Very low
Compatibility w/ closed cavities	N	N	N	N	N

nevertheless. The SVM of this category, all compatible with closed cavities, are listed in our table as *Sublimable compounds* (see page 99), which consist of harmless organic materials, and as *Cetyl alcohol* (see page 99), poured in its liquid form followed by solidification due to natural cooling to allow further processing. The former sublimates around 150 °C independently of the atmosphere, and the latter evaporates or decomposes at 200 °C in air, requiring a supplementary dwell around this temperature. Both are applicable to unfired LTCC to help keeping the right shape during the lamination, but sublimable compounds can be screen printed as inserts, while cetyl alcohol can be used as a filling material only, to fill pre-formed cavities (see Figure 3.23). We will not forget to mention that although PRANONSATIT et al. experimented in 2005 with success *polymer resin ink* as SVM on alumina (see page 100), this method might not be suitable to green LTCC depending on the resin. In effect, it the resin polymerisation occurs at too high temperatures (typically 200 to 300 °C) for unfired tapes, it would accelerate their drying or even start the organic binder burnout. For already sintered tapes however this could be an option for open structures, but the burnout temperature of the resin (450 °C) would prevent any support during sintering.

b) SVM that burn out during sintering The second category concerns *carbon-based pastes* (HANSU BIROL) or tapes (KENNETH PETERSON) that can either fill pre-formed cavities or, as

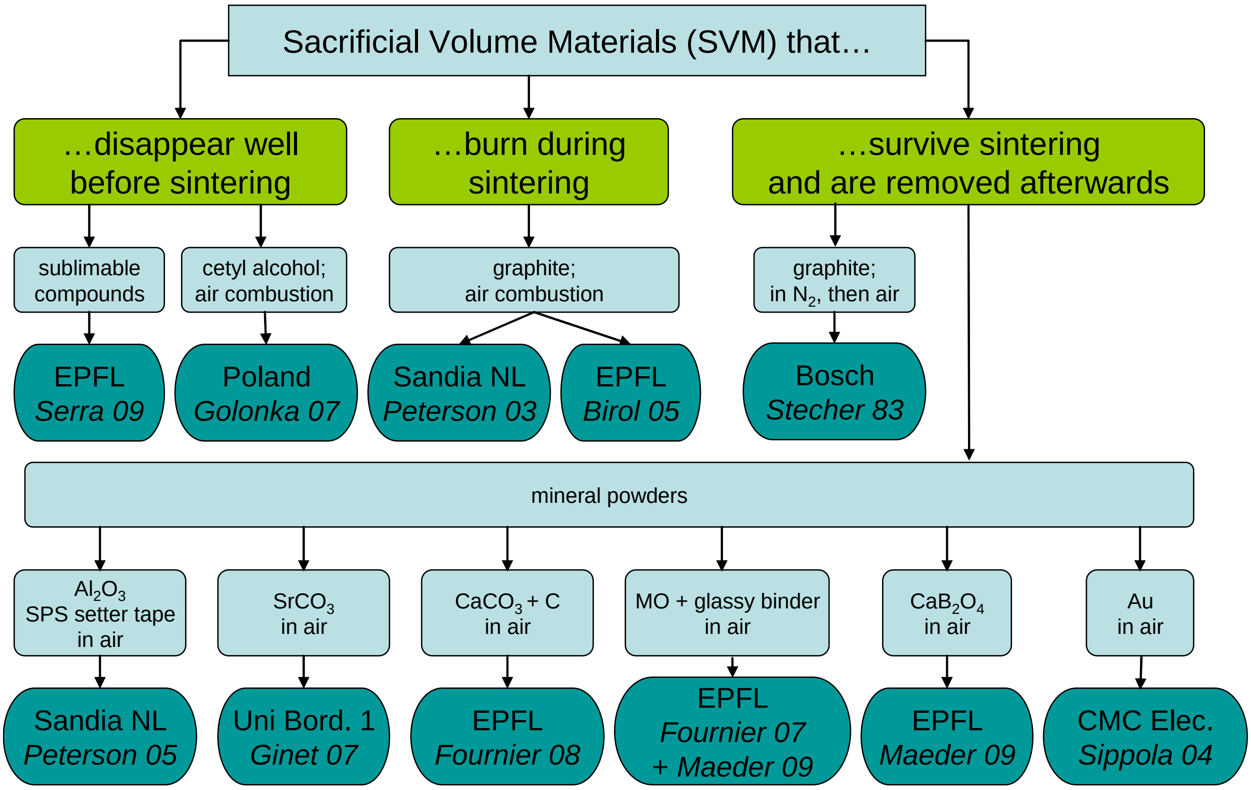

Fig. 4.1: Chart of Sacrificial Volume Materials (SVM) classified first in function of the removal occurrence, and second in function of the chemical compound. For each method the institutions, lead researchers and years of first publication are mentioned.

it has been implemented by the cited scientists, be used "as is" without prior channel definition (see illustration of Figure 4.4a and more on page 100 later). This method allows full pressure and high temperature lamination (something impossible to do with classical unfilled cavities), and, especially for closed cavities such as thin membranes, plays with the CO/CO_2 degassing effect to keep the desired form throughout the firing, despite the carbon burning before the sintering is finished (and hence before the LTCC porosity is closed). H. BIROL measured qualitatively in 2005 [110] that 780 °C is the porosity closure temperature of DP951 LTCC, but the complete burnout of carbon depends on grains size and this parameter must be fine-tuned when preparing the sacrificial paste. Carbon is however not suitable for "open" environments, as it can oxidize before the structure is sintered, leading to sagging and/or lateral deformation.

c) SVM that survive sintering and are removed or dissolved afterwards The third category forms the largest group, only suitable for open cavities. In this category, we distinguish methods that involve successive firing steps in N_2 and air (to preserve carbon-based SVM from burning out too early) from methods that fire SVM in air in one continuous cycle. The former is the "nitrogen analogue" of the carbon pastes of the previous paragraph, known as the "STECHER process" (see page 102), while the latter encompasses mineral powders. The "STECHER process" in its original form only makes sense on non-sintering substrates, because graphite does not sinter and is thus not compatible with the lateral shrinkage of most LTCC materials; we will therefore focus on methods with mineral powders, all involving simple firing in air:

- *Setter tapes of Al_2O_3*, also known as *SPS* for Setter Powder Sheets (see page 103 and also in section 6.2.5), are (usually) commercial materials that are delivered in the same form as green tapes, and thus can be cut to the desired shape before stacking. SPS are a uniform particle size Al_2O_3 material with an organic binder contained in a paper-thin sheet. The SPS binder burns away cleanly during firing, leaving a uniform distribution of setter powder in place of the fired parts. This powder must nonetheless be removed at the end of processing, either by mechanical action or by flushing, which can lead to clogging problems with nearby channels or fluidic ports: small particles are highly undesirable in microstructures. The advantages of the method are its ease of use and its chemical cleanliness, thanks to very low reactivity of Al_2O_3 grains with the LTCC.
- *Sacrificial layers based on $SrCO_3$* (mixed to a fugitive epoxy matrix, see page 105) have been successfully employed on alumina substrates. For LTCC, however, this sacrificial layer is essentially non-sintering, and not compatible with the lateral shrinkage of most LTCC materials; this is the same problem encountered by graphite sintering in N_2 atmosphere. Furthermore, the screen printing process is more cumbersome for the cleaning of screens: epoxy requires handling and cleaning separate from standard pastes, but can be advantageously replaced by polymers that are compatible with standard cleaning processes (see later).
- SVM made from a *mix of calcium carbonate and carbon* are explained in detail in section 4.4. A workaround has been found to prevent the mineral powder from reacting

with the glassy phase of the LTCC: the SVM is indeed a sandwich of three layers from two different pastes (requiring three screen printing steps, though); the inner layer contains a mix of C and $CaCO_3$ (acting as a skeleton during sintering, the proportion of C being varied to follow the tape shrinkage by pseudo-shrinkage by decomposition $CaCO_3 \rightarrow CaO + CO_2$ and $C + O_2 \rightarrow CO, CO_2$), while the outer layers contain only C (acting as an "anti-reactive buffer" between the mineral phase of the paste and the glassy phase of LTCC). The advantages lie in the compatibility with the free-sintering shrinkage of LTCC DP951, in the low reactivity during sintering and in the easiness of removal after firing: by mechanical action in the best cases, or by weak acid dissolution anyway. This mineral phase shows however almost no cohesion upon sintering, and can hardly prevent upward tape deflections that sometimes occur on elongated structures.

- SVM containing *MO + glassy binder* embrace pastes that contain a (refractory) metal oxide mixed with a glassy binder to ensure cohesion during, but also after the sintering. This is desirable for thin structures that have tendency to warp, twist, or erect during the sintering due to shrinkage mismatch stresses, but at the expense of a variable reactivity between the SVM and the other prints (conductors, resistors for instance) or the substrate, depending on the mineral content. For instance, when borax (anhydrous sodium tetraborate $Na_2B_4O_7$) is used as the glassy binder, it can react with and deteriorate the glassy phase of adjacent materials; this yield difficulties upon MSP dissolution with acids, due to a low selectivity. The metal oxides used in these SVM have negligible sintering; they are thus not suitable for free-sintering LTCC, but could be used on "zero-shrinkage" tapes.
  Two approaches have been explored in this class: first the present study with CaO and borax (the subject of section 4.3), which was later improved by my supervisor THOMAS MAEDER, leader of the Thick-film Technology Group, who replaced CaO with MgO, and borax with boric acid H_3BO_3 (or a limited amount of borax) as a "glue" between the MgO grains; see section 4.6 on page 134.
- SVM based on hydrated *CaB_2O_4* are issued from a mix of the former two methods; they present a good cohesion upon sintering (better than $CaCO_3$), and shrink more than MgO. Indeed, while MgO (refractory alkaline earth oxide) has negligible sintering, CaB_2O_4 presents a lower melting temperature and is sintering, thus making it compatible with normal-shrinking LTCC such as DP951. The new mineral pastes are dissolved by weak acid too, but they suffer from a high reactivity; this drawback results from the compromise accorded to the cohesion brought by the high boron oxide content. The case is described in section 4.6 too.
- *Au pastes later etched in KI* (potassium iodide), although they both show very low reactivity and offer cohesion upon sintering, are of little interest for industrial manufacturing, due to the expensiveness of gold; it would therefore require systematic recycling of the dissolved sacrificial material. We have not seen any report of use other than by SIPPOLA, which validated this method for a ceramic capacitive sealed gauge pressure in 2004 [117, 118].

Evolution of SVMs from 2004 to 2010 The improvements in the field of SVM can be noted by comparing the 2004 review of PETERSON et al. from SANDIA NATIONAL LABORATORIES [119] (one of the most prolific research group in LTCC) and the review presented in this thesis. As a reminder, in their article, they listed lamination variants used in conjunction with SVM:
Enclosed unfilled volumes have been envisioned in many areas of potential use with respect to LTCC, but conventional high pressure lamination poses problems for defining such volumes [120]. Techniques have been employed that first create openings in unfired ceramic tapes and then use uniaxial lamination or fine geometries to prevent the collapse of the open volumes. High pressure lamination of tape cast layers can be used in conjunction with a filler material, either in the form of:

a) *a temporary insert (patent of* MIEHLS, *1993 [121]),*
b) *an insert that can be etched after firing (*ESPINOZA-VALLEJOS, *1998 [122]),*
c) *an insert that would disassociate during burnout and firing (again [122],* JONES *in 2003 [123, 124]),*
d) *or an insert that could be poured, shaken or flowed out after firing (patent of* CAWLEY, *1998 [125]).*

In some cases, this insert is cast in-place (patent of TRICKETT, *1989 [126]). In other instances, the insert is a discrete layer or stack matching the appropriate opening in a corresponding ceramic tape structure (patent of* ALEXANDER, *1997 [127]). Low pressure lamination without an insert through the use of an adhesive has also been described. (patent of* BURDON, *2003 [128]).* As a reminder, the use of adhesives was extensively covered in section 3.4.3.
It is interesting to trace a parallel between the above classification and the one proposed in this thesis: the class (a) techniques correspond to my first category ("before sintering"), (b) and (d) are confused in the third category ("after sintering"), while the (c) technique is clearly the second category ("during sintering", i.e. graphite in air). Since 2004 the techniques have seen nice improvements: most of the citations were patents that do not seem to have made technological breakthroughs, and we have now many controlled or promising techniques:

- for class (a), sublimable / evaporable compounds such as polyhydric alcohols and cetyl alcohol;
- for class (b) and (d), most of the mineral powders ($CaCO_3$, MO+glassy binder, $SrCO_3$, CaB_2O_4);
- only methods of class (c) existed already: first the method of PETERSON allowing high-pressure and high-temperature lamination of buried cavities, but also the method developed by BIROL for thin membranes at the same time and published the same year in [129].

4.2.2 Detailed review of SVM methods

We present here a review of the existing sacrificial volume materials methods, except our contributions, which are the subject of the next sections.

Sublimable compounds In 2009, my colleague Nathalie Serra of the EPFL-LPM successfully created microfluidic and test structures with a new type of sublimable (i.e. evaporable in the solid state) SVM: non-polymeric polyol-type organic materials, also known as plastic crystals. The organic compounds are numerous: mixes of polyhydric alcohols, TME/TMP and TME/NPG in a suitable cyclohexanol-based solvent mixture. TME-TMP stands for Trimethylolethane/pentaglycerine and Trimethylolpropane respectively, NPG for Neopentyl glycol.
The overlying structures were in silicone-graphite or ethylcellulose, as depicted in Figure 4.2; the study was presented at IMAPS EMPC in Rimini [101]. Although the substrate was alumina and not LTCC, the technique is still interesting for the lamination of green tapes, as these SVMs totally vanish around 150 °C, which is below the beginning of LTCC organics burnout (~200 °C). Furthermore, cyclohexanol (the main solvent contained in the paste) turned out to be one of the least agressive solvent for green tapes from our preliminary tests. The first tests of sublimable compounds on LTCC are expected for 2010 in our laboratory.

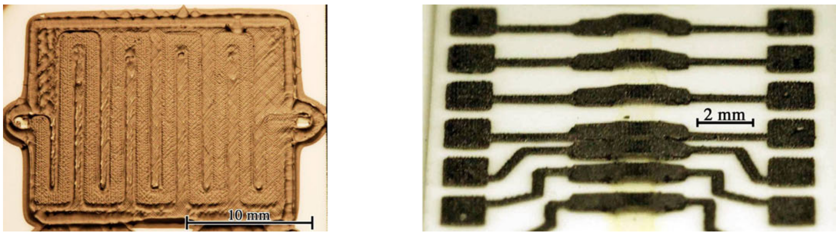

(a) *Left:* Microchannels covered with silicone-graphite. *Right:* Ethylcellulose bridges after evaporation of the underlying TME-TMP sacrificial layer (the central yellowish color witnesses of the remaining colorant).

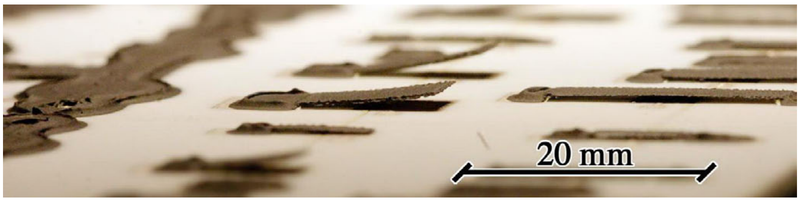

(b) Cantilevers (left) and bridges (right) in silicone-graphite.

Fig. 4.2: Examples of application of SVM sublimable compounds produced at EPFL-LPM by N. Serra and presented at IMAPS EMPC 2009 in Rimini [101].

Cetyl alcohol The use of cetyl alcohol was introduced in section 3.4.3, as it is part of the process of Malecha and Golonka [84,85,99] of Wrocław University of Technology, Poland. The alcohol is heated above 49 °C (m.p.) and poured in its liquid form into a pre-formed cavity, and, by natural cooling, it solidifies back to allow further tape processing (i.e. stacking

(a) Plan view of planar inductor.

(b) Isometric view of self-assembled inductor.

Fig. 4.3: State-of-the-art self-assembled screen-printed microwave inductors from Pranonsatit et al. [130]. Note on (b) the out-of-plane erected loop, which is the result of both tensile stresses during firing and gravity, as the substrate was suspended upside down for the firing.

and lamination, see Figure 3.23 on page 88). It later evaporates / burns out around 200 °C in air, requiring a supplementary dwell around this temperature.

This sacrificial material is applicable to unfired LTCC to help keeping the right shape during the lamination, but it can be used as a filling material only (and not as an insert), to fill cavities obtained by prelamination.

Polymer resin ink Pranonsatit et al. experimented in 2005 with success polymer resin ink as sacrificial on 96 % alumina to create self-assembled screen-printed microwave inductors (Figure 4.3). As explained in [130], they first screen printed Ferro Ag3350 low temperature silver paste to create the planar inductor. With the self-assembled inductors, two layers of 921 registration ink were deposited. After drying to remove excess solvents, the silver conductor structural layer was then printed onto the hardened sacrificial layer. The sample was placed upside down and fired at 450 °C in air, simultaneously burning off the carbon sacrificial layer. Tensile stresses within the conducting track where exploited during this final firing stage, to leave an out-of-plane self-assembled inductor depicted on Figure 4.3b. Note the out-of-plane erected loop, which is the result of both internal stresses during firing and gravity, as the substrate was suspended upside down for the firing.

Nonetheless, this SVM is not suitable for use on green LTCC because the resin polymerisation occurs at too high temperatures for the unfired tapes (see above in section 4.2.1 on page 93).

Carbon-based sacrificial layers (processing in oxidizing atmosphere) Carbon-based sacrificial layers that burn out during firing are useful for structuration of LTCC, overall for closed cavities that conserve their shape thanks to the degassing brought about by oxidation of carbon [110] (see discussion below), such as:

$$\mathrm{C\,(s) + O_2\,(g) \rightarrow 2CO\,(g)} \tag{4.1}$$

For open structures like cantilevers, this kind of SVM goes away too fast to provide mechanical support during sintering. Using them for delicate structures such as thin membranes can be difficult, due to a very high process sensitivity [7, 113, 129]. This approach has first been studied

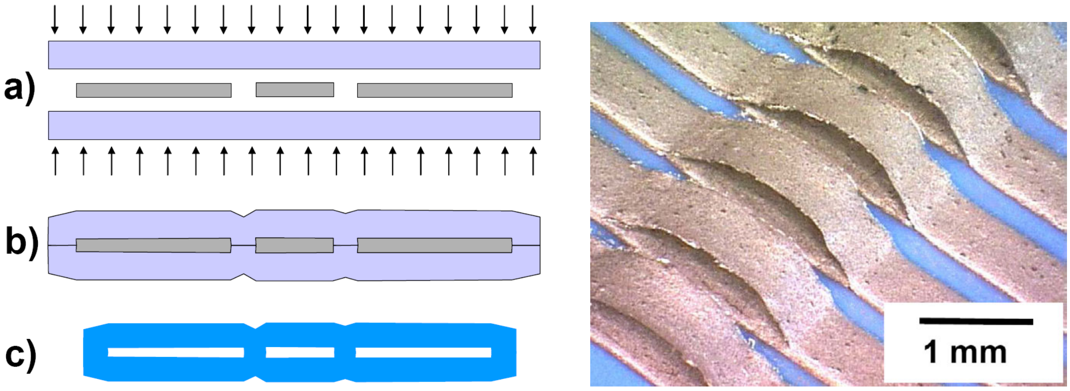

(a) Cross-sectional sketch of one sacrificial volume technique. a) tape layers and sacrificial material are collated (arrows indicate lamination), b) laminated result, c) fired appearance.

(b) Thick-film, free-standing conductor loops above thick-film lines on LTCC were created using sacrificial materials.

Fig. 4.4: Illustrations of 2004 state-of-the-art techniques from K. A. Peterson et al. of Sandia National Laboratories, Albuquerque, New Mexico, USA. [119]

for LTCC by Mário Ricardo Gongora Rubio et al. from São Paolo in 2001, who produced an excellent review of the then-existing techniques with highlight on the process steps (see [5]). They were followed by Kenneth A. Peterson et al. from Sandia National Laboratories, who favored high pressure lamination variants in 2004. In [119] they described their technique just after their review (cited at the end of section 4.2.1 on page 98):
Each of the above descriptions, that uses a sacrificial (fugitive) material, has the point in-common that a cavity is first created and then filled with a closefitting insert. We have demonstrated a technique whereby the sacrificial volume is formed during lamination by the deformation of the unfired ceramic tape around sacrificial materials and the resulting bonding of compatible areas without the use of a preexisting cavity [107]. We have accomplished this in several ways, with materials of various form and compliance. One such technique is shown in the sketch of Figure 4.4a. In (a), the LTCC tape and sacrificial material are collated. The arrows indicate that the stack will be laminated. (b) shows the result after lamination with the LTCC tape bonded in sections between sacrificial material. Finally, in (c), the clean removal of the sacrificial material during burnout and firing leaves sacrificial volumes.

A sheet or tape material with an appropriate pattern is one of the forms they have used for sacrificial material. Materials used as sacrificial materials in solid form include a low molecular weight sheet of a polymer (such as polypropylene), commercial carbon tape (TCS-CARB-1 [131] by TFT Thick Film Technologies, formerly Harmonics, Inc.), and assorted other materials and shapes, including mandrels defined with stereolithographic techniques. More SVM application from Sandia were published in 2005 in [108, 109].

Carbon-based sacrificial materials were also studied by Dr. Hansu Birol [7, 49, 110], and employed successfully for "closed" environments such as thin membranes (up to 20 mm in diameter for a spacing of 40 µm, see Figure 4.5) or narrow channels typically found in microreactor and mixers. For the manufacturing of thin membranes, our group leader T.

Maeder analyzed in [132] that the degree of swelling was found to strongly depend on many process parameters, such as the heating rate during firing, the width of the output ports and the sacrificial carbon layer thickness. Clearly, at high temperature, there is a competition between some pressure-evolving mechanism and the release of this pressure through the output ports and, below the porosity closure temperature of the LTCC, also through the porous LTCC tape. The nature of this pressure-evolving mechanism still hasn't been exactly determined: large swelling values, corresponding to an inner volume increase of a factor ≥ 3, have been observed, while the largest expected volume increase factor is only ca. 2, corresponding to the reaction: $C + O_2 \Rightarrow 2CO$. A solution to this clue might lie in graphite having a much more complex oxidation mechanism than the above reaction suggests [133]. Especially, oxygen absorption occurs before desorption of CO/CO_2, which could explain pressure evolution by dominant desorption towards the end of the firing cycle. Whatever the actual mechanism is, it must be understood and quantified in the future in order to achieve tight control of the membrane geometry.

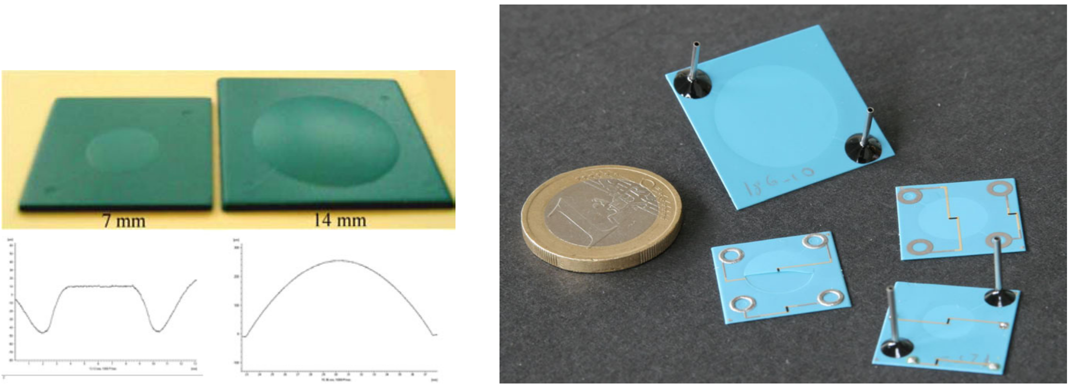

(a) Membranes with diameters of 7 and 14 mm, both fired at 5 °C/min heating rate. The corresponding surface profiles are shown below the image.

(b) Various membrane diameters: one 7 mm and two 14 mm pressure sensors with screen-printed piezoresistors on membrane and as reference (bottom right), and one 30 mm simple membrane. The post-firings were followed by completion of inlet and outlet ports with tubes or solder pads.

Fig. 4.5: LTCC membranes made with carbon-sacrificial paste in our group by H. Birol et al. at EPFL-LPM since 2004 [110].

Graphite in N_2 Pioneering, but little-known work on carbon and other sacrificial layers was carried out on classical thick-film technology, already in the early 1980's at Bosch by G. Stecher et al. [134–136]. Somehow, however, these devices did not achieve large diffusion. To our belief [132], this is due to the relatively complex processing, which involved successive firing steps in both nitrogen and oxygen, as well as the combination of unusual materials. For carbon layers, their procedure can be summarised as follows Figure 4.6:

1) Print & dry carbon layer onto zones that must be free-standing.
2) Print, dry and fire in nitrogen a porous, nitrogen-firing dielectric.

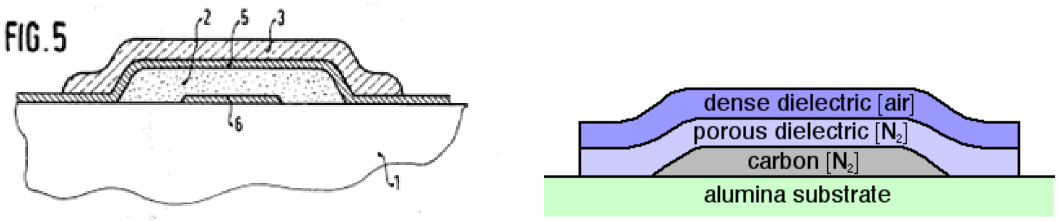

(a) Sketch issued from the patent [134].

(b) Our interpretation [132] of the of the basic layer sequence of the Stecher process.

Fig. 4.6: State-of-the-art structures created with mineral sacrificial layers: schematic cross-section views of the nitrogen process developed at Bosch by Stecher in 1983. Carbon is first printed and fired in N_2 atmosphere, then covered by a porous dielectric fired in N_2 too; this allows the carbon to be burned in air and the CO_2 to degas through the open porosity of the dielectric. The fragile hollow shape is then consolidated with dense dielectric, which is fired in air.

3) Burn out the carbon layer through the porous dielectric by heating in air.
4) Print, dry and fire in air dense dielectrics layers to build the basic structure.
5) Print the required additional layers such as conductors and resistors, . . .

While the process may look relatively straightforward at first glance, the first layer of step (4) is quite critical, due to the need to print onto the relatively weak porous dielectric, a difficult task that can make the process unreliable. Moreover, printing onto the porous carbon and dielectric layers can be difficult due to solvent loss into the pores by capillarity. Therefore, simpler, less critical sacrificial layer methods are needed; unlike the early thick-film work, however, no firing in nitrogen is envisioned.

Setter tape of Al_2O_3 as a sacrificial material This sort of SVM, also known as *SPS* for *Setter Powder Sheets* (see also in section 6.2.5) was first introduced by K. A. Peterson et al. from Sandia National Labs in 2005 [108]. SPS are (usually) commercial materials that are delivered in the same form as green tapes, and thus can be cut to the desired shape before stacking. SPS are a uniform particle size Al_2O_3 material with an organic binder contained in a paper thin sheet. The SPS binder burns away cleanly during firing, leaving a uniform distribution of setter powder in place of the fired parts. It seems however that this does not prevent the LTCC from shrinking, as would be the case when used externally in constrained sintering. Here is an extract of their publication that describes their process:
By treating a commercial setter tape from TFT *[131] as a sacrificial material, [...] we have been able to create "functional-as-released" moving parts. "Functional-as-released" in this context means that aside from removing the sacrificial material, no additional assembly is required. [...] Release consists of blowing the setter particles out of the structure, either with compressed gas or some other particular working fluid for the device. The technique we are using is to place a material in contact with the desired layers that prevents tape bonding, but then occupies the space during firing. An expansive thin layer that would sag upon firing is restrained from doing so. Deformation during lamination can be used to tighten the tolerance on a hub for a wheel. The concept for a simple wheel is shown in Figure 4.7a. [...] A space is*

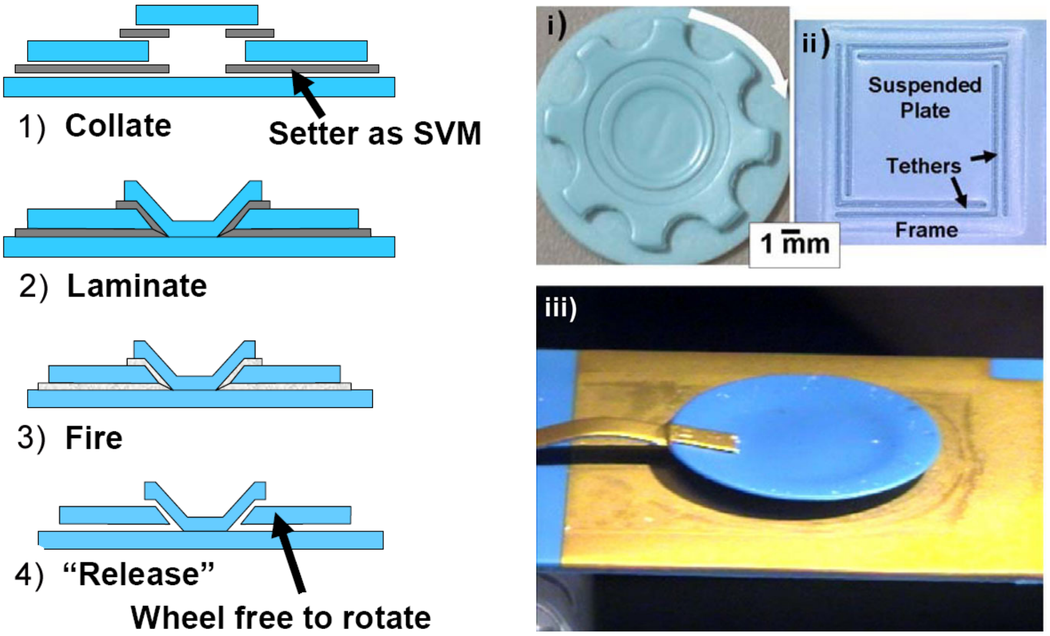

(a) Simplified illustration of "functional-as-released" LTCC wheel.

(b) *(i)* Freely rotating "functional-as-released" wheel. *(ii)* Suspended square plate tethered to outer frame. *(iii)* Suspended structure: cantilevered capacitor plate (Ø12 mm).

Fig. 4.7: State-of-the-art 2005 structures made with setter tapes as SVM; adapted from illustrations of K. A. PETERSON et al. from SANDIA NATIONAL LABORATORIES [108, 109].

defined that permits the hub for the wheel to fuse to the substrate, but keeps the wheel from sticking to the hub or to the substrate. [...] One factor to be considered is the large differential shrinkage between the setter layer (1 %) and the LTCC layer (12–15 %). Although it becomes a loose powder, trapping the material in certain ways can give rise to problems seen in laminated object manufacturing. This problem can be mitigated by using the supporting material in a pattern, such as support posts or rings, or coated with carbon SVM.

The fired wheel can be seen on Figure 4.7b (i), along with two other suspended structures: a square plate tethered to outer frame (ii) and a cantilevered capacitor plate (iii).

Other mineral-based sacrificial layers For more "open" structures, structuration with a sacrificial material that survives the firing step and supports additional layers, then is etched away by an acid as in MEMS technology, would be much more straightforward. Unlike setter tape (see above), such a structuration method also leaves no particles, which are highly undesirable in microstructures. For hints as to what materials could be suitable for such a task, we start back in 1969 with an article from VERMILYEA [137] about the rates of dissolution of natural Brucite, optical grade MgO, and commercial $Mg(OH)_2$ in aqueous solutions. MgO first reacts with water to form an $Mg(OH)_2$ layer and the rate is controlled by dissolution of the $Mg(OH)_2$. The information is interesting for SVM: there is no notable inhibition at low pH by substances such as phosphates & borates like $H_2PO_4^-$ and $H_2BO_3^{--}$. It is also not necessary to use a very low pH for the solution, because of the limitation by diffusion. This is expected, as MgO and $Mg(OH)_2$ are strong bases.

Another indication to use metal oxides such as MgO for SVM was given in 1993 by KOTANI et al. who designed and fabricated a La-modified $PbTiO_3$ (PLT) pyroelectric infrared sensor with a microcavity by MgO surface micromachining in H_3PO_4 [138]. Although this study (involving thin films) was much different from our topic (embracing thick films), it worth mentioning because of the weak acid employed. The microcavity under the sensing element was formed by etching the front surface of the substrate in order to improve the thermal properties. As the concentration in phosphoric acid decreased and Pt diffusion into MgO substrate increased, the side etch rate of the MgO substrate increased from 1.9 to 3.4 µm/min at 80 °C. The sizes of the fabricated sensor, sensing area, and etching holes were $1\times2\,\mathrm{mm}^2$, $200\times240\,\mu\mathrm{m}^2$, and $60\times120\,\mu\mathrm{m}^2$, respectively. We learn from this work that it is not worth using high H_3PO_4 concentrations to dissolve MgO: it is too destructive and does not improve the etching rate significantly. Here is what came next in literature:

$SrCO_3$ mixed to a fugitive epoxy matrix Sacrificial layers based on $SrCO_3$ (mixed to a fugitive epoxy matrix), introduced in 2007 in classical thick-film technology by CLAUDE LUCAT, PATRICK GINET, et al. [139–144], are quite convenient because this material has low reactivity and hygroscopicity, does not significantly decompose (to $SrO + CO_2$) at normal thick-film firing temperatures ($\leq 900\,°C$), and yet easily dissolves in relatively weak acid solutions; an example of application is presented on Figure 4.8. In this technique, the lack of cohesion and large porosity in the fired states facilitates etching, but requires co-firing of the SVM with the overlying structure layer (e.g. dielectric or conductor). It is desirable to avoid porosity in the dried state, because it would "steal" solvent from overprinted layers ; thus, epoxy resin was chosen as the binder of the SVM, fully plugging the interparticle space in the sacrificial material, and giving a non-porous layer after polymerization.
For LTCC, however, this sacrificial layer is essentially non-sintering, and not compatible with the lateral shrinkage of most LTCC materials. Last but not least, the use of epoxy is cumbersome in screen printing for the cleaning of screens: epoxy requires handling and cleaning separate from standard pastes. Also, the need to burn away large amounts of resin can be a quality issue in large production: a more classical binder system would be preferable.

Lead bi-silicate glass etched in HF Glass as a sacrificial material was discussed by M. R. GONGORA RUBIO et al. with lead bi-silicate etched in buffered HF in the excellent overview [5]. This method suffers from serious problems: poor solubility and selectivity:

- Due to limited solubility of the glass frit, and because it is dense, it is difficult to remove all the material.
- Ceramic green tapes are glass-ceramic composites and when exposed to BHF will etch at a rate comparable to the lead bi-silicate frit. The reactivity of glass with LTCC during firing is an issue for the selectivity upon dissolution.

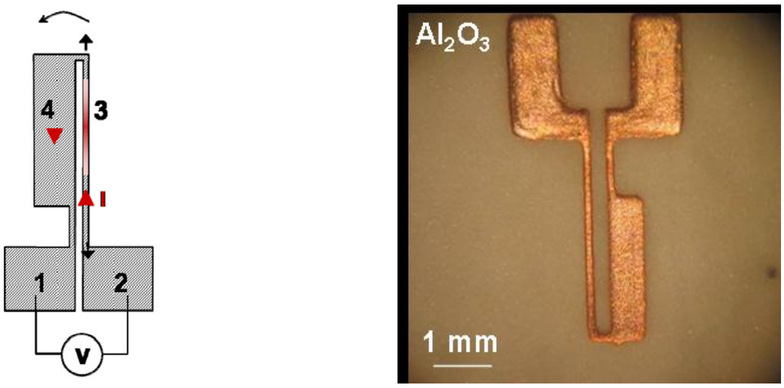

(a) Principle of actuation.

(b) Picture of a fabricated actuator, in copper on alumina substrate.

Fig. 4.8: State-of-the-art structure created with mineral sacrificial layers: a thermal actuator with asymmetric dilatation, made with a method using $SrCO_3$ and epoxy as sacrificial material [141, 143].

Thus came the idea to combine a (glassy) binder (in small quantities) to a soluble powder that would be less reactive, and still somewhat porous (to ease its dissolution).

Mineral SVM attempts at our laboratory: $CaO + B_2O_3$ Prior to this thesis at the LABORATOIRE DE PRODUCTION MICROTECHNIQUE (EPFL-LPM), my colleagues Dr. HANSU BIROL and Dr. THOMAS MAEDER had explored chemically dissolvable mineral sacrificial pastes based on mixtures of CaO (refractory) and B_2O_3 (melts at ca. 450 °C) system [7, 49, 112]. Unexpectedly, shrinkage was found to be small, ca. 7-8 %, regardless of the B_2O_3 content, and the films remained porous. This was ascribed to the high volatility of free B_2O_3 and to the high melting points of its compounds with CaO, hindering sintering. Although the open porosity made for very easy etching with acids (fuming HCl 37 %, FLUKA 84419), the low shrinkage did not allow successful co-firing with LTCC, as the Figure 4.9 can attest.
This work from BIROL was the premise of this chapter's work; attempting to improve this situation is the subject of the next section: replacing B_2O_3 with borax ($Na_2B_4O_7$, sodium tetraborate), because it is known to reduce volatility and enhance sintering.

Discussion on the dissolution of LTCC substrate When using acids for dissolving sacrificial materials, the substrate gets dissolved as well. ACHIM BITTNER et al. from SAARLAND UNIVERSITY studied in 2009 in depth the porosification process of fired low temperature co-fired ceramics LTCC substrates [19]. As a reminder, "DUPONT 951 LTCC tape consists of corundum, anorthite and a glass phase, originating after firing from a lead silicate glass [145]". A TEM-micrograph of commercial LTCC is provided on Figure B.1 on page 220.
BITTNER observed that phosphoric acid, well known as etchant for aluminium and alumina-based thin films, also attacks (at high temperature) the Al_2O_3 grains implemented in the glass matrix. For their experiments they used DUPONT 951AX LTCC tape (254 µm thick) laminated and fired standardly, and then etched in H_3PO_4 at 90 °C and 110 °C for 8 h; this

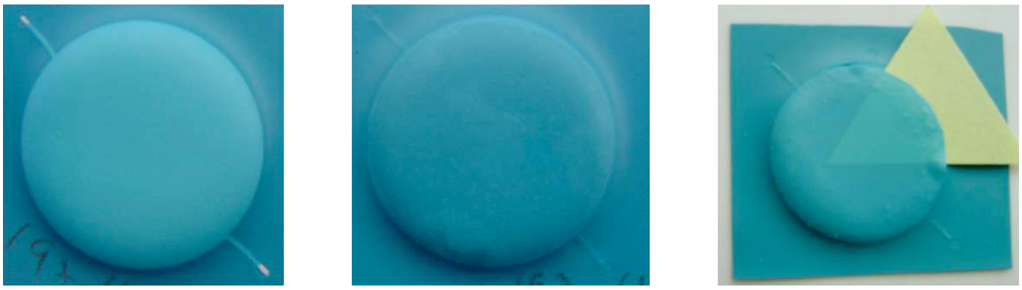
(a) Before etching. **(b)** After etching. **(c)** Spacing of a semi-open LTCC structure shown by a paper insert.

Fig. 4.9: Photographs of LTCC membranes formed with a $CaCO_3$-based mineral sacrificial paste ; the deformation due to shrinkage mismatch between the mineral sacrificial paste and the tape is obvious on all figures. The white sacrificial layer, which is clearly visible at the channels' extremities on (a), is removed following etching by weak acid. This work from Dr. HANSU BIROL [7, 112] was the premise of this chapter's work.

created a porous layer in the tape surface about 10 µm and 25 µm deep respectively, as depicted on Figure B.2 on page 221.
They also etched LTCC substrates fired at different peak temperatures (800 °C, 850 °C, 900 °C, see Figure B.3a) and observed that the higher the firing temperature, the higher the penetration depth of the etching. The composition of untreated and porous LTCC samples analyzed by XRD spectroscopy (X-ray diffraction) is presented on Figure B.3b.

From the above, we can expect that employing H_3PO_4 at ambient temperature for dissolving sacrificial materials during some minutes should have a negligible impact on the LTCC substrate; unfortunately, this is more complicated than that. Indeed, although this turned out to be true for DUPONT GREENTAPE 951, our tests from last year [146] revealed that HERAEUS HERALOCK HL2000 and HL800 LTCC compositions were directly attacked by the acids (10 % acetic or phosphoric acid etchants); HL2000, especially, completely lost consistency, i.e. its glass matrix was entirely degraded. HL800 suffered extensive surface attack, but did show qualitatively much better chemical resistance than HL2000, as can be noticed on Figure 4.10.

"Zero-shrinkage" tapes HL800 & HL2000 More information about the HERAEUS HERALOCK "zero-shrinkage" LTCC tapes can be found in the articles [147–149]. Illustrations of the HL2000 tape, which is indeed a multilayered triplex, are depicted on Figure 4.11 with schematic cross-sections, and on Figure 4.12 for SEM and optical pictures. HL800 has a similar three-layer structure.

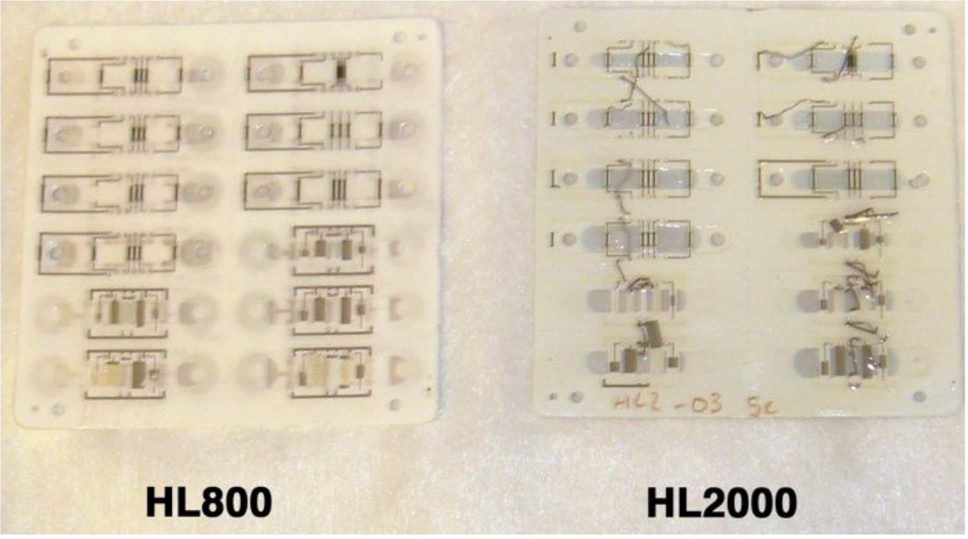

Fig. 4.10: Dissolution of HL800 (*left*) and HL2000 (*right*) circuits in 10 % acetic acid etchant; the HL2000 completely lost consistency and its screen printings. Presented by T. Maeder at IMAPS Rimini 2009 [146].

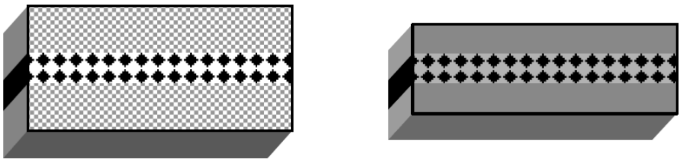

Fig. 4.11: Schematic cross-section of the three-layer Heraeus HL2000 tape, in the green state (*left*) and after sintering (*right*). [147, 148]

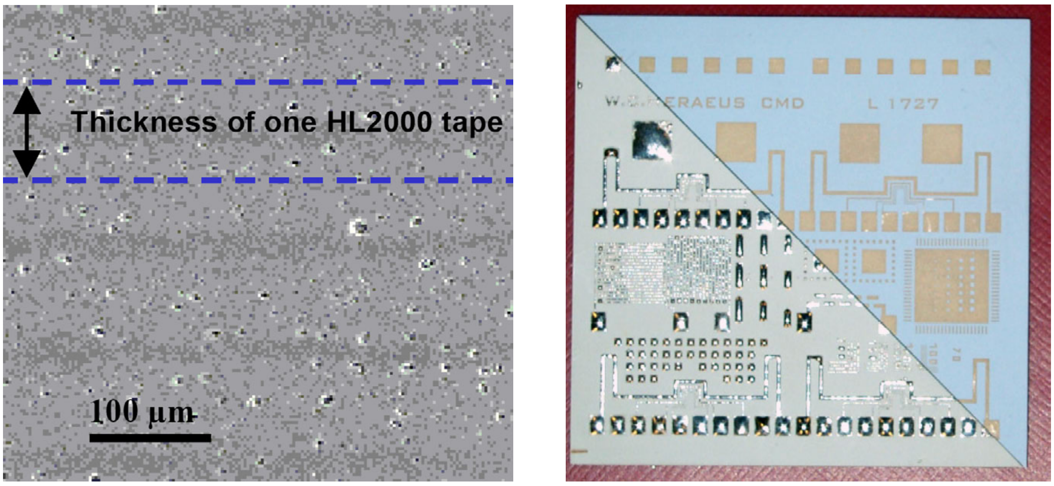

(a) Microstructure of a sintered laminate consisting of HL2000 tapes.

(b) Metallized HL2000 laminate before (*upper right half*) and after (*lower left half*) sintering.

Fig. 4.12: The “zero-shrinkage” Heraeus HeraLock HL2000 LTCC tape [147, 148].

4.3 Mineral paste formulation for alumina

4.3.1 Introduction and frame of the work

Cantilever beam force sensors based on LTCC and thick-film technology commonly apply piezoresistive strain sensing through thick-film resistors, and allow measurement of forces down to ca. 100 mN (see below the MilliNewton force sensor). Extension of this range down to µN...mN forces is attractive, because these sensors are robust and low-cost, but is no longer compatible with piezoresistive sensing. For such forces, it is more effective to measure the beam displacement rather than the strain; this requires an explanation developed in Appendix section B.3. The classical piezoresistive sensors and their limitations are presented, as well as the first direction of solution chosen by our laboratory: the replacement of alumina by LTCC to structure the cantilever beam. The second direction, abandoning the piezoresistive principle for a capacitive method, is the subject of this section.

The capactive sensor principle, enabled by a chemical solution

The second direction chosen by our laboratory to improve the initial piezoresistive sensor explores the way of sacrificial materials with chemical etching to create structures too thin for the classical approach. Mineral sacrificial layers (MSL) allow to go below the limit of ~50 µm for structures thicknesses; in effect, too thin LTCC tapes such as the 50 µm DuPont 951 suffer from strong deformations upon firing, as Birol experienced in [150]. MSLs, by ensuring a support throughout the stacking, lamination and firing process, enable to avoid the aforementioned deformations, but not the deformations of smaller order like localized bubbles or small warps due to internal elastic stresses induced by differences of thermal expansion; thus the sensor design is a compromise between ensuring a good shape and sensitivity.

As written above, piezoresistive strain measurement is not suited for thin bending structures; beam displacement is best measured with capacitive electrodes. This allows for purely passive measurements, but also active with electrostatic force cancelling to achieve higher sensitivity (with the help of extra electrodes, which can be combined [114, 151]). The capacitance involved for electrodes (2.5×2.4 mm) mounted on cantilevers of the size of the MilliNewton is relatively low (~ pF), but today's dedicated chips such as the Analog Devices AD7745/46 render the task easy, with multiple available configurations: differential, reference, temperature compensation, etc.

The challenge in creating this "variable capacitor" resides in the structuration of the cantilever – in our case, by the means of mineral sacrificial layers fired like standard thick-films, later removed by selective acid dissolution that leaves the cantilever free-standing.
The work of this section first presents the different structuration techniques, then the developed solution, followed by the prototypes that were realized in alumina (passive measurement), and discusses in depth the sacrificial paste composition and dissolution. The discussion focuses on design geometries, on foreseen improvements to facilitate dissolution, as well as on migration of the developed compositions to be LTCC-compatible.

4.3.2 Capacitive sensor principle

The goal is to make a micro force sensor of 1-2 mN range full scale behaving like a variable capacitor, and to determine the smallest measurable force. The principle is simple and depicted on Figure 4.13a: the following succession of pastes is screen printed and fired on alumina: conductor (lower electrodes + ground shield), mineral sacrificial paste (MSP), conductor (upper electrodes), and dielectric (i.e. the cantilever). The MSP must then be dissolved by acids (HCl or H_3PO_4). The challenge is twofold: the acid must act selectively (only the MSP must be affected and removed totally), and the MSP must not react with adjacent pastes or with the LTCC tape.

Once the MSP is removed, contacts are established on the electrodes by gluing standard DIL pins. The displacement of the cantilever (due to an external force) reduces the distance between the capacitive electrodes, and the variation of capacitance allows the measurement of the applied force. By adding a pair of reference electrodes and a non-moving cantilever of same characteristics, the capacitance measurement can be done differentially, significantly reducing perturbations induced by temperature and humidity.

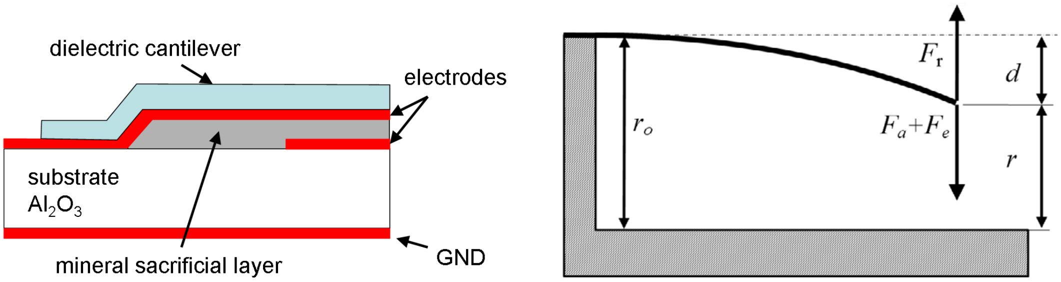

(a) Cross section displaying the layers and the mineral sacrificial paste.

(b) Forces for capacitive measurement (passive and active).

Fig. 4.13: Schematic representations of the capacitive cantilever force sensor in alumina.

Theory of the passive capacitive force sensor As can be seen on the schematic diagram of the forces in Figure 4.13b, the force to be measured (F_a) is applied at the tip of the cantilever, which bends and acts like a spring with an elastic return force $F_r = -k \cdot d$, where k is the spring constant and d is the displacement. The capacitance C between close parallel planar electrodes can be written as:

$$C = \frac{\varepsilon_0 \cdot \varepsilon_r \cdot A}{r} \tag{4.2}$$

with:

$\varepsilon_0 = 8.854 \cdot 10^{-12}$ [F · m^{-1}]	the dielectric constant ;
$\varepsilon_r = 1$	the relative permittivity of air ;
A	the electrodes area ;
r	the gap between electrodes.

By introducing r_0 as the initial gap between electrodes to Equation 4.2, the non-linear relation between applied force and measured capacitance is:

$$C\left(F_a\right) = \frac{\varepsilon_0 \cdot \varepsilon_r \cdot A}{r_0 - \frac{F_a}{k}} \tag{4.3}$$

The last force of Figure 4.13b, F_e, is an optional electrostatic force used in the case of active measurement. Unfortunately, this has not yet been tested, as the specific electronics were not developed; however dedicated electrodes are already implemented on the design for future tests. The theory of active measurement is presented in Appendix section B.4.

4.3.3 Sensor designs and geometries

Two beam designs have been tested: the simple cantilever (Figure B.9a left) and the bridge (Figure B.9a right), as depicted on page 227. Both geometries present pros and cons (see Table B.1); the best design will be chosen after extensive testing.
The goal is to avoid a too rigid beam, while providing at the same time a surface large enough to place the electrodes on the beam; the beam section will then be relatively large (a few mm) but very thin (40 µm) compared with the most sensitive MilliNewton force sensor (250 µm). In order to minimize the rigidity, and overall to decrease the influence of curling effects (cf. the interesting parenthesis of subsection B.5.2) due to firings or upon removal of the MSP, the beam deformations are concentrated in distinct zones by adding holes and hence by diminishing its cross section (Figure B.9b). The holes should be the largest possible, while keeping the minimal safety margins for screen printing.
Six variants have been selected, with variable overall lengths (7 to 15 mm), and presence or not of inner cut(s) and their lengths (1 to 6 mm), as listed in Table B.2 on page 228. The beam width was fixed at 3 mm for all variants (Figure B.10). Its spring constant k can be adapted by varying the beam length L or its thickness h upon screen printing. The holes' corners are rounded to avoid stress concentration.

Electrodes and capacitance The electrical pins and electrodes are placed as depicted on Figure B.9c. This allows using the same electronic setup for all variants, and in the future to add the active electrostatic feedback without hassle. On the mobile part of the beam, the two electrodes (measurement and active compensation) and their tracks are placed in a manner as symmetrical as possible to limit beam distortions during manufacturing, and during active measurements too.
We have supposed that the MSP forming the gap r between top and bottom electrodes will be from 40 to 60 µm. With a surface $A = 6\,\mathrm{mm}^2$, we can calculate for the different variants the no-load capacitance C_0, and for example the capacitance $C_{0.5}$ corresponding to a beam displacement $r = 0.5 \cdot r_0$. From Equation 4.2 we get:

- C_0 between 1.33 pF and 0.89 pF;
- $C_{0.5}$ between 1.77 pF and 2.67 pF.

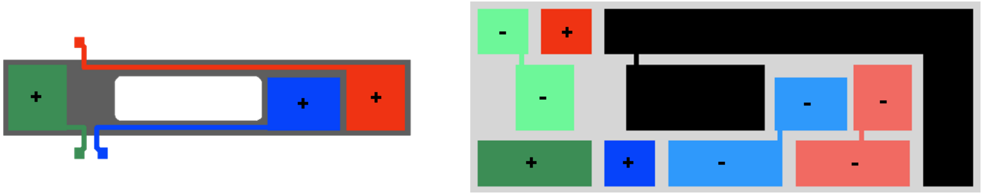

(a) Simple cantilever (*left*) and alumina base (*right*) virtually separated.

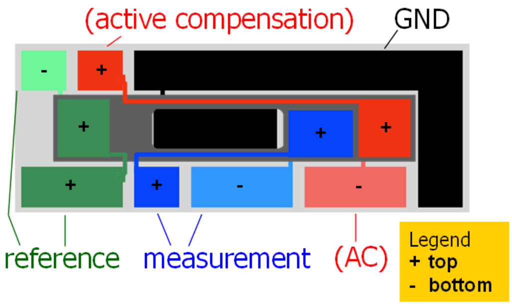

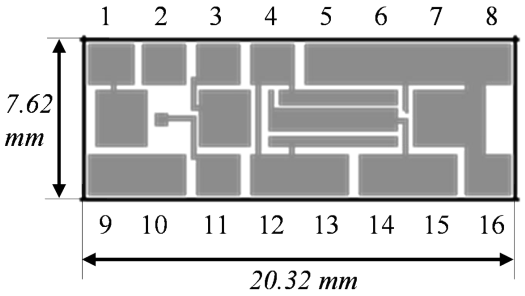

Pins	**Function**	**Pins**	**Function**
1, 9	Reference	2, 15	Compensation
11, 13	Measurement	8, 16	GND

3-7, 10, 12, 14: not connected

(b) Simple cantilever screen printed on alumina (resulting from the merging of (a) sub-parts). The + and - signs refer to the same set of electrodes.

(c) Repartition of pins on the alumina base for the bridge cantilever variant ; the non-connected pins allow mounting the different variants on the same electronic setup.

Fig. 4.14: Top-view disposition of pins and electrodes of the capacitive sensor for two variants: simple cantilever (a)+(b) and bridge cantilever (c).

We are therefore inside the range of measurement of the capacitive chip (maximum 4 pF). To summarize, the estimated capacitance is around 1 pF without force, and 2 pF at 50 % displacement.

4.3.4 Thick-film paste selection

Apart from testing different cantilever geometries as seen above, it is also possible to change the order, the type and number of screen-printed pastes. The following considerations have led to eight screen printing variants V1. . . V8 depicted on Table 4.2:

- It is mechanically favorable to have a sandwich cantilever (dielectric - conductor - dielectric) with the "soft" layer in the middle, to avoid an asymmetric bending due to thermal stresses.
- The passive measurement principle accommodates this sandwich easily. For active electrostatic compensation however, an additional dielectric layer in addition to air is not possible.

- The cantilever being mechanically governed by the dielectric layer, it is wise to print two or more dielectric layers on top of each other to ensure good mechanical stability and homogeneity.
- The goal is to measure the smallest possible forces; one variant with only one dielectric layer to lower stiffness is hence interesting.

Table 4.2: Screen printing variants for the capacitive alumina sensor. Variants V4 output the best results; V1-V2 and V5-V6 were fired correctly, but suffered from dissolution; finally V3+V7-V8 were unusable. See text for legend.

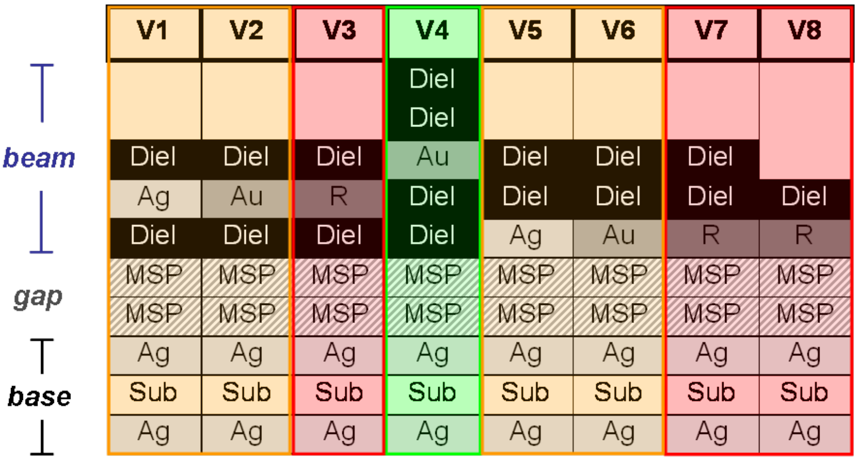

	V1	V2	V3	V4	V5	V6	V7	V8
beam				Diel				
				Diel				
	Diel	Diel	Diel	Au	Diel	Diel	Diel	
	Ag	Au	R	Diel	Diel	Diel	Diel	Diel
	Diel	Diel	Diel	Diel	Ag	Au	R	R
gap	MSP	MSP	MSP	MSP	MSP	MSP	MSP	MSP
	MSP	MSP	MSP	MSP	MSP	MSP	MSP	MSP
base	Ag	Ag	Ag	Ag	Ag	Ag	Ag	Ag
	Sub	Sub	Sub	Sub	Sub	Sub	Sub	Sub
	Ag	Ag	Ag	Ag	Ag	Ag	Ag	Ag

Legend of layers shown in Table 4.2:

Sub	0.635 mm thick, 96 % alumina substrate A476 from KYOCERA [152]
Ag	silver-palladium Ag:Pd paste (ESL 9635B)
MSP	mineral sacrificial paste (see later)
Diel	dielectric paste (ESL 4913)
Au	gold paste (DUPONT 5744)
R	resistor paste (DUPONT 2031)

The dielectric was chosen among three compositions from ESL (n°4903, 4913, 4924), after early dissolution tests (see later). While the ESL 4903 resisted to acids, it formed bubbles with the MSP; the ESL 4924 was totally dissolved by HCl. The screens used had a meshing/emulsion of 325/30 mesh/µm for conductors, 200/40 for dielectric and 200/50 for the MSP.

4.3.5 Sacrificial paste preparation

The original recipe of the work of Dr. Hansu Birol [112] consisted of $CaO + B_2O_3$, or $CaO + H_3BO_3$. The role of the CaO (Alfa Aesar 99.95%, 010923) is to be the skeleton of the paste, as its melting point is high (2572 °C). The H_3BO_3 or B_2O_3 acts as a binder during firing; it melts at 450 °C. The idea of Birol of using fluxing agent within an alkaline earth mineral matrix was explained in light of these results: H_3BO_3 dehydrates to B_2O_3 (glass) around 160 °C and then melts at 450 °C, which then wets and fills the porous CaO matrix. This leads to formation of a consolidated structure, which is not dense, thus etchable with the appropriate solvent.

Continuing his work, we decided to modify the initial MSP recipe because it gave a very porous paste. It would have not been an optimal a basis for two reasons (both however later turned out to be null and void):

a) A too high porosity is not good for future fine screen prints: if the paste solvent gets absorbed by the underlying MSP during the pass of the squeegee, adverse effects can occur like premature drying and cracks. We have since developed "rich" vehicles overcoming this issue (see subsection 4.6.1).

b) Hygroscopicity: a highly porous paste is prone to absorb air humidity, which is deleterious to CaO after firing (see later). This issue was solved by using MgO, which is less reactive.

It is worth mentioning that we decided to persevere using CaO for the skeleton instead of $CaCO_3$, MgO, or $SrCO_3$ (which I did not know at the time) from the experience of my predecessors. $CaCO_3$ was first tested by Birol [112], but in order to avoid possible complications brought about by the carbonate decomposition (such as bubble formation) in addition to his visual observations, we decided to continue the experiments with CaO.

Thus, we tried to substitute the boron oxide with borax (anhydrous sodium tetraborate $Na_2B_4O_7$, Riedel-de Haën granulated dry 98 %, 11648), known for its good vitreous and melting properties (melting point at 743 °C for the anhydrous form) and lower volatility, in order to better join CaO grains; borax alone dissolves well in HCl or H_3PO_4. As we are working on alumina, we are less subject to shrinkage issues than on LTCC – for the time being.

To determine the best CaO/borax mix, initial tests have been carried out with varying proportions. Both powders have been mortar grinded (Retsch RM100) for at least 1 hour before careful weighting (with a Denver Instruments balance) and mixing. Then an experimental organic binder was added to the mix, before passing through a tricylinder grinder (i.e. three-roll-mill EXAKT) to further reduce grain size and to get a homogeneous paste suitable for screen printing. The organic binder had the composition listed in Table 4.3; it was magnetically stirred for over 1 hour at 60 to 80 °C (Fischer Scientific stirrer). The equipment used can be seen on Figure B.4 on page 222.

Sacrificial pastes tested Seven pastes were prepared, with the following proportions of borax compared with CaO (in % volume / volume): 10, 20, 40, 50, 60, 70, and 80 %. Rapid tests of

Table 4.3: Experimental organic binder composition, used as paste vehicle (solvent + plasticizer + ethyl cellulose).

Component	Manufacturer	Code #	CAS #	Mass [g]	Mass [%]
Terpineol	Fluka (anhydrous)	86480	8000-41-7	32.00	64.5
Dibutyl Carbitol™ di(ethylene glycol) dibutyl ether	Sigma-Aldrich 99+ %	20,562-1	112-73-2	16.00	32.2
Ethyl cellulose viscosity 300 cP *	Sigma-Aldrich	20,065-4	9004-57-3	1.64	3.3

* measured as a 5 % solution in toluene/ethanol 80:20 (lit).

firings (in the SierraTherm belt air furnace, with a temperature profile 850 °C - 45 min) of all envisioned pastes on alumina showed the behaviors presented in Table B.3 on page 230.

Final sacrificial paste From the above experiments it turns out that the most suitable compositions are the 40 % and the 50 % of borax. The 40 % decomposed within a few days, so we decided to go with the 50 %. This was *a posteriori* a mistake, as it finally proved difficult to dissolve. Using the 40 % borax would had been smarter, but the subsequent screen printing operations would have needed to take place immediately afterward, in order to avoid short-term destruction by air humidity.

Thus, the 50 % powder mix was stirred with organic binder in proportions 60-40 % (mass-mass) respectively, as listed in Table 4.4. The same procedure as described before was used (mortar and tricylinder grinding).

However, no dispersant (acetylacetone, Sigma-Aldrich 99+%) was added in the final paste. Dispersant is usually added as 5 % of the powder mass to enhance screen printing pastes, but a test turned to disaster: upon paste stirring the mix suddenly heated, and after firing the resulting paste was yellowish, completely cracked and easily removable; probably a reaction between acetylacetone and CaO.

The sacrificial pastes were screen printed with a 200/50 screen mesh.

Table 4.4: Composition of final mineral sacrificial paste with 50 % borax and 50 % CaO (in % of volume of the mineral part). The mineral part was then mixed in proportions of 60-40 % (mass-mass) with the organic binder.

Component	Manufacturer	Code #	CAS #	Mass [g]	Mass [%]
Borax (sodium tetraborate) $Na_2B_4O_7$	Riedel-de Haën granulated dry 98 %	11648	1330-43-4	7.81	24.8
Calcium oxide CaO	Alfa Aesar 99.95% (metals basis)	010923	1305-78-8	11.06	35.2
Organic binder (experimental)	EPFL-LPM	see Table 4.3		12.58	40.0
Total				34.82	100.0

4.3.6 Results of pastes firings and dissolutions

Paste compatibilities upon firing The screen printing went relatively well, despite some tridimensional problems (vias filled by adjacent layers, tight margins). The MSL fired thicknesses were 30 µm after a first pass and 50 µm after a second pass, enough to ensure a good cantilever displacement range, but just enough to allow for good circulation of acid during dissolution.
Already at this stage, some paste combinations can already be discarded, as indicated by the colors of Table 4.2:

- Resistor-dielectric (V3, V7, V8) and MSP-Au-dielectric (V2) led to bubble formation (see Figure 4.15a for V2 and Figure 4.15b for V8), strongly affecting mechanical properties for the resistance variants.
- Strange black stains spread around the MSP for the resistor variants (V3, V7 and V8); however no other complications were encountered.
- V1 and V5, the silver versions of V2 and V6 respectively, presented intermediate results: although the firing went well, the dissolution test led to the mechanical destruction of most cantilevers in the arms.
- Some V2 sensors could have been used if their cantilever had not been curved upward after dissolution (Figure 4.16). V6 sensors, despite having their cantilever well separated, suffered from detached electrodes and broken cantilevers.
- V4 gave overall the best results: an alternative to V2 and V6, it isolates well the gold layer from the MSP with two dielectric layers.

Dissolution of sacrificial layer This step is indeed not yet under control for pastes containing large amounts of borax; especially the sodium oxide Na_2O of borax tends to react with adjacent layers and renders dissolution of buried MSP difficult. In particular, the Ag:Pd lower electrodes stick to the MSL and lose adhesion to the alumina substrate upon dissolution.
First tests were done with diluted HCl (Fluka 32%), but it was too strong and we switched to H_3PO_4 (Sigma-Aldrich, 98+%) to (hopefully) increase selectivity. Systematic tests were

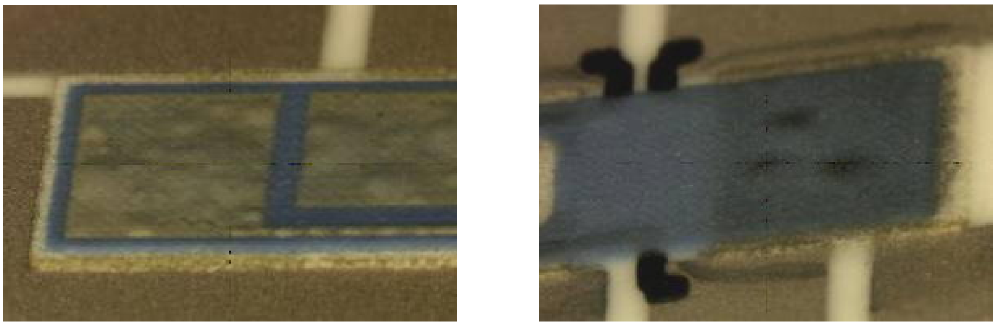

(a) Variant V2, cantilever electrodes **(b)** Variant V8, reference electrode

Fig. 4.15: Photographs of bubbles on thick-film cantilevers due to paste incompatibilities.

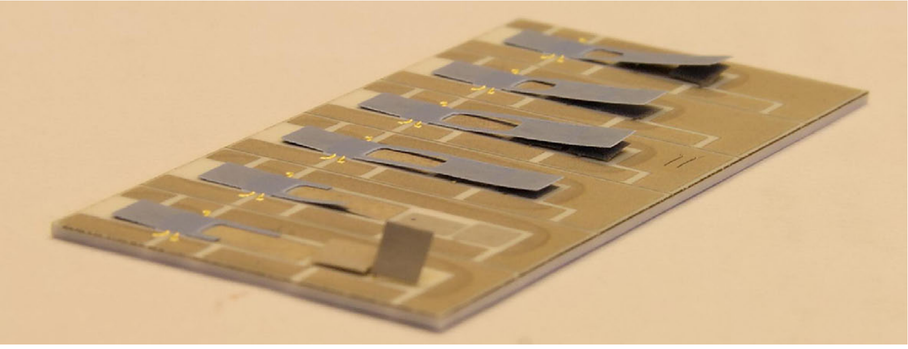

Fig. 4.16: Six cantilevers of variant V2 (Au-dielectric-Au) after 5 h 30 of dissolution in H_3PO_4. Note the detached lower Ag:Pd electrodes on some sensors. The whole fragment dimensions are about 45×20 mm.

carried out with alternating dissolution (1 hour) and rinsing (1 hour in DI water), in order to characterize the variants. This loop was repeated until all cantilevers of a variant were detached enough. Figure 4.16 shows the result of dissolution for variant V2 after 5 h 30 immersed in H_3PO_4.

The best results were obtained on sensors left 30 hours in 80-90 °C phosphoric acid, then thoroughly rinsed (first DI water for 1 to 8 h, finishing by IPA) and air dried at max 100 °C (at 150 °C the temperature bends and cracks the cantilever). Please refer to the report of my student Simon Wiedmer [114] for the listing of all intermediate variants.

Of course this procedure is way too long and the selectivity is not good enough for an industrial process; much better results will be presented in section 4.4 on page 121

Force measurements on sensor Please refer to section 5.4.1.

Assessment of design variants and flaws The different layouts proved to be relatively good; surprisingly, both sandwich and asymmetric cantilever designs were successful upon manufacturing and measurement. Nevertheless some design flaws were obvious:

- Variants with very long cantilevers and long inner cuts tend to be more quickly unusable than short ones, because they twist and tear easily.
- For bridge variants, the square via in the middle of the dielectric layer (i.e. variants PT and PP of Table B.2 on page 228) turned out to be too small (300 µm×300 µm) and hence impossible to fill properly, because it is located in a hole of the sacrificial layer that gets clogged by the dielectric paste. Indeed this ESL 4913 ink is relatively liquid, and upon screen printing it flows in the hole and clogs it, as schematized on Figure 4.17 and depicted on Figure 4.18b (to be compared with Figure 4.18a).
- Conductor tracks located close to one another can sometimes touch each other after screen printing, causing a short circuit. This is especially the case with the Ag:Pd paste (ESL 9635B, see Figure 4.18d), whose print definition was much lower than the gold

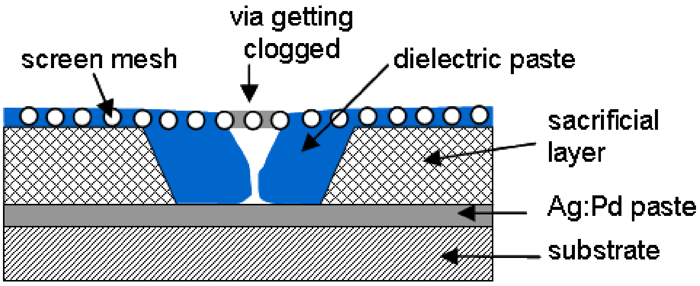

Fig. 4.17: Via getting clogged due to overflowing of the dielectric paste into a tailored hole in the sacrificial layer: there is no more room for the next conductor layer to make connection with the underlying Ag:Pd layer.

paste (DP 5744, see Figure 4.18c), despite using the same screen mesh (325/30). This can be prevented by increasing their spacing of 100 µm to 200 µm.

- The current layout is relatively complicated as it allows wiring all electrodes separately; however we are wiring electrodes by pairs on our signal conditioning chip, and at least one electrode of each pair is connected on the same pin; we could thus simplify the layout by linking, for instance, all the bottom electrodes.
- It is necessary to screen print at least two layers of dielectric paste to form a robust-enough cantilever beam. Adding a third or a fourth layer increases the beam thickness and rigidity only slightly, this can hence be afforded. Furthermore the dielectric becomes less fragile and the probabilty of pinholes decreases with an increased number of layers: the process reproducibility probably increases too.

4.3.7 Conclusion of this study

The manufacturing of a capacitive microforce sensor has proved to be feasible in thick-film technology on alumina with mineral sacrificial layers, but not yet on DP951 LTCC, due to shrinkage and dissolution issues. The manufacturing process, involving the dissolution of a mineral paste made of CaO and borax in a weak acid, is nonetheless too long and not yet completely controlled: the interactions of the mineral paste with adjacent electrodes is currently too strong, yielding a poor ratio of functional sensors after dissolution.

Sensor performance As described in subsection 5.4.1 on page 173, the sensor shows a force range of ~2 mN with a resolution of ~1 % of full scale, which is quite good for passive measurement. Active measurement with electrostatic counteraction was eventually not implemented.

Mechanics Both sandwich and asymmetric cantilever designs proved to be successful. Simple cantilevers tend to be easier to dissolve than bridges; however no extensive tests could be done on mechanical aspects.

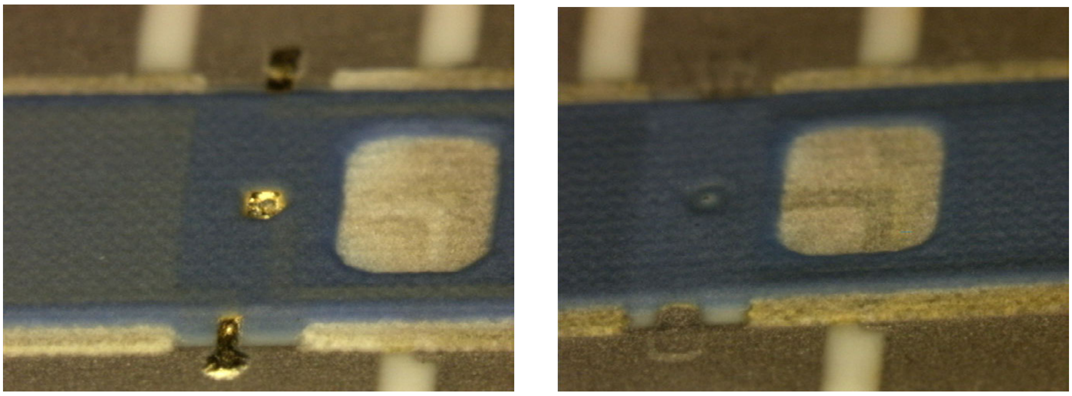

(a) Via of V4 well defined.

(b) Via of V5 clogged by dielectric paste.

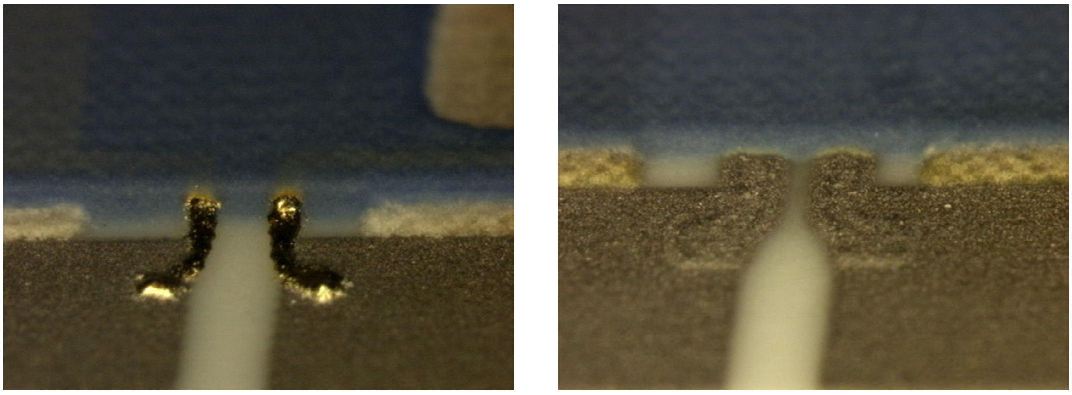

(c) Electrodes of V4 well defined.

(d) Electrodes of V5 too close to each other (bad printing definition).

Fig. 4.18: Details of variants V4 (diel 2x-gold-diel 2x) and V5 (Ag:Pd-diel 2x) highlighting design flaws. For an idea of thescale, the blue dielectric cantilever is 3 mm wide.

Chemistry From a chemical point of view, resistor paste has seen strong interactions with dielectric upon firing; silver conductors fired apparently well, but turned out to be defective upon dissolution. Finally gold conductors were the best choice, despite some bubble deformations.

Regarding the mineral sacrificial paste (MSP), the volume ratio of the mineral powder tested was 50 % CaO + 50 % $Na_2B_4O_7$, but it would have been more interesting to test the 60 % CaO + 40 % $Na_2B_4O_7$ version. In effect, this latter paste contains less sodium, but must be processed faster due to its higher hygroscopicity. It turned out that the borax, presumably its sodium oxide Na_2O content, tends to react with and degrade adjacent layers, rendering dissolution difficult; this observation is *a posteriori* not surprising, knowing that sodium oxide is a highly reactive flux that strongly degrades the acid resistance of glasses.

Continuation of research

At this point, the research can be oriented in two directions:

a) With the intention to stay on substrates that do not shrink laterally, by improving the MSP/SVM composition to reduce its reactivity with adjacent layers upon firing, facilitate its dissolution and avoid self-destruction due to moisture, and by adapting the organic vehicle to address screen printing issues; this is developed in the Perspectives section in subsection 4.6.1.

b) By diverting to shrinking substrates (i.e. like DP951 LTCC) with the adaptation of the mineral compound, the glassy binder and the organic vehicle (to reduce the solvents aggressiveness on the tape). Rapid tests carried out right after this phase of the study led to an interesting solution towards reducing the sodium content by making a paste with 60 % volume of CaO, 15 % of borax and 25 % of H_3BO_3 (or B_2O_3, almost equivalent). Although the new paste shrinkage should be the same as with the former recipe, the new ink was swiftly tested on DP951 LTCC, yielding predictable disastrous results, as Figure 1.10 on page 25 can testify. To conform to this LTCC tape, the MSP shrinkage has to be increased (from 7-8 % to 15 %). At that time we got the idea to add bismuth borate BiB_3O_6 [153], known to melt at 726 °C (it is congruent), but we never tried this compound eventually. After reflection, using an eutectic of the system Bi_2O_3-B_2O_3 would allow for a lower melting temperature, even an adjustable temperature.
The migration of the MSP to LTCC will be developed in the next section.

4.4 Mineral paste formulation for LTCC

4.4.1 Introduction

In the field of three-dimensional silicon micro-electromechanical systems (MEMS), the use of sacrificial materials removed at the end of processing has been studied for nearly thirty years and is now standard. However, it is more seldom used in thick-film and LTCC technology. So far, only silk paper or methods for closed cavities (such as carbon-based fugitive phases) have been available on LTCC. Mineral sacrificial pastes (MSP) have been successful on alumina substrates (see [139] and section 4.3), but not yet on free-sintering LTCC due to the shrinkage mismatch between the MSP and the LTCC that inevitably leads to strong deformations [113]. We must nonetheless mention the case of SCS (self-contrained sintering) tapes such as the Heraeus HeraLock, also known as "zero-shrinkage" tapes: the case is very interesting too, as the MSP organic binder must be adapted to those of the tapes, but the problem is quite different because of the near absence of in-plane shrinkage. At the time of this study we were not using HL products; its was however later studied by my supervisor T. Maeder (see section 4.6).

This section presents a novel way to make free-standing structures on LTCC under unconstrained sintering, using mineral sacrificial pastes made of carbon and calcium carbonate. The volume ratio of the final mineral powder is 28 % $CaCO_3$ and 72 % C, which is then mixed with an organic binder in mass proportions 60 % - 40 % respectively. The remaining material is easily removed after firing by dissolution in diluted weak acid (H_3PO_4).

Frame of the Work This work took place in the development of a capacitive LTCC anemometer for the MC2, a 10-gram indoor slow flyer used for bio-inspired neural network research by Zufferey et al. [154] from the Laboratory of Intelligent Systems (EPFL-LIS), which is depicted on Figure 5.30 on page 176; its speed ranges from 0.5 to 3 m/s. The motivations are explained in subsection 5.4.2.

4.4.2 Studied sensor: the capacitive anemometer

The physical principle that lies behind this capacitive anemometer is simple, and nearly the same as for the sensor on alumina of subsection 4.3.2: electrodes are deposited on adjacent surfaces of LTCC tape facing each other, one being the base and the other one the moving cantilever. At the electrodes position, the tapes are initially separated by a gap r_0 formed by the mineral sacrificial paste (MSP). After firing the MSP is dissolved, leaving a free cantilever. It is easy to understand that the wind pushing on the cantilever produces a force that bends the cantilever, moving down the top electrode, and thus the gap r will decrease as the electrodes get closer. It induces an increase in capacitance that will be used to calculate the relative air speed of the slow flyer; the underlying theory is explained hereafter. Figure 4.19a depicts a schematic view of the sensor, not yet striped of its mineral sacrificial layer, which lies between the base and cantilever.

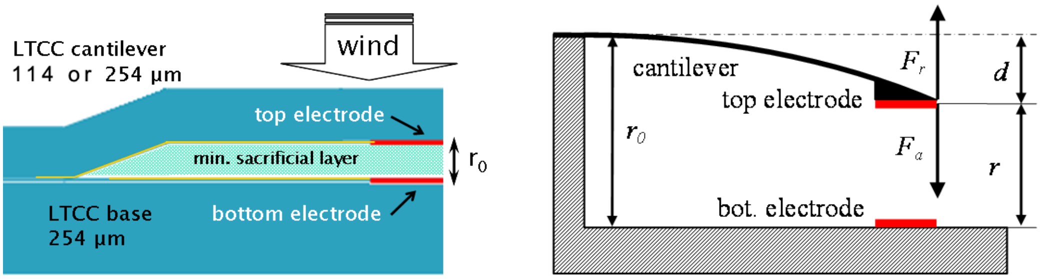

(a) Cross section of the sensor not yet stripped of its mineral sacrificial layer (fitting the gap of height r_0). Unfired tape thicknesses are indicated.

(b) Forces and distances; electrodes are considered to stay planar throughout the cantilever movement.

Fig. 4.19: Schematic representations of the capacitive anemometer (cantilever microforce sensor) in LTCC

Theory of the capacitive force sensor The same theory seen in section 4.3.2 applies: the force to measure (F_a) is applied at the tip of the cantilever, which bends and acts like a spring with a return force $F_r = -k \cdot d$, where k is the spring constant and d the displacement; figure 4.19b schematizes the mode of operation. Given the small displacement of the cantilever, the capacitor formed between the electrodes can be assumed to be planar. The capacitance can be written the same as Equation 4.3 developed on page 110:

$$C\left(F_a\right) = \frac{\varepsilon_0 \cdot \varepsilon_r \cdot A}{r_0 - \frac{F_a}{k}}$$

4.4.3 Mineral paste composition determination

As seen in subsection 4.3.5, the attempt to improve the mineral sacrificial paste by replacing B_2O_3 with borax ($Na_2B_4O_7$, anhydrous sodium tetraborate, m.p. 743 °C) gave mitigated results. Altough the feasibility of mineral sacrificial paste in standard thick-film technology on alumina substrates was shown using a paste with 50 % borax $Na_2B_4O_7$ and 50 % CaO (% volume) mixed with an organic binder, the removal of this layer was problematic. As described in section 4.3.6, it proved to be possible by dissolution in H_3PO_4 at 80 °C for 30 hours, followed by rinsing in deionized water for some hours, and drying in air at 100 °C, which is cumbersome. The main reason was because the sodium oxide Na_2O contained in borax tended to react with the adjacent layers (hence degrading them), which then tended to lose adherence to the substrate when exposed to the H_3PO_4 etching medium. Thus we tried a paste containing less sodium, i.e. 60 % vol. CaO, 15 % borax and 25 % H_3BO_3; the reactivity with conductors was decreased, but not the shrinkage mismatch (see item 2).

Still, the underlying goal to obtain a MSP suitable for LTCC was not reached, due to shrinkage and dissolution issues. To conform to DP951 LTCC the shrinkage had to be increased (from 7-8 % to 15 %); the pursued developments have reached this aim, which is the subject of the following paragraphs.

Here is the list of criteria with which the MSP must comply. It must:

Table 4.5: List of minerals used for MSP preparations, with specific masses used in calculations, as well as melting points. The calcium carbonate $CaCO_3$ was used in the second part of tests.

Mineral	Manufacturer	Code #	CAS #	Particle size	Density ρ [g/cm^3]	Melting point [°C]
CaO	Alfa Aesar 99.95% (metals basis)	010923	1305-78-8	< 10 µm	3.35	2572
C	TIMCAL	TIMREX KS5-44	7782-42-5	27 µm	2.25	-
H_3BO_3	Sigma-Aldrich 99.99 %	33 906-7	10043-35-3	-	1.44	160
$CaCO_3$	Alfa Aesar 99.5 % (metals basis)	11403	471-34-1	5 µm	2.93	800

- . . . ensure physical support of 3D structure before and during the sintering, and possibly offer some cohesion;
- . . . produce no deformation of the LTCC;
- . . . be chemically compatible with electrodes;
- . . . be easily applied by screen-printing;
- . . . be easily removed after firing (by dissolution or other mean).

To reduce the workload associated with screen printing, rapid tests were carried out on leftover LTCC (DP951 254 µm) to eliminate the most unsuitable paste compositions. Manual screen printing was then done through a simple metallic screen to refine the MSP compositions until an acceptable solution was found. The final tests were carried out with different variants of paste superpositions and conductor tracks (standard and PTC resistor, or Ag:Pd conductors). The results are presented hereafter.

List of minerals and organics Table 4.5 summarizes the minerals used for MSP preparations. Note that the specific mass may vary depending on manufacturer, and is sometimes listed as a "density range"; for example CaO is stated at 3.25-3.38 by Alfa Aesar).

Only the boric acid H_3BO_3 was mortar ground (1 hour, Retsch RM100), because of agglomerates. Others were fine enough to be used "as is". All powders were carefully weighted (Denver Instruments) and thoroughly mixed. Then the mix was gradually added to an experimental organic binder that has the composition listed in Table 4.3 on page 115, and which was magnetically stirred for over one hour at 60 to 80 °C. The proportions of mineral powder and organic binder are 60 and 40 % (mass-mass) respectively, for all pastes listed subsequently.
To save time, none of initial test pastes were further grinded. Only the last screen-printed series of paste were passed through a three-roll mill (EXAKT); the operation only slightly improved the geometry of deposited paste.

Table 4.6: Initial MSP tests on leftover DP951 LTCC with calcium oxide, carbon and boric acid: volume proportions of the mineral part, and resulting observations: LTCC deformations, gap quality and easiness of removal. The paste O8 is interesting in terms of deformation but lacks a skeleton to support the upper structure.

Code	Volume ratio [%]			Initial MSP results on leftover DP951 LTCC		
	CaO	C	H_3BO_3	LTCC deformations	Gap quality	Mean of removal
O1	60	0	40	strong	bad	manual wiping
O3	50	20	30	average	average	manual wiping
O4	50	0	50	strong	bad	manual wiping
O7	100	0	0	very strong	very bad	manual wiping
O8	**0**	**100**	**0**	**none**	**very small**	**acid + US bath**

Initial tests of MSP: CaO, C and H_3BO_3 The initial tests were done directly without borax, to eliminate the earlier encountered problem of sodium reactions with electrodes. For the shrinkage adaptation we had thought of using bismuth borate [153], known to melt at 726 °C, but it was not attempted as the developed solution was satisfactory enough with calcium and carbon only ; it is always preferable to avoid using components leading to possibly toxic sub products such as bismuth salts.

Table 4.6 presents the pastes used for the initial MSP tests with their mineral volume proportions. These pastes were deposited on leftover DP951 LTCC tape by hand with a spatula, and some samples were covered with another LTCC tape to form a sandwich. The subsequent analysis focused on the deformation of the LTCC, on the quality of the gap and on the mean of removal. For this latter, *manual wiping* means that the fired MSP could be simply removed by sliding it with a finger, while *acid + US bath* means that the MSP needed to be dissolved in H_3PO_4 in an ultrasonic bath for 5 min.

This easiness of removal contrasts with the long dissolution process necessary for the sodium-containing pastes of subsection 4.3.5, which lasted at least 30 h (section 4.3.6); as such, it is a significant improvement. It must be mentioned that a dense layer is not necessary in case of LTCC, facilitating dissolution. It will be shown later that porous MSPs may be used in classical thick-film technology as well.

The pastes 02, 05 and 06 were made with intermediate values of proportions, and as their properties did not differ much, they were omitted from the above table.

Results of initial tests The results of this series are not good; the samples all suffered from deformations of LTCC and present a bad gap quality. However, the MSP was very easy to remove (by wiping a finger on it):

- Figure B.12 on page 231 shows a 1-layer LTCC sample printed with paste O1 and its strong deformations.
- A 2-layer cantilever LTCC sample made with paste O3 is displayed on Figure B.13: the deformations are more localized. Although the base is less affected, the cantilever is too distorted.

- Only the O8 paste (made with 100 % carbon) showed no deformation, but the gap was nearly nonexistent (Figure B.14). This is explained by the almost complete combustion of C before the sintering, leading to the sagging of the cantilever on its base. This is no surprise; the carbon fugitive phase has been used so far with success only in closed cavities, and with structures that are rigid enough to avoid sagging.

It can also be noted that although the pastes were initially white or black (depending on their carbon content), they all turned out white after firing (if there was anything left to be seen), as Appendix Figure B.12, Figure B.13 and Figure B.15 can attest, because of the remaining calcium oxide.

Improvement of MSP: sandwich of $CaCO_3$ and C From the first series of tests it was concluded that:

- carbon C was beneficial, but useless if deposited alone;
- calcium oxide CaO was useful too, but only in small proportions;
- boric acid H_3BO_3 did not bring improvements.

Hence we tried a combination of $CaCO_3$ and carbon in the hope that the volume lost during firing by oxidation of the carbon and decomposition of $CaCO_3$ to CaO [94], according to Equation 4.4, would allow this material to better follow the shrinkage of the LTCC.

$$CaCO_3(s) \rightarrow CaO\ (s) + CO_2(g) \tag{4.4}$$

Thus, new tests were carried out with $CaCO_3$ and C only: they are listed in Table 4.7. The pastes O10 and O11, rich in $CaCO_3$ (respectively 100 % $CaCO_3$ and 50 % $CaCO_3$ - 50 % C), gave very bad results (strong deformations), so the amount of calcium carbonate was reduced to give the pastes T7...T10, which exhibited much better results[3].

Table 4.7: Improved MSP tests on leftover DP951 LTCC with calcium carbonate and carbon only: volume proportions, and resulting observations: LTCC deformations, gap quality and easiness of removal. The paste T9 is very interesting, as it shows nearly no deformation.

Code	Vol. ratio [%]		Improved MSP results on leftover DP951 LTCC		
	$CaCO_3$	C	LTCC deformations	Gap quality	Mean of removal
O10	100	0	very strong	very bad	manual wiping
O11	50	50	very strong	very bad	manual wiping
T7	9	91	nearly none	OK, but small	acid
T8	19	81	nearly none	glued on 1 side	acid
T9	**28**	**72**	**nearly none**	**good**	**acid**
T10	38	62	slightly on the base	good	acid

Appendix Figure B.15 shows the results of the best paste (T9) made with 28 % $CaCO_3$ and 72 % C, here used for a test sandwich-cantilever. The final shape is clearly very good, and the

---

[3] Their ratio numbers are not round, because the wrong specific mass (2.71 instead of 2.93) had been taken for mass calculations

Table 4.8: Tests of sacrificial materials with different silk papers: number of layers and resulting LTCC deformations, gap quality and easiness of removal. None is usable for the foreseen application.

Code	Silk paper		Results		
	Type	# of layers	LTCC deformations	Gap quality	Mean of removal
O12	1	7	none	cantilever broken	acid + US bath
O15	2	7	none	no gap!	acid + US bath

MSP has totally vanished after dissolution/removal. All the pastes of the T sere can be simply removed by a quick stir in H_3PO_4 followed by DI H_2O rinsing.

Complementary initial tests: silk papers Besides MSP, silk paper was also envisioned as a sacrificial layer. Table 4.8 summarizes these attempts, all unsuccessful, apparently due to insufficient amounts of minerals in the paper. Despite the LTCC suffered no deformation, the cantilever either collapsed on the base or it simply broke. The silk paper solution was not further investigated; it does not mean that it must be disregarded, but it is not dispensable by screen printing anyway.

4.4.4 Fabrication of free-standing structures

The good results obtained with paste O8 and T9 opened the way for the prototyping of the microforce sensor, with committed screen printing instead of rapid screen printing through a metal mask. Electrodes and MSP are deposited on the base tape 254 µm thick, while electrodes are printed on both faces of the cantilever to prevent asymmetrical cantilever deformation; such deformations were observed in previous projects due to a mismatch of shrinkage between the paste and the tape. The top electrode will therefore have no nominal electrical function, but can be used as a ground shield.

The sensor size was chosen to be compatible with the existing socket of the capacitive sensor demo-board, i.e. 12.7×25.4 mm. Different geometry variants were designed, by varying the cantilever length, its width, and the presence or not of a hole in it. For rationalization reasons, the sensors were produced in batches containing two sensors of each variant mounted head-to-head. This head-to-head mounting with the cantilevers joined together was favored to leaving the cantilevers free for the following reasons:

- The top LTCC layer being only 114 or 254 µm thick, the intrinsic rigidity of the tape is not sufficient to ensure it will not collapse during manipulations;
- If the cantilever is free to move before the end of the sintering, strong deformations can take place during lamination and firing.

Figure 4.20 shows a base tape and a cantilever tape, both in green state but screen-printed and ready for stacking; the 2×7 sensors and the geometry variants are clearly visible. Figure 4.21

displays the same sensor assembled and laminated (Figure 4.21a), as well as fired but with MSP undissolved (Figure 4.21b).

The sensors are singulated after firing by laser scoring along post-stamp-like cuts present only in the base tape ; the operation requires multiple rapid passes (laser parameters 80 %, 2 kHz, 1 mm/s) and must be done carefuly in order not to break the fragile cantilevers.

The choice of the electrode type and of the MSP combination is of primary importance: it must ensure the compatibility between MSP and electrode, as well as a sufficiently large gap between the cantilever and the base. The selection is described hereafter.

Screen printing variants Beside the geometry variants, of little interest for this chapter, the screen printing operations were also varied in sequence and in the choice of paste to experiment different “sandwich” combinations. Three kinds of electrodes were tested:

a) Ag:Pd	DuPont 6142D capacitor electrodes;
b) PTC resistor	ESL 2612-I;
c) 1 kΩ/□ resistor	DuPont 2031.

The underlying idea behind the resistor electrode is to prevent destructive short-circuits when the cantilever will be in contact with the base and possibly to give a better shrinkage & TCE capabitility with LTCC, i.e. less stresses. Concerning the Ag:Pd choice it was dictated by the DuPont assortment (DP6142D is specially made for capacitor electrodes), but other inks like Ag DP6145 would probably be suitable too; to the contrary, the Ag:Pd DP6146 would yield too strong deformations on so few LTCC tapes.

Three kinds of MSP "sandwiches" were also experimented:

1) a four-layer made of C - $CaCO_3$ - $CaCO_3$ - C; in Table 4.9 $CaCO_3$ is named O10;
2) a two-layer of T9;
3) a three-layer made with C - T9 - C, where T9 is 28 % $CaCO_3$ and 72 % C.

Table 4.9 lists the 8 variants tested, the observed deformations of LTCC and cantilever, as well as the color of the fired mineral sacrificial paste. Unlike for initial tests that all turned to white, the observed colors were white, beige, red or black, due to reactions with electrodes. The results are as follow:

- The variants V2 + V3 with tracks of PTC ESL 2612-I present a red coloration, and despite a better gap quality for V2, more deformations for V2 than V3 (Figure 4.22a). V2 was selected for pin mounting and capacitive tests, but S. Wiedmer reported it to be too sensitive to temperature variations, resulting in a useless sensor (see section 5.4.2).

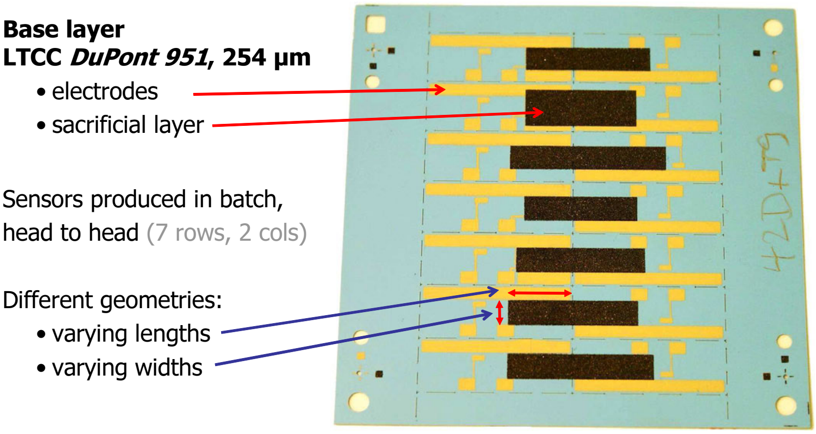

(a) Bottom layer (bases) with DP6142D electrodes (yellow) and mineral sacrificial layer (black). The post-stamp-like cuts later used for singulation by laser scoring are visible.

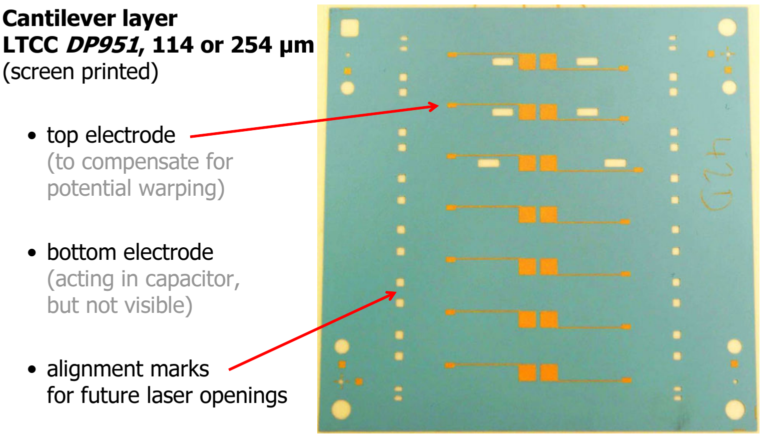

(b) Top layer (cantilevers) with electrodes on both sides, after screen printing but *before* lasering.

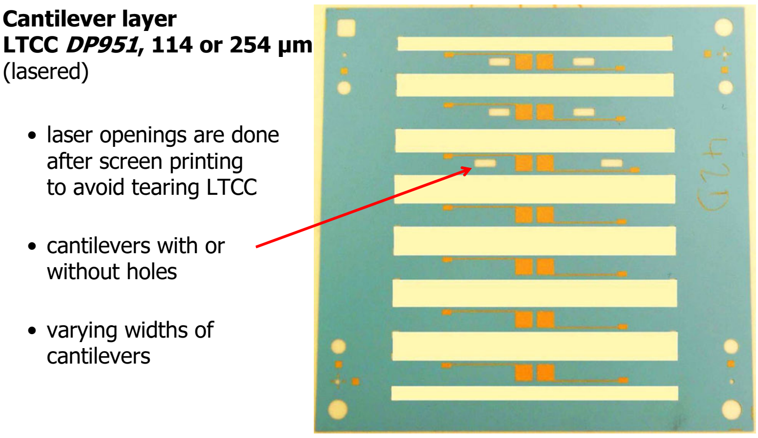

(c) Same as (b) but *after* lasering.

Fig. 4.20: Unassembled LTCC circuit of variant V5 with base (a) and cantilever layers (c), containing 2×7 sensors mounted head-to-head. The intermediate manufacturing step of the cantilevers layer is represented on (b). The tape dimensions are 72×72 mm.

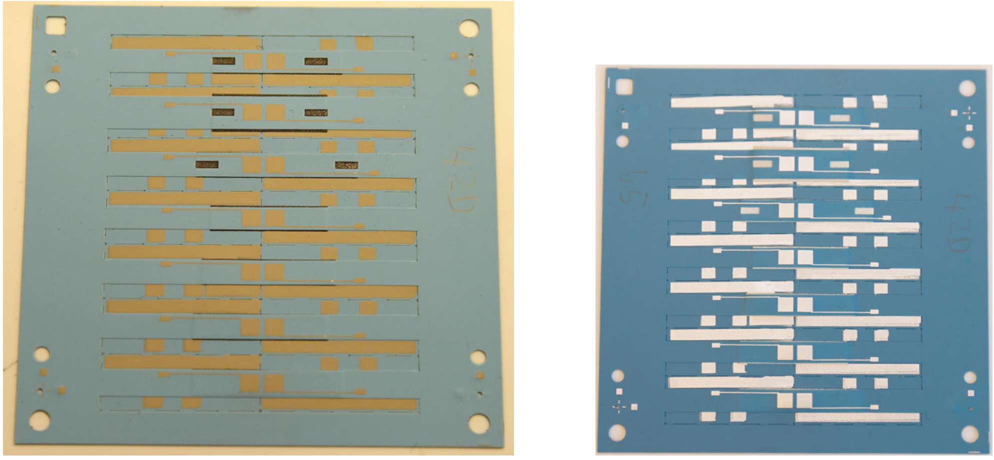

(a) Circuit assembled and laminated, but unfired ; the MSP is clearly visible in the cantilever holes (black) and under the embossed cantilever.

(b) Circuit fired ; the MSP is still visible (with a granular texture), but it turned to white as carbon burned.

Fig. 4.21: LTCC circuit of variant V5 assembled from subparts (a) and (c) of Figure 4.20. Note the dimensional variations due to shrinkage: from 72×72 mm to ∼62×62 mm.

Table 4.9: Variants of screen printing: track type, number and order of MSP depositions, and resulting observations: LTCC deformations and color of fired MSP. Legend: Ag:Pd means DP6142D capacitor electrodes; PTC means ESL RESISTIVE 2612-I; "1 kΩ/□" means DUPONT RESISTIVE 2031. For O10 and T9, see Table 4.7. The variants V2, V6 and V7 gave the most interesting results (one of each track type) and were further tested as capacitive sensor.

Variant	Track	MSP		Results	
		# of layers	Order of deposition	Deformations	MSP color, fired
V1	Ag:Pd	4	C-O10-O10-C	Important cantilever deformation in height	White
V2	**PTC**	**2**	**T9-T9**	**Good gap but more deformations than V3**	**Red coloration**
V3	PTC	3	C-T9-C	Bad gap despite nearly no deformations	Red stains
V4	Ag:Pd	2	T9-T9	Slight deformations of cantilever and base	Beige
V5	Ag:Pd	2	T9-T9	Despite more def. than V6, good results	Beige
V6	**Ag:Pd**	**3**	**C-T9-C**	**No deformations**	**Beige**
V7	**1kΩ/□**	**3**	**C-T9-C**	**Nearly no deformations**	**Black stains**
V8	1kΩ/□	2	T9-T9	Slight deformations of base	Dark grey - black

- The resistive paste DUPONT 2031, of value 1 kΩ/□, was present in variants V7 and V8. Although the LTCC deformations were small or nearly absent (Figure 4.22b), the capacitive tests conducted on V7 were unsatisfactory, because of the instability of measurements;
- The last kind of tracks, Ag:Pd DuPont 6142D, used with the variants V1, V4, V5 and V6, gave interesting results. The V1 variant, of which the MSP was made with C enclosing pure $CaCO_3$, was totally useless because of very strong cantilever deformations (Figure 4.22c top). It seems that the MSP grew too much, and it kept doing so for some

days afterwards under ambient humidity (see Figure 4.22d). The hydratation process of CaO-based compounds into $Ca(OH)_2$ calcium hydroxide is a well-known reaction accompanied by a volume expansion (cf. IGUCHI [155]); the base reaction is:

$$CaO\ (s) + H_2O\ (l,g) = Ca(OH)_2\ (s) \qquad (4.5)$$

IGUCHI also observed a slow hydration rate and a large volume expansion for $3\,CaO \cdot Al_2O_3$; the probability that some of these compounds were created at the boundary between the MSP and the LTCC exists, but is low for Al_2O_3 as it is little reactive below 900 °C; however, this is more probable for the oxides of the glass: B_2O_3, PbO, SiO_2, etc.

- The variants V4 (Figure 4.22c bottom) and V5 presented more deformations than the V6 (Figure 4.24a), so they were not tested. Of all the variants, V6 gave the best results: no LTCC nor cantilever deformations, easy MSP removal and stable measurements (see later).

The MSP of V6 is made of a sandwich displayed on Figure 4.23: C-T9-C, with T9 made with 28 % $CaCO_3$ and 72 % C. It was screen printed on the base in three successive steps:

1) A layer of paste containing 100 % carbon mixed with a binder was screen printed and dried for 10 min at 120 °C.
2) The paste T9 was printed on top of the first layer with the same screen, and similarly dried for 10 min at 120 °C.
3) Another carbon layer was finally printed on top of the two inks, and dried under the same conditions. The resulting sandwich is displayed on Figure 4.23a.

The good results of this triple-layer sandwich can be explained like this: as tested with the paste O8, the carbon in contact with LTCC in the upper and lower layers does not create deformations. The T9 in the inner layer serve as skeleton for cantilever while the carbon is oxidized. The volume lost by carbon combustion and decomposition of $CaCO_3$ to CaO allows the altering MSP to follow the shrinkage of the LTCC.

Lamination After screen printing the tape were carefully stacked on a pin alignment fixture. To accommodate for the extra thickness induced by the MSP, pseudo-isostatic lamination was applied with the help of a 15 mm thick, Ø 120 mm constrained rubber pressing from the top (see subsection 3.3.1 on page 70); it lasted 10 min at 25 °C under 80 bar (8 MPa). The pressure was chosen low to avoid damaging the fragile cantilevers.

LTCC firing All samples were fired in a lamp air furnace (see subsection 2.2.7 on page 40) with a modified temperature profile; compared to those displayed in Appendix A, it featured a long organic burnout to ensure complete combustion (300 min from 330 °C to 450 °C), followed by a sintering ramp of 2.5 K/min peaking at 875 °C with a dwell of 30 min.

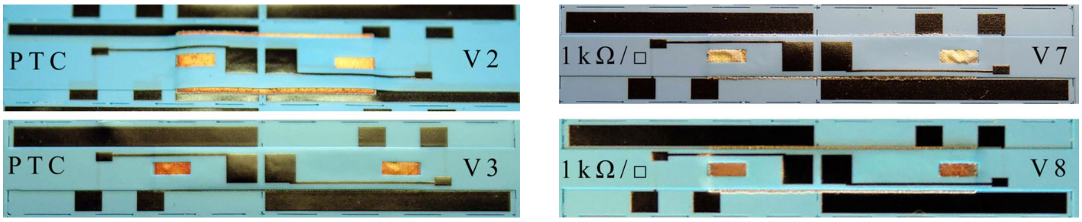

(a) PTC variant V2 (top) and V3 (bottom). Note the red coloration of the MSP, visible through the hole in the cantilever. LTCC deformations are restrained.

(b) DP2031 variants V7 (top) and V8 (bottom) ; both suffered little deformations, but were electrically instable.

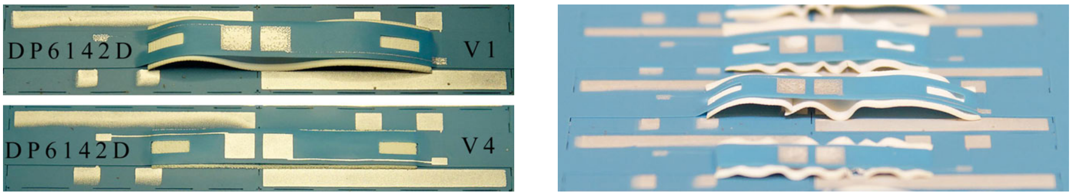

(c) DP6142D variants V1 (top) and V4 (bottom). The V1 showed an extreme case of cantilever deformation just after firing, while it was moderate for the V4

(d) Same sensor of variant V1 as displayed on (c) top after 10 days of hygroscopic absorption in air: the deformation of the undissolved MSP due to its continuous growth is clearly visible.

Fig. 4.22: Results of fired LTCC samples of defective screen printing MSP variants, grouped by electrode type.

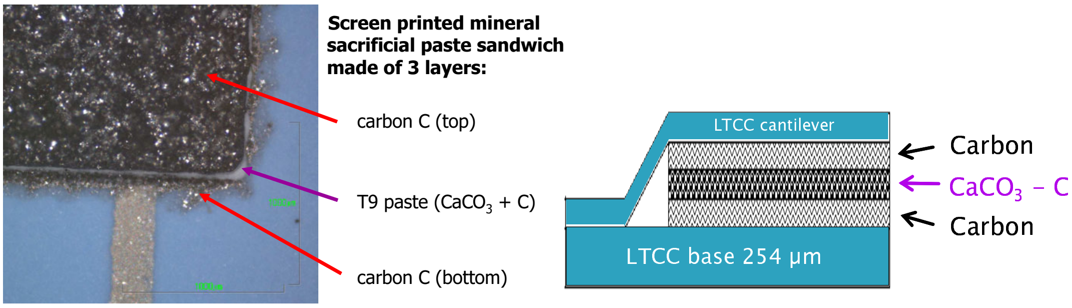

(a) Top view of a freshly screen printed MSP sandwich on LTCC base. Note the electrode track exiting at the bottom.

(b) Schematic cross section of the sensor and of the MSP sandwich ; electrodes are not represented.

Fig. 4.23: Mineral sacrificial paste sandwich composed of carbon on outer layers, and of paste T9 (a mix of $CaCO_3$ and carbon) on inner layer.

MSP dissolution The MSP removal of the last samples was made by wiping a finger in the cases it was naturally accessible. However, dissolution by stirring in diluted H_3PO_4 at ambient temperature for 15 min, followed by simple DI H_2O rinsing and air drying was often necessary. It resulted in the sensor depicted in Figure 4.24c and Figure 4.24d, with a clearly visible gap. Some alterations of electrodes and of tape surfaces were observed for some sensors, as depicted on Figure 4.24b; we did not notice an electrical malfunction however.

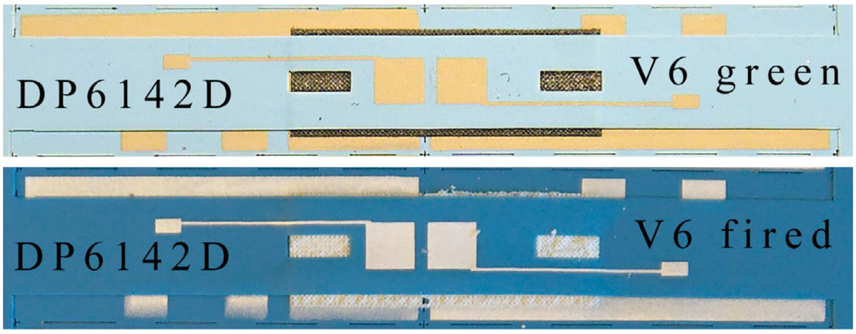

(a) Screen printed sensor with DP6142D electrode showed in green (top) and fired states (bottom).

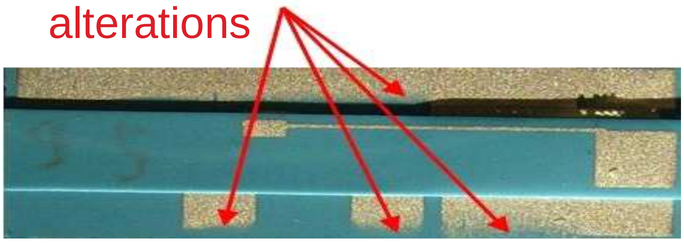

(b) Some alterations of electrodes and of tape surfaces were observed for some sensors; we did not notice an electrical malfunction however.

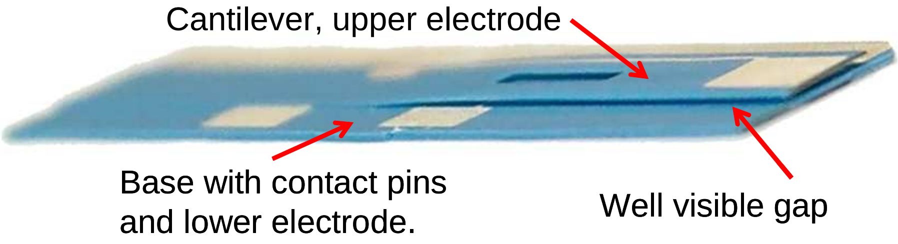

(c) Capacitive sensor after removal of sacrificial layer. The gap is neat and well visible between the cantilever and the base. The electrodes are the light grey squares ; the contact pins/wires have not yet been mounted.

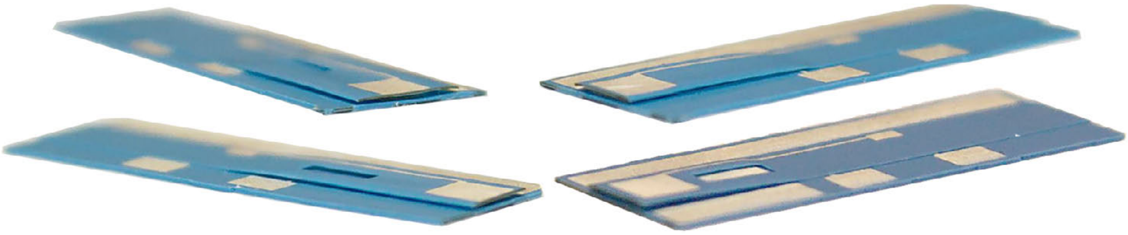

(d) Same as (c) with different cantilever geometries. Some twisting in the cantilevers can be observed, due to the asymmetric track layout.

Fig. 4.24: Photographs of the V6 variant that turned out to be the best both in geometric and electrical qualities.

4.4.5 Sensor performance

Please refer to section 5.4.2 on page 177 for capacitive sensor measurements and performance.

4.4.6 Improvements of the Sacrificial Paste

The abovementioned results are promising for the creation of other free-standing structures. However, the considered C-T9-C sandwich is not yet optimal; it can probably be improved by refining the components ratio of the mineral paste composition. The use of another LTCC system such as the HERAEUS HERALOCK, with ±0.2 % of shrinkage, would be a logical next step; it was indeed later investigated by T. MAEDER in [146], who found it had a bad chemical resistance to etchants (see section 4.6).

Moreover, switching to an aqueous solution (per example polyvinylic alcohol) instead of an organic-based solution for the pastes binder (i.e. replacing the Terpineol by other solvents) could reduce problems encountered at screen printing, such as embrittlement of thin tapes (50 µm) due to over-absorption of solvent by the LTCC. With MAEDER et al. we presented in [94] in 2008 two alternative screen printing vehicles for the processing of sacrificial materials and low-firing thick films: 1) a non-aggressive glycol-based vehicle for screen printing thick sacrificial layers onto thin LTCC, and 2) a "high non-evaporables" vehicle for mineral / carbon sacrificial materials allowing subsequent overprinting in the dried state. Their formulation, processing and applications are discussed with regard to the physical and chemical properties of the solvents, plasticizers and binders.

Summary of paste (in)compatibilities Based on experience in this work and other projects, here is a summary of the paste (in)compatibilities encountered upon co-firing with our C-T9-C MSP sandwich:

Conductor	DUPONT 6142D (Ag:Pd): good compatibility.
Conductors	DUPONT 6145 (Ag), DUPONT 6146 (Ag:Pd): not yet tested.
Resistors	DUPONT 2031 (1 kΩ/□), ESL 2612-I (PTC 100 Ω/□): physically OK, but requires more testing as S. WIEDMER experienced electrical instabilities [114].
Resistors	DUPONT 5092D (PTC 100 Ω/□) and CF011 (10 Ω/□): more testing needed due to strong deformations, as depicted on Figure 5.50 on page 193.

4.4.7 Conclusion of study

A novel method of structuration of free-standing structures on LTCC has been proposed and successfully demonstrated. It differs from previous methods in the sense that it is compatible with the LTCC shrinkage, it is not limited to closed cavities, and also because it uses mineral sacrificial layers deposited by screen printing, in the form of a three-layer sandwich. The bottom and top layer are pure carbon, to avoid LTCC deformations due to contact with minerals. The

middle layer is a mix of 28 % calcium carbonate $CaCO_3$ and 72 % carbon C. All layers are mixed with an organic binder in mass proportions 60 % - 40 % respectively. The $CaCO_3$ acts as skeleton after the carbon combustion during the firing, as it gets transformed into CaO (of higher melting point, 2 572°C).
The remaining material is easily removed after firing by dissolution in diluted weak acid (H_3PO_4), successive rinsing in deionized water and air drying at 100 °C. This easiness of removal is a huge improvement on the first phase of the study; it contrasts with the long dissolution process necessary for the sodium-containing pastes of subsection 4.3.5, which lasted at least 30 h (section 4.3.6).

To summarize: the advantages lie in the low reactivity during sintering and in the easiness of removal after firing, while the drawbacks are a three-step screen printing process and almost no material cohesion upon sintering: this method can hardly prevent upward tape deflections that sometimes occur on elongated structures.
Regarding the possible improvements for this mineral paste, I see two ways:

- The refinement of the mineral paste, by fine-tuning the compounds proportions to allow a tailored shrinkage compatibility and an easier dissolution (for example with water instead of weak acids);
- The replacement of the organic paste solvent (currently Terpineol) to make it less aggressive to unfired LTCC tapes and to allow its use with other brands.

4.5 Application of sacrificial pastes to sensors

For reading consistency, the section treating about the performance of the sensors developed earlier in this chapter was separated from the sensors' performance analyses and placed in the chapter devoted to sensors. Please refer to section 5.4 on page 173.

4.6 Latest MSP improvements and perspectives

4.6.1 Improvement of non-shrinking MSP

My supervisor, the Dr. Thomas Maeder, continued the ongoing research of non-shrinking mineral sacrificial pastes on the basis of the abovementioned research. In [156] we published the following:

While $SrCO_3$, $CaCO_3$ or Al_2O_3 provide mechanical support during firing, their lack of sintering results in insufficient cohesion. Lateral (XY) constraint is therefore not always guaranteed, and structures may lift or curl due to internal stresses arising during sintering. Therefore, what is needed is a material similar to $SrCO_3$, but with a slight amount of local sintering / bonding between the powder particles to impart a minimum of cohesion and thus stabilize the overlying structures. The degree of sintering and assorted shrinkage must remain low for good dimensional stability and to maintain large open porosity, allowing rapid chemical etching.

A search for appropriate substances revealed two potential candidate compounds, which are studied: 1) MgO + sintering aids, and 2) borates, such as calcium metaborate, CaB_2O_4:

- MgO is a well-known sacrificial material for surface micromachining of MEMS [138] and, if "dead-burned", is sufficiently stable in its oxide form towards ambient humidity, at least for a short time. Being refractory, it is expected to require a limited amount of sintering aids to hold the grains together, and B_2O_3 and/or borax ($Na_2B_4O_7$) are envisioned for this purpose. Borax is less volatile and provides better bonding, but the deleterious effects of its sodium content limits the maximum tolerable amount.
- CaB_2O_4 was also explored, due to its commercial availability[4] and moderate melting point of 1154 °C [157], which leads us to expect limited sintering at ca. 850 °C.

Paste reformulation Last but not least, there is an additional issue that needs to be addressed for classical thick-film technology (but not for LTCC): printability over highly porous films, as is desired for the sacrificial layer, is usually very poor, as the pores prematurely extract the solvent of the overlying paste, impeding proper levelling or even leading to clogging of the screen mesh. To overcome this issue, paste formulation must also be studied, with two main options:

1) The sacrificial layer paste may be formulated to be less or not porous in the dried state, so that overprinting is possible. This may be accomplished with classical pastes by increasing "non-evaporables" [94] or by using an epoxy resin as vehicle [139], and requires the sacrificial layer and the first subsequent one to be co-fired.
2) Alternatively, the paste for the first overlying layer is formulated to be tolerant for porous layers. This route – if successful – is compatible with both co-firing and standard sequential firing.

This work therefore aimed at developing a complete thick-film mineral sacrificial paste process, using MgO or CaB_2O_4 (+ additives if needed) as sacrificial compounds, and suitable paste formulations to allow overprinting in the dry or fired state. $SrCO_3$ was also tried for comparison purposes. While classical thick-film technology is used here, the developed processes may of course be also adapted to LTCC. The developed process was illustrated by fabricating cantilevers and bridges using different thick-film dielectric compositions (see Figure 4.25).

Dielectric reformulation for overprinting Printing of standard commercial thick-film inks over the fired sacrificial layer is problematic, even when using coarse screens; as expected, vehicle loss into the very porous layer resulted in strong premature drying and clogging of the screen mesh. This is presumably due to the high particle loading of standard pastes, making them sensitive to vehicle loss, coupled with a vehicle of relatively low viscosity apt to rapidly escape into the pores of the sacrificial layer, a situation depicted on the left of Figure 4.26. Therefore, we reformulated the three commercial multilayer dielectric inks, ESL 4903, 4904 and 4913 by adding various volumes of a "rich" vehicle (e.g. viscous and having a high binder

---

[4] Sigma-Aldrich

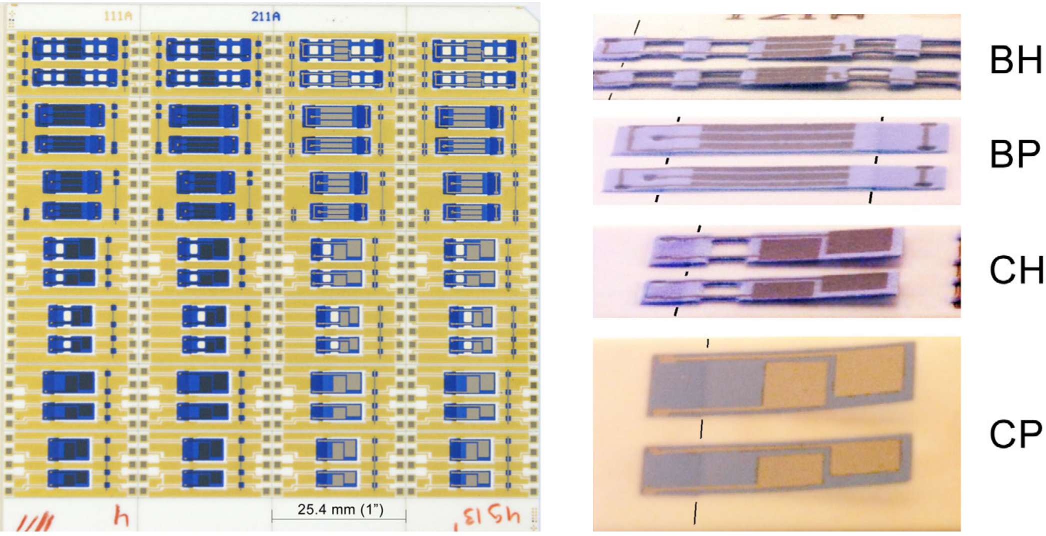

(a) Cantilever / bridge test substrate. *Left 2 columns:* + 1 layer dielectric over conductors; *Right 2 columns:* bare conductor.

(b) Examples of structures, illustrating stress-induced curling of cantilevers and buckling of bridges. Black lines: suspended / unsuspended boundary.

Fig. 4.25: Test structures developed by T. MAEDER and W. HRAIZ after evolution of my mineral paste. *Legend*: BH: bridge, with hinges; BP: bridge, plain; CH: cantilever + hinges; CP: cantilever, plain. Dielectric: ESL 4913 (BH); ESL 4904 (others) [156].

concentration), whose formulation is given in Table 4.10. This roughly leads to the situation depicted on the right of Figure 4.26:

- The particle loading of the ink is lowered, which leads to a larger tolerance to vehicle loss.
- The vehicle part of the ink must become more viscous to offset the decrease in particle loading and thus conserve approximately the same paste viscosity. This increased viscosity considerably slows down its escape into the pores of the sacrificial layer.

By testing iteratively, we found that the optimal proportions of commercial paste and extra vehicle for overprinting were ca. 70-30 % for ESL 4903, 72-25 % for ESL 4904 and 60-40 % for ESL 4913. A similar "rich" formulation was used for the final version of the sacrificial layer ink, as this allowed easy variation of the thickness through successive deposition and firing of multiple layers, e.g. the sacrificial layer can be printed onto its fired self.

Results This new study led to the following results: of the different examined candidate materials for sacrificial layers, CaB_2O_4 exhibited some initial sintering, giving a quite ideal porous, yet mechanically stable layer structure. However, it tended to crackle at large thicknesses, presumably due to its use in hydrated form. Therefore, MSPs based on MgO with H_3BO_3 as a sintering aid were used, avoiding borax, which tends to diffuse into and degrade underlying and overlying films. Although this combination was found to be quite suitable for the manufacture of suspended thick-film structures, it was still somewhat mechanically too weak. Therefore,

Table 4.10: Formulation of "rich" vehicle additive for overprinting inks onto sacrificial layer (ca. 40 % volume added to commercial paste) [156].

Type	**Compound**	**Parts** (by mass)
Solvent	Terpineol	10
	DBC *dibutyl carbitol*	5
Binder	EC-46-48 *ethylcellulose with 48% ethoxyl content, medium grade ("46 cP")*	3

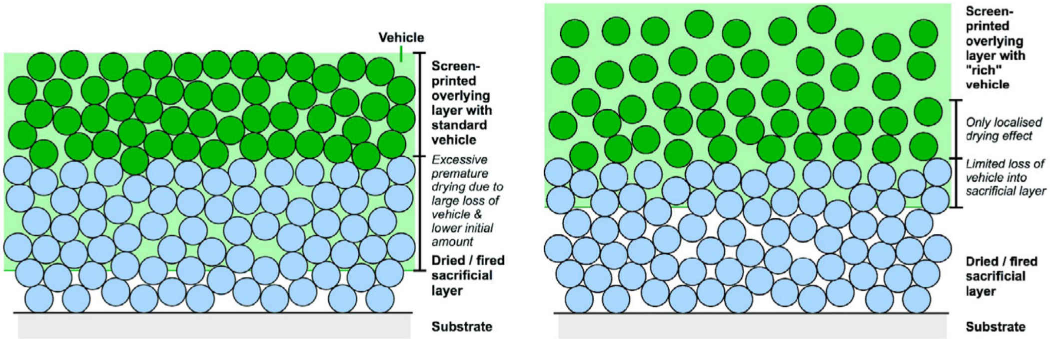

Fig. 4.26: Schematic comparison of printing paste over porous layer with two different vehicles: standard (*left*) and "rich" (*right*). Image courtesy of T. Maeder [156].

further development work is needed, with several options possible to improve the sacrificial layers, such as coating MgO (promising first results obtained), using CaB_2O_4 or other borates in anhydrous form, or applying mixtures of these compounds to tune the sintering behaviour. Satisfactory results for suspended structures were obtained both with co-firing and post-firing. However, co-firing was quite process sensitive, easily giving rise to inhomogeneous dielectric layers over the sacrificial one, and post-firing was therefore preferred. Co-firing should, however, not be a problem with LTCC, due to the much higher thickness of LTCC tapes. Post-firing thick-film compositions onto porous fired sacrificial layers requires adjustment of the ink vehicle formulation of the first overlying layer to ensure trouble-free screen printing over the porous sacrificial film. This was achieved by increasing the amount of vehicle, e.g. lowering the powder volume fraction, and correspondingly increasing the vehicle viscosity (by increasing the binder concentration) to maintain a good printable rheology.

Based on these developments, cantilever and bridge structures based on commercial thick-film dielectric and conductor compositions were fabricated and successfully released using acetic or phosphoric acid solutions. Compared with the initial attempt that used CaO and borax, problems due to Na diffusion or reaction with ambient humidity were entirely avoided – acid resistance of layers was not significantly affected by contact with the sacrificial layer.

4.6.2 Toward application to "zero-shrinkage" LTCC

Our team, led by Dr. THOMAS MAEDER, pursued the research by adapting the MSP recipes presented in this thesis to make them suitable for "zero-shrinkage" HERAEUS tapes [147–149]. In [146], we examined new MSP processes to achieve slender suspended structures in LTCC technology. To this end, materials based on MgO (refractory alkaline earth oxide, negligible sintering) and CaB_2O_4 (lower melting temperature, sintering) were formulated and applied to both classical (shrinking in XY direction) and "zero-shrinkage" LTCC materials: DP951, HERAEUS HL2000 and HL800 (shown as fired single tapes on Figure 4.27a; note the excessive self-warpage of HL800).

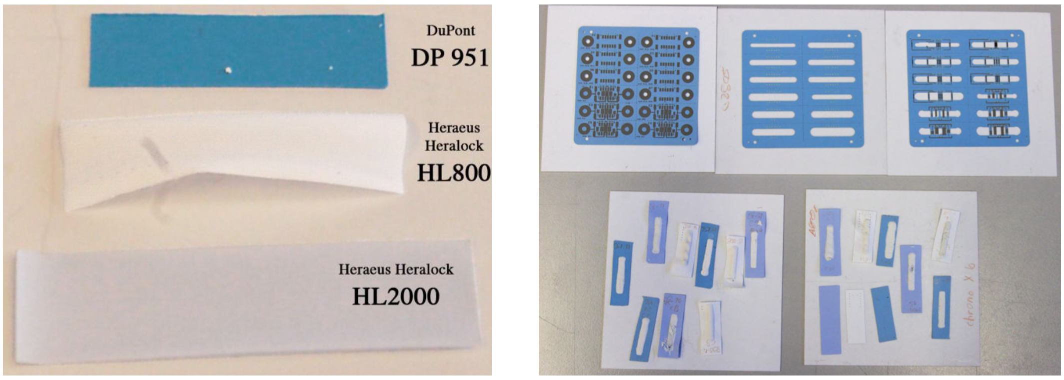

(a) Fired single layers of three different LTCC tapes, some suffering from self-warpage; from top to bottom: DP951 (flat), HL800 (heavily deformed) and HL2000 (flat but with curled edges) [146].

(b) *Top*: test structures (flow sensors and capacitive suspended bridges) on DP951; *Bottom*: quick tests of various MSPs on DP951, HL2000 and HL800.

Fig. 4.27: Tested tapes, structures and MSP materials.

Compared with the devices laminated between two flat metal plates, the MSP method allows a much wider process window to obtain undeformed structures; (pseudo-)isostatic lamination is possible, ensuring good interlayer bonding on the whole surface of the device.

Formulation of the MSPs to have some cohesion (rather than turning into loose powder) is advantageous for later handling and in order to avoid curling up of cantilevers. Initial quick tests were done on single LTCC tapes to rapidly determine the most suitable compositions for each tapes; the best and worst results are displayed in Table 4.11.

After selection of the most suitable paste for each tape, the MSPs exhibited reasonably good printing and firing compatibility with the LTCC tapes; the test structures were flow sensors (see Figure 4.27b and Appendix section C.2) and capacitive suspended bridges. Printings on DP951 are depicted in Figures 4.28a and 4.28b; HL800 is shown on Figure 4.28d; for HL2000 please refer to Figures 3.18c and 3.18d.

Nevertheless, a lower reactivity of the vehicle solvent system with LTCC would still be desirable, and some more fine-tuning is still needed on DP951 to more exactly match the MSP and LTCC shrinkage. This is of course not an issue on HL2000 and HL800, which is a considerable advantage of these two tapes.

Table 4.11: Quick tests carried out on single LTCC tapes to determine, for each tape, the best MSP among five.

	DP951	HL2000	HL800
worst case	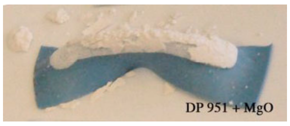	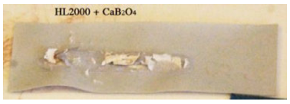	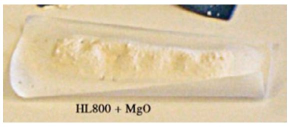
best case	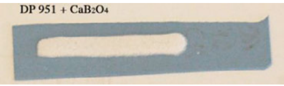		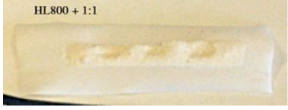

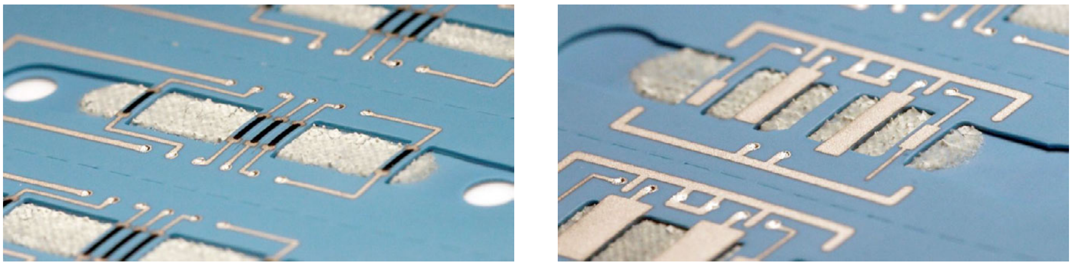

(a) DP951, flow sensor with thermal bridges.

(b) DP951, suspended capacitive bridges.

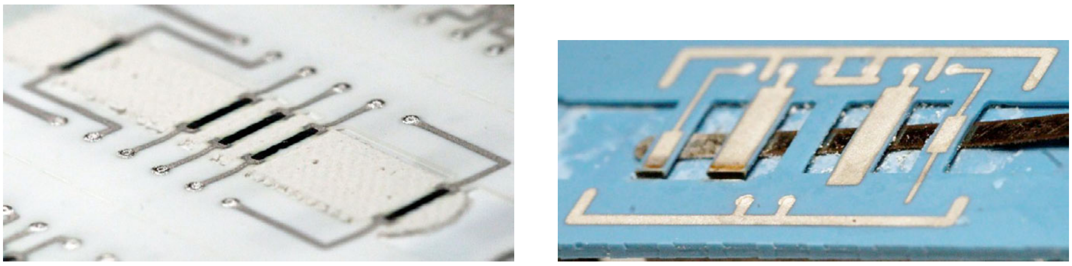

(c) HL800, flow sensor with thermal bridges.

(d) The bridges of (*b*) after MSP dissolution and laser cutting of the left two suspended structures. See from the white stains how part of the MSP reacted with LTCC.

Fig. 4.28: Flow sensors and suspended bridges structures tested with the improved MSP compositions. Collaborative work with G. Boutinard Rouelle and T. Maeder of EPFL-LPM.

The acid etching characteristics of the structures, however, did not match our expectations. DP951 was in general unaffected by the 10 % acetic or phosphoric acid etchants, but the surface in contact with CaB_2O_4 exhibited some damage (see Figure 4.28d), in contrast to our earlier studies with $CaCO_3$ [112], most likely due to B_2O_3 sublimation and reaction with the LTCC surface, locally affecting its chemical resistance. Nevertheless, the structures could be etched away successfully, albeit with some residue.

The HL2000 and HL800 LTCC compositions, in contrast to DP951 (which is known for its good chemical resistance [18]), were directly attacked by the acids; HL2000, especially, completely lost consistency, i.e. its glass matrix was entirely degraded. HL800 suffered extensive surface attack, but did show qualitatively much better chemical resistance than HL2000. This poor performance, in line with other studies [158], is not necessarily intrinsic, as we did not optimise the firing conditions, which we intend to do in later studies. Moreover, the MSP compositions, which used relatively unreactive coarse MgO powder and CaB_2O_4, still need to be optimised to etch away in more benign conditions.

Perspectives Future work will therefore first concentrate on optimising the LTCC firing conditions to achieve maximal chemical resistance for the “zero-shrinkage” LTCC compositions (not necessarily optimal for other considerations) and characterization of the materials in a wider range of etchants. Furthermore, the formulation of the MSPs for HL2000 and HL800 will be refined to allow more benign etching conditions. One possible path is to switch to finer, more reactive MgO powder, without any "binder" such as CaB_2O_4 or with a more soluble one, in order to increase its etching rate. On DP951, efforts will focus on decreasing the boron of the MSP loss while keeping the desirable sintering and shrinkage characteristics of CaB_2O_4. Finally, the formulation of the screen printing vehicle will be further refined to minimise solvent interactions with the LTCC tape during drying.

There is also an elegant alternative that we tested: as the HL tapes get directly attacked by the etching acids, we thought of an hybrid tape sandwich made of DP951 - HL2000 - DP951. The DuPont tapes provide the chemical resistance and an increased thickness, whilst the HeraLock dominates the shrinkage (keeping it close to zero). We conducted quick tests with laser cutting leftovers of the abovementioned flow sensors; the sandwiches (see Figure 4.29) were made of DP951-HL2000-DP951, with various thicknesses of DP951 to assess the shrinkage behavior. Cyclohexanol solvent was used as surface softener, and lamination was coarsely done by hand. It turns out that symmetrical sandwiches (with two DP951-254 µm) yield a flat output with relatively good tape bonding, while asymmetrical samples (with one DP951-50 µm and one DP951-254 µm) were rolled. Concerning the chemical resistance, it proved to be good, as Figure 4.29c can attest.

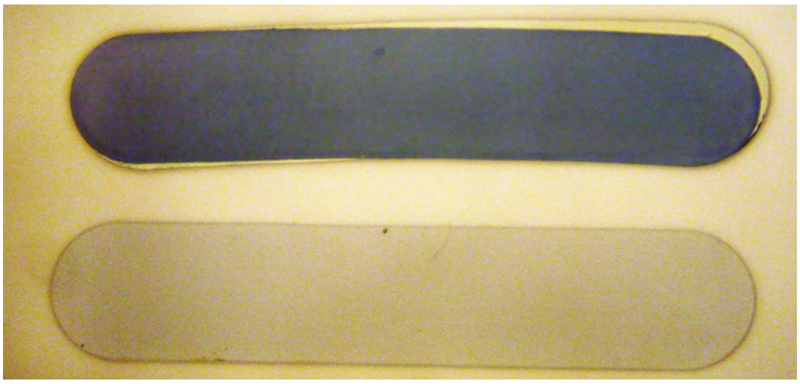

(a) Top view of fired test samples: a symmetrical sandwich (with two DP951-254 µm) showing a relatively good flat output (*top*), and a single HL reference sample to compare dimensional changes (*bottom*): the sandwich shrinkage is clearly blocked. Fired dimensions are around 25×4 mm.

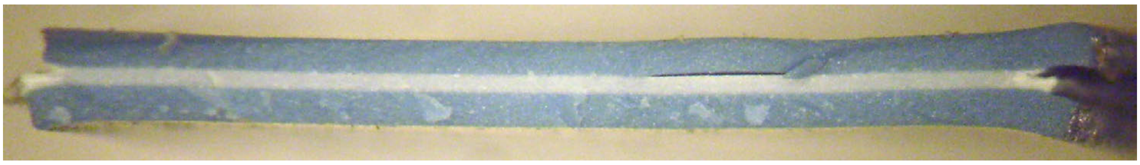

(b) Cross-section of fired symmetrical test sample (with two DP951-254 µm) showing a relatively good flat output. In spite of the presence of a small delamination, the tape bonding is good.

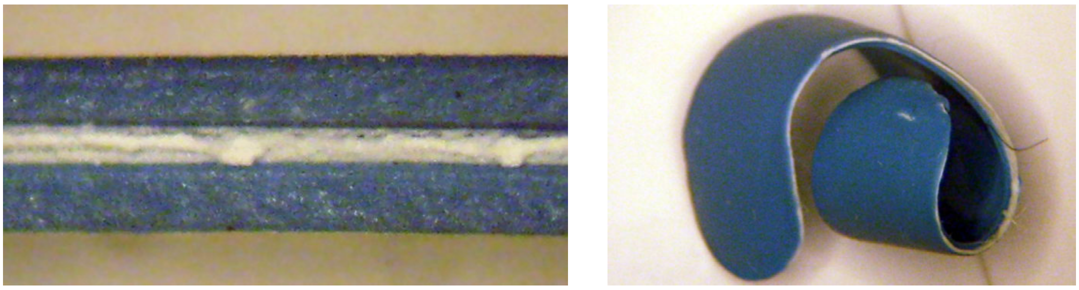

(c) Edge of symmetrical (with two DP951-254 µm) fired sample showing a good flat output, and limited attack after dissolution in weak acids. Thicknesses are around 205-90-205 µm.

(d) Rolled up asymmetric sample (DP951-50 µm on one side and DP951-254 µm on the other), made to demonstrate the effect of unbalanced pull on each side of non-shrinking HL2000 during sintering.

Fig. 4.29: Quick tests made with laser cutting leftovers of the abovementioned flow sensors to evaluate the idea of three-tape sandwiches. The sandiwches were made of DP951-HL2000-DP951, in order to combine the chemical resistance of the DuPont and the absence of shrinkage of the Heraeus. Various thicknesses of DP951 were tested, to assess the shrinkage behavior. Cyclohexanol solvent was used as surface softener, and lamination was coarsely done by hand. Presented by T. Maeder at IMAPS Rimini 2009 [146].

4.7 Conclusion

This chapter has proved possible to manufacture open structures in thick-film technology with mineral sacrificial volume materials (SVM), which are etched away after firing by weak acids like diluted phosphoric acid H_3PO_4 or acetic acid. So far, only closed cavities made with fugitive phases (carbon) were available to structuration. Our SVM materials, depending on their composition, are compatible with standard hybrid technology (alumina substrates), with “standard shrinking” LTCC tapes such as DuPont GreenTape 951 or with “zero-shrinkage” LTCC tapes like the Heraeus HL2000.

SVM for alumina The SVM for alumina were first made of CaO (skeleton) and borax (glassy binder, sodium tetraborate $Na_2B_4O_7$) mixed with an experimental organic binder, but it turned out that the sodium oxide Na_2O freed during the firing was too reactive and adverse reactions occured with adjacent layers, yielding poor dissolution conditions. The latest improvements in our laboratory led to the development of mineral SVM based on MgO with H_3BO_3 as a sintering aid, avoiding borax, which tends to diffuse into and degrade underlying and overlying films. Although this combination was found to be quite suitable for the manufacture of suspended thick-film structures, it was still somewhat too soft. Therefore, further development work is needed, with several options possible to improve the sacrificial layers, such as coating MgO (promising first results obtained), using CaB_2O_4 or other borates in anhydrous form, or applying mixtures of these compounds to tune the sintering behaviour.

We also demonstrated that post-firing thick-film compositions onto porous fired sacrificial layers requires adjustment of the ink vehicle formulation of the first overlying layer to ensure trouble-free screen printing over the porous sacrificial film. This was achieved by increasing the amount of vehicle, e.g. lowering the powder volume fraction, and correspondingly increasing the vehicle viscosity (by increasing the binder concentration) to maintain a good printable rheology.

Based on these developments, cantilever and bridge structures based on commercial thick-film dielectric and conductor compositions were fabricated and successfully released using acetic or phosphoric acid solutions. Compared to the initial attempt that used CaO and borax, problems due to Na diffusion or reaction with ambient humidity were entirely avoided – acid resistance of layers was not significantly affected by contact with the sacrificial layer.

SVM for “normal-shrinking” LTCC: DuPont 951 The technique proposed for the DP951 involves successive screen printing of pastes made of carbon C and calcium carbonate $CaCO_3$ in a sandwich manner; the pastes were experimental, but easy to prepare from commonly available ingredients with standard equipment. The sacrificial materials are dissolved after firing by gentle stirring in diluted weak acids (H_3PO_4) at ambient temperature for 15 min, followed by simple DI H_20 rinsing and air drying. The whole process is compatible with industrial screen printing manufacturing, and their is room for improvement: the sandwich paste composition can be refined to allow for a better dissolution, or even to bypass this step. In effect, some of the manufactured samples had mineral paste leftover that could simply be removed by wiping a finger on it. Hence, gentle air blowing or water dissolution can be envisaged in place of weak acid dissolution.

The next efforts for SVM on DP951 are described next.

SVM for "zero-shrinkage" LTCC: Heraeus HeraLock Our team extended the research of SVM for so-called zero-shrinkage LTCC tapes, i.e. Heraeus HL2000 and HL800. To this end, materials based on MgO (refractory alkaline earth oxide, negligible sintering) and CaB_2O_4 (lower melting temperature, sintering) were formulated and applied to both classical (shrinking in XY direction) and "zero-shrinkage" LTCC materials: DP951, Heraeus HL2000 and HL800.

The acid etching characteristics of the structures, however, did not match our expectations. DP951 was in general unaffected by the 10 % acetic or phosphoric acid etchants (it is known for its good chemical resistance [18]), but the surface in contact with CaB_2O_4 exhibited some damage, in contrast to our earlier studies with $CaCO_3$ [112], most likely due to B_2O_3 sublimation and reaction with the LTCC surface, locally affecting its chemical resistance. Nevertheless, the structures could be etched away successfully, albeit with some residue.

Future work will therefore first concentrate on optimising the LTCC firing conditions to achieve maximal chemical resistance for the "zero-shrinkage" LTCC compositions (not necessarily optimal for other considerations) and characterization of the materials in a wider range of etchants. Furthermore, the formulation of the MSPs for HL2000 and HL800 will be refined to allow more benign etching conditions. One possible path is to switch to finer, more reactive MgO powder, without any "binder" such as CaB_2O_4 or with a more soluble one, in order to increase its etching rate. On DP951, efforts will focus on decreasing the boron of the mineral paste loss while keeping the desirable sintering and shrinkage characteristics of CaB_2O_4.

Finally, the formulation of the screen printing vehicle will be further refined to minimise solvent interactions with the LTCC tape during drying.

Chapter 5

Application to sensors & microsystems

We present in this chapter different sensor applications: an industrial compressed air multisensor[1]*, a microreactor for measuring chemical reaction thermally, a thermal anemometer for an indoor slow flyer and an array of microthrusters for satellite orientation.*

*The focus of this chapter will be mainly on the SMD (surface mount device) multisensor in LTCC technology specially designed for standard industrial compressed air (*section 5.3*). It combines the measurement of pressure, flow, and temperature, with its integrated signal-conditioning electronics. Such a sensor can be mounted onto an integrated electro-fluidic platform by using surface mount technology, as a standard electronic component would be on a printed circuit board, obviating the need for both wires and tubes; the fluidic connections are insured by solder rings, in parallel with the electric ones – which was never achieved before.*

Usually, fluidic sensors in LTCC are dedicated to one physical quantity and need external electronics. The device presented is the combination of two independent sensors developed previously: one measuring pressure, the other one measuring flow and temperature. Although being at its first iteration, our integrated sensor already exhibits exploitable performances, though not optimal of course; the power consumption can be readily reduced and we explain how and why.

Capacitive sensors that were structured with the mineral sacrificial layers developed in the previous chapter are proposed in section 5.4. The other sensors are presented as examples of the vastness of LTCC structuration possibilities; they were not thoroughly characterized like the first sensor.

Key words: LTCC, Integrated multisensor, Pressure, Flow, Temperature, SMD mounting, Capacitive sensors, Microreactor, Thermal anemometer, Array of microthrusters.

---

[1] *Adapted from the conference paper n°8539 presented at the Eurosensors XXIII Conference 2009, Lausanne (Switzerland):* Y. Fournier, G. Boutinard Rouelle, A. Barras, N. Craquelin, T. Maeder, and P. Ryser, SMD pressure and flow sensor for compressed air in LTCC technology with integrated electronics *[159], and from the Master project of Jean-Bastien COMA [160].*

5.1 Introduction

Our laboratory being active in the development of ceramic sensors, sensor integration & packaging and in their industrialization, it was natural to orientate our research towards sensors designed for the industry. As we had a long-term partnership with an industrial company active in the pneumatic field, I decided to focus the main effort of the applicative part of my thesis onto the development of an integrated multisensor that can measure various physical quantities of standard industrial compressed air. It combines the measurement of pressure, flow, and temperature, with its integrated signal-conditioning electronics. The sensor can be mounted onto an integrated electro-fluidic platform by using surface mount technology (SMT), as a standard electronic component would be on a printed circuit board (PCB), obviating the need for both wires and tubes; the fluidic connections are insured by solder rings, in parallel with the electric ones.

Although having undergone one iteration only, our integrated sensor already exhibits exploitable performance, though not optimal of course; the power consumption can be readily reduced and we explain how and why.

Five other sensors are presented: two microforce sensors, a chemical microreactor, a thermal anemometer, and an array of solid-propellant microthrusters. These sensors are the results of semester or master projects carried out in our laboratory; the usage is that PhD students direct undergraduate student projects in addition to those directly linked to their thesis, and ensure the formation of students on the machinery necessary to manufacture the circuits. This requires an important amount of time, which is done at the detriment of the thorough completion of the projects (i.e. complete sensor characterization and modellization, plus second iterations and industrialisation), but at the benefit of acquiring and transmitting a practical know-how of utmost importance.

Therefore, the presented sensors must be seen as technological demonstrators that slightly deviate from the classical scientific approach regarding their development: one can expect from a scientific project that first theoretical models are studied in detail, and that the subsequent design is optimized, before the first manufacturing iteration, from a nice modeling made with complex finite-element simulations or other appealing computer-aided tools. Our experience proved that this would be a bad approach for projects involving R&D in LTCC: the interactions between the ceramic, the printed inks and the manufacturing conditions are so process-specific that it is – for the time being – pretentious to expect an output as planned. We experienced so much unforeseen behavior that we adopted a different approach when designing a new LTCC circuit:

- First we try to mimic as much as possible former successful designs: innovations should be done step by step and not many at the same time, to avoid potential unforeseen deleterious interactions.
- Simple theoretical models are used for the thermal, mechanical, and electrical aspects. As a rule of thumb, if they can be done with pencil and paper it is reasonable; complex mathematical simulations are already too much.

- The layout is performed on a specific software (for instance HYDE, see section 2.1.1) that offers electrical verification and 3D viewing. Geometrical and screen printing variants are most of the time possible thanks to the generous surface of LTCC tapes; this allows important time savings. Finally, a thorough control of the laser cutting output files and of the screen mesh plotting files is strongly recommended.
- The first manufacturing iteration (firing) takes place, sometimes on partial circuits if an internal structure must be masterized before building complete (buried) circuits. Feedback is provided by the different circuit variants distributed on the same batch, and by the screen printing variants of the different batches. Sometimes too many deformations or paste incompatibilities have arised at this step; we must then return to modifying the design. Otherwise after individualization and inspection, the best samples continue the process with the mounting of pins, wires, fluidic fittings as necessary.
- The best samples are placed on test benches and the first measurements can take place, yielding a first characterization. Practice can be confronted to theoretical expectations.
- The whole process repeats iself from the second step, usually with a reduction of variants, leading to a second, even third manufacturing iteration. The complex modelings and simulations make sense only after the second or third iterations, when all the unexpected technological problems have been solved.

As one can expect, one design & manufacturing iteration with a subsequent characterization can last from two to six man-months, which corresponds to the duration of students projects. Thus, only one iteration per project is executed in general, unfortunately.

5.2 State of the art of microfluidic devices

Before entering into the core subject of this chapter, it is relevant to first review what can be done with LTCC, and also what existed beforehand – a necessary justification for our work. The devices presented next were not all known to us at the beginning of this thesis; the following state of the art presents both former designs and some of the realizations unveiled by the "LTCC Community" in parallel to our efforts.

5.2.1 Flow sensors

The literature contains many examples; we list four of them.

- Gongora Rubio et al. described in the admirable overview [5] the meso-scale gas flow sensor they realized in 1999 in LTCC technology. The basic sensor structure consists of a thick-film resistive heater and two thermistors printed on a thermally isolated bridge in a cavity. The device measures the mean temperature in bridge using two thermistors; this temperature is related to flow in the cavity. This configuration utilized five layers of DP951-254 µm. The famous picture of this sensor is displayed on Figure 5.1a.

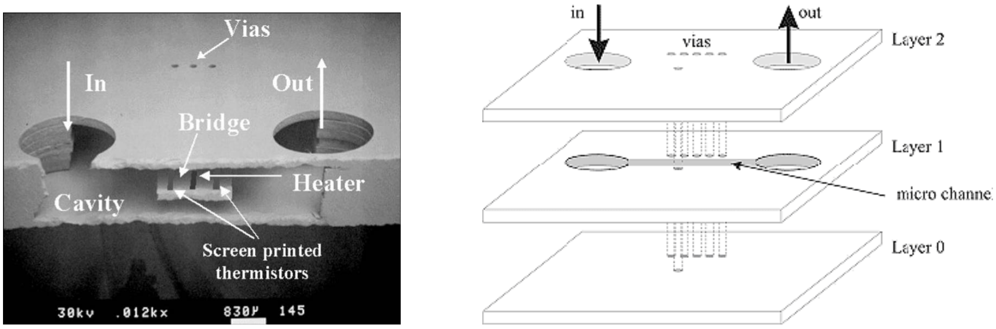

(a) Cross section of the gas flow sensor of Gongora Rubio [5].

(b) Schematic of the mass flow sensor of Güleryüz & Smetana [161].

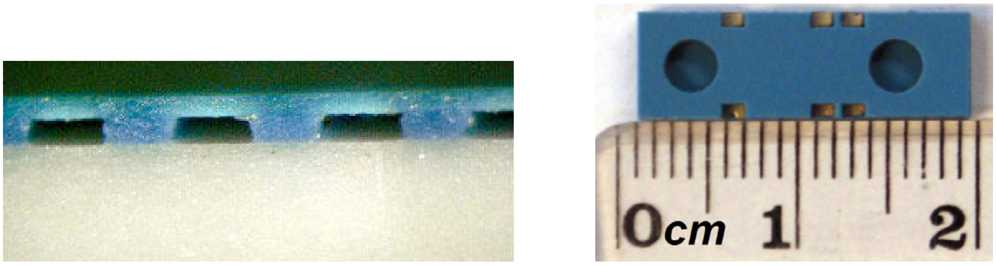

(c) Cross-section of photoimageable channel closed with LTCC, showing an excellent adhesion. By Magonski [162].

(d) Three-element gas flow sensor of Jurków & Golonka [97].

Fig. 5.1: Examples of flow sensors in LTCC.

- Güleryüz & Smetana published in 2005 [161] about a mass flow sensor realized in CeramTec GC LTCC. It is based on the same principle as the preceding example; the schematic is shown on Figure 5.1b. It operates on the calorimetric principle.
- Magonski et al., in 2005 too [162], successfully tested a thick-film photoimageable technology (Fodel, see section 6.2.3) combined with LTCC as an effective method of realization for a micro flow sensor. A cross-section of the device is displayed on Figure 5.1c.
- A three-element gas flow sensor in LTCC, manufactured with the help of Cold Chemical Lamination (see section 3.4.2), is proposed by D. Jurków in [97]; however the sensor has no integrated electronics, as depicted on Figure 5.1d.

5.2.2 Pressure sensors

In this field too, the literature abounds in examples. Here are four of them:

- Piezoresistive and piezoelectric thick-film pressure sensors, both in thick-film and in bulk PZT materials (Lead zirconate titanate, still one of the most suitable material for this application [163]), was extensively studied by Slovenien research teams among which Marina Santo Zarnik, Darko Belavic, and Marko Hrovat. Their published

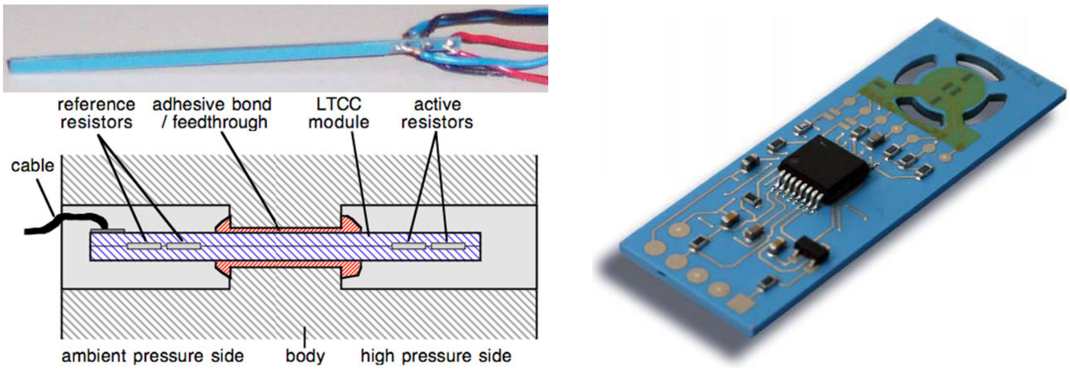

(a) Ultra-high isostatic pressure sensor photo (*top*) and schematic cross-section of the immersed-resistor principle (*bottom*) of EPFL-LPM [168].

(b) Photo of integrated pressure sensor with decoupled membrane – FRAUNHOFER IKTS [167].

Fig. 5.2: Examples of state-of-the-art LTCC pressure sensors.

numerous articles on the modellization of screen-printed resistors onto membranes, and on the realization and testing of such sensors [164–166]. They also published on PZT actuators on LTCC; see section 6.2.1.

- A good example of pressure sensor with integrated electronics was done by the FRAUNHOFER IKTS in Dresden, Germany. UWE PARTSCH presented in IMAPS OULU 2007 [167] the realization of Figure 5.2b. It presents interesting similarities with our multifunction integrated sensor of section 5.3, except that it measures only pressure, while we treat flow and temperature too.
- An article on ultra-high isostatic pressure sensors, depicted on Figure 5.2a, was co-published with BAMDAD AFRA and THOMAS MAEDER in 2007 [168]. This was a novel "isostatic" pressure sensor concept, whereby the sensing element is immersed in the pressure fluid. This method in principle allows the measurement of very high pressures (demonstrated up to 1200 bar), because materials stresses within the sensing beam are all compressive. LTCC beams with hermetically embedded thick-film piezoresistor bridges have been fabricated, packaged and characterised as sensor elements. The observed sensitivity is comparable to the response expected from the LTCC and piezoresistor materials properties.
- Integration of silicon on LTCC was demonstrated by BECHTOLD of VIA ELECTRONIC in 2008 [169]. They successfully bonded LTCC to an Si-glass wafer by anodic bonding at 400 °C and 1500 V.

5.2.3 Multifunction sensors

Optico-fluidic sensor of TU Dresden In 2004, M. R. GONGORA RUBIO reported in [170] about a development of an optical and fluidic sensor from the TECHNICAL UNIVERSITY OF DRESDEN, as can be seen on Figure 5.3. Apparently the LTCC is used as a fluidic platform

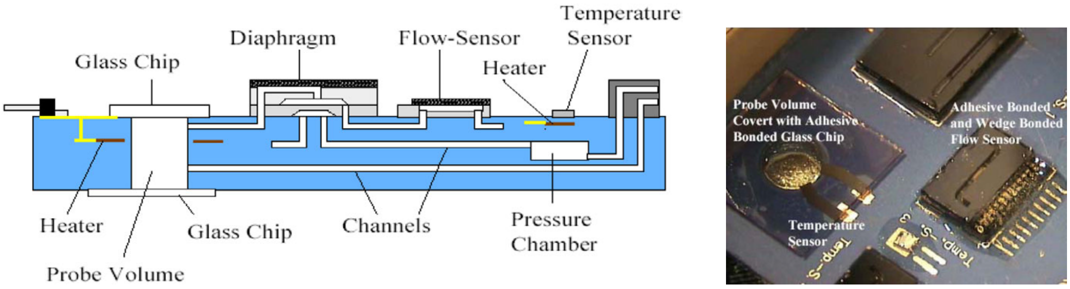

(a) Schematic cross-section.

(b) Sensor covered with protective resin.

Fig. 5.3: Integrated opto-fluidic sensor from TU Dresden [170]. Compared with our multifunction integrated sensor (section 5.3), where all the active sensor parts (but the electronics) are in LTCC, the LTCC substrate is here a fluidic platform only: all sensors and MEMS are mounted on surface, except buried heaters.

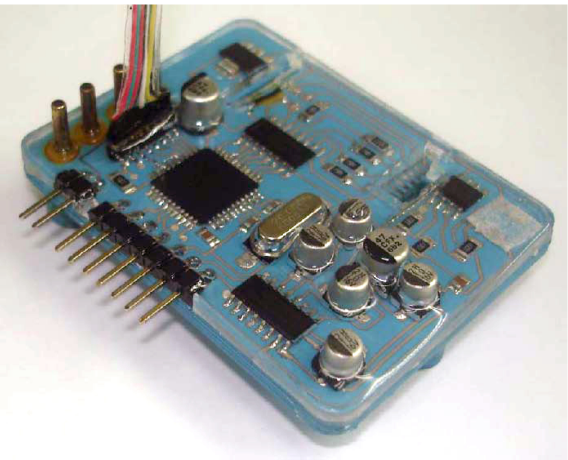

Fig. 5.4: State-of-the-art LTCC photometer device for phosphate ion determination of water pollution from fertilizers; PDMS is deposited over the circuit for environmental protection. Presented by Da Rocha in 2008 [171].

only: all the sensors and MEMS are mounted on surface, except for buried heaters. This is to be compared with our multifunction integrated sensor (section 5.3) where all the active sensor parts (but the conditioning electronics) are in LTCC.

Photometer Device for Phosphate Ion Determination The construction and evaluation of a miniaturized photometer device for phosphate ion determination was presented by M. R. Gongora Rubio at CICMT 2008 in Munich, Germany [171]. The device is an LTCC continuous flow system for the monitoring of the eutrophication process of water ponds due to pollutants. It allows the detection of fertilizers (nitrites, ammonium & phosphorous species), of dissolved oxygen and of heavy metal contamination in lakes. It is depicted on Figure 5.4; the LTCC is covered with PDMS for environmental protection. Polydimethylsiloxane is one of the most widely used silicon-based organic polymer.

5.2.4 Hot plates, humidity and gas sensors

These devices are presented together, because they usually share common thermal elements in their working principle. We present here two gas sensors, several microheaters, a humidity sensor and a gas viscosity sensor.

For modern gas sensors, low power consumption is expected; compared with standard devices on alumina, LTCC sensors consume less power due to their lower thermal conductivity (2 to 5 W/m·K [75] instead of 24 W/m·K for the A-476 96 % of KYOCERA [152]). In addition, LTCC technology offers the possibility to structure sensor substrates to almost any desired shapes; this is perfect for minimizing the thermal consumption.
PISARKIEWICZ presented in 2003 a gas sensor made with an LTCC hotplate mounted on a TO-5 package [172]; it is depicted on Figure 5.5a.
JAROSLAW KITA, from the UNIVERSITY OF BAYREUTH in Germany, published in 2005 an interesting article [173] with several pictures of his hot-plate gas sensor realizations in LTCC (see Figure 5.5b). He performed thorough thermal characterization, and concluded that although laser cutting enables to obtain thin beams (as low as 200 µm fired, minimizing thermal dissipation), maximal reduction of beams cross-section is not recommended, because of poor mechanical stability. The further reduction of power consumption should be achieved by reduction of the hot-plate dimensions.

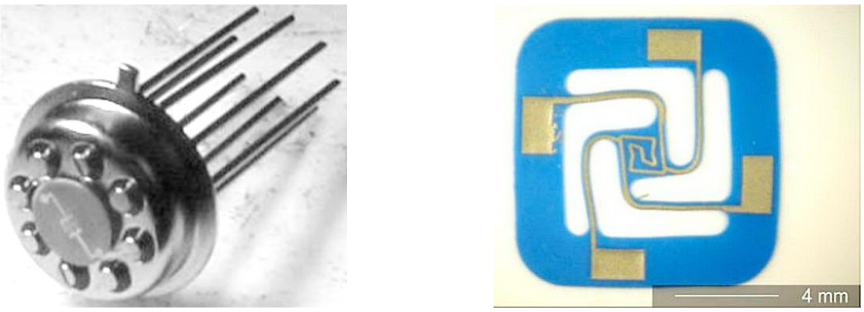

(a) LTCC hotplate on TO-5 for gas sensor [172].

(b) LTCC hotplate (KITA [173]).

Fig. 5.5: Two state-of-the-art LTCC hotplates and gas sensors.

Another type of micro-heaters was presented in 2005 by PETERSON of SANDIA NATIONAL LABORATORIES int the admirable review of non-microelectronic meso-scale applications [108, 109]: heated LTCC tubes (Figure 5.6). These curiosities were made by two differents methods: by rolling a sheet (device *(1)* of Figure 5.6a and those of Figure 5.6b), and by stacking (the device *(2)* of Figure 5.6a is made of 300 layers of DP951-254 µm).

We will not forget to mention the integrated oxygen-getter & sensor module developed by my supervisor, Dr. T. MAEDER, presented at IMAPS CICMT 2008 [174]. This device, intended for the atmosphere control of packages, was tested in various getter geometries (meander or rectangular, see Figure 5.7). It consists of a Pt-heated LTCC micro-hotplate carrying an active (getter and sensitive) material, whose state may be monitored by measuring its electrical resistance. Preliminary studies for an appropriate active substance were carried out using Fe,

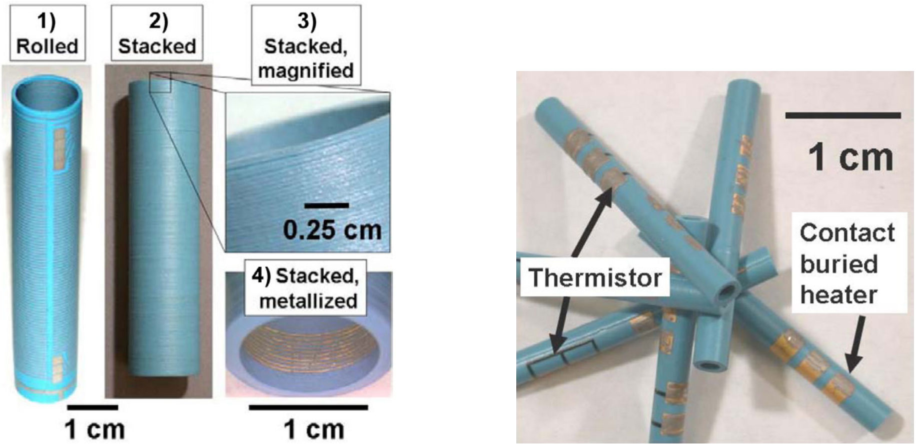

(a) Fired LTCC tubes: *(1)* Rolled, *(2-3)* Stacked, *(4)* Metallized and stacked.

(b) Miniature rolled heated tubes with thermistors simplify point-of-use heating.

Fig. 5.6: State-of-the-art LTCC heated tubes made by Sandia National Laboratories [109].

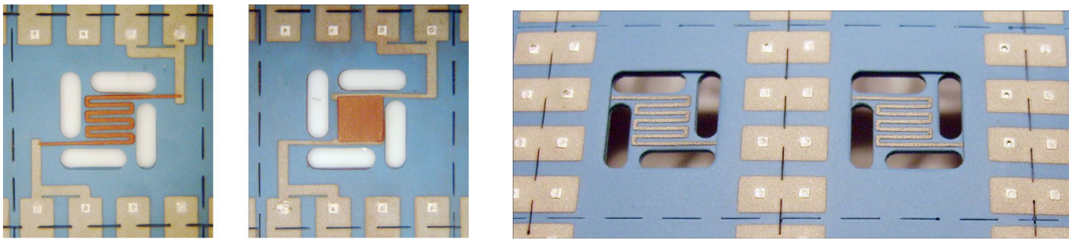

(a) Top side: getter. *Left:* meander geometry; *Right:* rectangular geometry.

(b) Bottom side: heaters; resistance ca. 5 Ω.

Fig. 5.7: Oxygen-getter module presented by T. Maeder at IMAPS CICMT 2008 [174].

first fired as Fe_2O_3, then reduced to Fe in a N_2:H_2 (4 % H_2) ambient. The results show that, in principle, this method is validated, and that conductive porous metal films may be produced in this way. However, the mechanical integrity of the films was still too low, indicating insufficient sintering of the reduced Fe, together with probable decomposition of the glass frit. The results were overall mitigated.

A humidity sensor of thermal conductive type was designed by Smetana in 2006 [175]. The measuring principle is based on the resulting difference between the thermal conductivity of dry air and that of water vapor at elevated temperatures. The device is made by the assembly of two different LTCC tapes with glass sealing: the substrate is made with 1 layer of ESL 41020-114 µm, and the cap is made of 3 layers of CeramTec GC-320 µm. The sealing glass is the paste ESL 4011C. A schematic view and a picture are displayed on Figure 5.8.

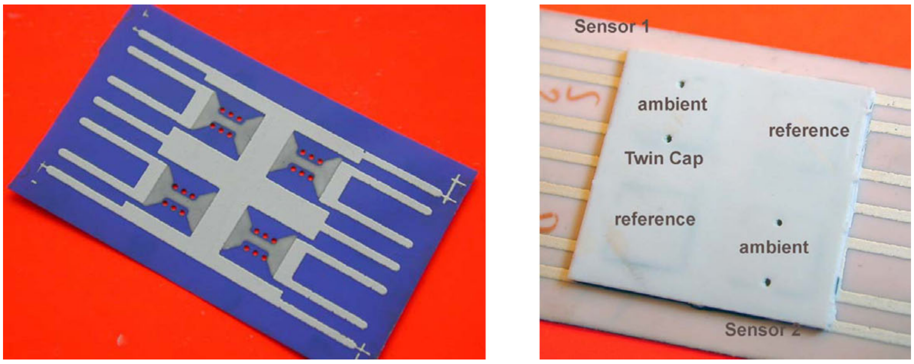

Fig. 5.8: Humidity sensor made of two different LTCC tapes, by Smetana [175]. *Left:* H-shaped sensor element arrays placed on a LTCC-substrate ESL 41020-114 µm. *Right:* A pair of humidity sensors with a mounted cap (top view). The LTCC cap is made with the CeramTec GC tape tape (240 µm fired thickness).

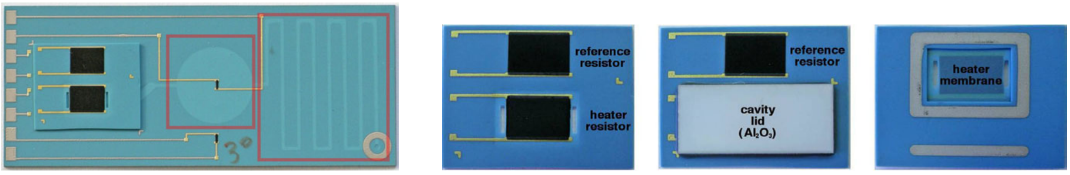

(a) Top view picture; the sensor three parts are, from left to right: heater module, integrated pressure sensor and meander.

(b) Heater modular; top view (*left and center*) and bottom view (*right*).

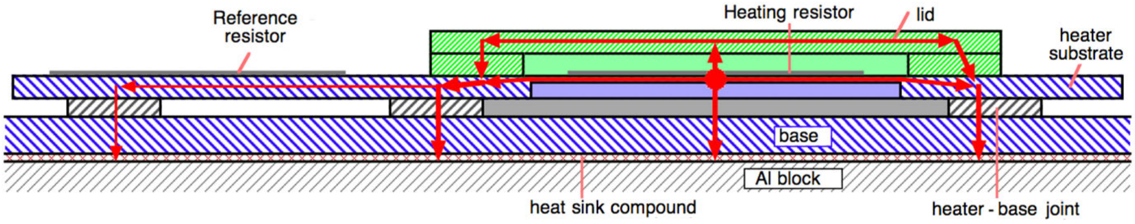

(c) Schematic cross-section with thermal flow (in red).

Fig. 5.9: LTCC gas viscosity sensor measuring the "Wobbe index", developped at EPFL-LPM [176].

Finally, our laboratory also developed a gas viscosity sensor for measuring the "Wobbe index"[2] in gas heating appliances (Figure 5.9). The device comprises a meander (fluidic resistor), a pressure sensor (membrane with thermal element) and a modular heater (assembled by soldering). The pressure sensor is issued from the research of Birol [113], and was modular in the early version before being integrated in the sensor substrate. The project was presented by T. Maeder at IMAPS 2007 Deutschland [176].

---

[2] The Wobbe index is an indicator of the interchangeability of fuel gases such as natural gas, liquified petroleum gas (LPG), and town gas.

5.2.5 Miscellaneous sensors

Back in 1998, BAUER listed in [177] different variants of lamination techniques and presented an LTCC electronic circuit with a buried, wire-bonded die and fitted with fluidic microchannels for cooling. Other fluidic devices are listed next.

Fluidic micromixers GONGORA RUBIO listed in [170] 3D serpentine mixers in LTCC, and Kaminski published in [178] a Y-mixer with microchannels made from the assembly of a single-tape central LTCC structure with two PMMA lids. As one could expect, the channel made in a single LTCC tape suffered from deformations. To circumvent this problem, a solution exist by splitting the channel accross two LTCC layers, which we did in our microreactor presented on section 5.5.
An LTCC enzymatic microreactor was presented by MALECHA, GOLONKA et al. in 2007 [179]; the device is simply made of three different LTCC layers, which are then covered with a PDMS lid for fluidic ports. THELEMANN listed similar mixing structures in 2007 [18], along with an interesting long-term dissolution test of DP951 (see section D.2 on page 241).

Microfluidic diode In the conference paper of CICMT 2008 [180], M. R. GONGORA RUBIO et al. present the development and characterization of a hybrid microfluidic diode structure based on LTCC technology associated to a sapphire valve seat and a sphere as a mobile part, as shown in Figure 5.10. The proposed diode structure is comprising two metallic input/output flanges, the LTCC body, a net structure made from LTCC or a metallic mesh embedded in LTTT (Low Temperature Transfer Tape, see section 6.2.4 on page 212) ceramic material and a sapphire ball valve seat and sapphire ball.

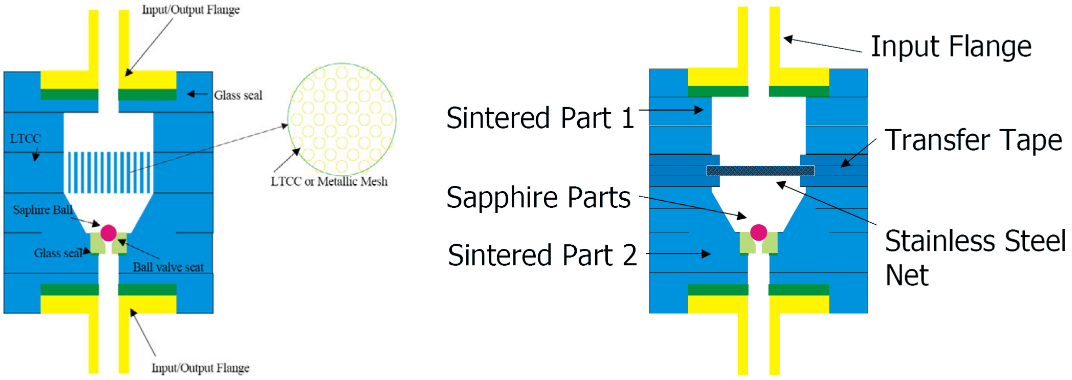

(a) Variant with LTCC core; the net is in LTCC too.

(b) Variant with a core in LTCC and LTTT (Transfer Tape); the net is in stainless steel.

Fig. 5.10: Two design variants of a microfluidic diode presented by M. R. GONGORA RUBIO at CICMT 2008. The glass seals, the sapphire ball and the flanges are common to both variants [180].

5.3 Integrated multisensor

5.3.1 Industrial needs and state of the art

The introduction (see section 5.1) presented the technological background of this project. We will now approach the industrial needs that motivated it.
Over the past years, the fields of sensors and microfluidics in LTCC technology have been explored, adding new possibilities to this material initially developed for high-density electronics and packaging. Research has led to the emergence of micro-heaters, flow sensors, pressure sensors, micro-reactors, fluidic mixing channels and bioreactors. However, these devices were mainly developed as stand-alone products without integrated signal amplification and conditioning, and not suited for industrial applications with surface mounting technology (SMT).

On the commercial market, many fluidic sensors of various types are available and offer high-precision measurements ($\leq 0.3\,\%$ of full scale). They usually require to be physically mounted vertically or horizontally by tightening, and to be connected with large gas fittings (e.g. G1/2"). The electrical lines transit through connectors such as the DB9 or standard copper wires. These sensors are generally priced well above 100 USD, and are sometimes coupled to regulators (for pressure or flow). Such devices are well suited for precise measurements; however, their performances, dimensions and price are much too high for diagnostics or safety purposes. There is clearly a need for simple, easily mountable, low-cost, low-precision, yet reliable fluidic sensors, in particular in the pneumatic industry to monitor valves and actuators. As we will see next, the sensor we propose is innovative in many points.

Evidently, such a complex sensor cannot be designed directly from scratch; its final development is the result of merging prototypes issued from students projects and the fruit of our initial former experience for the assembly method by soldering (section 2.3). Our laboratory had previously developed different kinds of sensors in standard thick-film technology and in LTCC, aimed for the low-cost, mass production industry; for instance, a prototype of micro-flow sensor for liquids [181] was integrated in a disposable microreactor driven under LabView (see section 5.5). However two key prototypes were at the origin of the new integrated sensor:

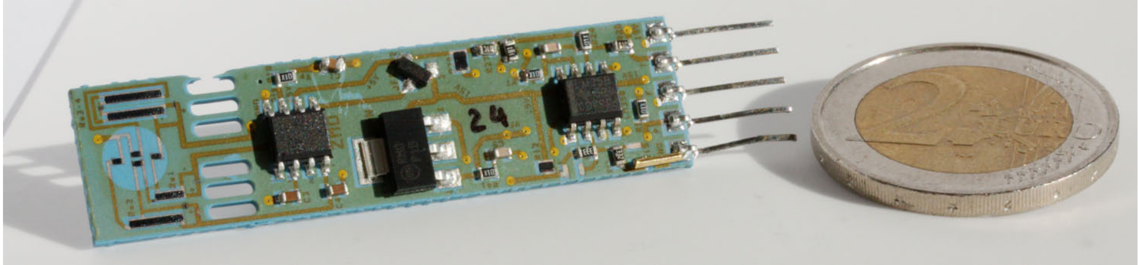

Fig. 5.11: Our innovative LTCC fluidic multisensor with integrated signal conditioning electronics. It allows measuring compressed air pressure, flow and temperature. It can be entirely mounted by soldering on its bottom face (see Figure 5.19), thus making it a true *electro-fluidic SMD device* on its own – which was never achieved before. The five pins on the right are for test purpose only.

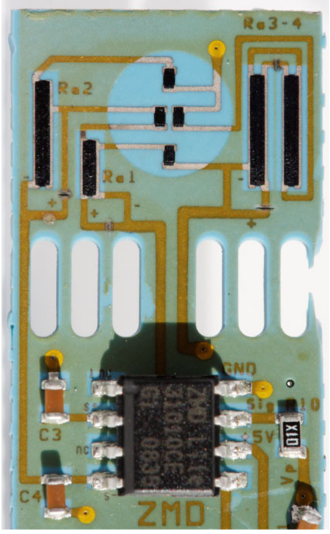

Fig. 5.12: Pressure sensor section with its piezo-resistive bridge and ZMD signal conditioning electronics [183]. The outermost right arm was accidentaly broken, without impact on performance.

1) An SMD pressure sensor with integrated electronics was realized in 2008 [182]; it is shortly described in the Appendix section C.1 on page 232.
2) A flow sensor demonstrator followed in 2009 to determine the most suitable measurement principle (calorimetric or anemometric) [182]; its development is summarized in section C.2 on page 236. The anemometric principle proved to be sufficient for coarse measurements, i.e. typically required by applications involving diagnostics.

In this application we propose, for the first time, a combined SMD sensor in LTCC for measuring gauge compressed air pressure, flow and accessorily temperature, integrating signal conditioning electronics for linearization, adjustment and (for pressure and flow) temperature compensation (Figure 5.11). The pressure measurement is based on thick-film piezoresistors mounted in Wheatstone bridge on an LTCC membrane (Figure 5.12); the nominal range is 0…6 bar, with a repeatability of 0.1 %, and a precision of 1 %. The air flow measurement is based on the anemometric principle, with a heating/sensing thermistor placed in the flow; see Figure 5.13. The intended range is between 0 and 100 NL/min when using a bypass (only a fraction of the total flow is measured). Finally, two thermistors upstream and downstream give the fluid temperature.

The design of the integrated SMD sensor is described in subsection 5.3.2, with manufacturing steps in subsection 5.3.3. The performances and limitations of each fluidic function are analyzed in subsection 5.3.4, as well as the LTCC issues encountered.

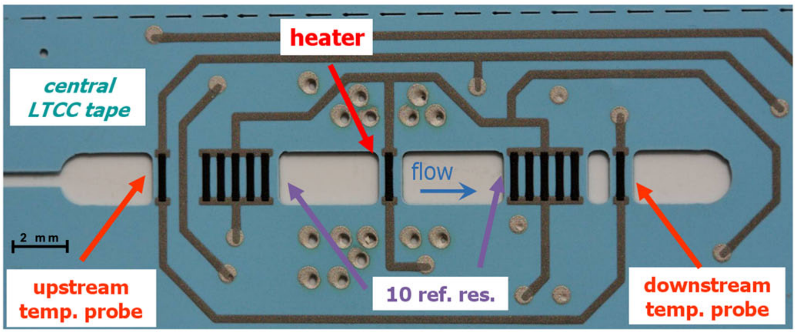

Fig. 5.13: Central LTCC tape (T3) showing the flow + temperature sensor sections. The heater resistor is surrounded by Ag thermal vias; conductor tracks are in Ag:Pd.

5.3.2 Design considerations and fluidic functions

Design guidelines

The integrated sensor was designed with the following guidelines, with the goal of achieving an easily manufacturable and mountable device. Most of the requirements had been validated with the prototypes of Appendix C.

1) Pressure sensor principle: piezoresistors in full Wheatstone bridge on a membrane. LTCC must be able to sustain an air pressure of at least 10 bar (nominally 6), in a non-aggressive fluid.
2) Flow sensor principle: anemometric, with 1 heating thermistor suspended on a bridge in the airflow. Aimed range is between 0 and 100 NL/min with a bypass. The reaction time should not exceed 3 s.
3) Temperature sensor: amplification of a resistive bridge comprising thermoresistors placed toward inlets. The intended range is 0. . . 100 °C.
4) Mounting-induced stresses should not affect the sensor measurements (mainly for the pressure).
5) The device must be compatible with surface mount technology (flip chip). No external wires and no tubes for connections; all connections must be at the bottom, except for test pins.
6) Electronics for processing the signals must be integrated, with a maximum of five electrical connections: power, the three signals (one for each physical quantity), and ground.
7) Laser trimming should be restricted to easy operations:
    a) Coarse trimming of the pressure measurement bridge offset;
    b) Trimming of the differential temperature setpoint of the flow sensing resistor;
    c) Trimming of the temperature signal at room temperature. Cumbersome trimming under pressure or flow, which requires additional fluidic connections to the sensor, should be avoided.

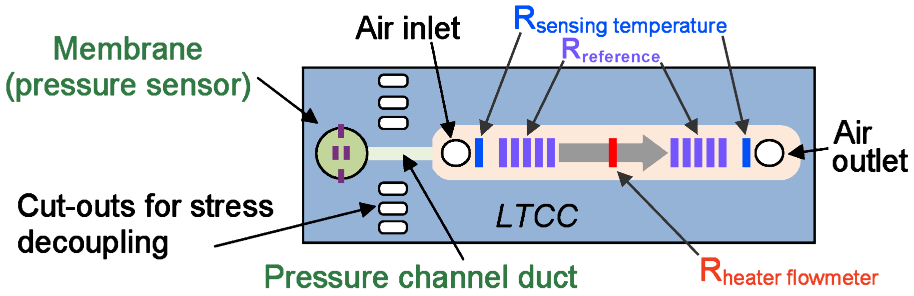

Fig. 5.14: Schematic top view of the integrated sensor, showing the placement of the fluidic functions and the elongated shape of the circuit.

8) Heating of the sensor body by heat flowing into the LTCC from the power transistor and the flow-sensing thermistor must be minimized, which entails providing a good thermal path through the LTCC to well-dimensioned solder pads at the bottom of the device.

Mechanical arrangement

Due to the rather contradictory aspects of the fluidic functions involved, the placement of the sensing elements and the overall shape of the circuit are of capital importance. While the pressure sensor has to avoid heat and mechanical stresses, the thermal flow sensor must be at the same time insulated from external influences, and evacuate parasitic heat efficiently to the outside. Furthermore, the temperature sensor should measure the actual fluid temperature, and not the result of the flow measurement.

These considerations rapidly led to the selection of an elongated shape for the device, as depicted on Figure 5.14. The fluidic inlet and outlet form the outermost parts of the bottom attachment footprint of the circuit, with the electrical connections lying in between. The pressure sensor is placed free-hanging beyond the outermost attachments to isolate it from mounting stresses. As this free-hanging zone is small in relation to the overall device, mechanical stability remains ensured. Figure 5.15 displays a semi-transparent 3D view of the sensor.

Flow sensor section

On the former prototype (section C.2), two thermal mass flow measuring principles were tested: *calorimetric* (heat diffuses faster than air flows, very sensitive but limited to $< 5\,\mathrm{NL/min}$), and *anemometric* (flow goes faster than heat diffuses, less sensitive but compatible with high flows). The latter principle was therefore adopted for the industrial device aimed for in the present work. A bypass arrangement may be used to extend the flow range even further, as depicted in Figure 5.16.

The flow sensing circuit is a Wheatstone bridge, with one branch consisting in thick-film thermistors in the channel (1 heating/sensing resistor R_{+hi}, plus 10 identical ones in parallel forming R_{+lo}, as reference, cf. Figure 5.13) and the other branch consisting of two fixed reference resistors R_{-hi} and R_{-lo}. In the left branch of the bridge, the choice to use 10 resistors

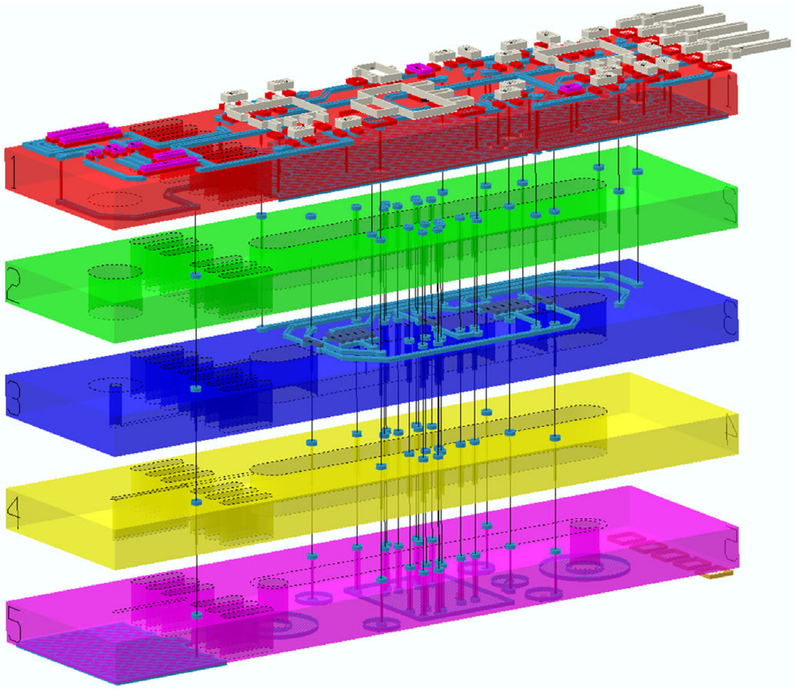

Fig. 5.15: 3D, semi-transparent exploded view of the integrated sensor, showing the five LTCC tapes.

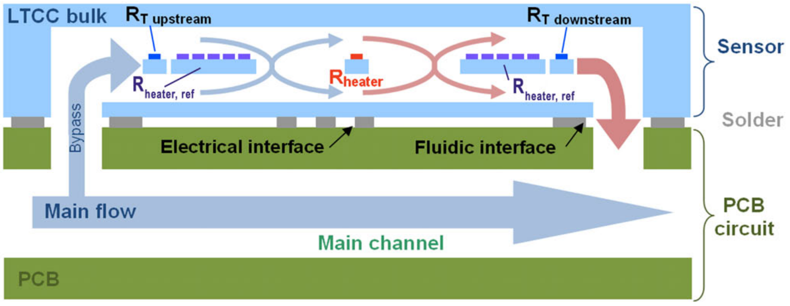

Fig. 5.16: Schematic view of the flow + temperature sensor sections when mounted on a fluidic PCB, depicting the bypass and thermistors.

vs. the heater was dicted by the assumption that a 10:1 ratio would yield negligible heating in the reference elements. We realized after the first manufacture iteration that the optimal number of resistors, in order to get the best signal over electric power ratio was inferior to 10; a number of 2 would theoretically yield the highest signal, while greatly simplifying design and manufacturing.

We aimed to regulate the central heating resistor R_{+hi} ca. 40 K above the reference one R_{+lo}, estimating this was a good compromise between sensitivity and power consumption. This is done by introducing a controlled nominal inbalance in the bridge, which is actively corrected during operation by the temperature rise. Temperature regulation is carried out by an amplifier (Figure 5.17) whose output is buffered by a power NPN transistor and fed to the Wheatstone bridge. To ensure a valid measurement, a minimal bridge supply voltage is ensured by a pull-up resistor in parallel with the transistor. This bridge supply voltage is also the output signal, and

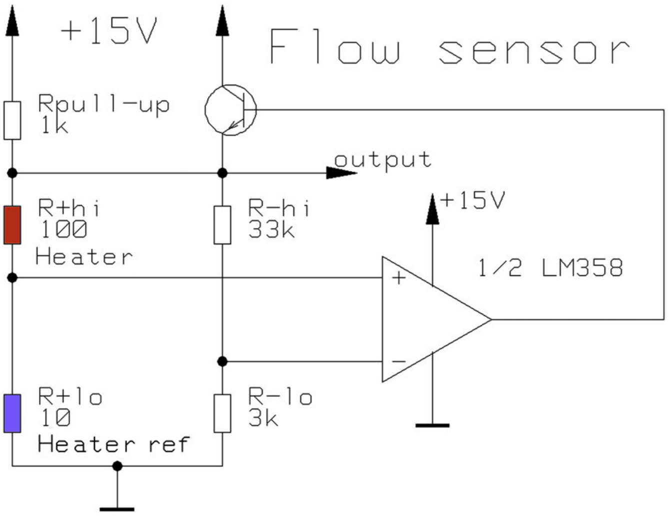

Fig. 5.17: Simplified electrical schematic of the flow sensor section. It is basically a Wheatstone bridge with an amplifier, whose buffered output heats the measuring resistor to regulate its temperature.

increases continuously with the flow.
Several design features were implemented to optimize heat management:

- The heating resistor was thermally decoupled from the LTCC sensor body as much as reasonably possible.
- In order to minimize the effects of the heat leaking from this resistor to the device, its surrounding zone is provided with an array of thermal vias connected to the bottom ground solder pad for heat extraction.
- The NPN power transistor is implanted close to the same thermal vias.
- An Ag ground plane is located under tape T1 to improve heat dissipation from the top SMD components to the bottom solder pads. It however does not extend under the pressure membrane to avoid biasing the piezoresistors.

Pressure sensor section

To decouple the pressure membrane from the mechanical and thermal stresses (due to soldering during assembly, heat dissipation, etc.), it is advantageous to position it in a cantilever fashion at one end of the circuit, and to place oblong cuts to further mechanically decouple it from the main part of the sensor (Figure 5.12 and Figure 5.14).
Measurement of the former demonstrator (Appendix section C.1), fitted with the ZMD31010 signal conditioner [183], gave outstanding results: the repeatability of the sensor was better than 0.1 %. Schematics of the layout can be seen in Figure C.4 on page 234. Hence, only a few changes were necessary for the new design: lower values of the coarse offset adjustment resistors, and the addition of a MMBF 4492 JFET transistor to get a constant 5 V voltage supply for the piezo-resistive bridge and the ZMD chip (with the V_{gate} pin of the ZMD chip driving the gate of the JFET). The whole sensor is supplied at 15 V.

Temperature sensor section

For the temperature measurement, it was decided to use two thermistors in series, one close to each fluidic connection to measure the average of inflow and outflow and thus be insensitive to flow inversions. This compound thermistor is in series with a fixed one in a half bridge arrangement, and the resulting signal is amplified.

5.3.3 Experimental

Manufacturing

Sensors are produced in batch of four per fired circuit, with three variants of flow channel width: 2.0, 2.5 and twice 3.0 mm. The dimensions of a fired sensor are 50×12.7×1 mm after singulation.

LTCC tapes Based on the previous attempts of Appendix C, the tape system chosen is the DP951PX (254 µm unfired thickness). Thinner tapes (114, 165 µm) are a possible choice for the membrane, but this less conservative choice would require more testing in order to ensure reliability. The sensor consists of five different LTCC tapes (T1-T5), which were sometimes doubled (for a total of five to eight layers) as described below:

T1	top lid (printed on both faces, with Ag ground plane below)
T2, T2b	upper channel (vias only)
T3, T3b	thermistor bridges
T4, T4b	lower channel (vias only)
T5, T5b	floor (printed on both faces)

The unfired, printed tapes are all shown on Figure 5.18. All tapes were 254 µm thick unless specified otherwise. Some manufacturing variants were produced:

- T3 was tried using 114 or 165 µm thick tape, in order to decrease conduction heat losses.
- T5 was doubled (T5b) to increase lid rigidity (see tape issues in section 5.3.4).
- T3 was doubled (T3b) to create a sandwiched version of the thermistor bridges (desirable for media separation, in case gases more aggressive than air must be measured).
- T2 & T4 were doubled (T2b, T4b) to increase channel height and increase the distance from bridges to floor & lid.

The retained pastes are Ag DP6141 for vias, Ag:Pd DP6146 for tracks and pads, Ag DP6145 for the inner ground plane, DP2041 (10 kΩ/□) for piezoresistors, and DP5092D (100 Ω/□) for thermistors; all are cofired. In post-firing there is an overglaze on both faces (DP QQ550, but ESL G-481 would suit too), and finally a lead-free 96.5 Sn-3 Ag-0.5 Cu solder paste on top for the SMD components.
The reason why Ag (e.g. DP6145) was not selected for the tracks of T3 is due to a known

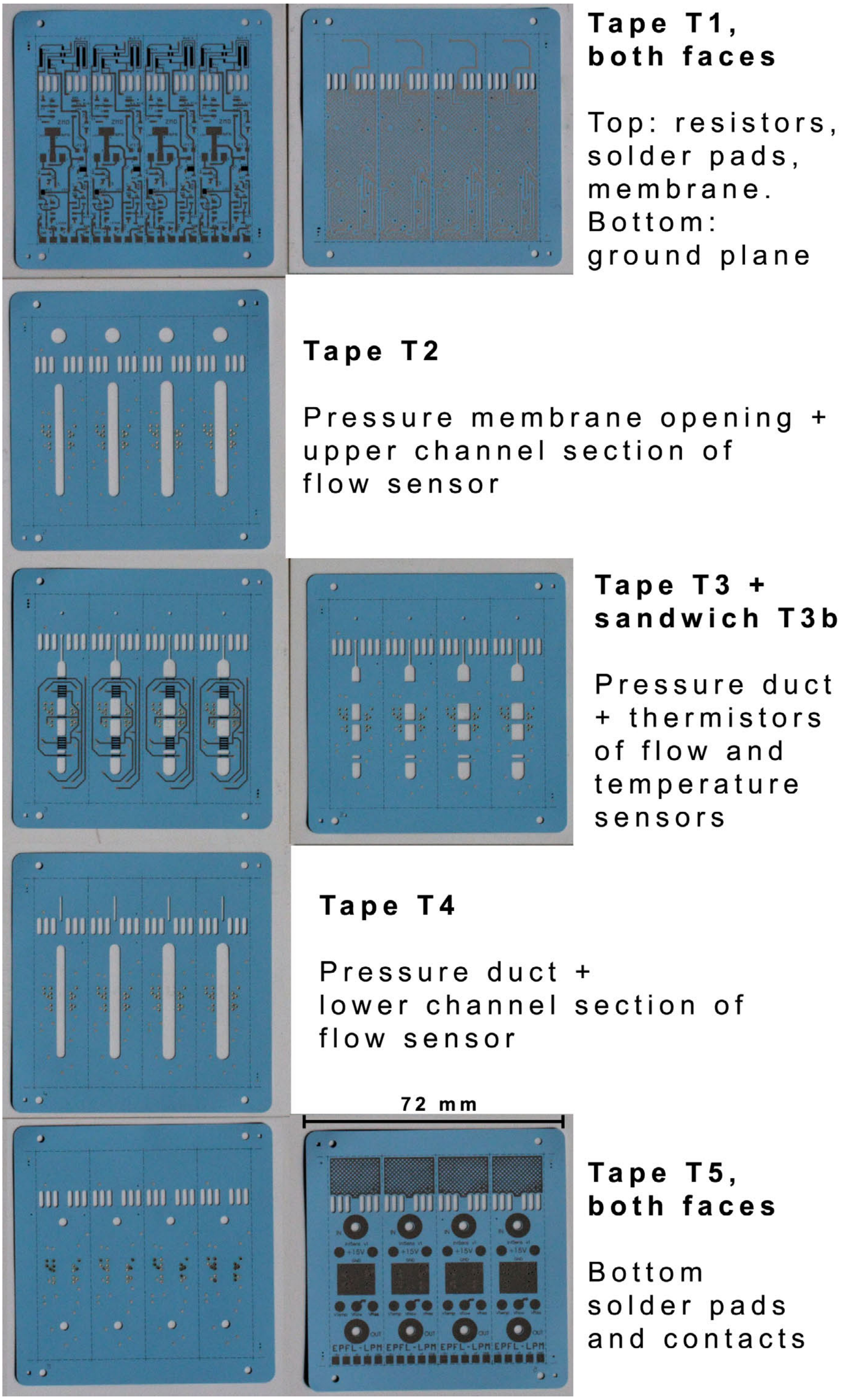

Fig. 5.18: Top view displaying all five LTCC tapes of the integrated sensor (unfired), screen printed and ready for stacking and lamination, with bottom faces of tapes T1 and T5.

incompatibility with the PTC resistor terminations. Gold terminations, similarly to those used for the flow sensor and microreactor of section 5.5, would also be a good solution; however, this would either require an additional screen printing (the gold paste cannot be directly linked to the Ag via fill), or the via fill should be replaced by the DP6138 Ag:Pd.

LTCC processing After removing the MYLAR protection tape and pre-conditioning at 120 °C for 30 min, the LTCC tapes were laser cut using our Nd:YAG trimming laser (see subsection 2.2.3). The tapes were then screen printed with an AUREL 900T (subsection 2.2.4) in the following successive order, when applicable:

- Vias filling (holes Ø 0.2 mm, catch pads Ø 0.7 mm; thermal vias Ø 0.4 and 0.65 mm respectively);
- Conductor printing (linewidths 0.15. . . 0.5 mm);
- Resistor printing (active length 1.6 mm, width 0.3 mm, measured dried thickness 27. . . 34 µm).

Between each print, the tapes were allowed to level at room temperature for 5 to 10 min and dried for 3 min at 100 °C in an air oven. After printing, the tapes were stacked and uniaxially laminated between protection sheets (MYLAR or LDPE foil). The whole procedure is described in subsection 3.3.2 on page 74.
After removal of the protective sheets, the stacks were placed on standard alumina substrates and fired in a lamp furnace (ATV PEO-601 [58]) with an air flow of 200 L/h. The firing profile was standard, with a long organic burnout to ensure complete combustion (200 min from 250 °C to 450 °C), followed by a 5 K/min sintering ramp and 30 min dwell time at 875 °C. The overglaze (acting as anti-solder mask and protection) was printed and post-fired (510 °C) separately in a belt oven (see subsection 2.2.8).

Mounting of SMD components, singulation and assembly on PCB The SMD components were soldered on top of the substrates using Sn-Ag-Cu solder. This was followed by singulation of the devices, and mounting them onto fluidic test PCBs using a lower-melting Sn-Pb or Sn-Bi solder. These PCBs consisted of three FR4 epoxy plates: base (bottom), channels (middle), and orifices & contacts (top), stacked and glued together. The final result can be seen on Figure 5.19.

Pressure calibration First, a coarse adjustment of the raw bridge offset was carried out by digital laser trimming of the adjustment thick-film resistors, to bring the offset within the ~60 mV/V accepted by the ZMD chip. Then, the calibration procedure of the ZMD chip was carried out with the help of the ZMD SSC EVALUATION KIT (for programming) and with a DRUCK DPI520 pressure regulator (max 5 bar gauge, precision of 0.1 mbar). The pressure signal was set to deliver between 0.5 and 3.5 V for a range of pressures from 0 to 6 bar (gauge). The calibration went as follows:

- Pressure stabilized at 0.0 bar → measurement of first raw bridge value;

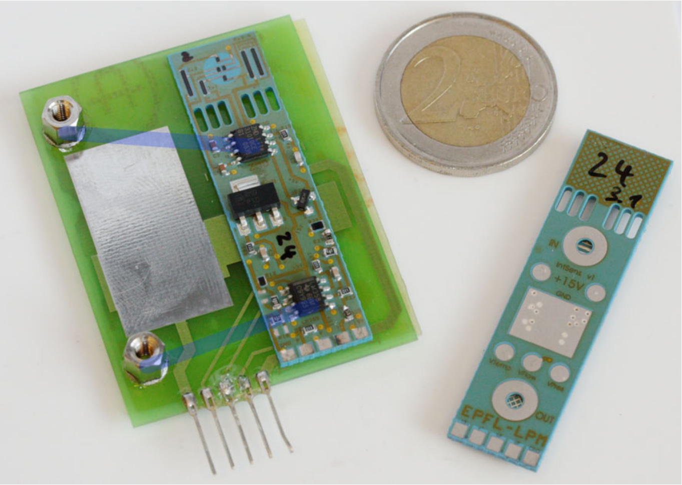

Fig. 5.19: *Left:* integrated sensor mounted on fluidic PCB with channels highlighted in transparent blue. *Right:* bottom face of LTCC sensor showing contact and solder pads, as well as (greenish) overglaze protection.

- Pressure stabilized at 4.5 bar → measurement of second raw bridge value;
- Computation of the signal conditioning coefficients (gain and offset), and writing into the chip EEPROM.

Measurements

Flow measurements A Voegtlin GSC-C4TA-BB26 regulator (0 to 20 NL/min; accuracy ± 0.3 % of full scale) was used as flow reference. No bypass was used in the pneumatic layout, and the PCB was placed downstream of the regulator. Two kinds of measurements were executed:

- At 20 NL/min, the power supply was gradually increased from 0 to 14.8 V to evaluate the behavior of the sensor and determine the nominal temperature rise of the measurement thermistor.
- At constant voltage in normal regulation mode, the flow was gradually varied and the output voltage recorded.

Pressure measurements The measurements were carried out by connecting the inlet to the Druck regulator and by closing the outlet, as follows: three ramps back and forth in a row, each going from 0 to 4 bar, and back from 4 to 0 bar; each ramp is made by steps of 0.5 bar. Once the desired pressure is set on the regulator, the software waits long enough (5 s) to allow stabilization, and records the pressure output voltage.

Temperature measurements Due to a lack of gas supply with adjustable temperature, it was at the time impossible to test and calibrate the sensor with a flowing gas. Measurements were therefore carried out in a HERAEUS air oven from 30 to 100 °C by steps of 10 K, exposing the whole sensor assembly to the temperature. For each step, the output voltage was first measured directly after powering up the sensor with 12 V, and again after 5 min to assess the influence of sensor self-heating.

5.3.4 Results and discussions

This chapter is divided between structural issues and measurements of each fluidic function.

LTCC issues

Deformation of suspended bridges To verify the integrity of the suspended bridges, the first firings consisted of incomplete LTCC circuits – only tapes T3 to T5 were stacked. The first manufactured bridges exhibited strong buckling, mostly downward but also upward in some cases, a problem clearly amplified with thin tapes (Figure 5.20b). On the contrary, the two parallel resistors blocks yielded less bending, which is thought to be due to the presence of some camber along the channel axis (the wide blocks assume a tile-like shape), which increases their rigidity and makes them less likely to bend. The problem was even more surprising that the former prototypes (section C.2) were unaffected (Figure 5.20a). We misbelieved the origin of this flaw to lie in the too big difference of shrinkage between the bridge and the bottom lid; all attempts to increase the "drum-skin effect" (subsection 3.3.2) to get a flat bridge by differential lamination failed.

Indeed, KELLIS et al. from BOISE STATE UNIVERSITY observed a similar effect in 2009 [184] on silver paste (type not reported), as well as BIROL in 2005 during his work on DP9473 (an Ag/Pd paste for alumina) to adapt it to LTCC for co-firing [185]. In our case, the bridge deformations were due to too wide Ag:Pd conductor lines: a possible explanation could lie in the relatively strong expansion of the palladium upon oxidation inducing a locally important reduction of LTCC shrinkage, which in turns leads to the buckling of bridges. The effect was not revealed in the former prototype (Figure 5.20a, see section C.2), for the Ag:Pd lines were chosen very thin (0.15 mm) to minimize heat transfer through the conductors. In the new design, the linewidth was increased to 0.3 mm to prevent any line breakup due to dust or particles, as it occurred in the project described in section 2.4 on page 46. The effect was further amplified by the presence of voluminous thermal vias around the path of the conductor line, which broadened the paste deposition upon screen printing of the Ag:Pd.

For this reason, it was compulsory to redesign the tape T3 by assigning the smallest linewidth for all conductors leading to suspended bridges, and to invert the screen printing sequence order between vias and conductors. For the chemical incompatibilities already exposed, it was also impossible to replace Ag:Pd by Ag or Au for these tracks.

Miscellaneous

- Some complete LTCC sensors exhibited considerable bending in their length, yielding a camber of ~0.4 mm when laid onto a flat surface (Figure 5.21). We believe this camber

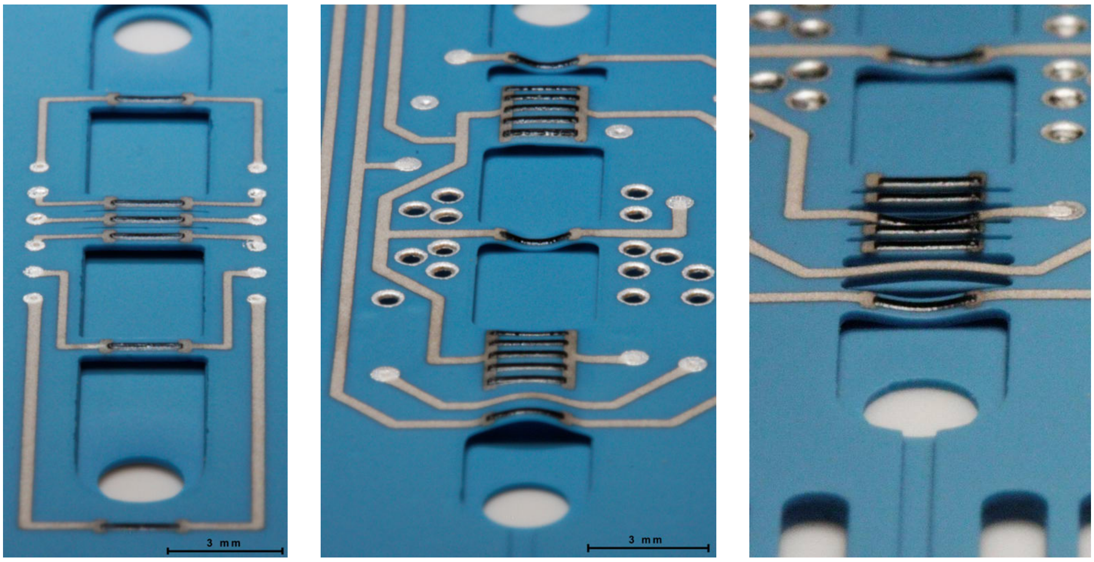

(a) Flow sensor proto: intact bridges because narrow Ag:Pd tracks leading to resistors are narrow (0.15 mm); induced deformations are thus negligible.

(b) Integrated sensor: strong deformations of suspended bridges. Note the difference of buckling between resistor blocks, single resistor bridges, and full conductor bridge due to the thick Ag:Pd conductor tracks (0.3 mm).

(c) Integrated sensor with lasered cuts between resistors: only suspended bridges with leading Ag:Pd tracks are buckled; those with terminations only are flat.

Fig. 5.20: Close-ups on voluntarily incomplete LTCC flow sensors to assess a manufacturing issue.

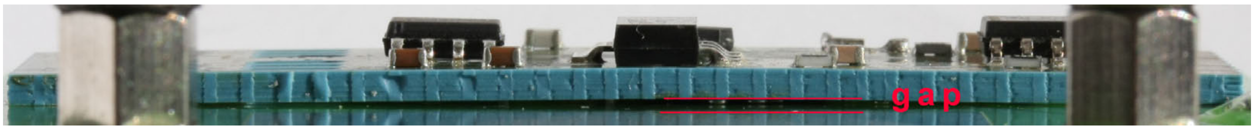

Fig. 5.21: Side view of integrated sensor mounted on PCB depicting convex sensor bending. Note the gap in the middle, which yields a camber of ~0.4 mm.

may be due to the large Ag:Pd ground solder pad at the bottom of tape T5, for the same reasons exposed in the previous paragraph.

- The outermost arm of the oblong pressure section cut-outs had a tendency to break up upon manual singulation (Figure 5.12), due to the singulation stamp-like cuts placed too close to the arm.
- For variants of thinner central tape, a sandwich (by doubling tape T3) was employed to minimize the warping effect. The lamination of this sandwich often led to the separation of the tapes, even before the firing: the lamination conditions must still be optimized in order to achieve good interlayer bonding while keeping deformations low.

Flow

Characterization vs. supply voltage First, the flow was set at the maximum value the controller could deliver, e.g. 20 NL/min, and the supply voltage gradually increased from 0 to 15 V. The high flow maximizes cooling of the sensing resistor, i.e. it allows measurement of the "cold" sensing bridge output. The behavior of device #23-2.0 is given in Figure 5.22. One can clearly see three different supply voltage ranges:

1) 0.0. . . 2.2 V: amplifier not active ($\mathrm{LM358}$ working at < 2 V, but emitter voltage is less than output);
2) 2.2. . . 8.0 V: amplifier saturated – insufficient voltage to balance bridge;
3) > 8.0 V: normal functioning – temperature controlled by amplifier.

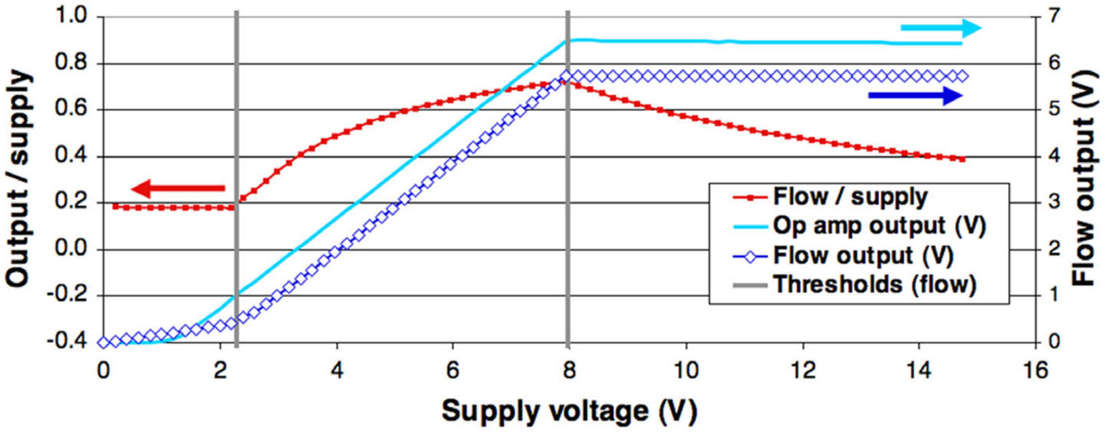

Fig. 5.22: Flow sensor voltage output vs. supply voltage for a fixed flow, showing three different behavior ranges.

The following aspects have to be borne in mind for such sensors:

- The pull-up resistor must give sufficient current to ensure reliable startup of the device, but not enough to passively heat the measuring resistor beyond its setpoint (which occurs more readily at no flow).
- The heating/measuring resistor must be able to reach its setpoint at the highest flow; for a given resistor, the bridge supply voltage must be sufficient.
- The $\mathrm{LM358}$ amplifier is not optimal for this application, due to its ca. 1.5 V saturation voltage drop relative to the positive supply rail and its relatively wide offset specifications; this can be improved by using a rail-to-rail device.
- It is better to use the bridge supply as an output rather than the output of the amplifier, as temperature changes affect the base-emitter voltage of the NPN transistor.

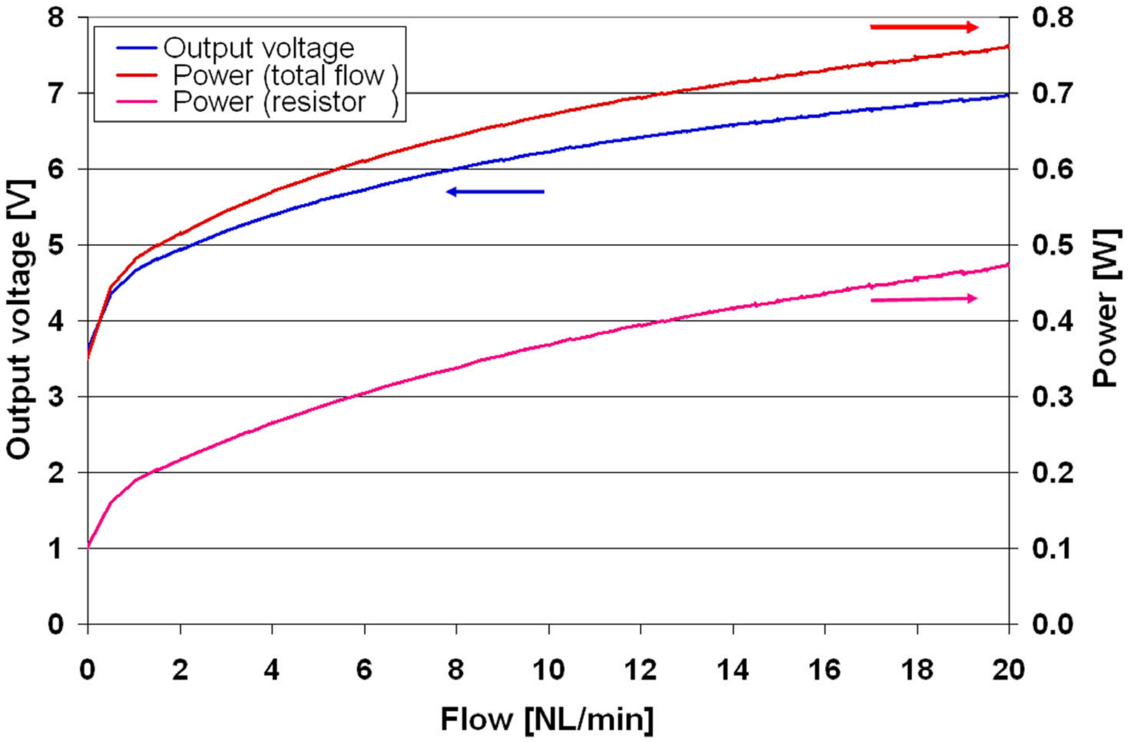

Fig. 5.23: Flow sensor voltage output response and power consumption vs. flow for circuit #23-3.1 under 10 V.

Characterization vs. flow The response of device #23-3.1 to flow, under a supply voltage of 10 V, is given in Figure 5.23. The output vs. flow (in blue) is evidently nonlinear, but is well correlated with the dissipated power (which is a square root with offset). The red curve is the total dissipated power of the sensor, while the fuchsia curve is the power dissipated by the heating resistor only. The total dissipation is relatively high, due to the linear regulation.

Pressure

Figure 5.24 shows the result of 10 pressure cycles on the signal, and the error vs. the original calibration step is plotted on Figure 5.25 (first and last cycle only). The total error is relatively low ($< 1\,\%$), and slowly drifted upward, an effect attributed to self-heating brought about by the flow sensor part (no flow and poor heatsinking), coupled with the temperature coefficient of the sensor offset (TCO). The selected ZMD conditioning chip can compensate TCO, so this source of error can be removed if necessary, although this adds one heating step to the calibration process.

The other main source of error is the slight 0.4 % decrease of span between calibration and measurement, which may originate from still imperfect decoupling of mounting stresses. Finally, the residual scatter may lie in the stability range of the pressure regulator.

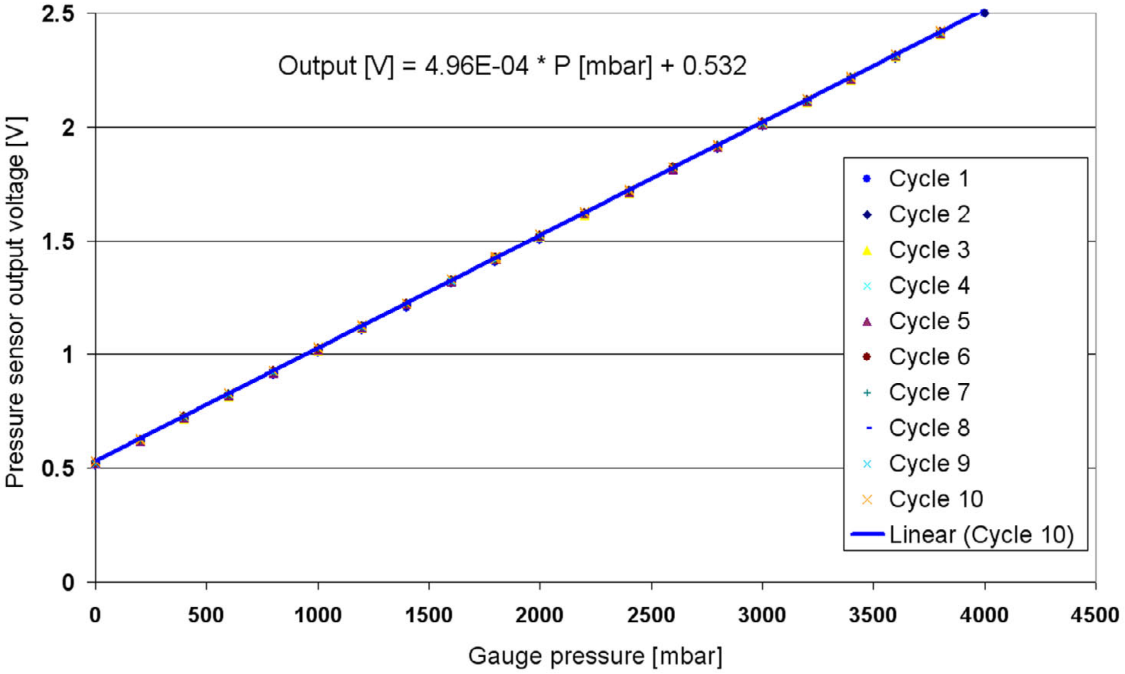

Fig. 5.24: Pressure sensor voltage output vs. gauge pressure for 10 cycles between 0 and 4 bar.

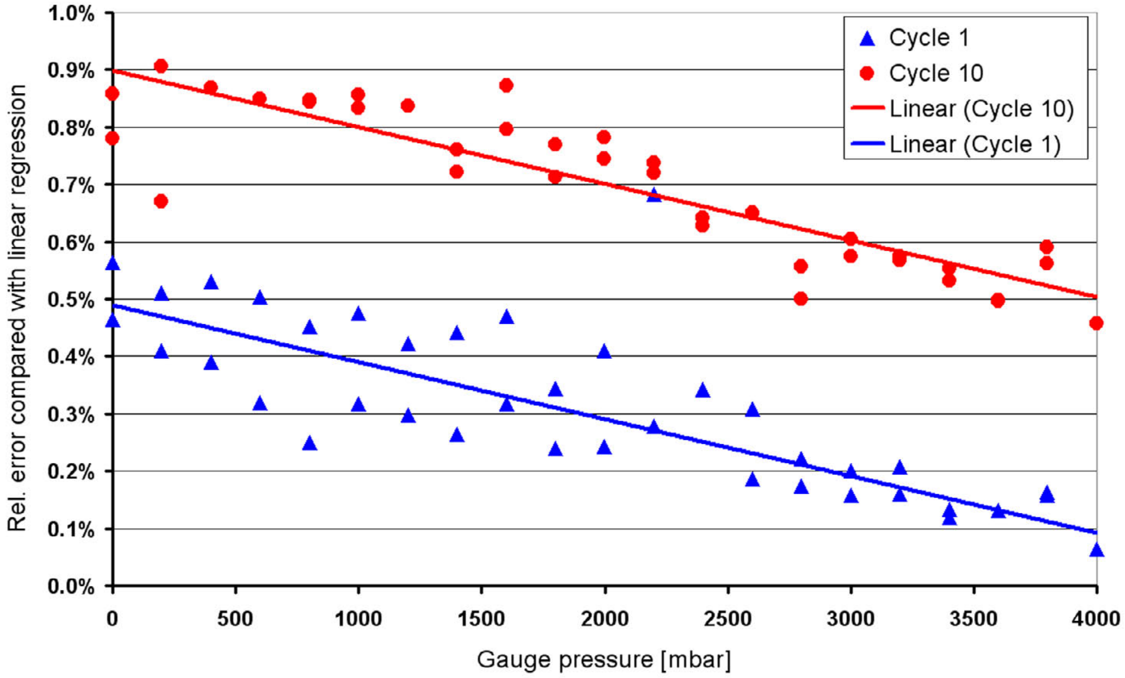

Fig. 5.25: Relative error of pressure sensor voltage output compared to a linear regression vs. gauge pressure for cycles 1 and 10.

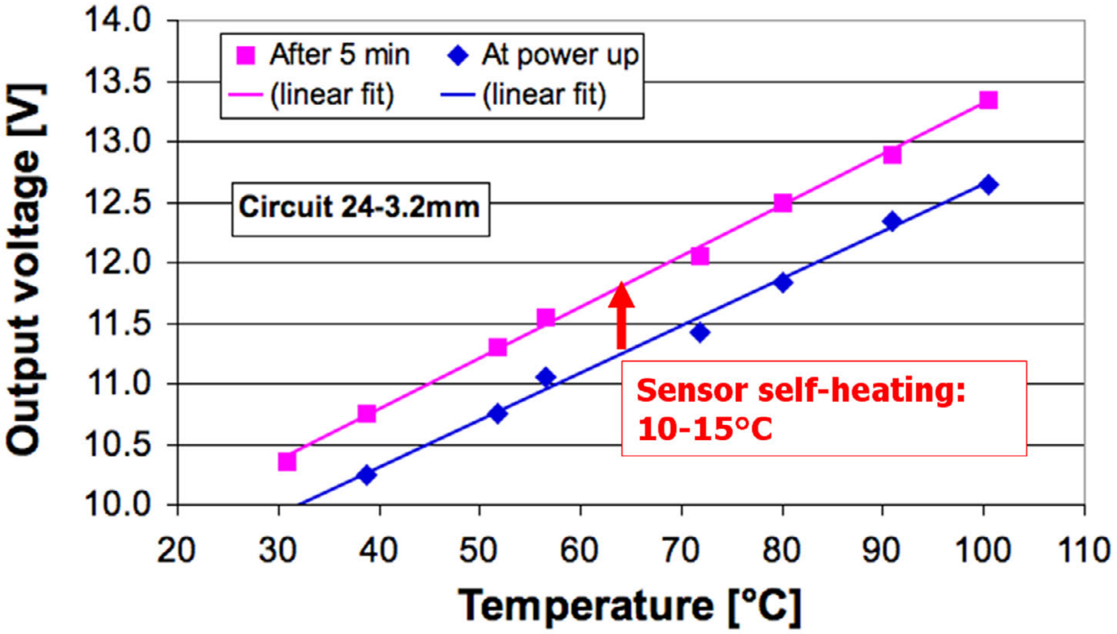

Fig. 5.26: Temperature output voltage vs. global sensor temperature, measured at t = 0 min since power up (blue), and at t = 5 min (fuchsia).

Temperature

The temperature output voltage presents a linear behavior with the global sensor temperature, as expected for this range. The graph of Figure 5.26 shows this in blue for the measurements at t = 0 min after power up, and in fuchsia for the measurements at t = 5 min. The sensor self-heating can clearly be seen with the vertical shift between the two trend lines, and is estimated to be in the order of 10 to 15 K.

5.3.5 Conclusion and outlook

A combined LTCC fluidic multisensor allowing measurement of standard industrial compressed air pressure, flow and temperature with integrated electronics was presented. This innovative device can be mounted with standard surface mount technologies onto an electro-fluidic platform, *de facto* making it a true *electro-fluidic SMD component* in itself. It comprises additionally its own integrated SMD electronics, and thanks to standard hybrid assembly techniques, gets rid of external wires and tubings – this prowess was never achieved before. This opens the way for *in situ* diagnostics of industrial systems through the use of low-cost integrated sensors that directly output conditioned signals.
The nominal ranges of measurement are 0...6 bar, 0...100 NL/min (tested up to 20 NL/min without bypass), and 0...100 °C, and are well adapted to industrial compressed air. Of course, they can easily be modified to suit other sensing needs.

Outlook Even in this first version, the pressure sensor section is already quite satisfactory (an overall precision of 1 % is achieved), as well as the temperature sensor part (which uses a "free" amplifier channel, and only requires a simple offset laser trimming step).
The flow sensor achieves robust and reproducible measurements, but its efficiency is quite low – the total power consumed is typically about three times of that needed to heat the measurement thermistor. The causes and possible solutions for this issue are discussed hereafter:

- **Heating resistor value too low.** The resistance must be designed to fit the combination of temperature differential setpoint and supply voltage, e.g. not to have excessive voltage headroom.
- **Thermal losses between heating resistor and sensor body:**
  - Further reduction of conductive and convective losses is still possible by minimizing bridge cross section and area, but fabrication issues must be taken into account;
  - A simple way to lower these losses is to decrease the nominal temperature rise of the heater – further tests are needed to determine the resulting compromise between precision and power.
- **Inefficient electronics:**
  - Use of a rail-to-rail amplifier would allow a 1.5 V bridge supply voltage gain (at same power supply voltage), lowering the overall required power.
  - More radically, switching to a pulsed-width modulation (PWM) mode of operation would essentially eliminate transistor losses, albeit at the risk of generating interference.

Besides optimization of the flow sensor power requirements, this first version of a fully integrated sensor highlighted many more points that can be improved:

- **Flow output voltage.** In this version, the flow output was connected to the amplifier output (with a small resistor in series), which makes the device relatively resistant against short circuits, but introduces some thermal drift due to the (temperature dependant) voltage drop V_{BE} between the base and the emitter of the NPN transistor. Directly connecting the bridge supply voltage (e.g. the transistor emitter) to the output removes this dependency, but requires adequate protection against short-circuits.
- **Wheatstone bridge of flow sensing circuit.** In order to obtain a better signal over electric power ratio, the branch consisting in thick-film thermistors in the channel will be simplified: only 2 resistors forming R$_{+lo}$ as reference will be implemented, instead of the current 10 identical ones in parallel.
- **Flow and temperature sensor trimming.** The SMD resistors used in this version will be replaced by printed ones, which can be trimmed to calibrate flow and temperature.
- **Overall bending of the sensor.** The sensor design should be changed (partitioning of the ground solder pad) or other tape / thick-film materials must be tested in order to avoid bending of the whole sensor.
- **Soldering.** The sensor mounting process can be achieved with the same Sn-Ag-Cu solder paste as for the top components, which is an advantage as Sn-Bi is relatively less common and ill suited in applications where relatively high temperatures are reached. This requires greater care during reflow and better topside solder pads, as the solder of the top components will melt a second time.
- **Layout.** The layout of the inner ground plane and lines must be improved to suppress bottlenecks, and voltage test points must be added on surface for pressure offset adjustment, and sensor integrity control.
- **Pre-cuts.** The stamp-like pre-cuts allowing singulation by breaking must be changed to avoid destroying oblong cuts of the over-hanged section.

5.4 Capacitive microforce sensors enabled with SVM

This section treats about the performance of the sensors developed in the previous chapter, in particular those mentioned in section 4.3 and in section 4.4. For reading consistency, the development of sacrificial materials was separated from the sensors' performance analyses.

5.4.1 Capacitive microforce sensor

Please refer to subsection 4.3.1 for the introduction and motivations of using sacrificial layers to design a new microforce sensor. The fabrication is covered throughout section 4.3.

Preparation of sensors and force measurements To test the sensors individually, they first needed to be singulated; our Nd:YAG 1064 nm trimming laser[3] was used for that purpose. The cutting, yielding sixty sensors per substrate, was a relatively long operation: circa 2 h 24 per substrate with the following settings: power 80 %, pulse frequency 2 kHz, galvo speed 0.20 mm/s.
A few sensors were good enough to be fitted with DIL pins, which were glued with ÉPOTECNY E212 conductive adhesive (see Figure 5.27a). The glue was manually dispensed with a syringe, and cured in an air dryer at 150 °C during 5 min.
To ensure a precise application of the force, a small drop of glue was deposited at the cantilever tip, imitating the ball of the MILLINEWTON force sensor (see Figure B.5); of course the mass of the "ball" had to be the smallest possible, to prevent the cantilever from bending due to its own weight.

A few prototypes (Figure 5.27) were tested with the demo-board of the ANALOG DEVICES AD7746EB chip. This demo-board, depicted on Figure 5.28, presents astonishing performances: its resolution is 4 fF, its linearity is ± 0.01 % and it is easily programmed by USB.

---

[3] [52], see subsection 2.2.3 on page 35

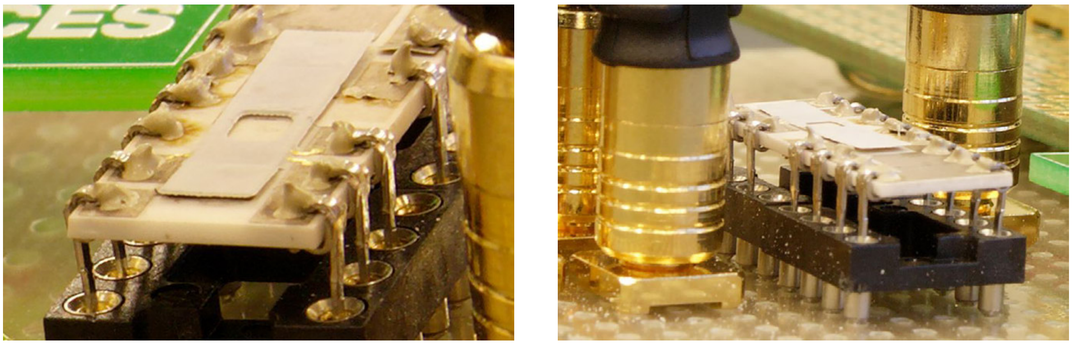

(a) Close-up on reference cantilever and pins glued with conductive adhesive.

(b) Front view showing a well-separated main cantilever.

Fig. 5.27: Photographs of thick-film capacitive cantilever force sensor prototype (variant V4) on alumina substrate, mounted on a DIL package linked to the AD7746 capacitive sensor (not shown, see Figure 5.28).

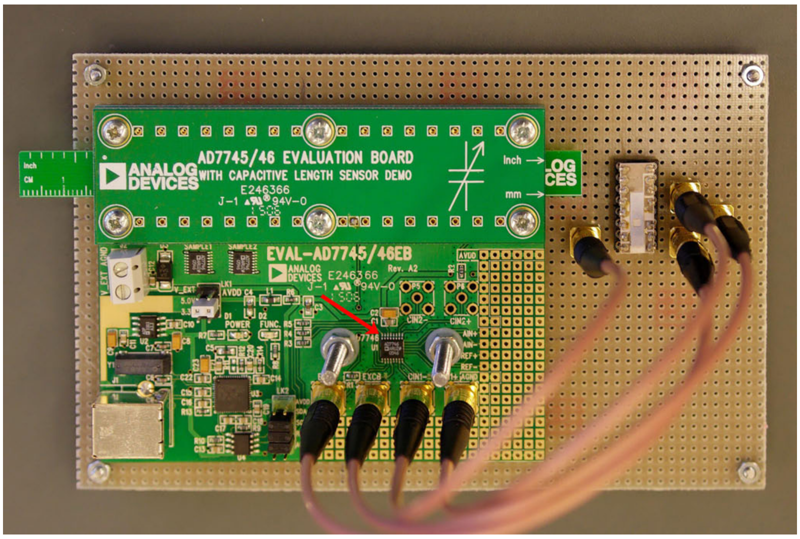

Fig. 5.28: The Analog Digital AD7746 capacitive sensor chip evaluation board (*left*), with the sensor indicated by the red arrow, and our cantilever force sensor mounted on a DIL package (*right*).

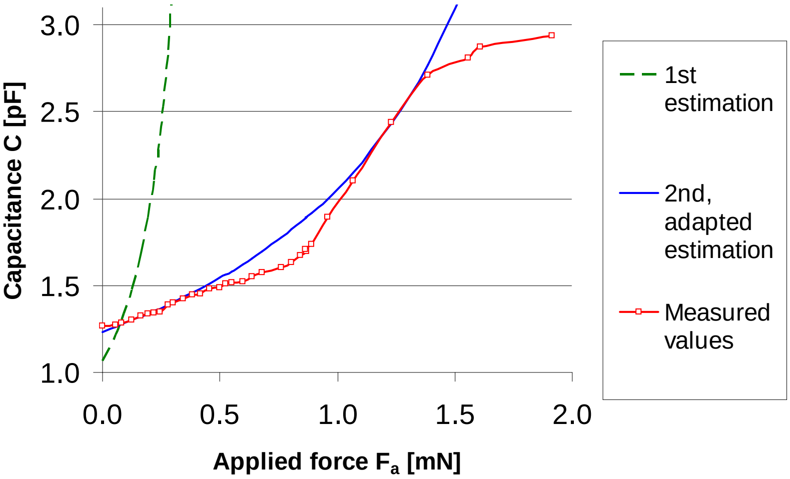

Fig. 5.29: Graph of measured capacitance (in red) in function of applied force on the cantilever of the thick-film capacitive force sensor prototype, along with *a priori* estimations (in green and blue).

The force applied on the cantilever tip was varied by depositing carefully weighted small triangular pieces of balsa wood ; the triangles were resting on two other feet of same height, in order to divide their resting force by three. This has been done in the same way as for the upcoming LTCC version of the sensor, depicted on 5.31b on page 177.

Sensor performance As can be seen on the graph of Figure 5.29, the first estimation of capacitance in function of applied force (green dashed line) was too pessimistic regarding measured sensitivity (red squares). Although the sensitivity is indeed lower, the capacitive AD7746EB chip has a range of ±4 pF (or 0-8 pF, displaceable up to +17 pF); thus, it would not be favorable to increase the sensitivity too much. Based on actual dimensions and

measurements (red squares), the estimation was adapted and the new one (blue line) fits reality rather well (except for the saturation that was not modeled, when the electrodes touch each other). The waves at the beginning of the curve are due to bad experimental conditions (laboratory door and window opened and closed, measurements made over 2 hours).
The achieved performance from the best sample, issued from variant V4, shows a force range of ~2 mN for a resolution of ~1 % of full scale, which is quite remarkable for passive measurement. To our astonishment, absolute or differential measurements show little differences; in differential, humidity affects the reference electrodes too, exceeding the hoped-for advantage of a double measurement.

Protecting from humidity Humidity is well known to have a strong influence on capacitive sensors; here is a solution to get protected from it. A *guard ring* electrode must first be added all around the measurement electrode (the bottom one, on the base). The role of the guard ring is to be exposed to humidity, and to be at the same voltage potential as the measurement electrode. The ring must be linked to the ground electrode, because the measurement electrode is considered a virtual mass by the capacitive chip. The ground electrode must also be extended on top of the cantilever, to act as a shield for the excitation electrode (the top one, under the cantilever). Ideally the measurement electrode should be further isolated by hermetic sealing with dieletric or overglaze (in neutral atmosphere) before applying the MSP; however, this solution prevents the possibility to do active measurements.

Conclusion As such, the sensor is at the early prototype stage and lacks integrated electronics, but it shows a good development potential. Unfortunately, active measurement with electrostatic counteraction was eventually not implemented, and hence could not be tested. The sensor was not further studied because the focus switched to the creation of an LTCC version of this sensor, the subject of next subsection.

5.4.2 Capacitive anemometer for micro-airplane

In this subsection we present a work that took place in a joint semester project [115] between our laboratory (the LABORATORY OF MICROENGINEERING PRODUCTION EPFL-LPM) and the LABORATORY OF INTELLIGENT SYSTEMS (EPFL-LIS). It consisted in the development of an LTCC anemometer for the MC2, a 10-gram indoor slow flyer used for bio-inspired neural network research by ZUFFEREY et al. [154], which is depicted on Figure 5.30; it's speed range is from 0.5 to 3 m/s. The motivation was to improve the anemometer robustness, because the one used so far was a simple wooden propeller mounted on a small electric motor, which needed to be frequently replaced due to the numerous crashes against walls during the neural network evolutions. Thus came the idea to use LTCC technology to develop a new anemometer with few or no mobile parts, and that would not need to be replaced so often. The requirements from ZUFFEREY [115] were as follow:

- The sensor must be crash-resistant to impacts of 3 m/s against hard surfaces;
- Its mass must not exceed 0.4 g, electronics included;
- The range of speed to be measured is from 0.5 to 3 m/s, with a resolution of 0.4 m/s;
- The sensor will be powered at maximum 3 V, the average current must not exceed 10 mA, and the peak power should be max 30 mW;
- The reaction time must be less than 50 ms, which is rather slow but still acceptable for an anemometer[4].

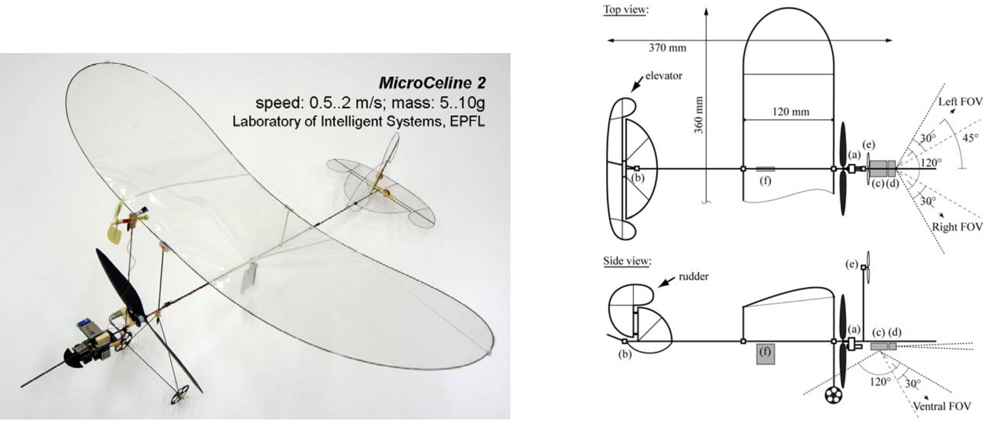

(a) The original anemometer (small yellow propeller) is placed in front of the wing above the main propeller.

(b) Schematic top and side views.

Fig. 5.30: Indoor slow flyer MC2 used for bio-inspired neural network research by the LABORATORY OF INTELLIGENT SYSTEMS (EPFL-LIS, [154]).

---

[4] In comparison, ZUFFEREY et al. measure nowadays the dynamic pressure every 20 ms (i.e. at 50 Hz) on their aerial robotics.

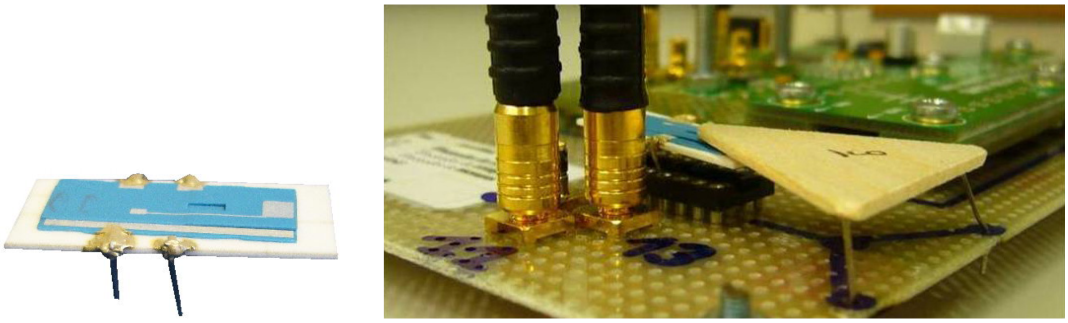

(a) Detail of the mount on alumina substrate and of glued pins.

(b) Sensor mounted on socket linked to the capacitor chip Analog Devices AD7746EB demo-board. A balsa wood triangle is pressing on the cantilever ; the effective mass pressing on the cantilever is one third of its global mass.

Fig. 5.31: LTCC capacitive force sensor mounted on alumina substrate to ease manipulations, and fitted with glued pins for electrical connections.

The challenge lies mainly in the mass limitation; all other points are easily achievable. Indeed, there were two anemometers developed in parallel, each sensor being the subject of a distinct semester project:

- A thermal sensor working like a hot-wire anemometer [186], discussed in section 5.6;
- A capacitive sensor that, when transposed to biology, would be mimicking the halteres of the fly; these latter help for controlling motion in flight. This anemometer is an evolution of the microforce sensor developed in thick-film technology in the previous section. The results obtained from the capacitive sensor prototype will be discussed in section 5.4.2.

Sensor manufacturing The fabrication of the sensor is described from subsection 4.4.3 on page 122 and beyond.

Results of capacitance measurements The best samples of the V2, V6 and V7 variants were first mounted on a small alumina substrate to ease manipulations, and fitted either with contact pins glued with conductive adhesive (Épotecny E212, Figure 5.31a), or with soldered wires. They were then measured in the same conditions as the previous sensor, as summarized hereafter. The demo-board of the AD7746EB chip (Figure 5.31b) has been again employed; the chip is the same as presented in section 5.4.1.
To run the tests, the sensors were plugged onto a socket linked to the demo-board with shielded BNC wires, and balsa wood triangles were used as weights to press on the cantilever at tip. The triangles were resting on two other feet, such as to divide their resting force by three, as can be seen on Figure 5.31b. Their masses were carefully weighted.

Of all the variants, only the V6 gave stable results. Among all the V6 sensors, only those with pins were measurable: those with wires were unusable, because of their longer length, giving birth to perturbations. For mechanical reasons an alumina substrate was glued under the LTCC base to ease the mounting of the contacts pins. The graph of capacitance in function of applied

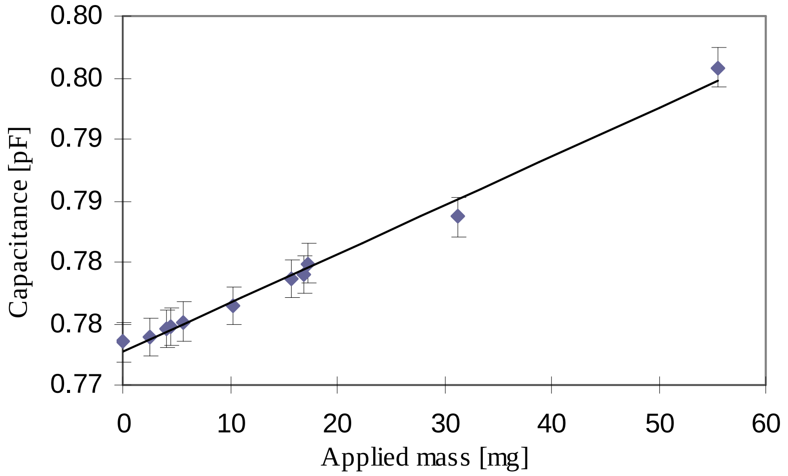

Fig. 5.32: Capacitance as function of applied mass for sensor #V6.8. The considered error is 0.2 %. The behavior is healthy and quite linear.

mass is plotted in Figure 5.32 for the best sensor of the V6 variant, the #V6.8: the output presents a healthy behavior and is quite linear, which bodes well for the continuation as an anemometer.

From microforce sensor to anemometer for slow flyer To be used as an anemometer, the best sensors were fitted with a "mustache" in balsa or ZTA[5] (see Figure 5.33), to allow the relative air flow to be sensed by the cantilever. To prevent breaking the cantilever, the mustache is mounted to act on the cantilever downward only, with a hinge made of glue at one extremity.

At this stage the sensor could not yet be mounted on the indoor slowflyer, so we found a solution for testing it in “wind conditions”. Blowing air with ventilators or in air vents proved to be difficult in the studied speed range (0.5 to 3 m/s): ventilators or ducted air blowers produce a turbulent, non-homogeneous air stream, and varying the air speed is not convenient; as for the professional large-section air vents available on the campus, their minimum air speed was in the range of 10 ±5 m/s. Thus we ended setting up an experimental bench with a travelling carriage and a reference anemometer; naturally, such conditions yield an important error, that we estimate of 2 % on the capacitance, compared with 0.2 % for the mass measurements.

The graph of speed measurements shown in Figure 5.34 proves that the concept is feasible and that the output is relatively linear despite rudimentary conditions; we expect that it is linear within a limited speed domain and for a low force. However, the hypothesis that the flow is laminar is probably wrong. For this we can calculate its corresponding Reynolds number; for standard air density and viscosity, a maximum speed of 3 m/s and a cross-section of 3 mm, *Re* is approximately 360:

$$Re = \frac{\rho \cdot v \cdot L}{\eta} \cong \frac{1.2\,{}^{\mathrm{kg}}\!/\!_{\mathrm{m}^3} \cdot 3\,{}^{\mathrm{m}}\!/\!_{\mathrm{s}} \cdot 0.003\,\mathrm{m}}{0.00003\,\mathrm{Pa{\cdot}s}} \cong 360 \tag{5.1}$$

---

[5] Zirconia Toughened Alumina

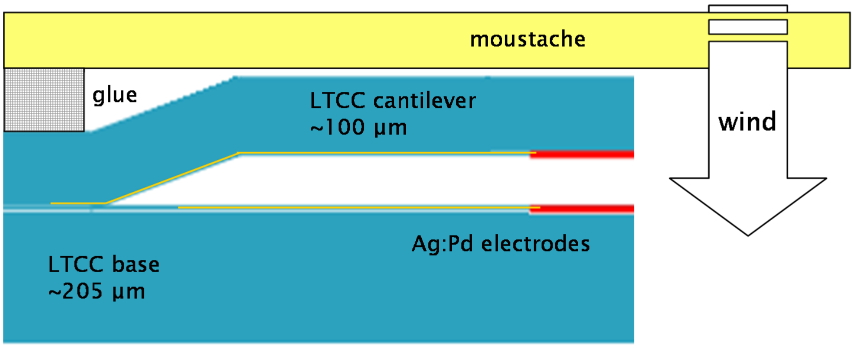

(a) Schematic cross-section of a sensor fitted with a mustache that is mounted such as to act on the cantilever downward only, in order to prevent breaking the cantilever. The MSP, filling the gap between the cantilever and the base, was dissolved beforehand. Fired tape thicknesses are indicated.

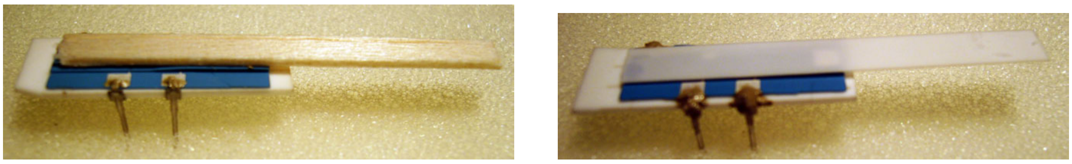

(b) Mustache in balsa wood. The gap under the cantilever is visible on the right side of LTCC.

(c) Mustache in ZTA.

Fig. 5.33: Illustrations of capacitive anemometer prototypes mounted on alumina support with glued pins and fitted with lightweight mustaches to be more sensitive to air flow.

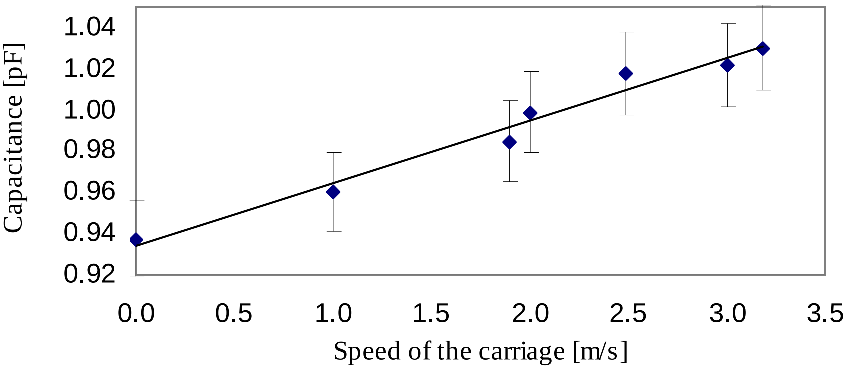

Fig. 5.34: Capacitance as function of speed of the travelling carriage. The error is 2 %, due to rudimentary measurement conditions.

According to flow studies of this geometry [187], this value of *Re* lies in a complex transition regime.

Linearity was not a requirement from Zufferey anyway: for the simple indoor slow flyer, 3 to 5 distinct "speed" outputs were sufficient for the sensor, as the airplane microprocessor would use an implemented Lookup Table to compute speed. As such, it is evident that the sensor is far from being optimal and merits further developments.

Regarding the packaging of the sensor, various solutions were sought and tested. An appropriate shell was made out of white foam typically found in postal parcels (Figure 5.35): this was the best compromise between lightness, efficiency and convenience of use. This solution was only tested by manual throwing against hard surfaces, and not on a real slow flyer; we can nevertheless reasonably consider the conditions of this test to be harsher than real crashes.

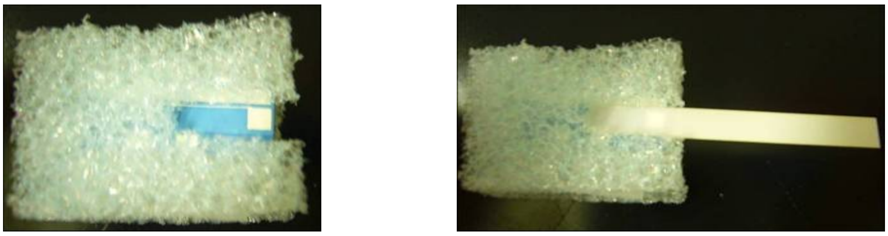

(a) Packaged w/o mustache. **(b)** Packaged with a mustache in ZTA.

Fig. 5.35: Anemometer packaged with white foam typically found in postal parcels.

Conclusion The aim of the semester project was to design a capacitive anemometer in LTCC for an indoor slow flyer, in the form of a cantilever microforce sensor fitted with a mustache extended in the air flow. The principle of speed extrapolation by capacitance measurement was demonstrated and the concept proved. Various designs were tested and turned out to be successful; surprisingly, we observed a low influence of the hole in the cantilever.
However, the prototype was left at its early development and needs further research before being embedded on a plane. In particular, the mustache and the foam packaging must be tested in real conditions, and the AD7746EB chip must be integrated on the sensor.

5.5 Microreactor

In 2005, one of our first LTCC device realizations was a chemical microreactor fitted with a calorimeter, designed to study the exothermic mixing of two strong reactants such as HCl and NaOH. The project was carried out in the frame of the Master project of Raphaël Willigens, chemist from the University of Liege in Belgium [17], and was presented by T. Maeder in [188]. The development occured in two phases: first, the setup of a liquid flow sensor; and second, the microreactor itself, by integrating two of these flow sensors in parallel, in order to measure the flow of each reactant before entering the mixing meander of the calorimeter.

5.5.1 Precursor: flow sensor demonstrator

My first electro-fluidic LTCC realization at EPFL-LPM was this liquid flow sensor prototype, in early 2005. It was designed to be compatible with surface-mount technology (with soldered M3 nuts as fluidic ports), and to be able to measure aggressive liquids, it featured thermistors screen-printed on LTCC surface, instead of being buried in the channel (cf. flow sensors of subsection 5.2.1). The device, of dimensions 25.4×12.7 mm, is depicted on Figure 5.36.

This work has demonstrated the feasibility of a low-cost, media isolated, chemically-resistant, surface-mountable micro flow sensor using low-investment technologies such as LTCC and screen printing. Water flows between 12 µl/min and 5 ml/min have been measured with a power consumption of 40 mW; however the sensibility is the greatest between 0.02 and 1 ml/min. Please refer to our IMAPS Bruges 2005 publication [181] for a detailed description.

5.5.2 Microreactor development

Design The reactor is made of three parts, as highlighted on Figure 5.37: the pre-heating serpentines, the individual flow sensors, and the mixing calorimeter with its reactor meander.

The sensor has two fluidic inputs were reactants enter, and one output; the fluidic fittings are metallic tubes glues with Grafted Maleic Anhydride Polyethylene (Figure 5.38). Each of the inputs passes through a first serpentine meander in order to be pre-heated (see below), and then through an integrated flow sensor before being mixed together in the reactor meander. The flow sensors are nearly identical to their precursor, except for the addition of cavities under their channels for a better thermal decoupling (Figure 5.40a).

The serpentines and the maze are made by decoupling the channels into “vertical” and “horizontal” portions spread on two layers, which is favorable for tape handling and channel integrity (Figure 5.37a). This elegant solution must be compared with the channel deformations that Kaminski reported for his PMMA-LTCC Y-mixer made out of a single LTCC tape [178]. The meander has an equivalent total length of 73 mm, which corresponds to a calculated minimum to allow a complete mixing of the reactants in laminar flow, for a flow of 100 µl/min and a reaction time of 2.6 s. The whole meander is located under a large thermistor to measure the endo- or exothermic reaction, thus making a calorimeter. Additionally, an Ag:Pd heating

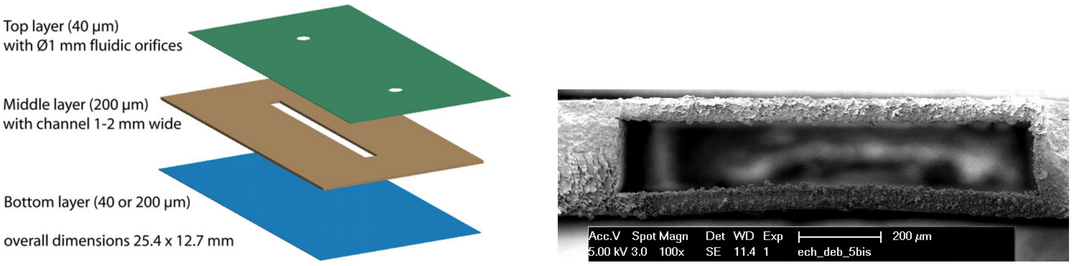

(a) Schematic of the three DP951 LTCC layers. **(b)** SEM cross section showing acceptable channel output geometry and good lamination.

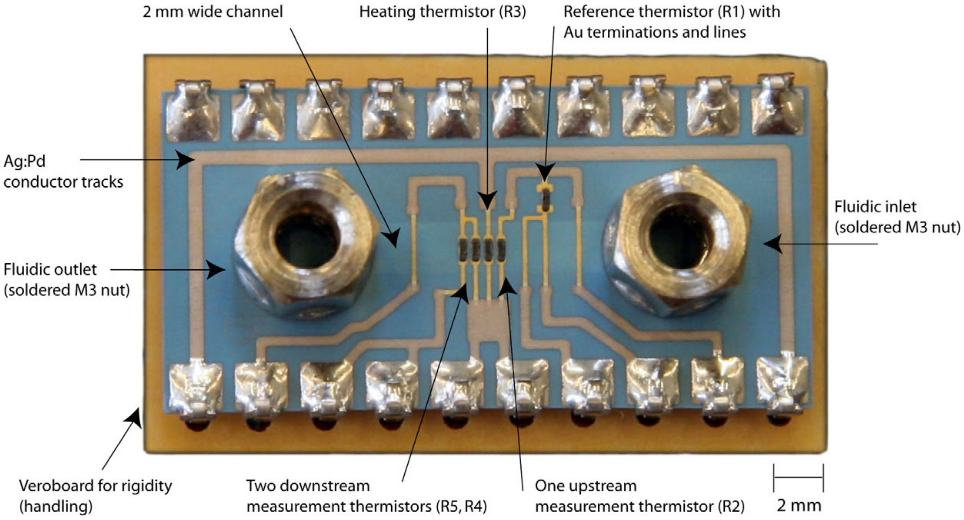

(c) Top view of flow sensor mounted on PCB for handling.

Fig. 5.36: My first electro-fluidic realization in LTCC at EPFL-LPM: an SMT flow sensor.

serpentine in ESL9635B screen printed on an alumina plate is glued under the microreactor to yield a uniform temperature all over the LTCC substrate (Figure 5.42b); this allows for the pre-heating of reactants too. An alumina cap is also glued on top of the LTCC substrate to minimize convection losses.

LTCC fabrication The LTCC substrate is made of five LTCC DP951 tapes of various thicknesses (Figure 5.39): 254 µm for tapes L1 (bottom lid), L2 (bottom fluidic channels) and L4 (top fluidic channels), while the thin layers of the flow sensors are made of 50 µm-thick tape (L3 and L5) to increase the signal sensitivity. The serpentine channels are 300 µm wide, and the flow sensor sections are 1.2 mm wide.

The first lamination trials on the flow sensors prototypes [181] were done along DuPont's recommendations, i.e. at a pressure of 206 bar, at 70 °C for 10 min; the fluidic structures had collapsed. The subsequent laminations were done with a pressure lowered to 80 bar (still at 70 °C for 10 min), this time with good results. The microreactors were then laminated with the same parameters; the quality of tape bonding after firing is very good, as the SEM pictures of cross-sections of Figure 5.40 can attest.

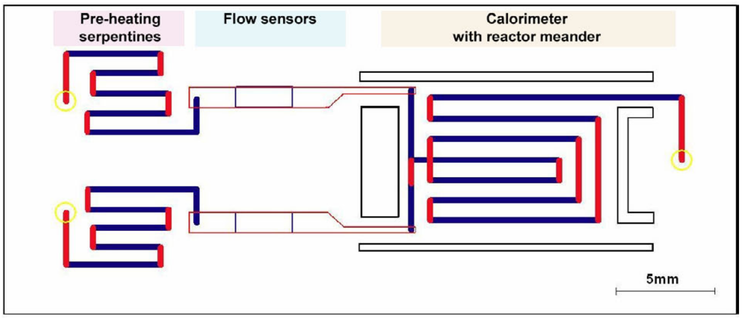

(a) Schematic of fluidic parts. Blue channels are lasered in tape L2, while red channels are cut in L4; yellow circles are ports in L5.

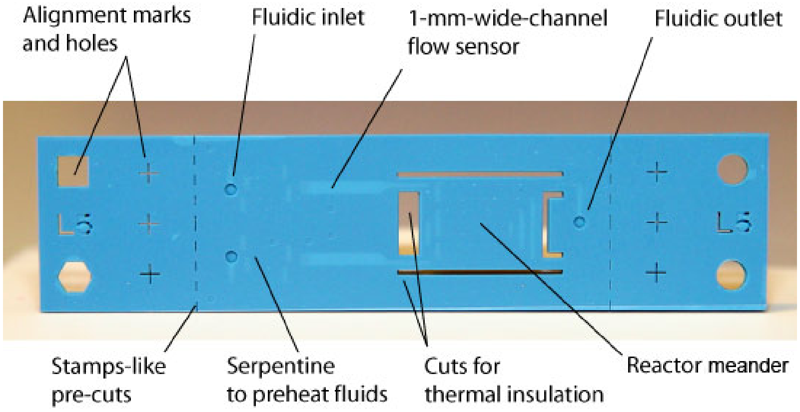

(b) Non-printed, non-singulated reactor; channels are visible in light blue.

Fig. 5.37: Top views of microreactor highlighting its three main parts: the pre-heating serpentine, the individual flow sensors, and the mixing calorimeter with its reactor meander.

Screen printing The electrical layout is displayed on Figure 5.41. The first screen-printed ink was the DP6145 Ag on tape L4, co-fired for buried tracks. After firing, the via fills and surface conductor lines were both made with post-fireable DP7484 Ag:Pd; it was followed on the bottom face by a ground plane of DP6145 Ag, post-fired this time, to create a thermally good conductive layer for the alumina heater. Then came the thermistors' terminations in DP5744 Au, followed by the PTC thermistors with DP5092D.
As this was our first attempt of co-firing inks on LTCC, the choice of pastes was not optimal and led to some problems of compatibility. At that time we had no complete ink assortment, and we had never tried using vias. For instance, the DP7484 Ag:Pd post-fired vias teared off the co-fired DP6145 Ag lines; this forced us to manually repair broken electrical connections with conductive glue. Seen with the experience of today, filling vias in post-firing was non-sense; using DP6141 Ag for via fill and DP6146 Ag:Pd for co-fired tracks would have been more appropriate.

Testing & conclusion We successfully measured an exothermic reaction by mixing HCl and NaOH, yielding water and NaCl at the output: $\mathrm{NaOH} + \mathrm{HCl} \rightarrow \mathrm{H_2O} + \mathrm{NaCl}$. The concentrations of both reactants were tested at 0.5, 1 and 2 M; the fact that the reactor

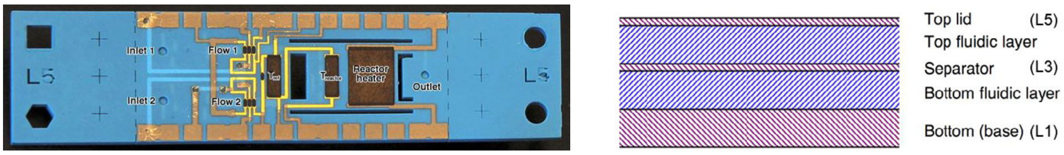

(a) Screen-printed, but not singulated, without ports nor alumina cap.

(b) LTCC layers stack from tape L5 (top) to L1 (bottom).

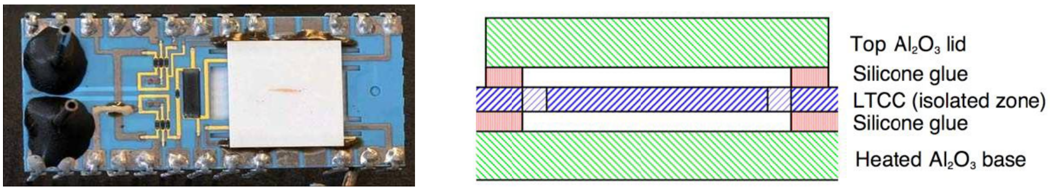

(c) Assembled; alumina cap on calorimeter, missing output port.

(d) At calorimeter location, showing thermally insulated LTCC.

Fig. 5.38: Top views of microreactor at different stages of fabrication and schematic cross-sections [188].

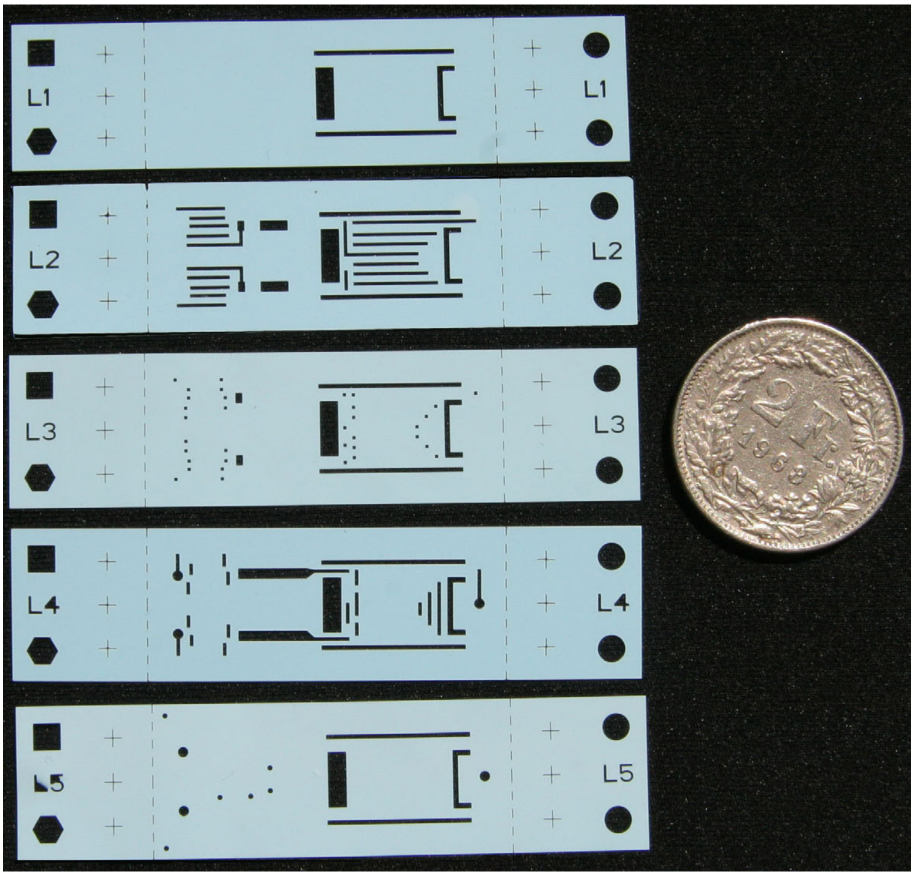

Fig. 5.39: Lasered LTCC tapes; layers L1, L2, L5 are in DP951-254 µm, while L3 and L5 are DP951-50 µm (note the light color difference).

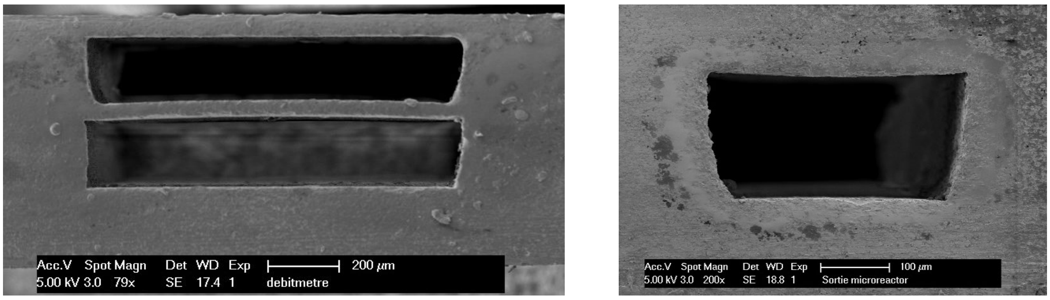

(a) Flow sensor: the top cavity is the flowmeter channel, while the bottom cavity is the thermal insulation.

(b) Outlet channel + bridge.

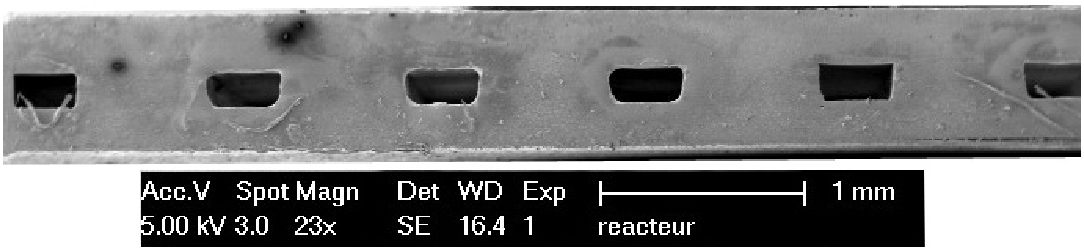

(c) Meanders in reaction zone; the secondary meanders are in another fluidics layer.

Fig. 5.40: SEM pictures of microreactor cross-sections at various locations.

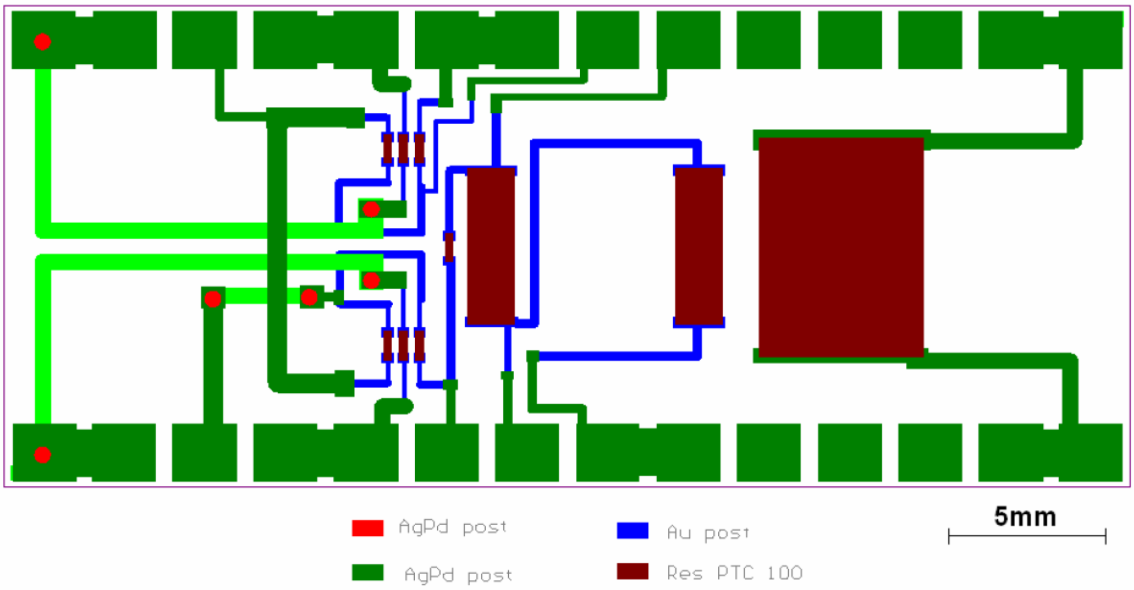

Fig. 5.41: Electrical schematic of microreactor. The light green lines are co-fired DP6145 Ag tracks.

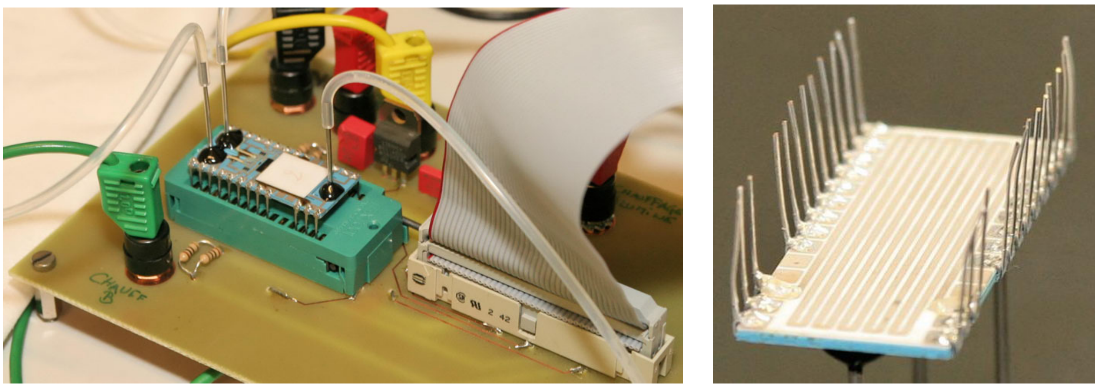

(a) Microreactor mounted on test bench to assess the calorimetric reaction of mixing two strong reactants. Its calorimeter is fitted with an alumina cap; the fluidic ports are glued metallic tubes.

(b) Heater serpentine printed on alumina substrate and glued on bottom face.

Fig. 5.42: Fabricated microreactor.

operated for at least several hours without apparent degradation also demonstrated the good chemical resistance of DP951.
Figure 5.42 depicts the microreactor mounted on a test bench; it was driven by an experimental software programmed under LabView. The report of Willigens [17] describes the procedure in detail.

This project demonstrated the possibility to create low-cost disposable chemical microreactors in LTCC technology. Simple lamination conditions were sufficient in regard to the channels geometries featuring small cross-sections and single layer for the height; larger channel cross-sections would require using our multiple sub-laminations technique (see section 3.3).

5.6 Thermal anemometer for indoor slow flyer

Similarly and in parallel to the capacitive anemometer project presented in subsection 5.4.2, this work took place in a joint semester project between our laboratory and the LABORATORY OF INTELLIGENT SYSTEMS. Please refer to the abovementioned section for the project motivation and the sensor requirements.

The present sensor was developed by PIERRE-ANTOINE THIVOLLE in 2007 [186]. It uses a thermal principle: a hot plate (a PTC resistor indeed) is in contact with the air flow whose speed must be measured. Heat is transferred to the flow by forced convection, and from the dissipated power we extrapolate the speed of the air flow.

Heating PTC thermistor on LTCC membrane The heating element was envisaged to be a thin tungsten wire (Ø 5 to 10 µm), but we concluded it was impracticable in our case; a PTC resistor on an LTCC membrane was chosen instead. The sensor substrate is made of two layers of DP951-114 µm; the bottom one contains a large cut to form the membrane, while the top one contains a pattern of holes (see Figure 5.43). These oblong cuts are intended to further thermally isolate the heating element from the sensor core, and also to help lower stress concentrations for the subsequent passage of the squeegee upon screen printing. Indeed, the PTC resistor is post-fired (DP5092D paste): the risk of membrane break up during screen printing is high. As always with PTC pastes, it is fired after conductor tracks (post-fireable ESL 9635B) but before the protective overglaze (ESL G-481).

We hence designed two variants of PTC/membranes: a small one (3.0×3.5 mm) and a large one (5.4×4.7 mm). We did a mistake however on the design of the oblong cuts, which were drawn parallel to the PTC: all membranes failed during the first screen printing trials of the PTC (right image of Figure 5.43). Therefore, it was necessary to modify these cuts by rotating them by 90°, making them perpendicular to the PTC (left image of Figure 5.43): this time, the membranes survived screen printing.

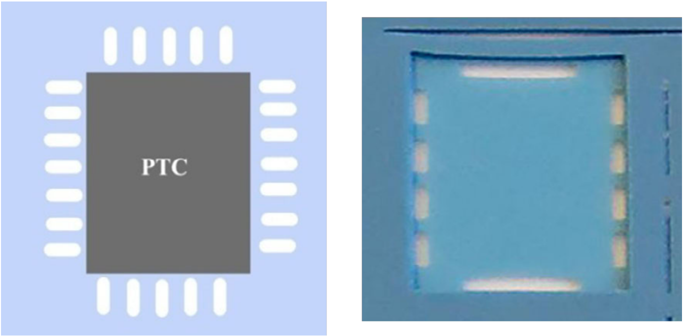

Fig. 5.43: PTC resistor on LTCC membrane for thermal decoupling. *Left:* schematic top view with perpendicular oblong cuts (robust design). *Right:* bottom face photograph of early failed attempt with parallel oblong cuts (fragile design).

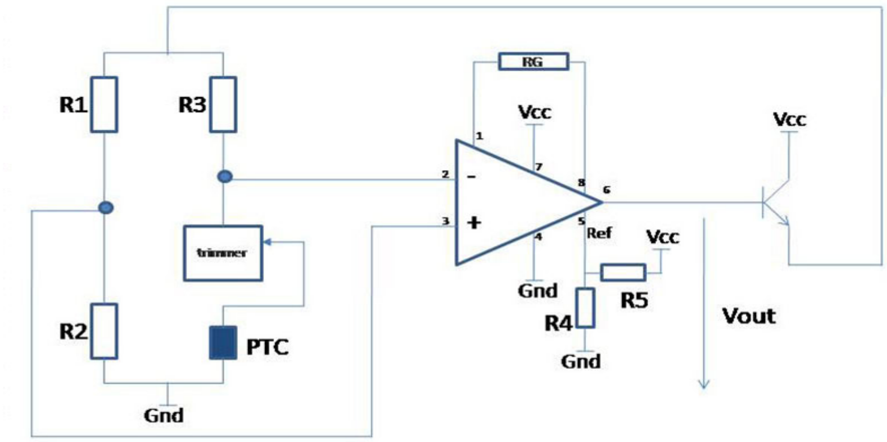

(a) Electrical schematic of sensor with constant temperature regulation.

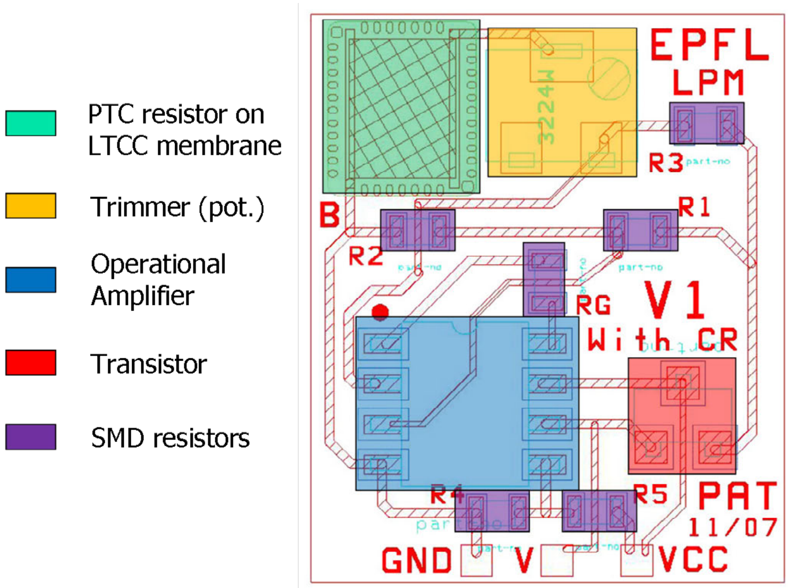

(b) Electrical layout of thermal anemometer with highlighted zones.

Fig. 5.44: Schematics of the thermal anemometer with heater functioning at constant temperature [186].

Electric layout The electronics were tested in two configurations for the regulation of the heating PTC: a) at constant voltage, and b) at constant temperature, with a closed-loop circuit. This second configuration (see Figure 5.44a) proved to be the fastest (with a reaction time of 0.28 s instead of 1 s); the temperature of the PTC resistor was measured at 33 °C for an ambient temperature of 22 °C. The electrical layout is displayed on Figure 5.44b.

Fabricated sensors Figure 5.45 shows two fired LTCC substrates: the left one is a top view of the correct membrane version (the fired overglaze in green), and the right one is a bottom view of first membrane version, showing tearing of LTCC along singulation stamp-like pre-cuts.

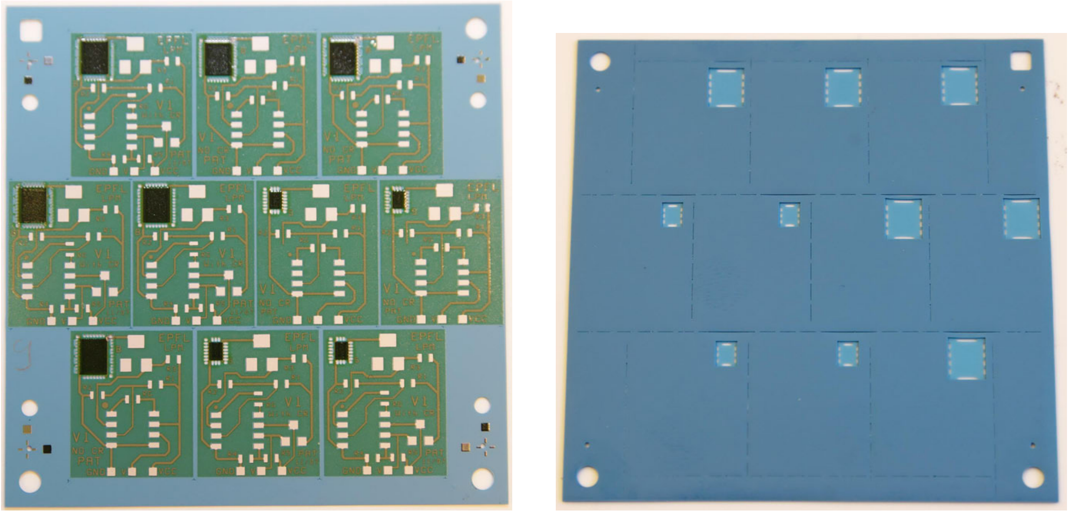
(a) (b)

Fig. 5.45: Fired substrates of sensors produced in batch: *(a)* Top view of new membrane version with fired overglaze (green). *(b)* Bottom view of first membrane version, showing tearing of LTCC along singulation cuts.

Figure 5.46 presents photographs of sensors with mounted regulation electronics, and also of a sensor packaged with foam as crash-protection (a kind commonly found in postal parcels).

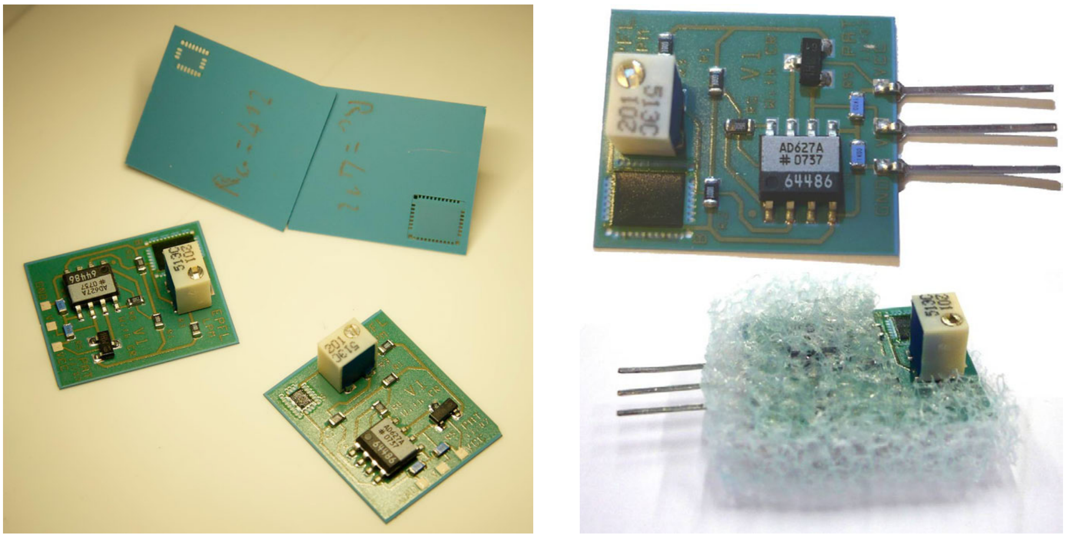

(a) Sensors fabricated with large and small membranes, top and bottom views.

(b) Sensor “naked” and packaged with foam, except at thermistor location [186].

Fig. 5.46: Photographs of fabricated thermal anemometers.

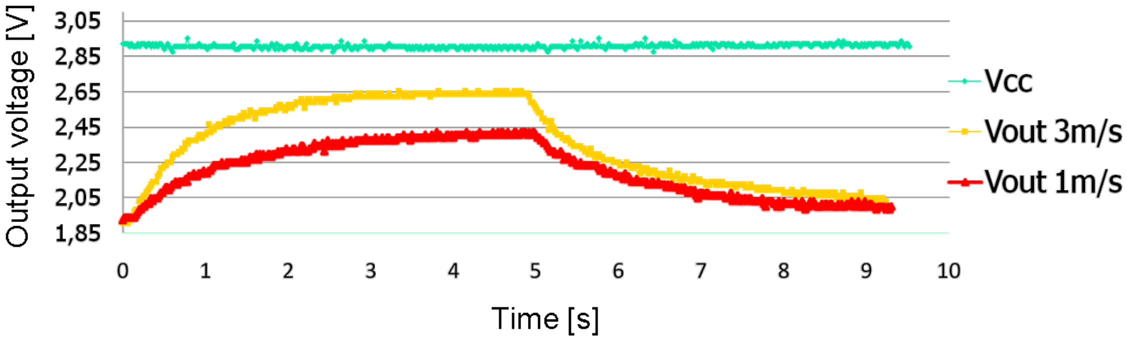

Fig. 5.47: Graph of sensor output voltage in function of speed measurement at different indicial air flows: 1 m/s (red) and 3 m/s (yellow). The slow sensor response time is clearly visible. The sensor supply voltage is 3 V. From [186].

Results & conclusion The best membrane variant proved to be the large one; coupled with the constant-temperature regulation, the sensor performed well regarding its supply voltage, its dynamic range of measurement, its resolution and its robustness. However, it failed fullfilling the requirements from Zufferey in terms of mass and response time: packaged with foam, it weighed 0.55 g (instead of max. 0.4 g), and its rising reaction time was 280 ms for an air flow of 3 m/s, almost six times more than the 50 ms allowed (see Figure 5.47). The current consumption was also somewhat high: between 10 and 20 mA (max. 10 mA).
As such the sensor is not optimized from the electronics and substrate surface (for the mass) points of view. Unless a much faster and lighter heating circuit is designed, the thermal anemometer is not suitable for the indoor slow flyer.

Nevertheless, this project allowed getting familiar with our design software regarding electronic circuits (useful for more complex designs such as the multisensor of section 5.3), and provided valuable information on the combination of PTC resistor printed on membranes with stress decoupling cuts, which we had never done before. This was possible thanks to the experience gained from the study of the influence of lamination parameters on firing shrinkage; the thin thermal membrane was decoupled from the sensor core while still staying flat by using the "drum-skin effect" (subsection 3.3.2).

5.7 Solid-propellant based microthrusters

This project was done in collaboration with Jaya Thakur from the Department of Mechanical Engineering of the Indian Institute of Science, in Bangalore, India. It was a good opportunity to explore LTCC structuration in another field, and to test printing of resistors onto sacrificial layers. The joint publication [189] is relating all the details; here is just a summary.

The introduction of micro-spacecrafts in the space industry has led to the development of various micro-propulsion techniques. Microthrusters are micropropulsion devices used in the microspacecraft for precise station keeping, orbit adjustment, attitude control, drag compensation and apogee kicking. The principle of operation of a solid propellant thruster is based on the combustion of a solid energetic material stored in a microfabricated chamber. In the current work, LTCC technology has been used for the realization of a solid propellant based microthruster structure. Hydroxyl Terminated Poly-Butadiene/Ammonium Perchlorate (HTPB/AP) is used as the propellant.

Layout and fabrication The principle of operation of a solid-propellant based microthruster is very simple. A solid energetic material is stored in a micro machined chamber which, upon ignition, burns and produces gases that are accelerated through an adapted nozzle to produce a thrust. The proposed LTCC solid propellant microthruster is fabricated by the lamination of individually processed layers of green tapes. The number of tapes we have used is either six or eight, depending on the design. The microthruster has a cavity (combustion chamber), a convergent-divergent nozzle and a thermistor embedded inside the cavity (Figure 5.48 and Figure 5.49b). Due to the major role played by the igniter in the successful functioning of the device, special attention was paid to its design to achieve a successful ignition. In order to minimize the power consumption and reduce the thermal losses to the substrate, some variants of microthrusters had their resistor insulated from the LTCC substrate by using a sacrificial layer of an experimental paste compatible with LTCC.

Using laser drilling, the cavities and registration holes for visual alignment during screen-printing are created in the tapes, with registration holes cut in every layer for alignment purposes. Stamp-like separation lines are also added in the design, providing an easy way to individualize the thrusters by breaking up the plate after firing. In addition, a small cut is also made at the exit of the nozzles to provide a reproducible geometry there, i.e. to keep the small inherent variability of the breaking process from affecting the flow of gases at the exit. Figure 5.49a shows the laser separation lines and the cavity at nozzle exit on tape 4.

Screen printing DP6146 Ag:Pd conductor paste was used to print the wire solder pads, the lead lines and the termination pads. After printing, the inks were first allowed to settle 5 min at room temperature, then dried in a ventilated oven at 120 °C for 10 min. The same procedure was applied for printing the experimental sacrificial layer (of the same composition, consisting of a carbon paste in organic solvents, as developed in section 4.4). However, not all circuits of the batch were fitted with sacrificial paste, as we had never tried the combination of

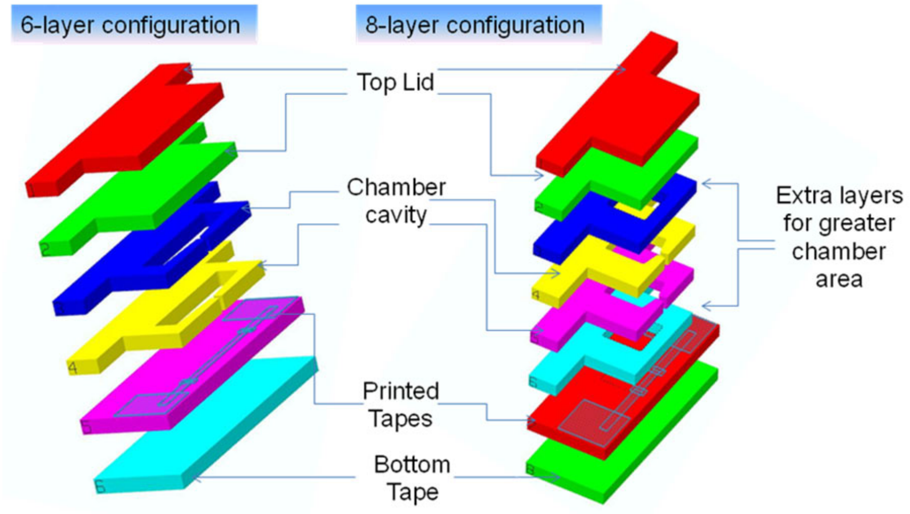

Fig. 5.48: Schematic model of LTCC microthruster [189].

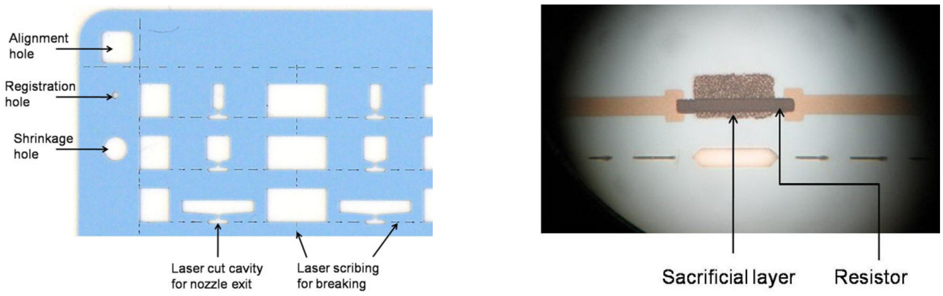

(a) Details of laser cut on tape 4.

(b) Binocular observation of a thermistor screen-printed over sacrificial paste and conductor track.

Fig. 5.49: Two manufacturing steps of the microthruster: laser cutting and screen printing [189].

sacrificial and resistor pastes before; we will see next it was a wise decision.
The next operation was the printing of the themistors. Two resistor pastes were tested: $\mathrm{DP\ CF011}$ ($100\,\Omega/\square$) and $\mathrm{DP5092D}$ ($100\,\Omega/\square$). Figure 5.49b shows the tape after resistor printing.

Firing The substrates were fired along a standard profile (peak at 875 °C). After firing, the stack was manually broken along the laser scribed lines to individualize thrusters. Soldering of ignition wires was then done at 250 °C, by preheating the co-fired thrusters on a hot plate to maintain the substrate at a sufficiently high temperature. This step had to be done before filling the cavity with propellant, as the ignition temperature of the propellant lied too close to that of the soldering step.

Unfortunately, none of the resistors screen printed over sacrificial layer presented a proper shape after firing. As Figure 5.50 can attest, strong buckling deformations can be observed at the extremities, close to the resistor terminations. There can be two reasons to this drawback: a) a

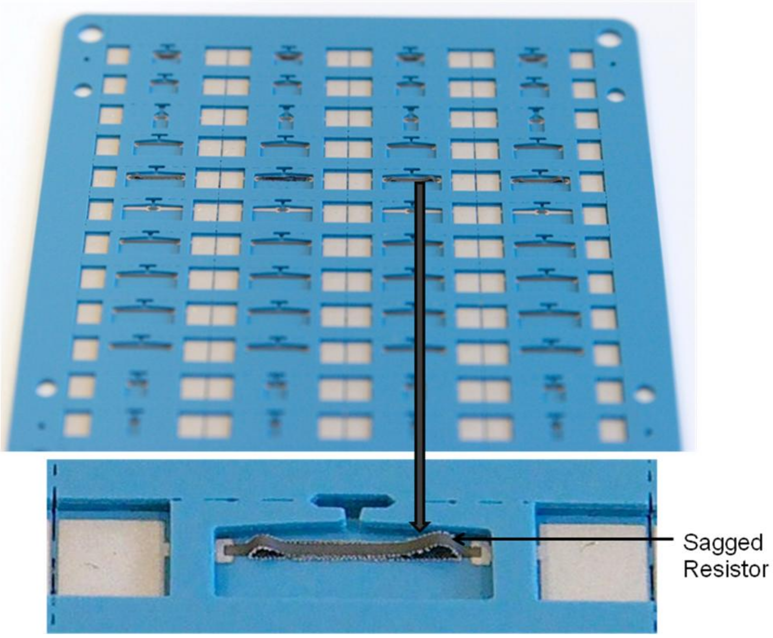

Fig. 5.50: Fired circuit of microthrusters in batch (*top*), and (*bottom*) close-up on the chamber of an LTCC microthruster revealing a mechanical buckling of the free-standing resistor upon sintering, or a chemical incompatibility between the $\mathrm{DP\ CF011}$ resistor paste and our sacrificial paste: the resistor, printed on top of the MSP, is clearly deformed at extremities (see arrows).

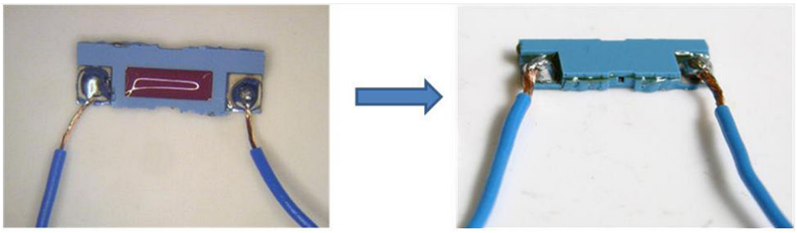

Fig. 5.51: Propellant filling and gluing steps [189].

possible chemical incompatibility of our sacrificial paste with the resistor, or (more probably) b) the resistor having no contact with the substrate upon sintering, and its own shrinkage being lower than that of LTCC tape, it suffered from compression at its extremities that resulted in strong buckling. Of course the resistor is useless with this out-of-plane shape: it is higher than the cavity, and would have been crushed at the time of filling the propellant anyway. Therefore, only the non-sacrificial versions of the microthrusters were further processed.

Propellant filling and final assembly Propellant filling is a very crucial step in the realization of the microthruster; cavity-free filling of a pasty propellant into blind holes featuring a substantial aspect ratio turned out to be difficult. The left image of Figure 5.51 shows a microthruster filled with propellant and with soldered ignitions wires.

The final step in the realization of the microthruster is gluing the lid; this was preferred to soldering the lid due to the risk of igniting the propellant accidentally; the ignition temperature

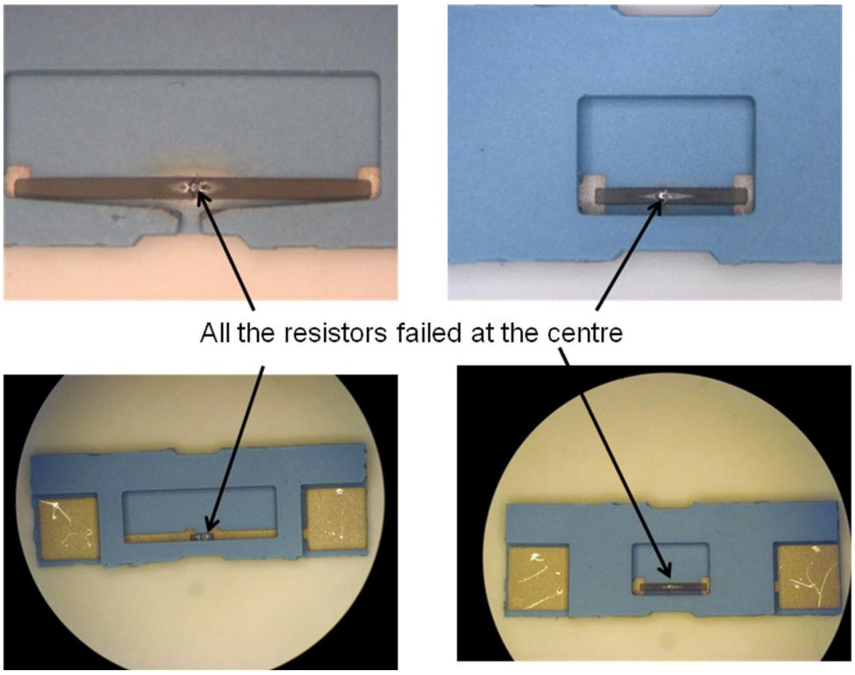

Fig. 5.52: Failure of overheated resistors (versions without sacrificial layer) [189].

of the propellant is expected to be in the range of 250-350 °C. The glue has to be strong enough to withstand the pressure (20 bar) and temperature increase generated by combustion of gases inside the chamber. Cyanoacrylate and LOCTITE 3430 epoxy were initially used for gluing, but could not withstand the conditions of combustion. Then EPOTEK 353 ND-T epoxy was successfully used for testing thrusters. This glue was applied on the whole surface of the top of the wall, the lid was applied to close the chamber, and the assembly was cured for 2 hours at 100 °C. The right image of Figure 5.51 shows a thruster after the curing of the glue and ready for testing.

Testing and results Control of the propellant ignition process in a microthruster is of critical importance for its applications; the repeatability of the temperature produced has to be ensured for reliable functioning of the microthruster. Characterization of the resistors was done using a power supply, a multimeter and an infra-red camera. Several trials were carried out to establish the proper heating power to ensure ignition and to check the resistor failure mode when overheated. In this case, failure was always found to occur at the centre of the resistor for the different studied variants, indicating reproducible ignition characteristics (Figure 5.52).

Preliminary combustion testing is done to check the integrity of the structure. Successful firing of the thruster was obtained after a few initial failures. Figure 5.53a (top) shows the picture of a structure that failed while testing its structural integrity. The thickness of the wall was subsequently modified to take care of the pressure levels. Another issue was failure due to insufficient strength of the glue bond, which occurred sporadically even after changing to the stronger EPOTEK 353 ND-T epoxy (Figure 5.53a, bottom): the dimensioning of the device must therefore be adjusted so that the adhesively bonded surfaces are large enough.

(a) Failed microthrusters due to insufficient wall thickness *(top)* and glue bond strength *(bottom)*.

(b) Mechanical jig used to hold the microthrusters and measure their thrust force.

Fig. 5.53: Failed and successful microthrusters [189].

An experimental set-up was made to test the viability of the design and acquire the characteristics of the LTCC solid propellant microthruster at near sea level (ca. 400 m). The setup consisted of a high-speed digital video camera to capture the propellant microcombustion, a MilliNewton force sensor (Figure B.5), a fixture to facilitate the positioning of the thruster on the sensor, an oscilloscope and a DC power supply (Figure 5.53b). LabVIEW software was used to capture the data on the computer. From the signals captured during the microthruster firing, the duration of combustion was recorded as 150 ms, and an average thrust of 19.5 mN was measured.

Conclusion In the present study, the design and fabrication of LTCC microthrusters has been briefly demonstrated. This type of microthrusters has high-level integration, better ignition efficiency and reliability, adjustable thermal characteristics and more design freedom compared with silicon based solid-propellant microthrusters. Effect of nozzle geometry, chamber geometry, resistor design had been studied to obtain different thrust and impulse levels. An LTCC-based solid propellant microthruster has been successfully tested to generate a thrust of 19.5 mN at an altitude of ca. 400 m.

It must be mentioned that only one iteration of design/fabrication could be done in the allotted time-frame of this project. In their current state, the microthrusters can only be reliably fired with the help of the mechanical jig, which plays a role of pressure container by preventing the lid from exploding during the propellant ignition. However we have no doubt that a slight increase of thicknesses of the walls, of the lid and of the glue bond will be sufficient to suppress mechanical failures upon firing.

Regarding the propellant, we observed that it had tendency to expand and spill out of the nozzle during the curing of the epoxy. This can be corrected by employing adhesives with lower curing temperatures or by fine tuning the propellant compounds proportions upon mixing.

5.8 Electro-fluidic platforms

In parallel to this thesis, we have carried out several industrial mandates that allowed to explore various configurations of fluidic platforms containing channels, crossings of channels (see example on Figure 5.54), as well as SMD electronics; we have gained valuable experience of what cavity geometry is susceptible or not to be successfully laminated and fired. This is closely related to the set of lamination parameters discussed in section 6.1.1.
Figure 5.54 shows two schematics of fluidic platforms with large, complex channels; some are crossing each other. The same circuits are presented after manufacture on Figure 5.55 and Figure 5.56, as well as on Figure 3.16 on page 77.

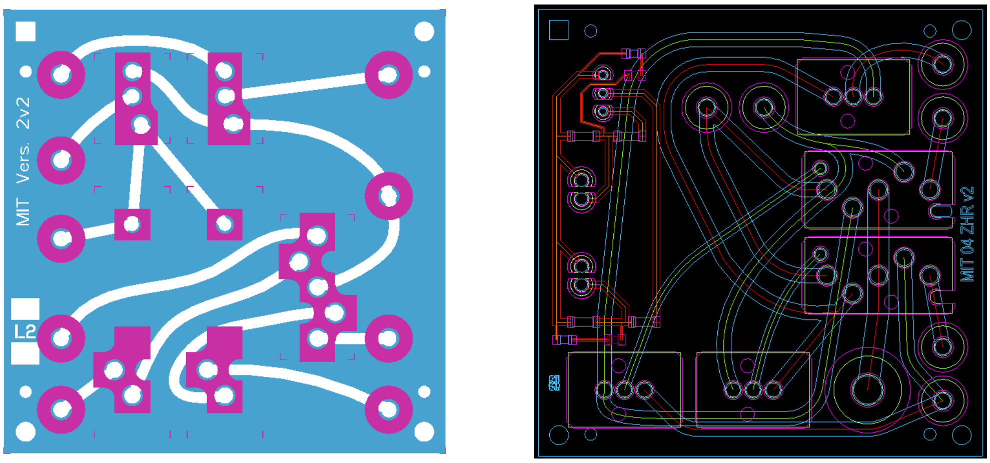

(a) Top view of layer L2 of circuit *MIT Vers. 2v2*.

(b) Transparent top view of circuit *MIT 04 ZHR*, with electronics driving electrovalves.

Fig. 5.54: 2D schematics of electro-fluidic platforms with complex channels and crossings.

Indeed, most of the fluidic platforms were already pictured throughout this document, to illustrate the different manufacturing steps; please refer to Figure 1.2 on page 17, Figure 1.9, Figure 2.2 on page 33, Figure 2.5 on page 37, Figure 2.6, Figure 2.8, Figure 2.11, Figure 3.3 on page 55, Figure 3.4, Figure 3.17 on page 78, Figure 3.19, and finally Figure 3.21 on page 85.

Fluidic fittings Concerning the fluidic fittings, our tests proved that classical soft soldering of M3 or M5 nuts onto metallized Ag:Pd ($\mathrm{DP}\ 7484\ /\ 6135\mathrm{D}\ /\ 6143$) solder pads yielded reliable bond strength and good hermeticity, compatible with industrial SMD manufacturing. The soldering quality is improved by employing vacuum in the molten state, in order to remove all trapped air bubbles from the solder joint (see section 2.2.8). We also soldered large brass adapters; these need to have a well-defined, symmetric solder pad, in order to prevent the adapter from rotating due to surface tension upon melting of the solder paste.
The soldered fluidic fittings coupled to our improved lamination technique allowed the producing fluidic circuits that sustained at least 100 to 250 bar under destructive tests – the best samples reaching 300 bar. With poor lamination, the circuits failed at 5 to 10 bar already.

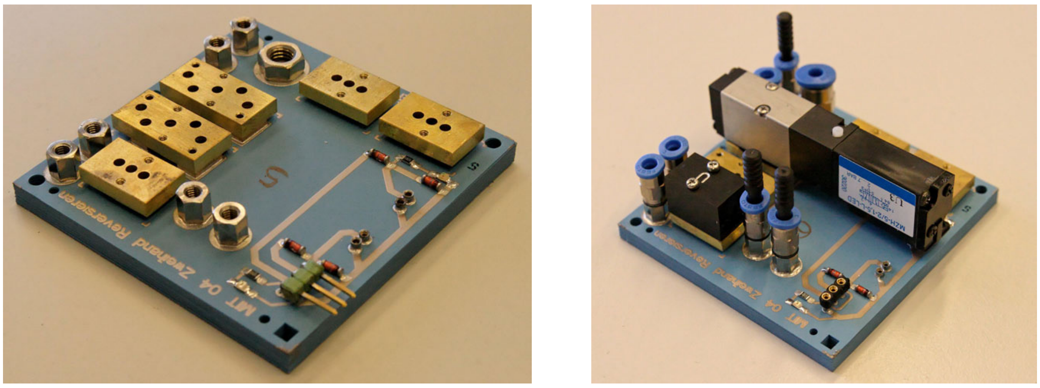

(a) Without valves or fittings. **(b)** With some valves mounted.

Fig. 5.55: Photographs of an electro-fluidic platform featuring SMD electronics for driving two standard solenoid electrovalves, as well as brass and nickeled brass fluidic adapters; note that external wires are limited to the three-pole connector. The circuit is the *MIT 04 ZHR* of Figure 5.54.

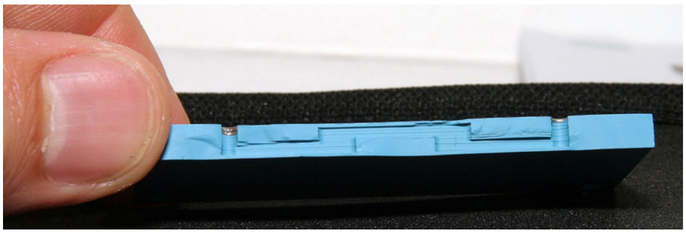

(a) Cross-section of a fluidic circuit showing large channel sizes and a zig-zag path; the whole stack is made of 22 layers of DP951-254 µm.

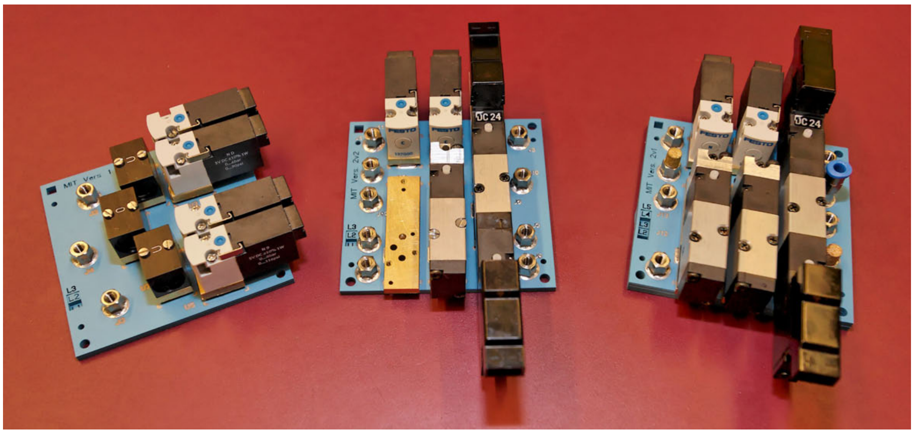

(b) Three different circuits with commercial fluidic components mounted. The central circuit is the *MIT Vers. 2v2* of Figure 5.54.

Fig. 5.56: More examples of a manufactured electro-fluidic platforms.

5.9 Conclusion

In this chapter we showed numerous applications of LTCC to sensors, microsystems and microfluidics devices. We saw in particular a multisensor for the pneumatics industry. An innovative industrial-grade potentially low-cost diagnostics multisensor for the pneumatic industry was developed, allowing the measurement of compressed air pressure, flow and temperature. The device is entirely mounted by soldering onto an electro-fluidic platform, *de facto* making it a true *electro-fluidic SMD component* in itself. It comprises additionally its own integrated SMD electronics, and thanks to standard hybrid assembly techniques, gets rid of external wires and tubings – this prowess was never achieved before. This opens the way for *in situ* diagnostics of industrial systems through the use of low-cost integrated sensors that directly output conditioned signals.

Our other realizations include capacitive microforce sensors, two kinds of anemometers (thermal and capacitive), a calorimetric microreactor for mixing strong reactants, a solid-propellant based microthruster, as well as diverse electro-fluidic platforms. Most of these realizations would have not been possible with the standard lamination and firing techniques used so far. Hence, we proved it was possible to circumvent the problems related to microfluidics circuitry: for instance, the difficulty to control final fired dimensions, the burden to produce cavities or open structures and the associated delaminations of tapes, and the absence of "recipe" for the industrialization of fluidic devices. These projects allowed us to gain valuable information in multiple domains:

- In the co-firing of mineral sacrificial pastes in slender LTCC structures;
- In the manner to laminate LTCC pressure membranes to ensure at the same time two contradictory aspects: a good tape bonding for stress resistance, and a flat shape with the "drum-skin effect". We also learned on the combination of thermal resistors printed on membranes with stress decoupling cuts;
- In the variable chemical resistance of different LTCC tapes;
- In the effect of co-firing Ag:Pd conductors with suspended LTCC structures, yielding strong deformations;
- In the type of cavity geometries susceptible or not to be successfully laminated and fired.

Chapter 6

General conclusion

This chapter begins with the recapitulation of our contributions to the research: first with improvements to LTCC technology, then with sensors and devices realized thanks to these improvements. We then discuss on the suitability of LTCC to microfluidics, and lists the applications where LTCC has a strong potential, its limitations, along with an appreciation of the different tapes we tested. This is followed by an outlook of what the future sensors and devices could be, and by an overview of the latest innovations in LTCC 3D structuring techniques, assembly and firing techniques. We give indications on where to orient research; for example with the study of unfired LTCC porosity, and with the testing of lamination of structures with different aspect ratios coupled to low pressure and solvents.

Key words: Innovations, 3D structuration techniques, High resolution machining, Firing enhancements.

In this thesis, we have first introduced in section 1.1 what *Low Temperature Co-fired Ceramic* is: a relatively new technology, originally intended for high-end electronics such as high frequency antennae, military-grade high-reliability circuits and automotive applications (car ignition systems). We then reviewed the general properties of LTCC, and compared it with competing methods such as PCB in FR-4 or purely prototyping methods. With regard to the dimensions of manufacturable structures, we showed that it could be positioned between MEMS (made up of components between 1 to 100 µm in size) and classical "macro microsystems" (components between 500 µm to 20 mm), thus filling the technological gap range from 100 µm to 500 µm.
I then undertook to demonstrate why LTCC is a promising technology for the industrial manufacturing of microfluidic sensors and devices, and listed the main related issues; for instance, the difficulty to control final fired dimensions, the burden to produce cavities or open structures because of the associated delaminations of tapes, and the absence of "recipe" for the industrialization of fluidic devices. The essence of this thesis lies in the solutions to the abovementioned problems: our contributions helped moving back the limits of LTCC structuration and enabled manufacturing devices that would have not been possible beforehand; we will recapitulate them now.

6.1 Our contributions to the research on LTCC

Our contributions to the LTCC domain can be split into two parts: the technological contributions with the new structurations methods and processing, and the contributions to innovative devices and microsystems that directly exploit the first improvements.

6.1.1 Technology

Processing

To compensate for the necessary reduction of lamination pressure and temperature to create fragile structures, we have developed a reproducible lamination technique (section 3.3) mixing pseudo-isostatic laminations with the help of a constrained rubber, and a classical uniaxial lamination between two metal plates. It requires the introduction of partial laminations that preserve crushable sub-parts from the pseudo-isostatic lamination, while ensuring a good tape bonding at locations where pressure would have been zero with a pure uniaxial lamination. This multiple-step lamination process is ended by a final metal lamination to join sub-parts together. The procedure requires a careful mastering of the processing conditions, as the deviation of lamination pressure between the sub-parts causes, later upon firing, stresses that can be fatal to the circuit due to an excessive difference of shrinkage (see next).
This complex workaround would be much simpler if we could work at (very) low lamination pressures with the help of methods such as Cold Chemical Lamination (CCL, see below); the differences between sub-laminations would be less critical upon firing, and the bonding of tapes would be ensured, still.

Regarding the lamination parameters adopted to fabricate our circuits, we discussed in detail (subsection 3.3.3) how the temperature, pressure and duration must be reduced depending on the type of circuit (with channels or not, with screen printings, in function of the tape etc.). As a general rule, narrow channels (200 to 500 µm) of low height (typically made of only one layer) can be laminated at nominal pressure (e.g. 206 bar for DP951), but with a lowered temperature (40 to 55 °C). Channels of medium size (0.7 mm to 2 mm) must be laminated at both lowered pressure (80 to 160 bar) and temperature (25 to 40 °C). Finally, complex fluidic structures involving long, high and large channels crossing each other must be laminated with an improved technique such as our multiple pseudo-isostatic sub-laminations and/or CCL, at low pressures (80 to 120 bar) and low temperature (25 to 40 °C).

Influence of lamination on shrinkage

As covered in section 3.2, we now have a better understanding of the shrinkage process in function of the lamination parameters. After testing the influence of various parameters with Design of Experiments, we could determine a simple linear model for the DuPont 951 in function of temperature and pressure; the number of layers and the lamination duration were the two other parameters retained for the study, but they turned out to have a negligible impact *on shrinkage*. However, they certainly play a role on the type of achievable structures and on

the quality of bonding of tapes upon sintering.
Our linear model must nevertheless be applied with caution, because we deviate from the manufacturer's lamination recommendations. In effect, for our study, the lamination temperature was limited to a range (25 to 55 °C) known not to provoke the collapse of structures of the studied design, while DuPont advises to laminate under 206 bar, at 70 °C for 10 min [9], and we expect the visco-plastic behavior of green tapes to become non-linear above 55 °C.
We also expect tapes from other manufacturers to exhibit the same general tendency of presenting a lower shrinkage after an increased lamination (and *vice versa*), but the dependence on pressure and temperature is probably different because of other (secret) organic binders employed. For instance, we know that the DP951 tape is based on acrylate polymers (PEMA/PMMA) [102], while others are based on PVA or PVB (HL2000 supposedly [88, 103, 104]).
Therefore, this study should be seen as a motivation to further study the influence of lamination, and is a call to LTCC suppliers to conduct similar experiments in order to adopt a standard shrinkage measurment technique. I am convinced that the future of LTCC structuration for microfluidics lies in the reduction of lamination pressure and/or temperature, and if end-users could dispose from models to better predict the shrinkage of their circuits, it would be a great leap forward for the community.

We also reviewed the latest innovative lamination techniques (section 3.4), among which Cold Chemical Lamination (CCL) based on solvents, Cold Low Pressure Lamination (CLPL) based on adhesives, and the use of sacrificial inserts, the frontier being often fuzzy with the evolution of methods.

Mineral Sacrificial Volume Materials

One solution to the problem of manufacturing cavities and open structures is the use of sacrificial inserts; in this field, I have open an exploration way with the use of *mineral* Sacrificial Volume Materials (SVM), also called Mineral Sacrificial Pastes (MSP), both on classical hybrid alumina substrates (section 4.3) and on standard shrinking LTCC (section 4.4), later dissolved by immersion in weak acids such as H_3PO_4. So far, only carbon fugitive phases were successful for definition of slender structures on LTCC, but only for relatively closed cavities such as buried channels or thin membranes.
The developed solutions are based on a sandwich of mineral compounds such as CaO, C and $CaCO_3$, which act as a skeleton during the sintering. The minerals are coupled to a glassy phase to join grains together, which is composed of boric acid H_3BO_3 or boron oxide B_2O_3, and of small amounts of borax (sodium tetraborate $Na_2B_4O_7$). Both are mortar ground and mixed with an experimental organic binder compatible with green tapes and with standard screen printing.
The dissolution is done by gentle stirring in diluted weak acid (H_3PO_4), successive rinsing in deionized water and air drying at 100 °C. In the best cases it was not even necessary: wiping a finger on the overflowed MSP was sufficient. The removal of MSP must however take place immediately after firing, as we experienced continuous grow of the leftover MSP due to the

ambient air humidity; the hydratation of CaO into $Ca(OH)_2$ is a well known reaction involved in the preparation of concrete.

My MSP compositions were later refined by colleagues of my group led by the Dr. THOMAS MAEDER, who pursued the research (section 4.6) both onto hybrid substrates and normal shrinking LTCC (DUPONT 951), but also onto "zero-shrinkage" tapes (HERAEUS HERALOCK HL2000 and HL800). To this end, materials based on MgO (refractory alkaline earth oxide, negligible sintering and much slower hydratation than CaO) and CaB_2O_4 (lower melting temperature, sintering) were formulated. Although the firings went rather well, we discovered that all LTCC tapes are not equivalent in regard to chemical resistance. In effect, though DP951 presents an excellent resistance to strong acids and bases [17–19] and was almost not affected by dissolution in 10 % acetic (CH_3COOH) or phosphoric acid etchants, HERALOCK tapes were directly attacked by the acids; HL2000, especially, completely lost consistency, i.e. its glass matrix was entirely degraded. HL800 suffered extensive surface attack, but did show qualitatively much better chemical resistance than HL2000. This poor performance, in line with other studies [158], is not necessarily intrinsic, as we did not optimise the firing conditions, which we intend to do in later studies.
Thus, the formulation of the MSPs for HL2000 and HL800 will be refined to allow more benign etching conditions. One possible path is to switch to finer, more reactive MgO powder, without any "binder" such as CaB_2O_4 or with a more soluble one, in order to increase its etching rate. On DP951, efforts will focus on decreasing the boron of the mineral paste loss while keeping the desirable sintering and shrinkage characteristics of CaB_2O_4.
In the future, gentle air blowing or water dissolution can be envisaged in place of weak acid dissolution; this would be ideal to protect adjacent layers from being attacked by etchants. Finally, the formulation of the screen printing vehicle will be further refined to minimise solvent interactions with the LTCC tape during drying.

As a more general contribution, we classified at the beginning of section 4.2 the existing Sacrificial Volume Materials, and presented an extensive state of the art. To our knowledge, such a work encompassing the latest techniques was not yet presented.

Two applications of MSP to sensors were also demonstrated: a microforce sensor in alumina (subsection 5.4.1), and a capacitive anemometer for an indoor aeroplane (subsection 5.4.2).

6.1.2 Devices

Exploration of fluidic platforms

We have explored various configurations of fluidic platforms containing channels and crossings of channels (section 5.8), and we have now a good idea of what cavity geometry is susceptible or not to be successfully laminated and fired. This is closely related to the set of lamination parameters discussed above in section 6.1.1.
Concerning the fluidic fittings, we proved that classical soft soldering of M3 or M5 nuts onto metallized Ag:Pd solder pads yielded reliable bond strength and a good hermeticity, compatible with industrial SMD manufacturing. The soldering quality is improved by employing vacuum in

the molten state, in order to remove all trapped air bubbles from the solder joint. We also soldered large brass adapters or complete sensors onto test fluidic PCBs with success, along with electrical connections.
Gluing of fluidic adapters is a also possible solution, experimented by many other teams for their prototypes.

The soldered fluidic fittings coupled to our improved lamination technique allowed the production of fluidic circuits that sustained at least 100 to 250 bar under destructive tests – the best samples reaching even 300 bar.

Application to sensors and to industrialization

We created several innovative sensors by direct application of the methods cited above, which would have not been possible beforehand. For instance, capacitive microforce sensors with free-standing cantilever beams or bridges (with a gap of 30 to 40 µm between the base and the beam) were possible to create thanks to mineral sacrificial materials (subsection 5.4.1).
Our integrated multisensor, measuring pressure, flow and temperature of compressed air was manufactured by successive pseudo-isostatic sub-laminations, ensuring good tape bonding despite large screen-printed areas (e.g. ground plane and buried tracks), later proved by pressure tests (section 5.3). It is a good example of functional packaging.
Another proof of the good lamination lies in the overpressure tests carried out on the piezoresistive prototypes of the pressure sensor part; those that were made with a DP951-254 µm membrane were nominally designed for working at 6 bar with a safety margin up to 10 bar, but we could not make them fail at 24 bar (the maximum applicable on our pressure system).

Other sensors, such as the thermal anemometer for indoor slow flyer (section 5.6), were designed based on the experience gained from the study of the influence of lamination parameters on firing shrinkage; the thin thermal membrane, notably, was decoupled from the sensor core while still staying flat by using the “drum-skin effect” (subsection 3.3.2).
The arrays of solid-propellant microthrusters (section 5.7) had their cavity laminated in multiple laminations, too. Sacrificial paste was also applied under the ignition thermistor, which revealed an unforeseen chemical incompatibility; more research is needed in this field, as there is no standardization in the composition of commercial pastes.
Already mentioned in the previous subsection, the capacitive sensors of section 5.4 with suspended structures of low-height gaps were made possible by the direct application of the mineral sacrificial pastes developed during this thesis. This allows measuring forces in the range of 0.01 to 2 mN on alumina sensor, and in the range of 5 to 600 µN on LTCC.

We also showed that it was possible to use LTCC for industrial sensor applications, by using standard assembly techniques such as gluing, soldering and wirebonding. A careful mastering of fluidic junctions by soldering yields the possibility to get rid of external wires and tubings, turning LTCC devices into SMD components, brightly demonstrated by the integrated multisensor of section 5.3 and by its pressure sensor ancestor (Appendix section C.1). This opens the way for *in situ* diagnostics through the use of low-cost integrated sensors that directly output conditioned signals.

6.1.3 Overall evaluation of the suitability of LTCC to microfluidics

In regards to the initial question of section 1.2.1 on page 25, LTCC is a technology adapted to the industrial manufacturing of microfluidic sensors and devices: the fabrication steps are all industrializable, and the prototyping fabrication steps differ little fundamentally from those used in mass production. For instance, mechanical punching can be used instead of laser cutting, as it is the case already for vias of the electronics industry. Nonetheless, the fabrication of channels, cavities and membranes obey rules that are dependent on the circuit geometry, on the type of LTCC tape, on the amount and type of inks screen printed, on the manufacturing equipment, etc.; it is for the moment not yet possible to predict with accuracy how to laminate a circuit in order to ensure the right output geometry *and* a correct bonding of tapes at the same time – at least not before a few iterations of testing. Consequently, thorough engineering and mastering of the know-how of the whole manufacturing process is still necessary to produce efficient LTCC circuits, to the contrary of older techniques such as classical thick-films on alumina substrates or PCBs in FR-4.

Notwithstanding its lack of maturity, the still young LTCC technology is in my sense promised to a long and bright future in both the microelectronics and microfluidics domains. The research around this material and its applications to microfluidics is in constant augmentation; still, the main research groups are not many, mainly located in Central and Eastern Europe, in USA, and in Brazil. Engineers have now a better understanding of the structuration possibilities, of the implications of lamination, and of the most common problems; they have all the tools in hand to manufacture complex microfluidics circuits. Let us review now the domains where LTCC is expected to be successful, and where it is not.

Application fields of LTCC

The applications were LTCC has the strongest potential, except high frequency electronics, are:

- **Harsh environments**:
    - **Hermetic packaging** of MEMS [45, 46];
    - Sensors functioning at **high temperatures or in corrosive atmospheres** and measuring pressure [168], flow, temperature, force, magnetic field [67, 68], etc.;
- **Integrated sensors** for low-cost diagnostic applications (section 5.3);
- Microreactors with complex circuitry for chemical analyses or, as disposable for dangerous testing (section 5.5, [17] and [176]);
- Niche **thermal applications** like **oxygen-getters** [174], **suspended heaters** [173], arrays of **microthrusters** thermally ignited (section 5.7 + [189]), **heat pipes and thermal cooling** of power electronics [190], or thermo-fluidic interfaces for MEMS with integrated temperature control [62];
- Special **custom shapes** enabled by almost infinite structuring possibilities.

Limitations of LTCC technology

In spite of its qualities, LTCC technology does have limitations, originating from its cost, mechanical properties (brittleness and limited strength) and from the achievable resolution.
For relatively simple devices produced on a large scale, **LTCC is not suitable** for the production of:

- **Large fluidic platforms or duct plates**, both because of its brittleness and of its cost (~1 €/dm^2/layer in mass production); it is preferrable to use classical techniques such as metal milling, plastic injection or reinforced PCB to create a duct plate, and to connect modular LTCC sensors onto it with the techniques we demonstrated.
- **For simple electric circuits**, where PCBs and classical hybrids on alumina are more competitive;
- Neither for **high-volume applications combining ceramic-metal or metal-polymer in a volumic shape** rather than by addition of layers; see HVPF in subsection 6.2.6.

At small dimensions, LTCC is limited by the modest resolution achievable by current industrial manufacturing techniques (lasering, punching, screen printing); the finest "conventional" manufacturable LTCC structures are in the order of 100 to 200 µm, for prints of 100 to 150 µm (line/space resolution). Fine laser tuning and micromachining (see later), as well as high-resolution printing techniques allow patterning structures down to 40 to 50 µm and prints of 20 µm line width, which still falls significantly short of the resolution achievable by MEMS manufacturing processes. Moreover, the manufacture of such fine structures partially negates the advantage of simplicity of common LTCC and thick-film processes, as it requires extreme caution and cleanliness during handling in the green state, screen-printing, lamination and co-firing.

Besides lateral dimensions, the tape structure of LTCC imposes limitations on the minimal achievable layer thickness, an important aspect for suspended structures requiring a high frequency response, such as thermal sources and sensors. Here again, MEMS proceses can reliably yield structure thicknesses down to ca. 100 nm, depending on size, while the finest available LTCC tapes are usually in the 20-50 µm range. Although this can be considerably improved (similar multilayer ceramic capacitor technology achieves layer thicknesses <2 µm [191]), this work has shown that achieving sound, undeformed thin structures with LTCC is currently a considerable challenge.

Finally, another current limitation is set by the absence of standards, both in commercial materials and fabrication processes for complex structures.

Appreciation of the different commercial LTCC systems We have seen that not all LTCC tape systems are equivalent; in Appendix section D.2 on page 241 we list the pros ans cons, with regard to microfluidics, of the commercial tapes frequently encountered in litterature.

6.2 Outlook

This section discusses present and future directions of research; as we will see, the field of research in LTCC is very vast and numerous research teams are currently active.

6.2.1 Sensors and microsystems

Other potentially promising applications of LTCC, but for which more testing is required with the current state of technologies, are reviewed below.

Microvalves The most famous prototype of microvalve tested so far is the 2001 attempt of Mario Ricardo Gongora Rubio et al. [5, 170] (see Figure 6.1). This project was just a demonstrator, and to our knowledge no extensive tests have been carried out afterwards. The hybrid microvalve was electomagnetic: the device had a multilayer coil, a fluidic system and a flexible diaphragm with a permanent magnet bonded in its topside. An assumption for the cause of this failure might be the difficulty to integrate powerful coils in LTCC.

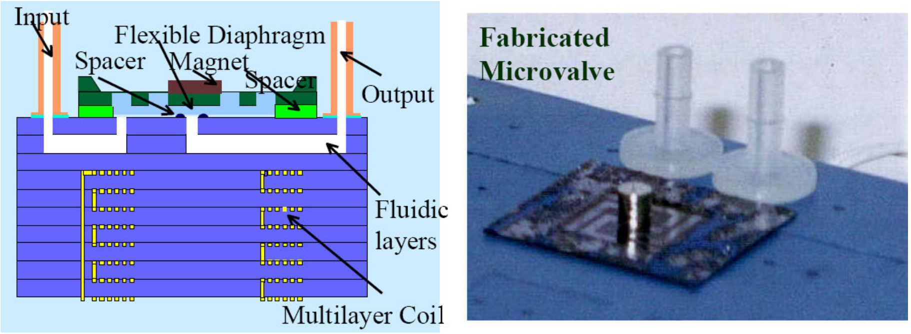

Fig. 6.1: Demonstrator of hybrid micro-electro valve by Gongora Rubio et al. [170].

Thus, other solutions have to be sought. At this meso-scale, it seems that piezoelectric bending actuators are more practical and have more favorable downscaling properties than traditional electromagnets. Nevertheless, the hermeticity of the joint (O-ring or other means) will always be a major problem, whatever the design. Hence, in our laboratory we had the idea of focussing on piezoelectric bending actuators in bulk PZT (Lead zirconate titanate, still one of the most suitable material for this application [163]). We thought of integrating the piezoelectric beam into a structure similar to our integrated sensor, with the idea to measure flow and pressure *in situ* to assess the valve functionning. The assembly methods envisioned are not many: gluing and soldering are the most relevant at this scale. Ideally, the bender should be clamped with an infinite rigidity, which is never the case. The assembly of PZT onto LTCC is problematic in the sense that PZT suffers from gradual depolarization at temperatures above 100-120 °C already. As most of the stable gluing and soldering operations rise above this temperature, it would require repolarizating PZT at 750 V or more after assembly. Then, there is still the problem of encapsulating the cavity containing the PZT beam inside an LTCC shell.

What about co-firing PZT with LTCC? Eastern European research teams (notably L. J. Golonka and A. Dziedzic in Poland, M. Hrovat, M. Kosec, D. Belavic and M. Santo Zarnik in Slovenia, S. Gebhardt and U. Partsch in Germany) have been working on PZT thick-films on LTCC in recent years [192, 193]. There are still numerous issues with these thick-films, mainly because of material interactions during firing [194, 195], and because the effect of clamping the thick-film to the substrate generates reduced effective values of d_{ij} coefficients. Work from Santo Zarnik et al. [163, 165, 196, 197] has shown that in the case of a thick-film realization, the deflection of the cantilever-type actuator is severely reduced in comparison with general bimorph structures (because of the stiffness of the ceramic substrate). In conclusion, it is not impossible to manufacture piezoelectric micro-valves in LTCC with the current technologies, but the force-displacement performances (i.e. the blocking force, and thus the maximal working pressure and maximum flow) would be at present rather low compared with classical techniques.

Bioimplants and medical applications Depending on the time-scale envisaged for a bio implantation, using LTCC in medical applications could be foreseeable or not. In effect, short-term (a few hours) contact of LTCC with body fluids would probably pass unoticed to the body, but long-term implantation (in weeks) could be problematic in case of materials leaching out of LTCC. Indeed, although the DuPont 951 tape (containing PbO) is known to exhibit good chemical resistance to strong acids and bases [17–19], a study of 2008 by Eitel et al. [158] on the biostability of LTCC materials for microfluidics and biomedical devices showed that all the studied tapes (Heraeus HL2000, CT2000 and DuPont 943, all lead-free) were unstable in both NaOH (1 M) and Simulated Gastric Fluid (SGF, made of 7 ml concentrate HCl and 2 g of NaCl diluted in 993 ml DI water). They however exhibited acceptable stability in Phosphate Buffered Saline (PBS) solution and Simulated Body Fluids (SBF, made of PBS plus 3 % Bovine Serum Albumin (BSA)). The study was conducted on 30 days by immersing screen printed and non screen printed tape samples in tubes containing etching solutions.
As we see, the LTCC tapes are unequal in regard to chemical resistance. Thus, more studies are necessary to assess the long-term stability and the potential toxicity of chemical species leaching out of LTCC, and research has to be done on the LTCC side to increase its chemical resistance.

6.2.2 Study of the LTCC tape materials

A study on the tape porosity would help in setting up new solvents for sacrificial inks, and to help in softening the surface layer of tapes for Cold Chemical Lamination. Measurements of the unfired tape porosity, vs. the laminated porosity and the fired state porosity would be interesting to know. T. Maeder observed in 2007 the following differences of unfired tape porosity during quick tests of binding LTCC together with propylene glycol (PG): the Heraeus CT700 was the most porous, followed by CeramTec GC; DuPont 951 was the most dense.
The presence of porosity in commercial LTCC tapes comes from the moderate amound of binder and plasticizer not being sufficient, for “reasonable” formulations, to fill the volume between the

mineral particles [36]; the actual formulation will be a compromise between strength, flexibility, and debinding properties. The plasticizer being somewhat volatile, tapes tend to become "rigid" after some drying following the opening of their sealing bag. More information about binders and their removal from ceramics can be found from the 1997 article of Lewis [198].

6.2.3 Various 3D structuration techniques of LTCC

Lamination

In order to draw the "map" of achievable LTCC structure geometries vs. lamination parameters, experiments on test structures with cavities of different ratios of height-width and of variable dimensions would be a logical first step to pursue the research we presented in section 3.3. Innovative methods to achieve low-pressure lamination should be sought. Locally softening the surface/adhesive bonding (CCL/CLPL methods) constitute a promising field of research, especially the formulation of materials and the development of reproducible application methods that achieve controlled surface modification and are compatible with thin LTCC tapes (see section 3.4.2 on page 84).

Injection of sacrificial materials after pre-lamination

B. Balluch & W. Smetana tested in 2008-2009 the injection of Sacrificial Volume Materials as filler into channels [40, 41]. The injected SVMs were in powder or liquid form; they tested PMMA (polymethyl methacrylate), PVA-S (special polyvinyl acetate) and HEC (hydroxethyl-cellulose). The injection system, depicted on Figure 6.2, is made of a steel mould with filter sheets and protective layers; an ultrasonic vibrator is used in conjunction with a vacuum system to draw the SVM into the microchannels. To prevent SVM-particles material from creeping into gaps between tapes, tapes were pre-assembled through the use of liquid adhesives of the same kind as those abovementioned (similarly to the CCL method). Foil inserts in PMMA 55 to 375 µm-thick were also used as filler for comparison.
They obtained mitigated results on CeramTec GC and Heraeus CT707 & CT800 tapes: the use of liquid SVM filler led to cracks (PMMA) or sagging (PVA+HEC), PMMA foil inserts films yielded cracks, as well as PVA+HEC powders. Only PMMA in powder led to a good channel output geometry.

Although we also got this idea, we never tried it as it requires a special vacuum apparatus, large openings and a circuit structure compatible with the necessary compression in the steel mould to inject the SVM. The risk of creating delaminations with SVM in the tape interstices must also not be neglected.

LTCC green tape micromachining

CNC micromachining R. K. Yamamoto and M. R. Gongora Rubio presented at the IMAPS CICMT 2008 conference a microplasma generator [199] (quickly introduced in 2004 in [170]), illustrated on Figure 6.3 and also published in the IMPS journal in 2009 [200]. This

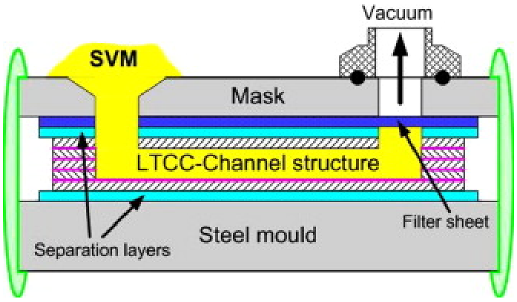

Fig. 6.2: Schematic of the SVM filler set-up tested by BALLUCH & SMETANA [40, 41].

device comprises a fine grid of LTCC studs (~500×500 µm) sparsed with holes in between the studs (see Figure 6.4c); the dense "forest" of studs forbids the use of two tapes and requires the LTCC tape to be finely *structured in its own thickness*. Plasma generation being beyond the scope of this thesis, the technological achievements that are here of interest are twofold:

- The use of LTTT transfer tapes to join co-sintered parts (already discussed in section 6.2.4 on page 212);
- LTCC green tape CNC surface micromachining (e.g. mechanical / laser milling without removing all the tape thickness).

Surface micromachining makes little sense for single thin LTCC tapes (like the DUPONT 951P2 50 µm-thick), but is of interest for tapes thicker than 200 µm (DP951PX 254 µm-thick, or CERAMTAPE GC (320 to 600 µm-thick), and even more for already-laminated tapes as is the case here. Laminates allow both a more robust circuit clamping during machining, and the creation of structures higher than the thickness of a single tape, with tool diameters down to 200 µm [200]. The process and an example of what can was done in this work is depicted on Figure 6.4.

An earlier reference to CNC micromachining of green tapes lies in the 2004 JPPA journal article of R. GORGES et al. [201], but the process was not described in detail.

Laser patterning / ablation The lasering of fine LTCC structures was tested by JURKÓW et al. in 2009 [202]. Direct structuration of alumina tapes and DP951 + HL2000 tapes using Nd:YAG laser system was investigated. The minimal features for commercially available green tapes milled with Nd:YAG laser were higher (ca. 40 µm) compared with those of the alumina tape tested, ML35A001, which was made with a latex of higher glass temperature (Tg).

YUNG & ZHUN studied laser ablation of green tape material by excimer laser (KrF, 248 nm), UV laser (Nd:YAG, 355 nm), and by infra-red laser (1090 nm) [203, 204][1]. The optical photos and SEM photos of the LTCC ablated by different kinds of laser sources are given in their papers, mostly via holes. The best results were obtained with the infra-red laser. HORVATH also conducted hole drilling tests with a tripled Nd:YAG laser [50].

NOWAK et al. reported in 2006 [104] about a novel "cold" self-cleaning technique for processing

---

[1] Each of them published the same article under both names in different journals...

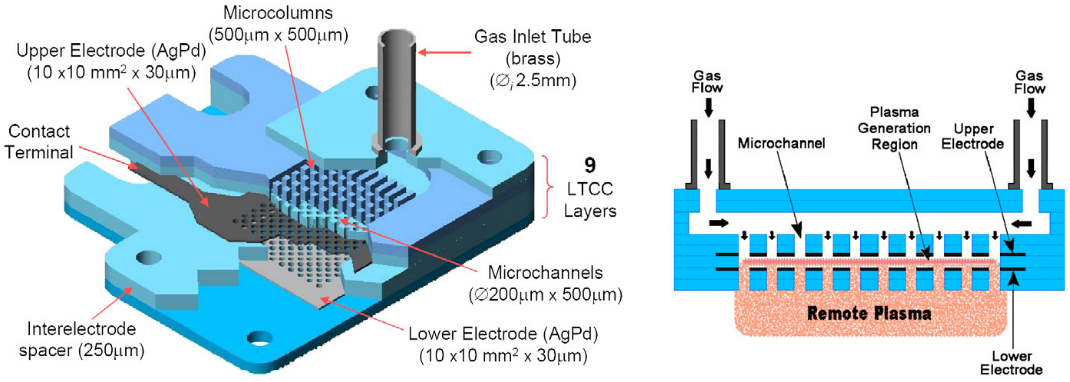

(a) Schematic 3D partial view.

(b) Device cross-section.

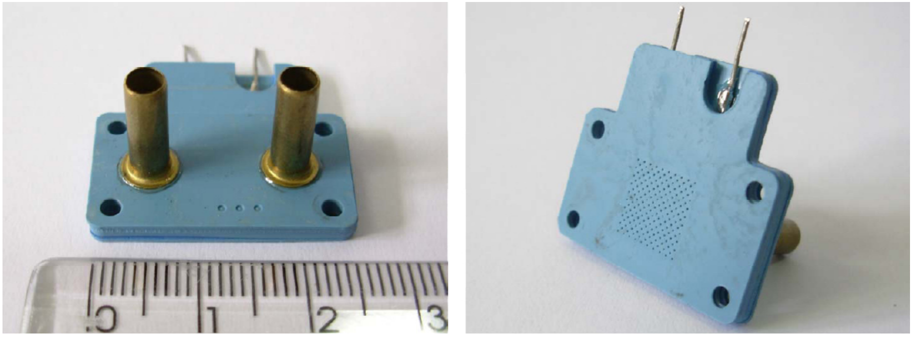

(c) Photographs of the fabricated microplasma generator. Note the micro-channels on the right image.

Fig. 6.3: Layouts and pictures of the microplasma generator presented by Yamamoto, Gongora Rubio et al. at the IMAPS CICMT 2008 conference [199].

LTCC in the green state at high resolution and high speed, using a low-power CO_2 laser. A particle ejection process involving both the ceramic grains and the organic binder produces material removal rates of $> 100\,\mu m$ per pulse. Lateral processing resolution of $50\,\mu m$ and depth resolution comparable to ceramic grain size with no heat-effected zone or other deleterious thermal effects were observed. The process was tested on HeraLock, HeraTape CT800 and Ceramtape GC. They also made a model of the key process parameters associated with "cold" laser ablation of ceramic materials in the green state [205].

High-resolution printing techniques

Direct Gravure Printing (DGP) M. Kittila et al. published in 2004 [206] about a Direct Gravure Printing (DGP) method for printing fine-line electrical circuits on ceramics; the idea is to fill a grooved silicone mould with the paste to be transferred on LTCC and then to apply LTCC on the mould with pressure: upon removal of the mould, the paste stays on the LTCC. They demonstrated that the method is an excellent technique to form narrow lines and structures with commercial silver pastes. With precise pressure control of the doctoring machine, lines down to $20\,\mu m$ in width were successfully printed on Heraeus CT2000 LTCC

(a) Printed circuit board CNC prototyping machine used to mill green LTCC.

(b) Sample of green tape micromachined in (a).

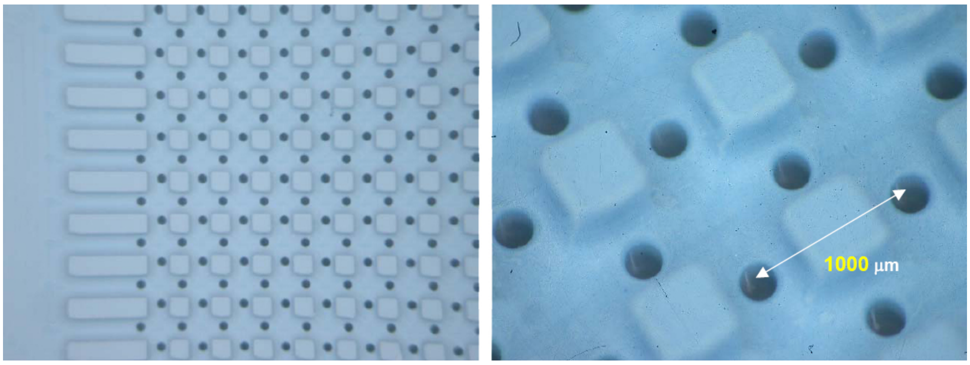

(c) Details of the green tape of (b) micromachined: microcolumns (left) and microchannels (right).

Fig. 6.4: LTCC green tape machining using CNC. [199]

without any special arrangements. Not all commercial inks are suitable to this process however; some exhibit a too strong adhesion to the silicone mould, which yields not clean printing surfaces after doctoring.

Photoimageable processes In contrary to LTCC technique, where different materials such as glass-ceramic composities and thick-film metallic pastes are co-fired in a single thermal operation, in the photoimageable process the ceramic structure is being built gradually step by step until the required thickness of dielectric is obtained.
The FODEL photoimageable ink technique, branded by DuPont, was first reported by Bacher in 2001 [207]. It combines the inorganics used in thick film with photoresist organics from the PWB industry. The process to image conductor lines and dielectric vias is photochemical; a polymerization reaction occurs when the materials are exposed to UV light through a photo-negative mask. The polymerized areas are "hardened" by the UV light while the unexposed areas are not changed. It is the unexposed areas that are washed away with a spray of water plus 0.8 % sodium carbonate during development of the image. A resolution of 50 to 75 µm is achieved for vias, and of 40 µm for gold tracks (with 80 µm pitch); this must be compared with the minimum 150 µm/150 µm line/space normally employed for standard screen

printing.
Magonski, Nowak et al. reported use in 2005 in [162] of Fodel dielectric 6050 first printed on 96 % alumina, then applied to Fodel 951-100 µm LTCC. Prior the lamination, the LTCC tape was preconditioned with thinner DP8250 to promote adhesion. They claimed the technique to be an effective method of realization of ceramic microfluidic devices.
Perrone, Mach & Müller recently published on miniaturized embossed low-resistance fine line coils in LTCC made using this technique [208]. Fine line embossed structures, with line widths and spaces of 50 and 75 µm, were respectively realized; the cross section of the embossed channels was about 50 µm. The advantage of the technique, in contrast to Direct Gravure Printing, is the embossement of the lines, which promotes a better tape bonding upon lamination and sintering.

6.2.4 Assembly techniques

Surface softening The idea of surface softening to improve the adhesion of tapes upon low pressure and low temperature lamination was extensively covered in section 3.4. This is, in our sense, one of the most promising way of research for the lamination of complex fluidic structures.

LTTT transfer tape LTTT (Low Temperature Transfer Tape), indeed a dielectric in form of tape instead of ink, is a cast film consisting of inorganic materials in a flexible organic matrix. They are designed to be fired on alumina substrates at a peak temperature of 850 °C. The green state handling characteristics are similar to LTCC.
Gold, palladium/silver, and silver based conductor systems are available for use with transfer tape. The flexibility in processing and the less stringent compatibility needs allow a wide variety of thick-film conductors to be used for metallizing the top layer.

The processing of LTTT closely follows the steps used in the well-established multilayer thick-film process, with the multiple dielectric printing per layer being replaced by a tape lamination step. A flow chart for preparing the transfer tape process is shown on the website of the APTA [209], while Table 6.1 is a comparison between LTTT and LTCC.
LTTT is commercially available by ElectroScience Laboratories (ESL), for both alumina and steel substrates:

ESL 41010-T is a flexible cast film of inorganic dielectric powder dispersed in an organic matrix, designed to be laminated to 96 % alumina. Its datasheet is available on the ESL website [210].

ESL 41030-T-200 is a flexible cast film of inorganic dielectric powder dispersed in an organic matrix, designed to be applied to a 430 type stainless steel substrate and fired at 850 °C. The 41030-T-200 film will yield a dense body after firing; datasheet available on [210].

An example of LTTT use was published by Yamamoto and Gongora Rubio recently in [199, 200], with the fabrication of a micro-plasma generator using a mixed LTCC and

LTTT Transfer Tape	LTCC Cofire Tape
Processing (Sequential)	Processing (Parallel)
Tape sheets cast	Tape sheets cast
Lamination to substrate	Lamination of layers
Metallization	Metallization
Component formation	Component formation
Advantages	Advantages
Strength	Low labor
Multiple fire	Single fire
Zero Shrinkage (X-Y)	Sheet inspection
Heat Dissipation	Multilayer capability

Table 6.1: LTTT & LTCC comparison (from [199, 200]).

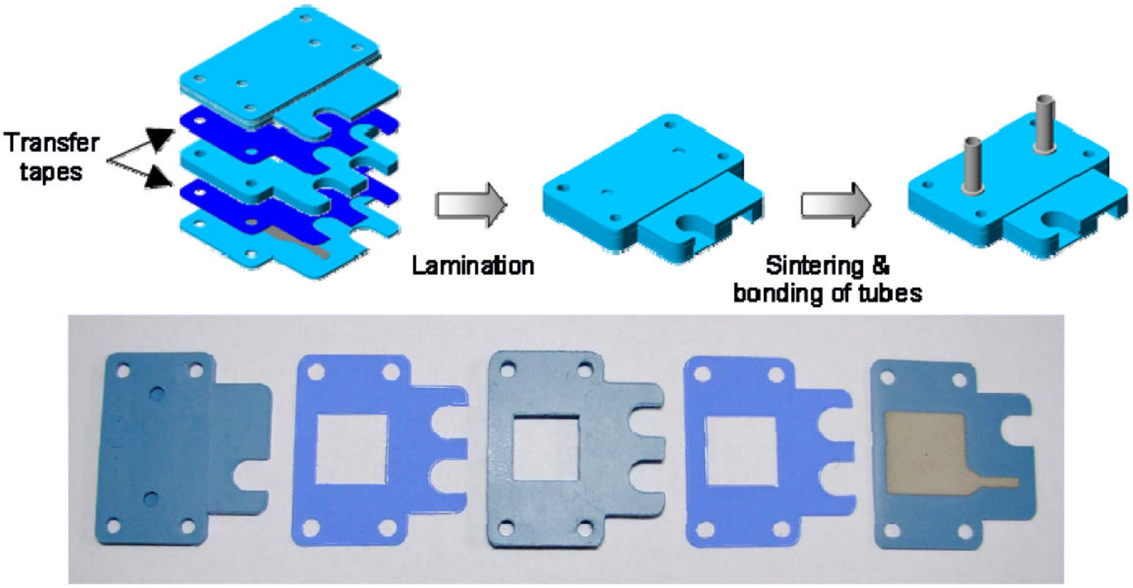

Fig. 6.5: Method of ceramic assembly with post-fire process using LTTT transfer tapes. Adapted from [199].

LTTT technology. Applications of mixed LTTT and LTCC ceramic tapes were developed for implementing structures with dielectric and magnetic materials to be used as integrated passive components displaying low-K and high-K layers for embedded capacitors and resistors. Figure 6.5 depicts the tapes used for the manufacturing of the device, and Figure 6.6 shows a comparison between two open cavity structuration methods: sacrificial carbon black tape vs. transfer tape.

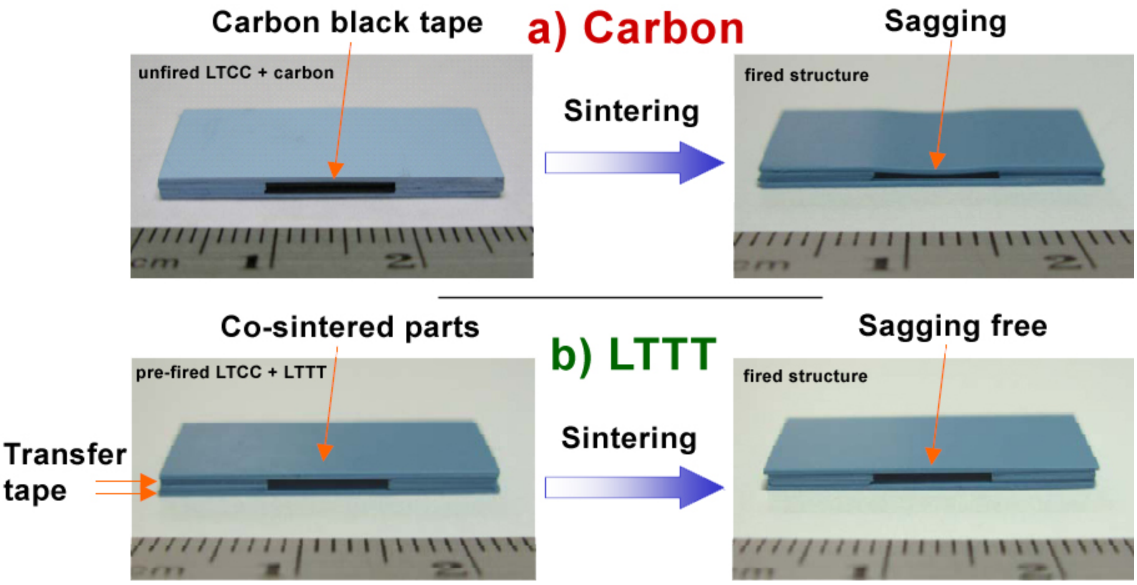

Fig. 6.6: Comparison between two open cavity structuration methods: sacrificial carbon black tape vs. transfer tape. **(a)** Co-fire method using carbon black tape as filler of open cavity: sagging occurs. **(b)** Co-fire & post-fire method using transfer tape: the resulting structure is sagging-free, thanks to the co-sintered partial initial parts. Adapted from a presentation given by M. R. Gongora Rubio at IMAPS CICMT 2008 [199].

Integration of ceramic materials Jaroslaw Kita et al., from University of Bayreuth, published in 2006 about an LTCC structure fitted with a buried glass window [211]; for this purpose they used HL2000 "zero-shrinkage" tapes and an additional glass-rich joining layer to compensate for the low glass content of the tape surface layer, and tested altogether three different types of ceramics: aluminium nitride (AlN), zirconia, and borosilicate glass. The process was successful for AlN and zirconia, but not for the borosilicate glass. Although it was possible to manufacture LTCC ceramics with a glass window, tests with the aim to cover LTCC ceramics with glass were not repeatable.

The idea was however not new: they cite two patents from Peterson et al. from Sandia National Labs dated in 2003 about a microelectronic device package with an integral window.

6.2.5 Firing techniques

Setter Powder Sheets (SPS) Coming back to the microplasma generator introduced in section 6.2.3, it is interesting to mention the firing process of the device. In [200], Yamamoto and Gongora Rubio write that the firing process parameters were standard, except that setter powder sheets (SPS) were used to ensure flatness of the electrodes structures, thus avoiding warping. This SPS, from TFT ([131] formerly Harmonics, Inc.), is a uniform particle size Al_2O_3 material with an organic binder contained in a paper thin sheet. The binder used in SPS is designed to burn out cleanly before the binders that are typically used in green tapes, leaving a uniform distribution of setter powder in place of the fired parts and thus preventing the formation of cracks and warping.

During the firing, the laminated green tapes are laid onto an alumina plate and covered with another porous alumina plate intercalating an SPS between the green tape and the alumina plate, as shown in the (c) of Figure 6.7. In comparison, most of the devices produced during this thesis were made with a bottom setter plate and no top cover plate (*a*); a few were fired with a top cover plate placed on the upper floor, not in contact with LTCC but making a "thermal cocoon" anyway.

Firing with or without top setter, as well as varying the setter was also tested by Sunappan [70]. He got better geometric results with top and bottom setters instead of only using the bottom one, and observed that the peak firing temperature of LTCC tape increased with increasing top setter load.

Observation of LTCC throughout the firing It would be very beneficial to observe the firing behavior of LTCC circuits throughout the burnout and sintering, in order to determine the origin of the deformations sometimes observed after firing. Corresponding prior studies on different systems [38, 81, 87, 212] show that considerable transient deformations can occur at various stages of the firing process.

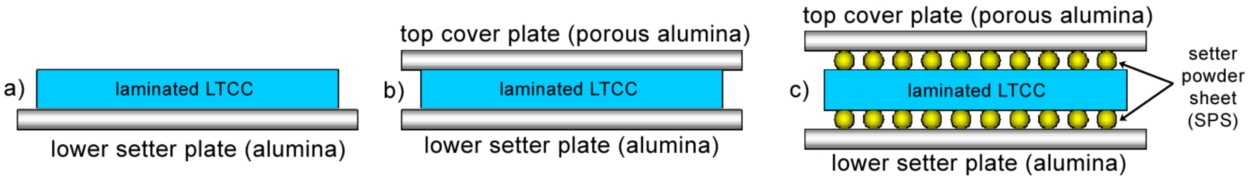

Fig. 6.7: Schematic side views of LTCC circuit firings with different variants of setter plates. (*a*) standard firing configuration; (*b*) firing configuration used by some teams; (*c*) setter powders deposited uniformly with SPS during green tape sintering resulting in a crack-free and flat structure. Adapted from [199, 200].

6.2.6 High-Volume Print Forming, HVPF

HVPF™ is a new method promoted by EoPlex Technologies (Redwood City, California, USA [213]) for manufacturing large volumes of complex metal-ceramic and hybrid components [214, 215], such as those depicted on Figure 6.8. However, the technology itself is not described in detail; it is only mentioned that it is based on “different print technologies” to effect successive deposition of different materials to build multilayer structures and create complex 3D shapes. It is claimed to be a high-volume manufacturing method for the production of low-cost components.

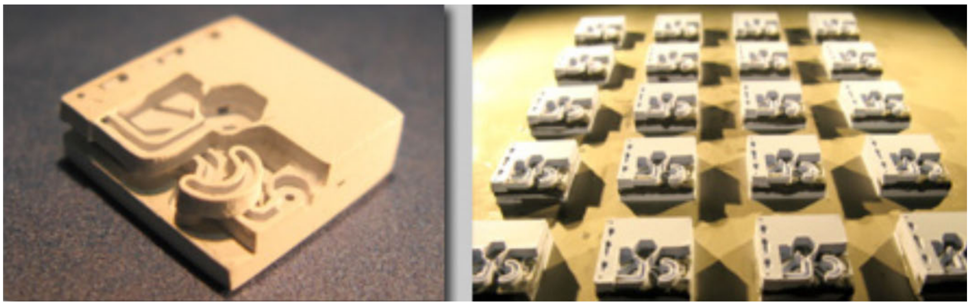

Fig. 6.8: Example of mass production of ceramic components with the HVPF process of EoPlex Technologies [213].

Appendix A

Firing profiles

A.1 LTCC firing

Here are different temperature profiles used with the ATV lamp air furnace [58] to fire LTCC circuits (see subsection 2.2.7):

A.1.1 Design of Experiments

Table A.1 lists the steps of the firing process used in the DoE experiments of section 3.2, the study of "Influence of lamination parameters on firing shrinkage". Figure A.1 shows the temperature profile used for the firings of LTCC experiments with mineral sacrificial pastes (see section 4.4). Please refer to subsection 2.2.7 for a description of the important aspects.

Table A.1: LTCC firing oven profile in air at 400 l/h for the DoE experiments.

	Step (actual temperatures)	Duration [h:min]	Total time [h:min]	Oven temp. [°C]	Slope [K/min]
1	Fast ramp	00:25	00:25	230	8
2	Ramp to 440 °C	01:30	01:55	450	2.4
3	Burnout dwell 100 min	01:39	03:34	450	0
4	Fast ramp	00:21	03:55	660	10
5	Sintering ramp to 875 °C	01:35	05:30	895	2.5
6	Sintering dwell 30 min	00:30	06:00	895	0
7	Natural furnace cooling	00:30	06:30	400	-16.5
8	Fast cooling	00:10	06:40	200	-20
9	Back to ambient	00:10	06:50	70	-13

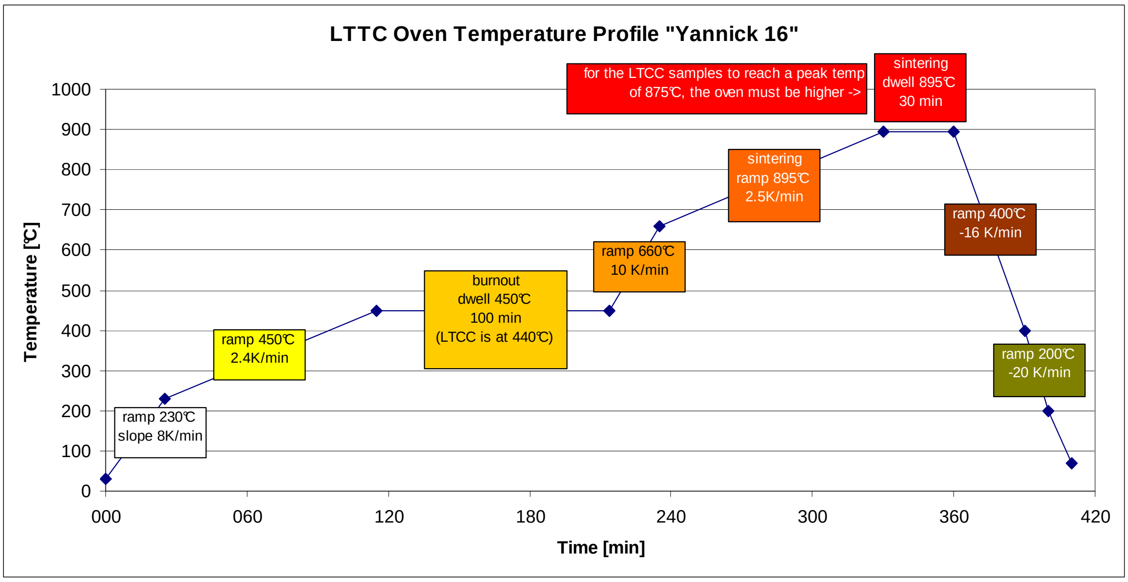

Fig. A.1: Temperature profile used for firings of LTCC during or DoE experiments on shrinkage. It features an organic burnout dwell of 100 min at 450 °C, and a sintering ramp of 2.5 K/min up to 895 °C (875 °C in reality) followed by a dwell of 30 min.

A.1.2 Multisensor

Figure A.2 shows the temperature profile used for firing our LTCC multisensor (see section 5.3).

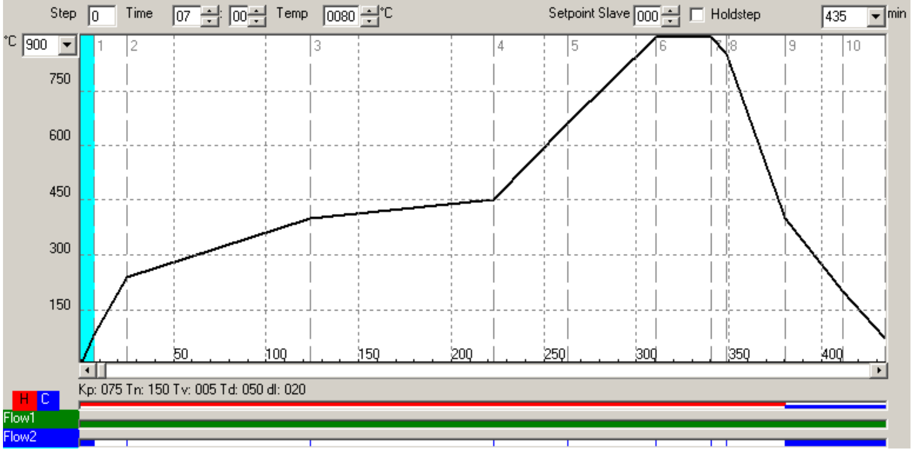
Step 0 Time 07 : 00 Temp 0080 °C Setpoint Slave 000 ☐ Holdstep 435 min

°C 900

Kp: 075 Tn: 150 Tv: 005 Td: 050 dI: 020

Fig. A.2: Temperature profile used for firing the LTCC integrated sensor. It features a medium organic burnout ramp (from 330 to 450 °C in 140 min), and a sintering ramp of 5 K/min up to 896 °C (to get a temperature of 875 °C at core) followed by a dwell of 30 min.

A.2 Soldering

Figure A.3 shows a typical temperature profile used with the ATV SRO702 [58] soldering oven (see section 2.2.8 on page 43).

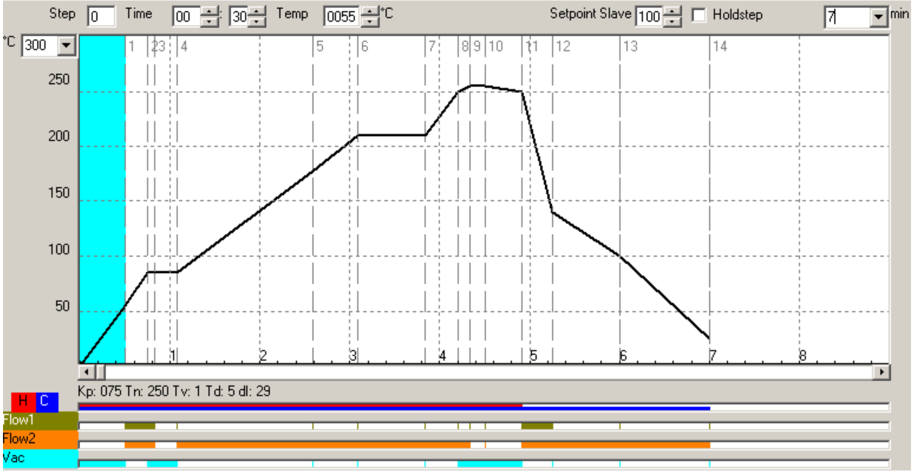

Step 0 Time 00 : 30 Temp 0055 °C Setpoint Slave 100 ☐ Holdstep 7 min

°C 300

Kp: 075 Tn: 250 Tv: 1 Td: 5 dl: 29

Fig. A.3: Temperature profile used for soldering the LTCC pressure sensor prototype. It features an atmosphere purge, a ramp up to just below the solder melting point (~220 °C) followed by a dwell to allow temperature uniformity. An short excursion (1 min) in the molten phase is performed up to 255 °C, along with a vacuum purge of 30 s to allow bubble degassing.

Appendix B

MSP and capacitive force sensors

B.1 State of the art

In section 4.2.2 on page 106 we discuss on the dissolution of LTCC substrates by etchants. Here is more information on the composition of LTCC tapes with TEM imagery.

A TEM-micrograph of commercial LTCC made by BLENDELL is proposed on Figure B.1. It is not mentionned if the method allows seeing light elements such as boron.

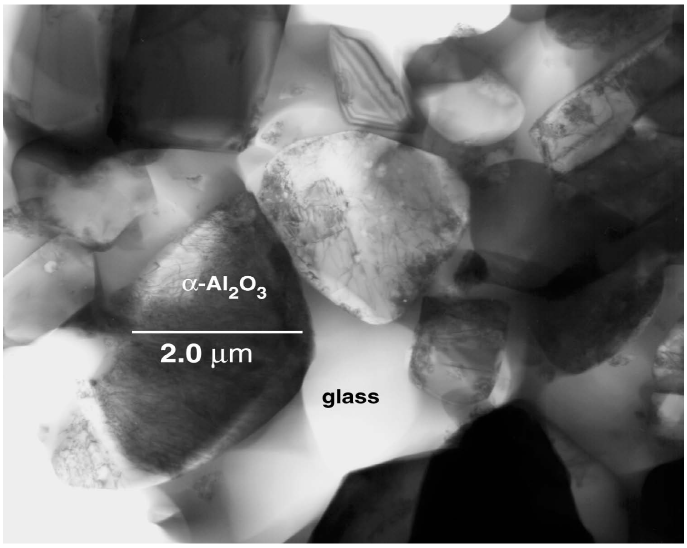

Fig. B.1: TEM micrograph of LTCC production device consisting of alpha-Al_2O_3 particles with sizes ranging up to 5 µm contained within a continuous glass phase. For this particular device, the glass phase was found to be a calcium-aluminum-silicate, containing various concentrations of Pb, Ti, Na and K. Source: [216].

Here are illustrations of the study by Bittner et al. on the dissolution of LTCC tape DP951 in H_3PO_4 [19]: Figure B.2 and Figure B.3.

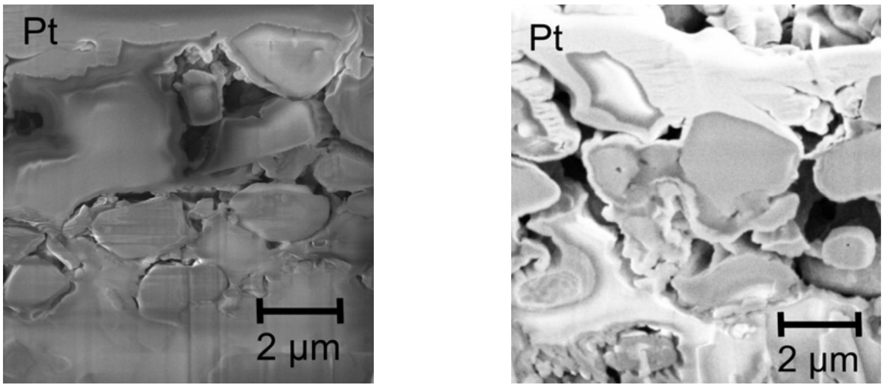

(a) Etching temperature: 90 °C **(b)** Etching temperature: 110 °C

Fig. B.2: TEM cross-sectional views on the microstructure of LTCC DP951 close to the surface after chemical etching for 8 h in H_3PO_4 at different temperatures [19].

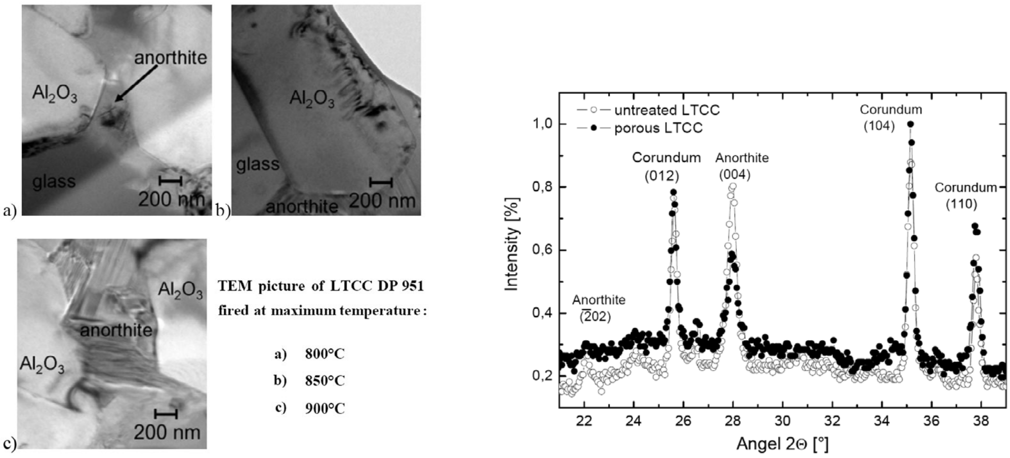

(a) TEM pictures of LTCC DP 951 fired at various maximum temperatures. **(b)** μ-XRD (X-ray diffraction) spectra of "as fired" and porous LTCC.

Fig. B.3: Two figures of the analyses on dissolved LTCC made by Bittner et al. [19].

B.2 Equipment

The equipement used for the preparation of the mineral sacrificial pastes of subsection 4.3.5 is shown on Figure B.4.

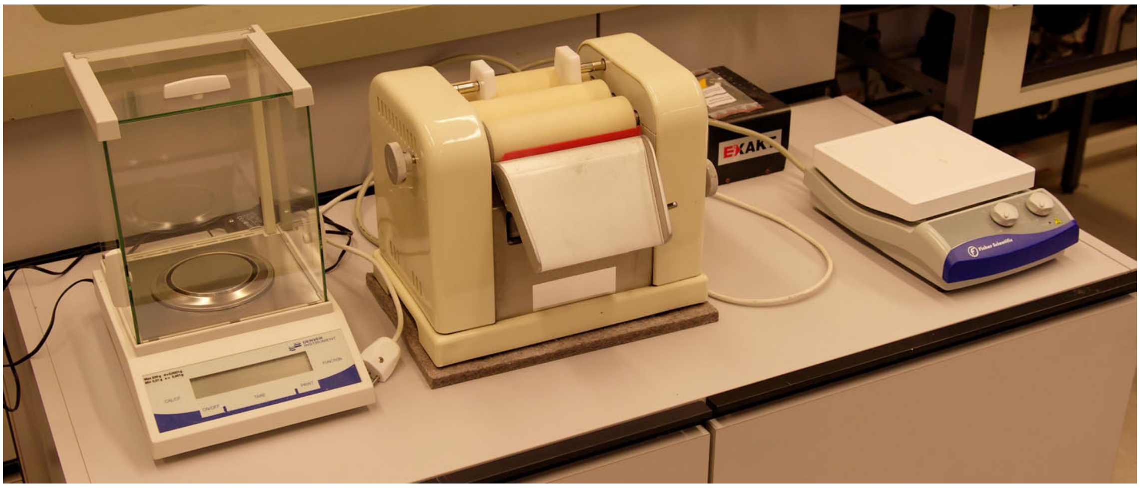

Fig. B.4: Equipment used to prepare the sacrificial pastes. From left to right: balance of precision (Denver Instruments), tricylinder (EXAKT), magnetic stirrer (Fischer Scientific). Not visible on the far right: mortar grinder.

B.3 Force sensors: from piezoresistive to capacitive

This section explains the transition of force sensors from piezoresistive to capacitve principle of measurement for low forces, as stated in subsection 4.3.1.

Force sensors: the classical piezoresistive approach

The MilliNewton, depicted on Figure B.5, is a robust force sensor working on the piezoresistive strain principle developed at the EPFL-LPM laboratory [6]. The range of forces for such "classical" sensors has been described in detail by Maeder et al. in [217]. Their results show that *a single sensor geometry cannot cover such a wide range of forces in an optimal way. For small forces (100 mN to ca. 2 N), simple cantilever force sensors are an excellent solution, achieving reasonable precision with a very simple design and compatibility with an SMD assembly process with solder or conductive glue. Characterization of solder joint strength shows that such joints can reliably withstand the bending moments resulting form the loading of the cantilever sensor up to ca. 2 N. Above this force, both solder joint and cantilever strength become critical in the cantilever design. Therefore, a 3-point or 4-point bending beam geometry must be selected, thereby extending the force range to ca. 100 N.*

An example of application can be found in a robotic interface to train hand and finger function developed by Dovat et al. [218], called HandCARE (Hand Cable-Actuated REhabilitation system), in which each finger is attached to an instrumented cable loop allowing force control

and a predominantly linear displacement. The device, whose design is based on biomechanical measurements, can assist the subject in opening and closing movements and can be adapted to accommodate various hand shapes and finger sizes.
Another example of application is the control of tensile strength in cloth threading machines. It is carried out by a hybrid thick-film sensor similar to the MilliNewton developed by Suphan et al. [219].

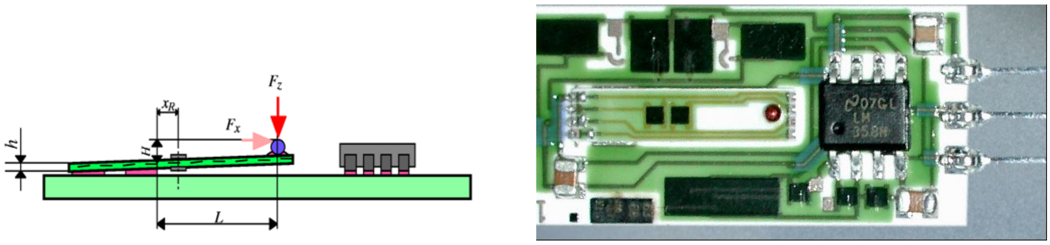

(a) Schematic side view. **(b)** Top-view picture.

Fig. B.5: Illustrations of the MilliNewton piezoresistive cantilever force sensor, produced at EPFL-LPM [6] (force range 20...2000 mN). The dimensions of the base are 25.4×12.7 mm, those of the cantilever are 15.6×3 mm and the force is applied onto the ball at the end of the cantilever.

Reasons of transition from piezoresistive to capacitive measurement principle

In almost all cases, the standard 96 % alumina used as a substrate material for thick-film electronics is also used for the sensor elastic element, in spite of its moderate strength and high elastic modulus [220].
For (very) low range force sensing (under 100 mN) however, classical alumina substrates have other drawbacks, as described by Birol in [221, 222]:

- Scoring and breaking (the standard thick-film individualization procedure) is not practical at very small dimensions, while laser cutting severely degrades the mechanical properties [223]. Moreover, very thin alumina substrates are very fragile and therefore difficult to handle (in the normal thick-film process), or not available at all. Practically speaking, the minimum reasonable thickness (to avoid excessive breakage during processing) for the alumina beam of the MilliNewton is ca. 250 µm, corresponding to a sensor with 400 mN nominal range.
- While solder assembly is reasonably reliable [224], it creates parasitic stresses [225]. Placement of the sensing resistors is therefore a compromise between maximizing signal (placement near the solder joint) and minimizing parasitic stresses (placement away from the joint). This effect is worsened by the impossibility to structure the alumina beam; to the contrary, LTCC allows narrowing the beam where the strain resistors lie, whilst keeping a large solder pad on a rigid plot. This helps retrieving some signal / sensistivity that is lost with decreasing nominal load - see next point.
- The nominal displacement increases with decreasing nominal load – the beam becomes too compliant, i.e. the sensitivity decreases too. For a constant displacement at full

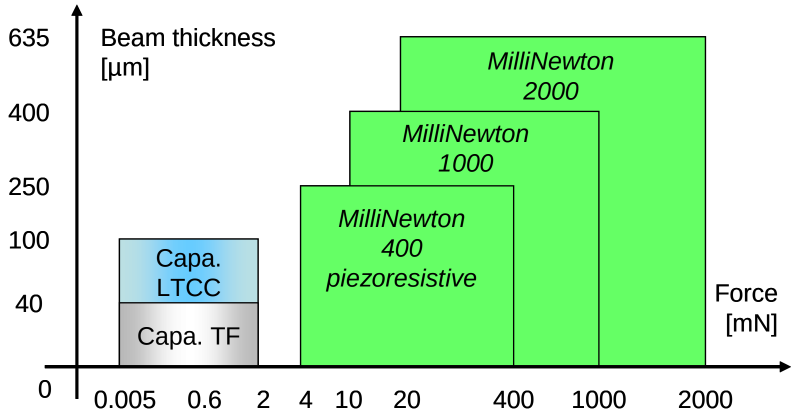

Fig. B.6: Schematic representation of the beam thickness vs. force ranges covered by various force sensor technologies (scales are not linear). "Capa. LTCC" stands for the LTCC capacitive sensor of subsection 5.4.2 and "Capa. TF" for the thick-film microforce sensor of subsection 5.4.1.

scale and for a beam thickness h the evolution of physical quantities evolves as follows (schematized on Figure B.6):

- The maximum curvature evolves in $1/h$, thus the curvature radius as $h/1$;
- The stress evolves in $1/h^2$;
- The capacitive sensitivity evolves in $1/h^3$.

Thus, two directions were taken in our laboratory to improve the initial piezoresistive sensor:

1) Substituting alumina by LTCC for the cantilever;
2) Abandoning the piezoresistive principle for a capacitive method.

The first direction was first explored by Hansu Birol and Marc Boers. As written in [49], their study is aimed at outlining the fabrication of a novel piezoresistive force sensor using LTCC technology, which operates at millinewton range, yet is compatible with low-cost thick-film fabrication process. Mechanical and electrical characterization of the device is explained in terms of processing conditions, including the principle of force sensing and materials employed. The reduction of warpage during firing by modifying commercially-available thick-film conductors is described, and the sensors are found to be efficient in responding to forces below 100 mN.

The study was completed by my colleague Nicolas Craquelin in 2009 by optimizing the cantilever layout and conducting finite-element simulations. His results, published in [226], prove that switching from a classical Al_2O_3-based thick-film beam (Figure B.5) to LTCC (Figure B.7d) allows using the design of a 3D structured beam (Figures B.7a, B.7b and B.7c) with increased sensitivity of the piezoresistive bridge, yet with largely conserved strength and stiffness. Another advantage of LTCC compared with alumina is a lower Young's modulus (approximately 3 times lower), more suitable for the measurement of small loads. Three thicknesses of the DuPont 951 GreenTape system were selected: 114, 165 and 254 µm (unfired); 51 µm tape was abandoned, as it tended to warp excessively during co-firing with

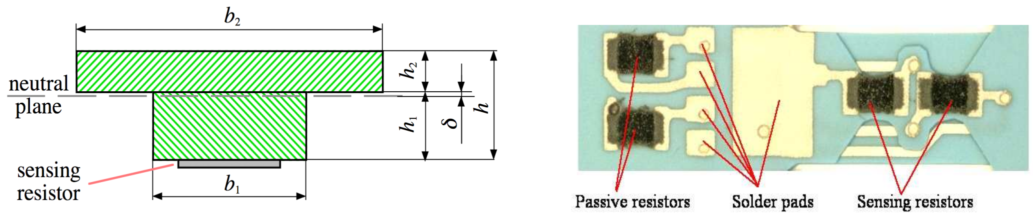

(a) Cross section of a bilayer LTCC cantilever (layer under tensile stress).

(b) Structured LTCC cantilever (b_1=1 mm, b_2=3 mm) shown screen printed on bottom side.

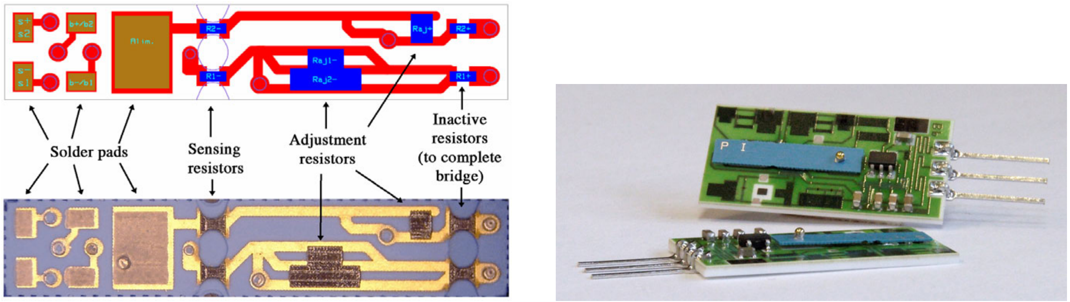

(c) Schematic layout and photograph of the bottom active face of the parallel variant of (d), where both sensing resistors lie side by side.

(d) Completed new low-range sensors using an LTCC beam (in blue). The sensing structured face is not apparent as it faces the base, but can be seen on (c).

Fig. B.7: Improvement of the MilliNewton force sensor by substituting its alumina cantilever with an LTCC version (force range 1. . . 100 mN). The base dimensions are 25.4×12.7 mm and the force is applied onto the ball at the end of the cantilever (15.6×3 mm). Pictures from [49] and [226].

conductors.

For the second direction, please go back to subsection 4.3.1.

B.4 Active measurement with electrostatic forces

This section explains the theory of the active compensation of capacitive sensors; please refer to section 4.3.2 for the schematic of the forces.

F_e is the optional electrostatic force used in the case of active measurement. An extra pair of electrodes can be used (or the existing pair if the measuring and acting signals are mixed) to attract the cantilever to the base. The electrostatic force is stated as:

$$F_e = \frac{1}{2} \cdot \varepsilon_0 \cdot \varepsilon_r \cdot A \cdot \left(\frac{U}{r}\right)^2 \tag{B.1}$$

The active electrostatic compensation principle lies in attracting the cantilever to an intermediate setpoint position $r_s < r_0$; any external applied force will modify the equilibrium, and the electrostatic voltage has to be decreased by the closed-loop feedback in order to maintain the reference position constant. Therefore, the elastic return force does not change, and we can write:

$$\Delta F_e = F_a \tag{B.2}$$

Thus, defining U_s as the voltage required to attract the unloaded cantilever to the setpoint r_s, we can rewrite Equation B.1:

$$F_a = \frac{1}{2} \cdot \varepsilon_0 \cdot \varepsilon_r \cdot A \cdot \left[\left(\frac{U_s + \Delta U}{r_s} \right)^2 - \left(\frac{U}{r_s} \right)^2 \right] = \frac{\varepsilon_0 \cdot \varepsilon_r \cdot A}{2 r_s^2} \cdot \left(2U_s \cdot \Delta U + \Delta U^2 \right) \tag{B.3}$$

If U_s is sufficiently high ($U_s \gg \Delta U$, superposition of a large bias voltage and a small variation), we can neglect the ΔU^2 term, yielding an essentially linear response of ΔU to the applied force:

$$\Delta U \cong \frac{r_s^2}{\varepsilon_0 \cdot \varepsilon_r \cdot A \cdot U_s} \cdot F_a \tag{B.4}$$

The Figure B.8 schematizes the applied force vs. electrostatic voltage graphic. However, one has to be careful with the voltage regulation, lest the system become instable when the electrodes are close to each other.

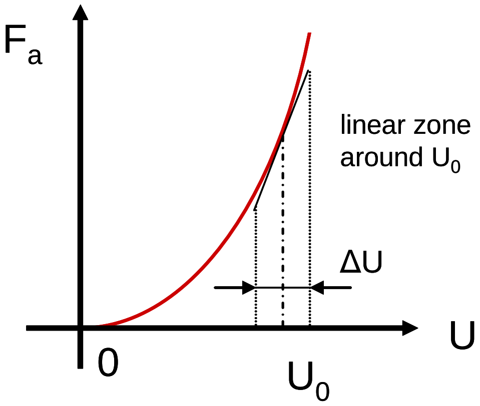

Fig. B.8: Graph of applied force vs. electrostatic voltage.

B.5 Microforce sensors on alumina

B.5.1 Sensor designs and geometries variants

The geometry designs of the microforce sensors of subsection 4.3.3 on page 111 are presented in Table B.1 and Figure B.9, and the variants in Table B.2 and in Figure B.10.

Table B.1: Comparison between the simple and bridge cantilever geometric designs (adapted from [114]).

Interesting properties for a force sensor	**Simple cantilever**	**Bridge cantilever**
Sensitivity to small forces	+	-
Insensitivity to the location of force application	-	+
Robustness	-	+
Risk of deformation upon firing due to differences in thermal dilatation	-	+
Usage of substrate surface (the lower the better)	+	-
Surface in contact with the etchant to dissolve the SVM	+	-

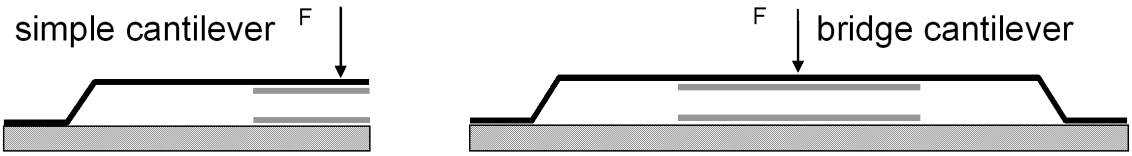

(a) Cross sections.

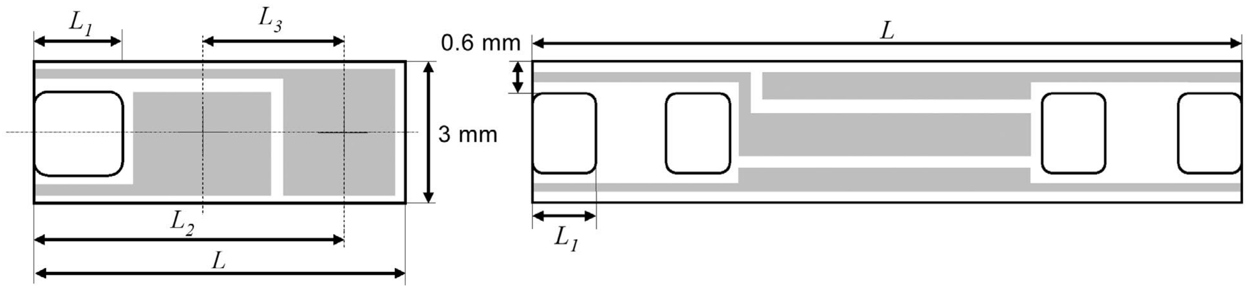

(b) Top view with dimensions, location of electrodes (gray) and of inner cuts (rounded rectangles).

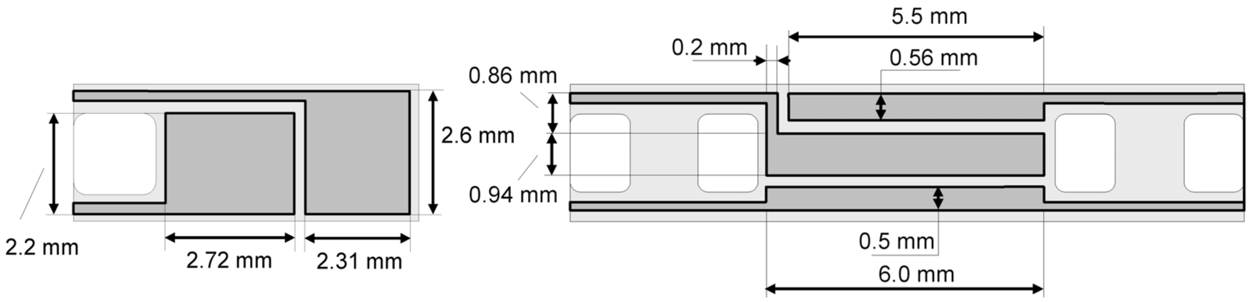

(c) Dimensions of electrodes.

Fig. B.9: Schematics of the designs of the capacitive sensors produced. For each view, *Left:* Simple cantilever design. *Right:* Bridge cantilever design.

Table B.2: The six retained geometry variants and their varying parameters.

Variant name	Cut length L_1 [mm]	Overall length L [mm]	Cantilever type	Holes in cantilever?	Top view shape of cantilever structure
S08T	1.9	7.8	simple	yes	
S10T	3.9	9.8	simple	yes	
S12T	5.9	11.8	simple	yes	
S12P	-	11.8	simple	no	
PT	1.4	14.8	bridge	yes	
PP	-	14.8	bridge	no	

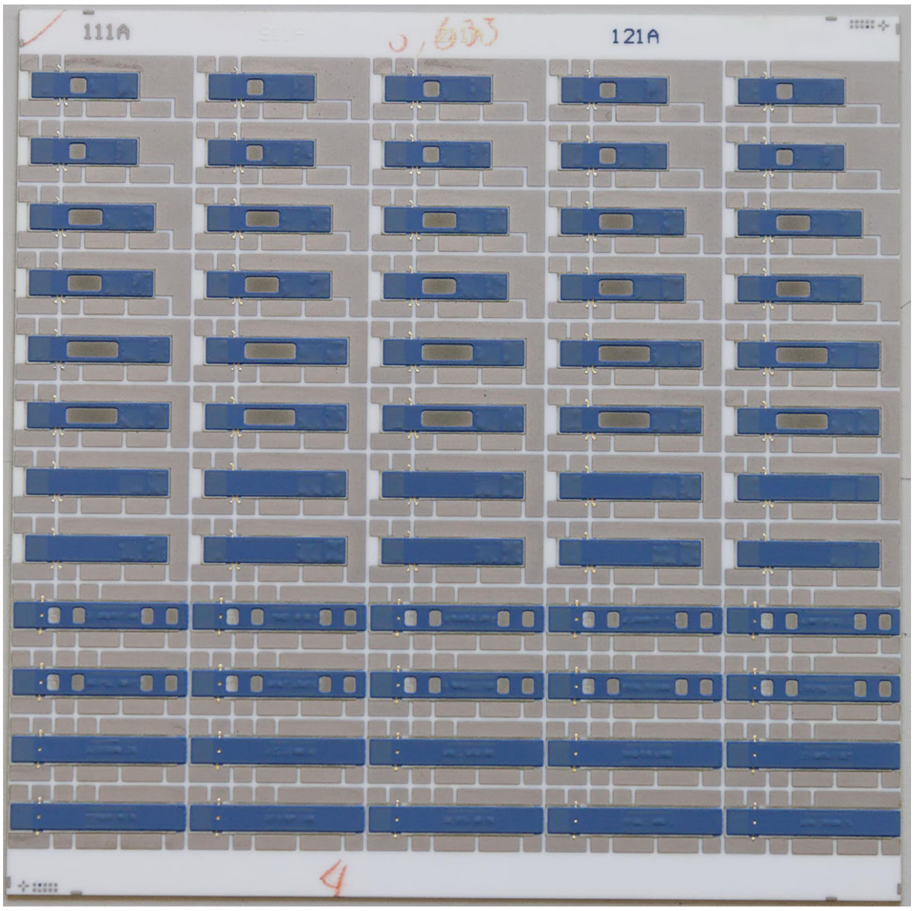

Fig. B.10: 4"×4" alumina substrate with ten samples for each six retained geometry variants; the upper six rows are simple cantilevers and the bottom six are bridge cantilevers. Dielectric is blue and silver-palladium grey.

B.5.2 Curling effect of suspended thick-film bridge

In subsection 4.3.3 (about the sensor designs and geometries of capacitive force sensors in alumina), we discuss on the rigidity of the beam that must not be too high to avoid losing sensistivity. Here is the report of the observation of an usual case. In 2004, Dr. Hansu Birol observed [110] an interesting curling side effect while creating a suspended thick-film bridge with a PTC resistor on LTCC (see Figure B.11). This side effect can be either beneficial (when a rigid structure is desired) or, as in our microforce capacitive sensor case, a drawback. Here is next how the structure was created and some remarks:

- The bridge is constructed using the following materials and order (all screen printed in green state): LTCC DP951, experimental carbon paste as SVM, dielectric paste, resistor paste (ESL 2612, PTC).
- The formation mechanism is a coupling of swelling and shrinkage of resistor paste. Swelling is believed to be the dominant one.
- The structure is mechanically very stable. One can touch on the bridge easily applying a reasonably high pressure.
- The bridge is curled from both sides, which prevents an effective measurement of thickness. This problem arises from shrinkage that is maximized in this (shorter) direction with respect to the longer direction.

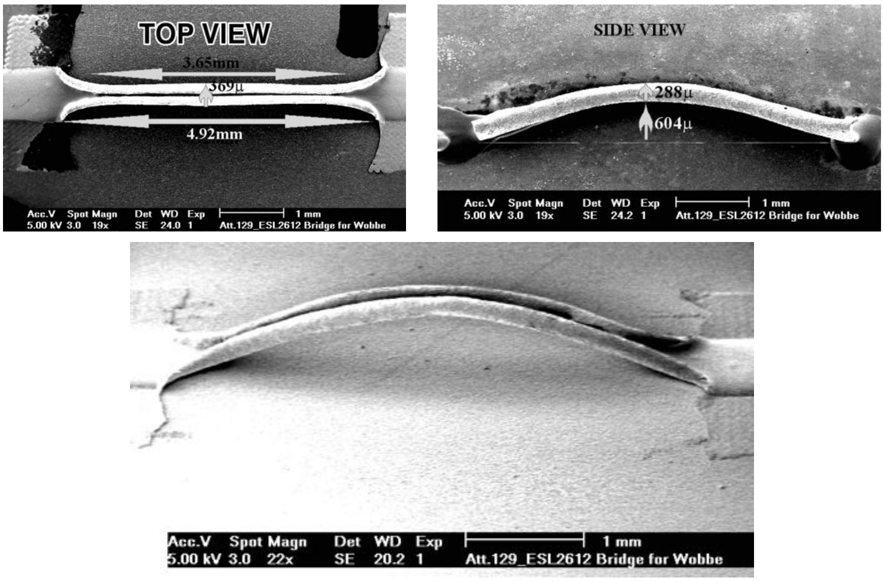

Fig. B.11: Lateral contraction and curling during firing of a thick-film PTC resistor bridge on carbon sacrificial paste fabricated on LTCC substrate (height from the surface $\sim$600 µm) [110].

B.5.3 Early tests of MSP on alumina substrates

Table B.3 lists the behavior of sacrificial pastes tested on alumina substrates discussed in section 4.3.5:

Table B.3: Behavior of sacrificial pastes tested on alumina substrates.

% of borax in CaO	Color	Aspect	Porosity	Hygroscopy	Tenue	Chemical reactions	Suitable?	Picture
< 40 %	very white	very powdery	porous	strongly	unbundled	?	no	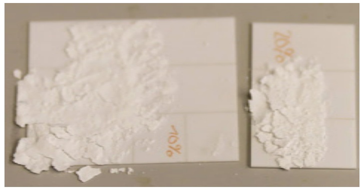
40 %	white	slightly powdery	?	yes, decomposed after 1 week	well bundled	?	yes if pro-cessed fast	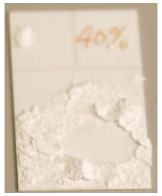
50 %	white	not powdery	slightly porous	no	not easily scratchable with nails	bubbles with resistor paste DP 2031	yes	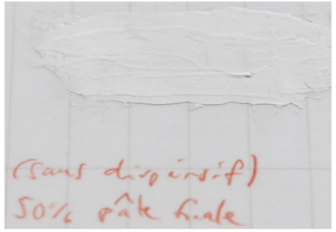
50 % with dispersant	white yellowish	slightly powdery	slightly porous	?	easily removable	?	no	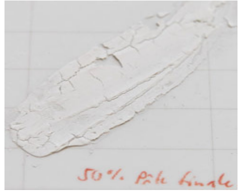
60 %	less white	not powdery	vitreous	no	scratchable with hard tool	bubbles with dielectric pastes	no	
≥ 70 %	transparent	not powdery	vitreous	no	nearly impossible to strip away	strong with dielectrics	no	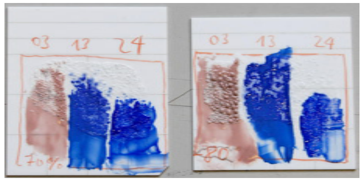

B.6 Mineral sacrificial paste on LTCC

The following figures illustrate the results of early tests of MSP on LTCC of section 4.4.3: Figure B.12, Figure B.13, Figure B.14 and Figure B.15.

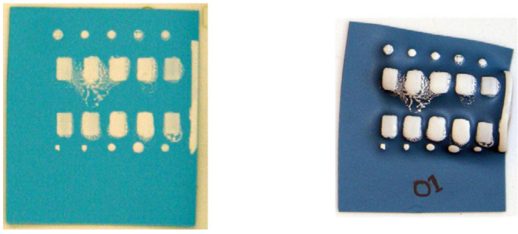

Fig. B.12: Test pattern of paste O1 (60 % CaO, 40 % H_3BO_3) printed on LTCC. *Left:* Green state; *Right:* Fired state; the strong deformations are clearly visible.

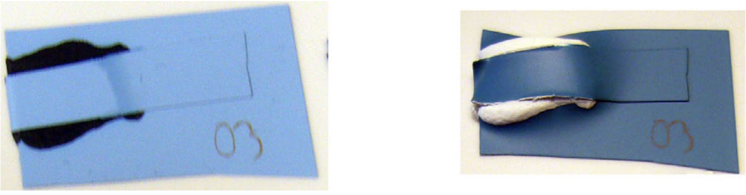

Fig. B.13: Sandwich-cantilever test made with paste O3 (50 % CaO, 20 % C, 30 % H_3BO_3) deposited on LTCC. *Left:* Green state; *Right:* Fired state; the cantilever is too much distorted.

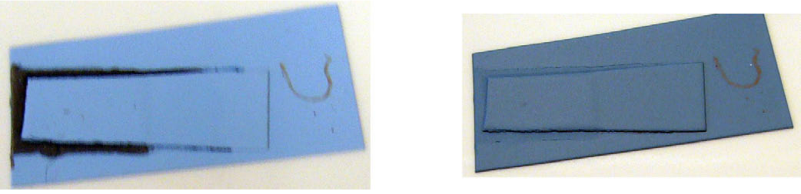

Fig. B.14: Sandwich-cantilever test made with paste O8 (100 % C) deposited on LTCC. *Left:* Green state; *Right:* Fired state; the LTCC is not deformed but there is nearly no gap due to sagging.

Fig. B.15: Fired LTCC sample of sandwich-cantilever made with paste T9 (28 % $CaCO_3$, 72 % C). There are nearly no base deformations and the cantilever shape is almost perfect. *Left:* Before paste removal (top view); *Right:* After mineral paste removal/dissolution (side view)..

Appendix C

Multisensor: precursor prototypes

The multifunction integrated sensor's development was split between two initial prototypes: a pressure sensor and a flow sensor, while the temperature would be extracted from the same thermistors used for the flow sensor. We summarize here each of these sub-projects for illustration purposes; please refer to our publication at IMAPS 2009 Rimini [182] for details.

C.1 Pressure sensor

The project of the SMD pressure sensor was carried out by Aurélie Barras in 2008 during her semester project [227]. The goal was to build and test functional prototypes demonstrating the compatibility with surface mount technology, the piezoresistive measurement principle coupled to an LTCC membrane, and the signal conditioning electronics. The intended range of pressure is 6 bar, with a safety margin at 10 bar. The supply voltage was fixed at 5 V, and the output signal should be ratiometric between 0.5 and 4.5 V.

Figure C.1 shows the manufactured sensor soldered on a fluidic test PCB (see Figure C.2), as well as a schematic cross-section highlighting the pressure path in zigzag.

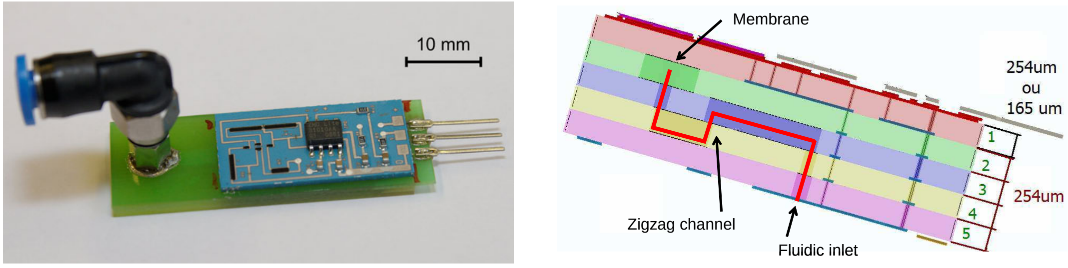

(a) Pressure sensor mounted on test fluidic PCB, with M3 inlet and 2.54 mm connector, showing its compatibility with surface mount technology.

(b) Schematic cross-section of LTCC layers and path of air pressure between fluidic inlet and membrane: zigzag channel for decoupling mounting-induced stresses.

Fig. C.1: SMD pressure sensor in LTCC.

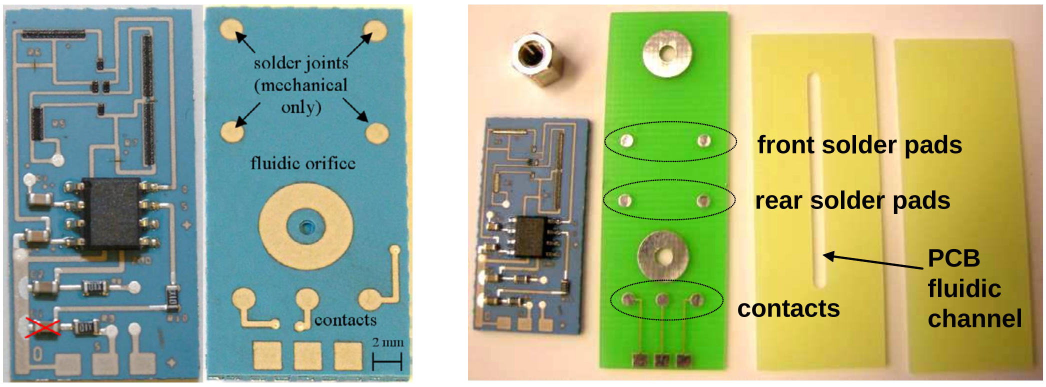

(a) **(b)**

Fig. C.2: LTCC pressure sensor at various stage of manufacturing. *(a)* Device ready to be mounted, after trimming and initial soldering. *Left:* top view; note the signal conditioner in the center (ZMD31010), the four resistors forming the full bridge at the top, and the tracks laser cut for offset trimming. The capacitor marked red must be strongly limited. *Right:* bottom view; note inlet and contact solder pads, as well as mechanical joints. *(b)* Top view of the sensor and of the not-yet assembled test PCB, made of three epoxy layers with contacts and diverse solder pads.

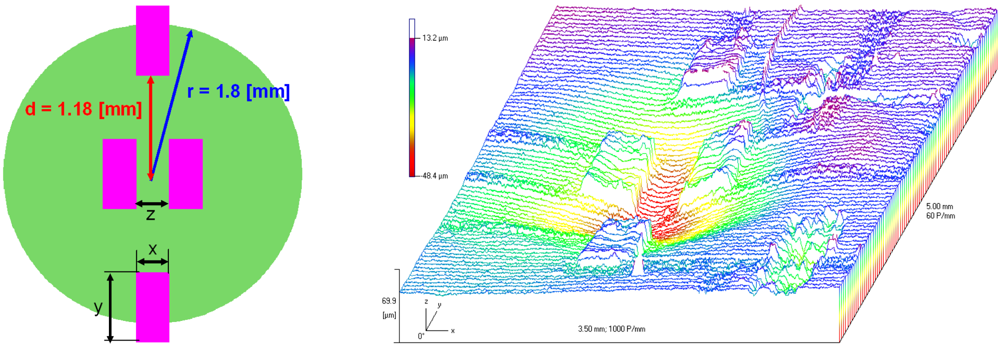

(a) **(b)**

Fig. C.3: Membrane and piezoresistors of pressure sensor. *(a)* Schematic placement of piezoresistors (pink) on the 3.6 mm-diameter LTCC membrane (green). *(b)* 3D profile of fired LTCC pressure membrane showing (exaggerately) a sagging of ~30 µm (UBM optical profilometer).

Mechanical layout To decouple the pressure membrane from the mounting-induced stresses, several solder joints were screen printed on the bottom face of the sensor along with electrical contacts (Figure C.2). Not all mechanical solder pads were subsequently used during soldering, in order to assess the influence of attachment location on the measurements.

The pressure membrane had a diameter of 3.6 mm; the location of piezoresistors is depicted on Figure C.3, as well as the optical profile of a fired membrane, showing a sagging of ~30 µm without notable influence on sensor performance.

Electrical layout The ZMD31010 [183] signal conditioning chip was chosen with the help of an earlier semester project by Olivier Thommen [228]. The schematic of the piezoresistor

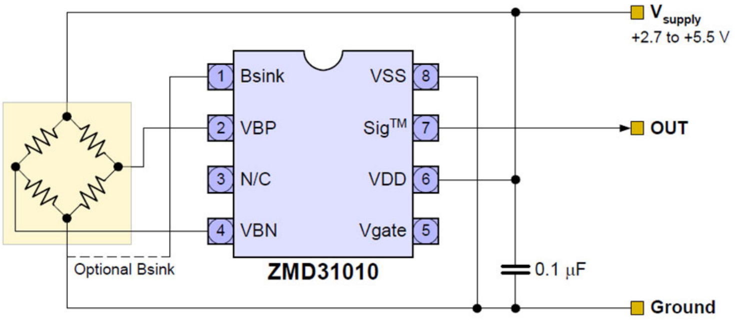

(a) Application circuit diagram of ZMD31010 signal conditioning chip.

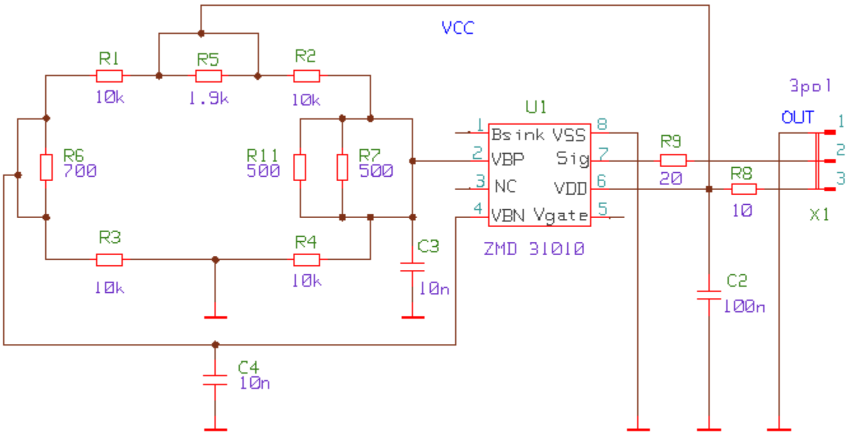

(b) Electrical circuit of sensor. R_7 and R_{11} form a single 250 Ω resistor, but were physically separated for layout reasons.

Fig. C.4: Electrical schematics – pressure sensor prototype.

coupled in Wheatstone bridge to the ZMD, as well as the whole sensor electrical schematic is displayed on Figure C.4.

Destructive tests A proof of the good lamination lies in the overpressure tests. Early prototypes were made shortly prior to this project. They were designed with a DP951-254 µm membrane and nominally designed for working at 6 bar with a safety margin up to 10 bar. In spite of this security, we could not make them fail at 24 bar (the maximum applicable on our pressure system). Those made with a DP951-165 µm membrane had a lower safety margin but failed between 12 and 14 bar (see Figure C.5), which is still above the calculated limit, hence very satisfying.

Results of pressure measurements Figure C.6 is the graph of pressure sensor measurements, i.e. the ZMD output voltage vs. the input pressure. The behaviour is perfectly linear; hence, we reused exactly the same design for our multisensor.

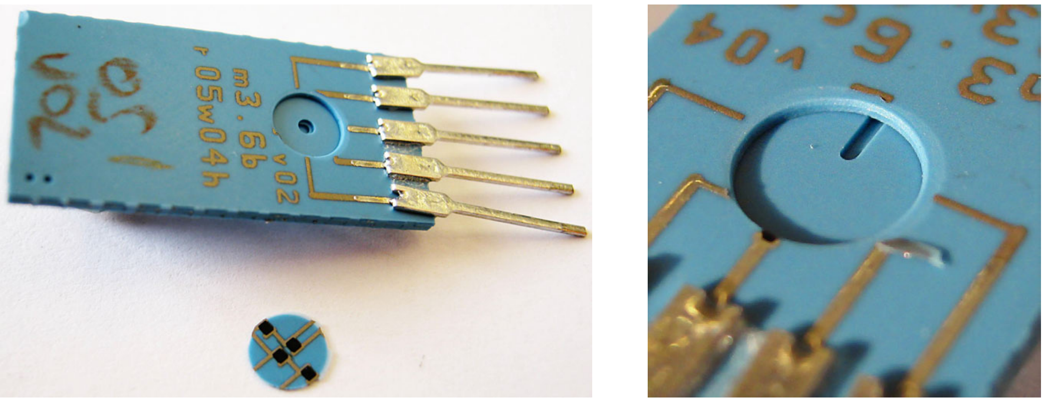

(a) A destructed sensor with its popped-up membrane laid beside.

(b) Close-up on another sensor with a simpler channel geometry.

Fig. C.5: Destructive overpressure tests carried out on early sensor prototypes made with an LTCC membrane of 3.6 mm diameter in DP951-165 µm: the sensor failed between 12 and 14 bar, which is very good, for their nominal pressure is 6 bar with a safety margin at 10 bar. Note how the breaks are clean; it proves that the maximal stress in the membrane is located at the edges and that it was homogeneous.

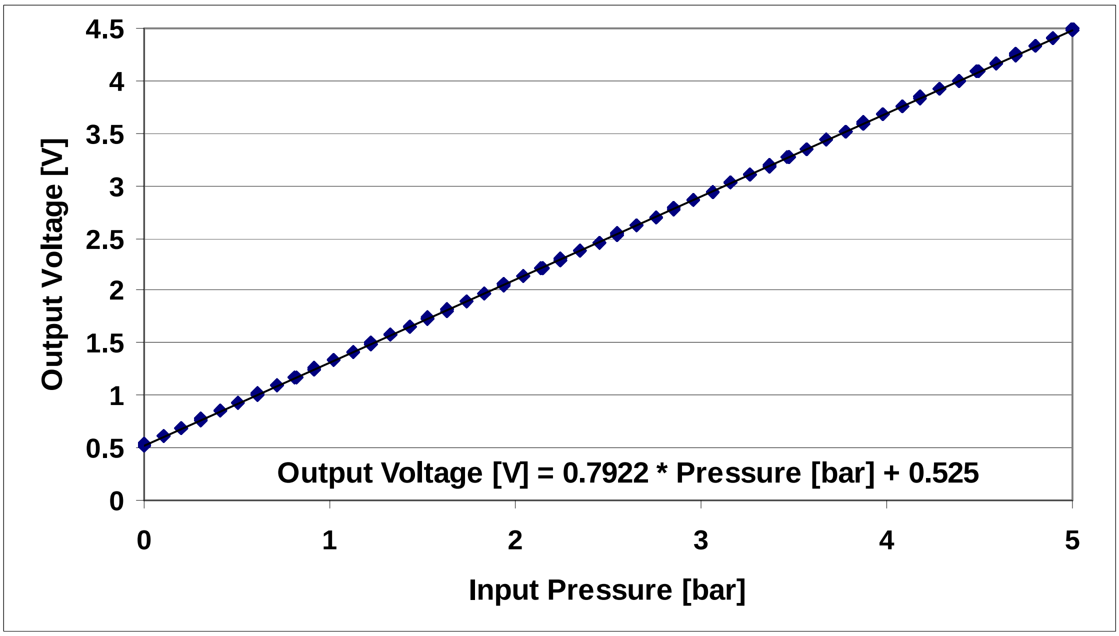

Fig. C.6: Graph of pressure ratiometric output voltage in function of input pressure for three ramps of pattern 0-5-0 bar each. The trend line is perfectly linear, without visible noise.

C.2 Flow sensor

The project of the SMD air flow sensor demonstrator was carried out by Grégoire Boutinard Rouelle in 2009 during his semester project [229]. The goal of his project was to build a functional demonstrator to determine the best measurement principle for low-cost diagnostics applications: calorimetric or anemometric, as well as the optimal channel geometry. The device must also be compatible with surface mount technology, but without the signal conditioning electronics (to the contrary of the previous project). The range of flow should from 0 to 100 NL/min (normalized liters per minute).

Mechanical arrangements The sensor structure is based on the the flow sensors presented in the state of the art of subsection 5.2.1, and is very similar to the multisensor later produced. It comprises five LTCC layers laser, two of them being laser cut to create channels. The central tape is supporting the bridges with thermoresistors: different bridge variants were produced. Figure C.7 show the schematics of one of these variants.
The two measuring principles could be studied at the same time with the adopted resistors configuration: the anemometric is function of heater power, and the calorimetric is function of the output voltage difference of the four sensing thermistors, which are placed upstream and downstream of the central heating resistor. The sensing resistors are electrically wired in Wheatstone half-bridges on the external test bench.

Manufacturing Indeed, two different structures were produced in batch on the same LTCC sheet (Figure C.8): the flow sensor, and suspended capacitive structures. This was because another research that was conducted in parallel: the testing of our latest mineral sacrificial paste (MSP) for different LTCC tapes (DP951, HL2000 and HL800, see subsection 4.6.2). Therefore, most of the pictures of the flow sensor manufacturing were already shown throughout

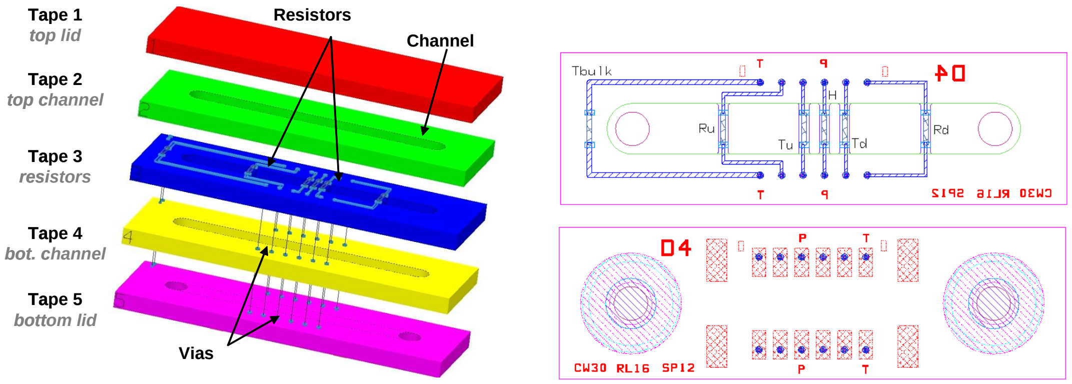

(a) Exploded view of LTCC layers.

(b) Top and bottom views of the flow sensor. Note the thermistors placement, and the connector solder pads with the vias beneath.

Fig. C.7: Schematics of the flow sensor demonstrator.

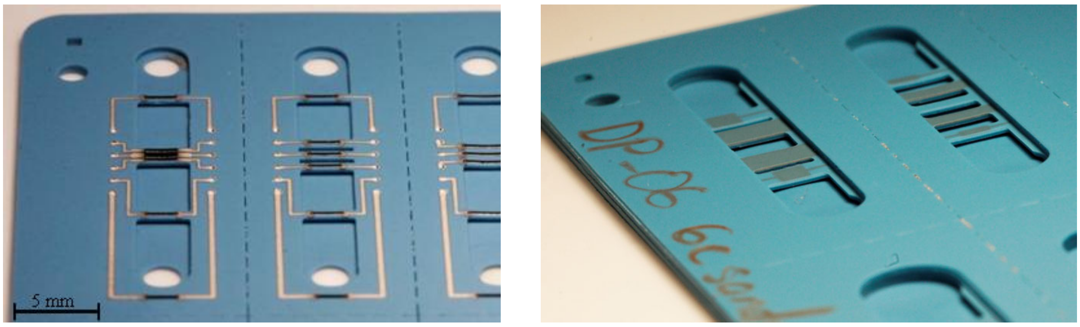

(a) LTCC flow sensors in batch, fired here without lid to show the thermistors. Channels are 3 mm wide and 24 mm long; inlets are Ø2 mm.

(b) Fired "sandwich" 6-layer circuit showing perfect test bridges; electrodes are visible through the 40 µm protective layer made with DP951-50 µm.

Fig. C.8: Firing of several different test structure on the same DP951 tape.

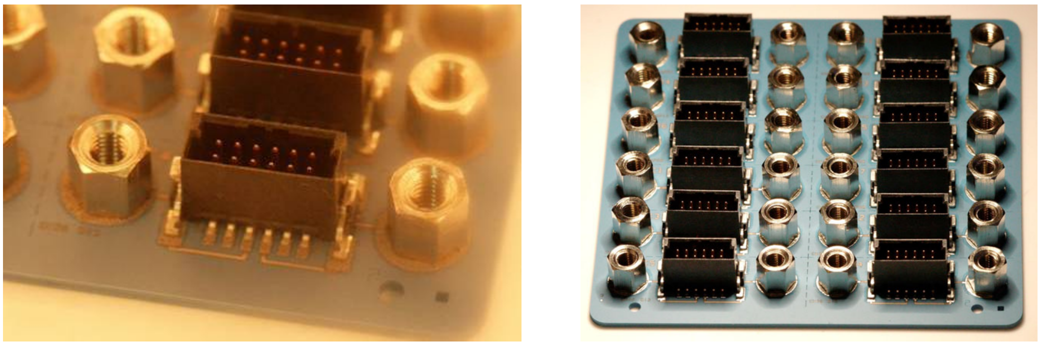

(a) Flow sensors undergoing final firing step.

(b) Final circuit after soldering, before singulation.

Fig. C.9: Soldering of M3 fittings and of ERNI low-profile 12-pin male connector.

this document; please see Figure 3.18 on page 80, Figure 4.27 on page 138 and Figure 4.28 on page 139 for our tests with MSP.

After firing, the flow sensors were screen printed one last time with solder paste, and an ERNI SMD connector was soldered along two M3 nuts as fluidic ports (similarly to our flow sensor of subsection 5.5.1). This is pictured on Figure C.9.

Air flow measurements The measurements of air flow resulted in the graph of Figure C.10. It turns out that the calorimetric principle (in green) presents a high sensistivity than the anemometric principle, but for a flow up to ~15 NL/min, compared to the ~110 NL/min of maximum flow tested. Above 15 NL/min, where the calorimetric signal is maximum, smart circuitry is necessary to discern on what "side of the graph" we are, which might hinder using low-cost electronics. To the contrary, the anemometric curve (in violet) is increasing constantly with a square root aspect: there is no problem of indetermination, and the signal can be easily linearized with passive electronics. For this reason, the anemometric principle was retained for the multisensor.

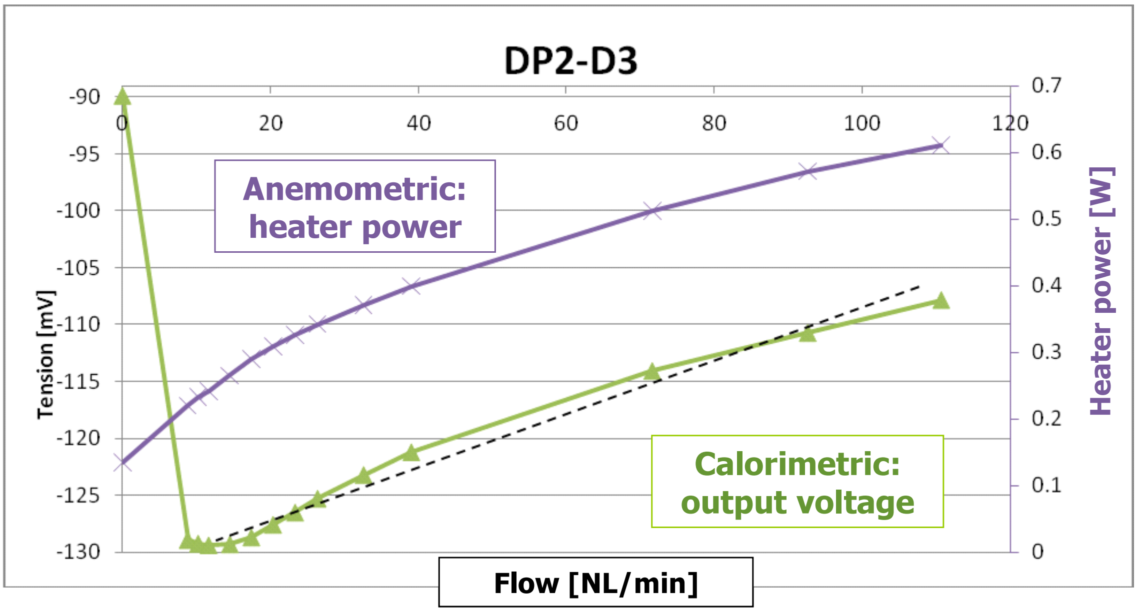

Fig. C.10: Graph of air flow measurements: output voltage and heater power vs. forced flow. Two measurement principle were studied: anemometric (in function of heater power, violet) and calorimetric (in function of output voltage, green).

Appendix D

Commercial LTCC tape systems

D.1 LTCC tapes suppliers

Regarding the manufacturing of LTCC green tapes, it is important to know that LTCC suppliers do not always perform the tape casting themselves; indeed, there are a few foundries on the planet that often cast LTCC for many suppliers at the same location. The 2001 article [1] from Reinhard Kulke et al. is an interesting introduction to LTCC and gives the list of tape casters; I counted 18 of them, located in the following countries: Austria (1), Finland (2), France (1), Germany (4), Korea (1), Japan (1), USA (7), Taiwan (1). The main suppliers are (data of 2001 updated with tapes availables in 2010):

CeramTec	GC
DuPont	GreenTape 951, 943 and 9k7 systems
ESL	410x0 system
Ferro	A6M and A6S
Heraeus	standard tapes HeraTape CT70x, CT800, CT2000, "zero-shrinkage" HeraLock HL2000, HL800, ferrite tapes AHT98-029, AHT03-003
NEG	Nippon Electrical Glass

Beyond these foundries, a number of companies (mostly huge manufacturers of electronics) have their own LTCC production facilities, which are not available to customers. Bosch, Hitachi and Murata are typical firms who manufacture their own LTCC products for the automotive, mobile communication and consumer electronic markets [1].

D.1.1 Types of inks

With regard to the composition of inks (i.e. pastes), Monneraye published in 1978 an extensive study [230] of materials used in classical thick-film technology, which required extensive adaptation to LTCC, since LTCC is fired at nearly the same temperatures alumina substrates are post-fired, with the addition of shrinking. The pastes available from suppliers are generally:

Conductors

Ag	for good conductivity at low cost.
Ag:Pd	for soldering pads (the Pd hinders the Ag from dissolving and interdiffusing into the solder paste), making links between gold and silver tracks (to avoid generation of voids due to the Kirkendall effect [231]), and surface conductors in general (less susceptible to electromigration).
Au	for special electronic applications and for bonding pads.
Pt	for special applications such as high-temperature heaters.
Cu	still rarely encountered, as it requires a carefully controlled low oxygen partial pressure during the sintering procedure [232]; used for tracks and vias.

Resistors

Constant	with values in series of 10, 100, 1 k, 10 k, and 100 kΩ/□ with a TCR ideally of 0.
PTC	*Positive Temperature Coefficient*, used to measure temperature or as heater, with a linear TCR usually of +3000 ppm [233, 234].
NTC	*Negative Temperature Coefficient*, used to measure temperature. They are usually non-linear and ca. an order of magnitude more sensitive than PTCs. However, it is difficult to fine-tune their value; buried thermistors exhibit much better long-term stability than the surface ones [234, 235].

Dielectrics In the first sense useless on LTCC as the substrate *is* the dielectric, but classical dielectric pastes can still be used as post-firing for cross-overs etc.

Overglazes Transparent or colored glassy protection used to protect a circuit from scratches and to stabilize laser-trimmed resistors.

Sealing glass Used to bond ceramic or metals at low temperature (~500-600 °C).

Sacrificial Not yet available from suppliers, these pastes, made of carbon and/or mineral oxides, are currently experimental and prepared by research teams.

D.2 Appreciation of the different commercial tape systems

Not all LTCC tape systems are equivalent; here are the pros ans cons, with regard to microfluidics, of the commercial tapes frequently encountered in litterature. We also give prices, normalized in €/dm^2/layer, for the tapes for which we got quotations during this thesis; this reflects the price for a low-throughput research laboratory, for a consumption of less than five kilograms of tape annually. The laser cutting characteristics are valid for our 1064 nm Nd:YAG laser (see subsection 2.2.3).

Tapes tested in our laboratory

CeramTec GC This tape, composed of alumina and anorthite, is nominally proposed in a green thickness of 360 µm (294 µm fired), but the supplier accepted to deliver us a test batch of 600 µm (490 µm fired). This increased thickness is of great help for manufacturing channels with a large cross section, but the X-Y shrinkage is rather high (16 to 19 %). However, laser cutting is very slow because of its white color, not absorbing the IR light of our machine. For comparison, we could cut at only 0.7 mm/s, compared with 3.0 mm/s for the DP951-254 µm, and at 10 mm/s for the CT700. The laser dust is easier to remove than with DuPont, but less than with Heraeus.
The system of inks is less developped than its competitors, but the tape proved to be compatible with foreign inks in post-firing; testing must be done for co-firing. We have no information regarding its chemical resistance. Its price ranges from 5.6 to 1.7 €/dm^2/layer for a minimum ordered quantity of 100 to 1000 sheets (202×222.5 mm each).

DuPont GreenTape 951 The DP951 is the most widely used and studied tape, and one of the oldest on the market. Offered in four unfired thicknesses (254, 165, 114 and 50 µm, fired ~210, 135, 95 and 40 µm respectively), it is associated with a complete system of co- and post-firing inks. The various thicknesses allow the manufacturing of large channels, of thin membranes as well as of structures of intermediate sizes all on the same circuit. Its chemical resistance is very good: a long-term dissolution test [18] carried out at room temperature during one year showed a good chemical resistance against exposure to strong acids or basic solutions. The worst case is the chemical resistance against NaOH, which corrodes both ceramic and glass, and is the only tested solution that causes a measurable stock removal.
Laser cutting is somewhat cumbersome, in the sense that the cutting speed is medium, and the generated dust is difficult to remove because melted particles stick to the tape surface. The light blue green material turns deep blue after firing. Its price is relatively high (data of 2009): for each thickness respectively 5.6, 4.1, 3.4 and 3.4 €/dm^2/layer for a minimum ordered quantity of 100, 200, 200 and 400 sheets (152.4×152.4 mm each, or 6”×6”).

Heraeus HeraLock 2000 The first “zero-shrinkage” tape available, HL2000 has been used and studied by many research groups. It is available in only one thickness: 133 µm (fired 91 µm), making it more appropriate for electronics than for microfluidics. The system of inks is complete, too. Its cutting speed is 9.0 mm/s (3x faster than DP951), and its color is very light mauve. Its chemical resistance proved to be the lowest of the tapes tested. Its price was originally high: 4.6 €/dm^2/layer in 2006 for a roll of 8"×3 m, the price dropped in 2009 to 1.7 €/dm^2/layer and the tape is now delivered in sheets of the same size as the DP951 (152.4×152.4 mm each, or 6"×6").

Heraeus HeraLock 800 Follower of the HL2000, it is available in only one thickness but with more Z-shrinkage: 120 to 130 µm (fired 82 µm). The HL800 [149] is in our sense still somewhat immature: it has a strong tendency to self-warpage, even without screen printings, and overall when fired with a low number of layers. Nonetheless, HL800 did show qualitatively much better chemical resistance than HL2000. In spite of its white color, its cutting speed is 9.0 mm/s (compared to 0.7 mm/s for GC). We give no price comparison for this one, as we got only free samples.

Heraeus HeraTape CT700 This tape has been available for a decade and is the Heraeus equivalent to the DP951. The available thickness makes it ideal for simple microfluidics (320 µm, 236 µm fired), but less for thin structures. The choice of inks available is very good, too. Its shrinkage is moderate in X-Y ($\sim 14.2\,\%$), but proved to be high in Z (26 %). Its laser cutting is very convenient: a high speed of 9 to 10 mm/s and almost no dust generated - or easily removed by blowing. Its color is light violet unfired, turning to dark violet after firing. Its price is low (data of 2006): 2.2 €/dm^2/layer for a roll of 280 mm×3 m, making it ideal for low-cost fluidic applications.

Tapes not tested in our laboratory

DuPont GreenTape 943 This lead-free glass/ceramic tape is oriented for high frequency applications; however, it is compatible with most of the ink system of the DP951. It is available in three unfired thicknesses: 254, 127 and 51 µm.

DuPont GreenTape 9K7 This lead-free new tape (2009) is oriented for high frequency applications; it must be sintered with a very long firing profile of more than 26.5 h, which is three times longer than what we used with DP951 [11].

ESL 410x0 We have no experience with these tapes; however, the system of inks is quite complete, and the tapes are compatible with their LTTT Transfer Tapes equivalent [210].

Heraeus HeraTape CT70x, CT800 and CT2000 We have little information about these tapes. We just know that the CT2000 is designed to allow production of high-performance wireless and multilayer circuits, and that is has a lower choice of inks than the CT700; for instance no resistor paste was available in 2006.

Ferro A6 Although it is one of the oldest tape (available in the nineties already along with the DP851 [127]), we have little information about this tape.

D.3 Appreciation of commercial pastes

Good experiences and issues we encountered with commercial pastes on LTCC are listed next. As the main tape system we used was the DP951, most of the listed inks are from DuPont.

Co-fireable conductor tracks

DP6145 Ag This paste yields low deformation upon firing, but it is difficult to solder due to a low wettabilty. It is also chemically incompatible when co-fired as a resistor termination for DP5092D PTC. For instance, it was used for the inner ground plane of our multisensor.

DP6146 Ag/Pd This paste yields important deformations upon firing, overall when used on surface and on suspended structures; we think it is because of its shrinkage being relatively different than the one of the tape (see section 5.3.4). To the contrary of the DP6145, it is easy to solder and is compatible with gold tracks and bonding pads. It is chemically compatible with PTC resistor terminations. However, it must absolutely *not be post-fired*, as this yields insufficient adhesion. We used it for the surface tracks and solder pads of our multisensor, as well as for the inner tracks leading to thermistors.

DP5742 & DP CDF-34 Au These pastes yield lower deformation than DP6146, and were successfully used to manufacture a complex MOEMS package (see subsection 3.3.1 and [45]). However, even a single co-fire in direct contact with Ag pastes yielded unreliable contacts, requiring the use of Ag:Pd as a transition composition.

Co-fireable (conductor) via fills

DP6138 Ag/Pd & DP6141 Ag These pastes provide reliable vias with DP951, with DP6141 having the advantages of lower cost and higher thermal conductivity (for thermal vias), and DP6138 allowing transition between Ag and Au.

Post-fireable conductor tracks

DP6135D & DP6143 Ag/Pd DP6135D was later replaced by DP6143; both were successfully used as solderable metallizations and exhibited high adhesion to LTCC.

Post-fireable overglazes These low-temperature cadmium-free encapsulant compositions are intended to form an insulating and protective layer over thick-film circuits and especially over thick-film resistors that are laser trimmed.

DP QQ550 This ink is best fired around 510 °C; under that T it is incompletely molten.

ESL G-481 & G-482 These pastes are relatively low-temperature firing, semi-glossy, acid resistant, screen-printable overglazes. The G-481 is green in colour and is used for the first coating over the resistor prior to laser trim. The G-482 is designed for use as the final glass coating. G-481 is fired between 580 and 625 °C, and was used for ca. ten years with good results as the standard overglaze in our laboratory. At 580 °C, the overglaze does not yet flow strongly, yielding a matte finish compatible with laser trimming.

Appendix E

Glossary

Alumina	Aluminium oxide Al_2O_3
Backing tape	Protective sheet on which the LTCC tape is cast, usually in boPET (biaxially-oriented PolyEthylene Terephthalate, branded under MYLAR, see below), which can be punched but must be removed prior to lasering.
Binder, permanent	Glassy phase present in many inks (resistors, dielectrics, overglazes, some conductors) and LTCC (=dielectric). It acts as a matrix for ceramic fillers, as a sintering aid and as an adhesion promoter (conductors). In modern dielectrics, it eventually reacts with the ceramic fillers and/or crystallizes.
Binder, temporary	Polymer that holds together the ink (after drying) or LTCC tape, and subsequently burns out during firing. In thick-film inks, it is initially dissolved in a solvent, where it imparts a suitable rheology (see *Vehicle*). Its properties in the dry state are often tuned by *Plasticizers*.
Blanking	Process of cutting raw LTCC "coils" into square and rectangular shapes with close tolerances.
Buried	Refers to a conductor, a thick-film resistor or a cavity trapped between inner layers of LTCC.
Burnout	Combustion of organic binders, including solvents and plasticizers remaining after drying, contained in tape and pastes during the firing. Typically occurs between 200 and 440 °C. Also applies to other carbonaceous matter such as graphite sacrificial paste, which however burns out at much higher temperatures, above 600 °C.
Cavity	Any cut in an LTCC tape other than a via. It can be open or buried.
CCL	Cold Chemical Lamination
Chip	Miniaturized electronic device usually found as bare die or packaged, e.g. as an SMD component. It can be an IC (integrated circuit), but not necessarily.
Circuit	A functional fired stack of LTCC tapes.

CLPL	Cold Low Pressure Lamination
Co-firing	Firing together pastes and tapes in the same step.
Die, dice, dies	A die (pl. dice or dies) is small block of semiconducting material (i.e. a "naked" chip).
DI water	De-ionized water.
DIL, SIL package	Dual In-Line, Single In-Line package.
DoE	Design of Experiments: methods to run tests rationally and efficiently, in order to gain time, to minimize the number of experiments, and to maximize the significance of the obtained results. DoE implies a careful selection of the experimental parameters and their ranges.
Drying	Removal of volatile solvents from freshly screen-printed pastes (before the next printing step, or before stacking and firing). Usually carried out in a well ventilated air oven or conveyor dryer.
Emulsion	Photosensitive polymer deposited onto the screen mesh that, after exposure and development, defines the print pattern and acts as a gasket between screen and substrate. Its thickness (20 to 105 μm) determines, together with the mesh, the process parameters and the paste properties, the amount of paste deposited.
Firing	The action to fire a ceramic in a furnace. For alumina and LTCC this is usually between 850 and 900 °C in air.
Functional phase	One of the four groups of materials composing the ink; it consists of metal powders (Pt, Pd, Ag, Au, etc.) in conductive inks, metals and/or metal oxides (RuO_2, $Bi_2Ru_2O_7$, Pd, Ag) in resistors, and ceramic/glass ($BaTiO_3$, glass) in dielectrics. (from [236])
GreenTape, green tape	Commercial name given by DuPont to their LTCC tapes; by extension it became common language (a "green" tape) to express unfired LTCC tapes. See also *Tape* below.
HTCC	High Temperature Co-fired Ceramic (sintered at 1400 to 1600 °C).
Hybrid technology	Refers to electrical circuits mixing thick-film depositions and SMD components. Unless not specified, alumina substrates are involved.
Ink	British name for *Paste*.
IPA	Isopropyl alcohol, or isopropanol.
Lamination	Pressing the stacked LTCC tapes, before the firing step, usually applying high pressure and temperature for a certain time. The lamination parameters are typically: pressure between 8 and 20 MPa (i.e. 80 and 200 bar), temperature between 25 and 70 °C and duration between 5 and 15 min.
Layer	Usually refers to successive paste depositions, but may also refer to tapes.

LTCC	Low Temperature Co-fired Ceramic (sintered below 920 °C).
LTTT	Low Temperature Transfer Tape
Mesh	The "backbone" of the screen, usually a stainless steel wire mesh. The meshing is given in meshes/inch (25.4 mm), and ranges from 80 to 400 mesh/in. The higher the meshing, the finer the printing resolution, the less paste is deposited.
MEMS, MOEMS	Microelectromechanical systems, Micro-opto-electromechanical systems
Modifiers	One of the four groups composing the ink; basically, small amounts of proprietary additives that control the behavior of the inks before and after processing. (from [236], also often called "additives").
MSL, MSP	Mineral Sacrificial Layer, Paste.
Mylar®	Commercial name of DUPONT polyester boPET backing tape; developed in 1952, it has nearly become a common name. See *Backing tape* above.
NTC	Negative Temperature Coefficient; usually employed when talking about resistors.
Pad	A small area of conductor for connecting wires or bonds (bonding pad), for soldering (solder pad) or for mechanical contact.
PAS / PLAS	Pressure Assisted Sintering / Pressure Less Assisted Sintering (in contrast to *UCS* and *SCS*).
Paste	Functional viscous ink with a rheology formulated to be suitable for screen printing. It can be printed onto unfired LTCC (by co-firing), fired LTCC (by post-firing), or alumina... The function can be conductor, resistor, via, sacrificial, etc. The ink consists of four distinct groups of intermediates, which are thoroughly mixed and blended, yielding a macroscopically homogeneous product: (adapted from [236]) 1) the "*Functional phase*" (ceramic filler for dielectrics, conductive oxide for resistors, metal powder for conductors); 2) the permanent *Binder* phase; 3) the *Modifiers*, which are specific to the type of ink; 4) the temporary *Vehicle*.
PCB	Printed Circuit Board.
PDMS	Polydimethylsiloxane; one of the most widely used silicon-based organic polymer.
Plasticizer	Organic compound whose purpose is to soften (i.e. "plasticize") and impart flexibility to the organic binder (*Binder, temporary*) of both LTCC tapes and dried thick-film pastes. Compared with the solvent, the plasticizer, added in smaller amounts, has a higher boiling point and mostly remains in the tape / paste after the drying step.

Post-firing	Firing pastes deposited onto already sintered LTCC.
Preconditioning	Heating LTCC tapes in an oven, to allow levelling by relaxation of the stress induced by the removal of the backing tape.
PTC	Positive Temperature Coefficient; usually employed when talking about resistors.
Punching	Process of using a punch press to push a punch through the unfired LTCC and into a die to create a hole in the workpiece. Usually used for vias.
Reflow oven	Oven used to melt solder paste and thus carry out soldering operations.
Release tape	Protective material used during lamination of LTCC tapes to avoid their sticking to press plates. *Backing tapes* in MYLAR are usually a convenient solution, at the expense of strong dust attraction due to their high electrostaticity. For rubber lamination, thinner food wrapping foils in PE are preferred.
Screen	Frame supporting an ink-blocking stencil, i.e. the pattern used for depositing paste by screen printing; may consist of a wire mesh and patterned emulsion (as in our work) or a patterned thin metal foil.
SCS	Self-Constrained Sintering (i.e. with "*zero-shrinkage*" LTCC tapes, in contrast to *UCS*).
SEM	Scanning Electron Microscope.
Sheet	Raw LTCC tape material as delivered by manufacturer (usually in sheets, but also in rolls).
Singulation	Individualisation of circuits when produced in batch from the same tape. It can be done by manual breaking stamp-like pre-cuts, by sawing with a diamond blade, or by laser scoring and manual breaking.
Slitting	Process of cutting coils to specified widths along the length of the coil.
SMD, SMT	Surface Mount Device, Technology. Can be applied here to an electronic component on top of a LTCC circuit, or to a whole LTCC circuit on top of a PCB (such as our multisensor of section 5.3).
Solder	Relatively low-melting (by convention < 450 °C) metallic alloy, used to carry out joining + interconnection of electronic components. Common electronic solder alloys are lead-free Sn-Cu-Ag ($T_\mathrm{f} = 220$ °C) or classical Sn-Pb eutectic alloy ($T_\mathrm{f} = 179$ °C).
Soldering	Joining two elements together with a *Solder* alloy, usually carried out in a reflow oven or with a soldering iron.
Solvent	Organic compound, usually a visquous liquid, used to dissolve the temporary polymer binder of a *Paste*, yielding a suitable *Vehicle* for dispersing the other solid components. As opposed to the *Plasticizer*, it evaporates during drying.
SPS	Setter Powder Sheets.

Squeegee	Rubber blade used to move the ink composition through the screen mesh.
Snap-off distance	Distance between screen mesh and substrate prior to the print stroke, e.g. when the squeegee is lifted from the screen.
Stacking	The action to align and pile up unfired but screen printed LTCC tapes, directly before the lamination step.
Standard LTCC	LTCC tapes that feature a shrinkage of 10 to 20 % in X-Y and around 20 to 25 % in Z, when processed with unconstrained sintering (*UCS*) (in contrast to "*zero-shrinkage LTCC*").
Substrate	The support of thick-film deposits; can be alumina, LTCC, steel, AlN, PCB (FR4), polymer etc.
SVM	Sacrificial Volume Materials
Tape	One level of LTCC, part of a stack/circuit. Usually refers to the unfired form.
TCE	Temperature Coefficient of Expansion.
TCR	Temperature Coefficient of Resistance, typically in [ppm/K].
TEM	Transmission Electron Microscope.
Thermal via	A via with a large diameter, filled with silver paste in order to efficiently conduct heat vertically through the device, thanks to its much better heat conductibility than the base LTCC material.
Thick film	The technology encompassing printing thick pastes (1 to 100 µm) on substrates (usually ceramic or metal).
Thin film	The technology involving depositing thin layers of 1 nm to 10 µm chemically or physically, per example by plating or techniques under vacuum (PVD, CVD, etc.).
Track	A line of conductor paste screen printed on LTCC.
Trimming	Coarse or fine adjustment of thick-film resistors, usually by laser.
UCS	Unconstrained Sintering (with standard LTCC, in contrast to *SCS*).
Vehicle	Of the four groups composing the ink, it encompasses the temporary organic components, which do not take part in the final product but are necessary for processing. It is composed of a solvent and a binder, and often also contains a plasticizer and dispersants. Initially, it is a viscous liquid that disperses the other groups of the ink, yielding a screen printable product. After drying (evaporation of the solvent), it provides a temporary mechanical bond for the mineral components. Finally, it burns out completely during firing. Note: Unfired LTCC tape is similar to dried paste (solvent evaporated after tape casting), but usually contains a much higher proportion of binder to give it sufficient strength for handling.

Via	Electrically (or thermally) functional hole made in a tape to connect the top surface to the bottom one. It can be either metallised on walls, or completely filled with paste. Typical diameter is 100 to 300 µm. Vias are punched or laser drilled.
Wire bonding	Method of making wired interconnections between an integrated circuit (IC) and a printed circuit board (PCB), using mainly Au or Al.
XRD	X-ray diffraction; an X-ray scattering non-destructive analytical technique which reveal information about the crystallographic structure, chemical composition, and physical properties of materials and thin films.
"Zero-shrinkage"	When talking about LTCC, concerns self-constrained (*SCS*) tapes that feature almost no shrinkage in X-Y, but up to 40 % Z (in contrast to *Standard LTCC*).
ZTA	Zirconia Toughened Alumina, ceramic material comprising alumina and zirconia.

For the sake of readability, the following brand names are mostly written without the ® or ™ signs and abbreviated; the list is non-exhaustive.

- DuPont™ (for example DP 5092D)
    - Mylar®, Tedlar®
    - GreenTape™ (e.g. DP951)
- W. C. Heraeus
    - HeraLock® Tape (e.g. HL2000)
    - HeraTape® (e.g. CT700)

- CeramTec (Ceramtape GC)
- ESL™ ElectroScience Laboratories (e.g. ESL 8837)
- Honeywell Riedel-de Haën® (Riedel-de Haën)
- Sigma-Aldrich
- Analog Devices (AD7746EB)

This thesis was written with the free open-source document processor LyX 1.6.5 and the document class "book (Memoir)".

Each entry of the Bibliography coming next is completed with back-hyperlinks of pages were citations are located.

Bibliography

[1] R. Kulke, M. Rittweger, P. Uhlig, and C. Günner. LTCC - Multilayer Ceramic for Wireless and Sensor Applications. *Journal PLUS (Produktion von Leiterplatten und Systemen)*, Ausgabe Dezember 2001:2131–2136, 2001. 15, 18, 19, 54, 68, 239

[2] IMST GmbH. http://www.ltcc.de. Kamp-Lintfort, Germany, 2010. 16, 40

[3] DuPont. *DuPont GreenTape Material System – Design and Layout Guidelines*, 2003. 16, 57, 58, 79

[4] E. G. Palmer and C. M. Newton. 3-D packaging using low-temperature cofired ceramic (LTCC). *Int. Journal of Microcircuits and Electronic Packaging*, 16(4):279–284, 1993. 15

[5] M. R. Gongora Rubio, P. Espinoza Vallejos, L. Sola Laguna, and J. J. Santiago Aviles. Overview of low temperature co-fired ceramics tape technology for meso-system technology (MsST). *Sensors and Actuators a-Physical*, 89(3):222–241, 2001. 15, 38, 61, 79, 92, 101, 105, 147, 148, 206

[6] Ecole Polytechnique Fédérale de Lausanne / Laboratoire de Production Microtechnique. Thick-Film Group and LTCC Technology. BM 3.142, Station 17, CH-1015 Lausanne, Switzerland, http://lpm.epfl.ch/ltcc, 2010. 15, 222, 223

[7] H. Birol. *Fabrication of low temperature co-fired ceramic (LTCC)-based sensor and micro-fluidic structures*. PhD thesis, #3696, EPFL, Lausanne, Switzerland, 2007. 16, 100, 101, 106, 107

[8] CeramTec. Specification of Glass Ceramic (Ceramtape GC), material datasheet, http://www.ceramtec.com/index/products/ltcc_ceramic_tapes//specification/00676,0123,0300,0555.php, 2010. 16, 76

[9] DuPont. *DuPont GreenTape 951 datasheet*, 2003. 16, 33, 34, 35, 40, 57, 201

[10] DuPont. *DuPont GreenTape 943 datasheet*, 2003. 16, 33, 34, 57

[11] DuPont. *DuPont GreenTape Material System – Design and Layout Guidelines*, 2009. 16, 18, 40, 79, 242

[12] Ferro. *Ferro A6 LTCC Design Guide*, 2002. 16, 33, 35, 57

[13] Heraeus. *Heratape CT2000 datasheet*, 2003. 16, 57

[14] Heraeus. *Heratape CT700 datasheet*, 2007. 16, 76, 79

[15] Heraeus. *HeraLock Tape HL2000 datasheet*, 2007. 16, 35, 52

[16] Heraeus. *HeraLock Tape HL800 datasheet DPIS*, 2008. 16

[17] R. Willigens. Microréacteur calorimétrique intégré en technologie céramique co-cuite à basse température (LTCC) [Integrated calorimetric microreactor in low-temperature co-fired ceramic technology (LTCC)]. Master project, EPFL-STI-IMT-LPM, Lausanne, Switzerland & ULG, Belgium, July 2005. 17, 181, 186, 202, 204, 207

[18] T. Thelemann, M. Fischer, M. Gross, and J. Müller. LTCC-based fluidic components for chemical applications. In *3rd Int'l Conference on Ceramic Interconnect and Ceramic Microsystems Technologies (CICMT)*, paper WA23, Denver, USA, 2007. 17, 139, 143, 154, 202, 207, 241

[19] A. Bittner, H. Seidel, R. Kautenburger, A. Roosen, and U. Schmid. Investigation on the porosification behaviour of fired LTCC substrates. In *5th IMAPS / ACerS Int'l Conference on Ceramic Interconnect and Ceramic Microsystems Technologies (CICMT)*, paper THA11, Denver, USA, 2009. 17, 106, 202, 207, 221

[20] Wikipedia. Definition of Microelectromechanical systems (MEMS). http://en.wikipedia.org/wiki/Microelectromechanical_systems, 2010. 18

[21] R. R. Tummala. Ceramics in microelectronic packaging. *American Ceramic Society bulletin*, 67(4):752–758, 1988. 18

[22] A. H. Feingold, M. Heinz, R. L. Wahlers, and M. A. Stein. Materials for Capacitive and Inductive Components Integrated with Commercially Available LTCC Systems. In *3rd IMAPS Annual Conference on Microelectronics and Packaging*, Herzelia, Israel, 2003. 18

[23] F. Schindler Saefkow, K. A. Jam, V. Großer, and H. Reichl. A 3D-package technology for fluidic applications based on Match-X. In *Actuator 2004*, Messe Bremen, Germany, June 14-16 2004. 19

[24] Advanced Liquid Logic Inc. Digital Microfluidics on PCB. 615 Davis Dr, Suite 800, Morrisville, NC 27560, USA, http://www.liquid-logic.com/, 2010. 19

[25] M.-A. Schneider. *Development of a novel microreactor-based calorimeter for the study of fast exothermal reactions in liquid phase*. PhD thesis, #3069, EPFL, Lausanne, Switzerland, 2004. 20

[26] J. R. Larry, R. M. Rosenberg, and R. O. Uhler. Thick-film technology: an introduction to the materials. *IEEE Transactions on Components, Hybrids, and Manufacturing Technology*, 3(2):211–225, 1980. 20

[27] J. E. Sergent. Understanding the basics of thick-film technology. *EDN*, 17(9):341–348, 1981. 20

[28] Wordsun. Festo: Leading manufacturer of aerosol filling equipment adopts integrated pneumatic duct plate technology. Marketing communications for engineering and technology companies, http://www.wordsun.com/release.php?id=640, 2008. 20

[29] Festo AG. Prototype of aluminium-epoxy resin fluidic platform. Private discussion, 2007. 20

[30] P. Gravesen, J. Branebjerg, and O. Sondergard Jensen. Microfluidics–a review. *Journal of Micromechanics and Microengineering*, 3:168–182, 1993. 21

[31] E. Verpoorte and N. F. De Rooij. Microfluidics meets MEMS. *Proceedings of the IEEE*, 91(6):930–953, 2003. 21

[32] D. Erickson and D. Li. Integrated microfluidic devices. *Analytica Chimica Acta*, 507(1):11–26, 2004. 21

[33] P. K. Khanna, B. Hornbostel, M. Burgard, W. Schäfer, and J. Dorner. Studies on three-dimensional moulding, bonding and assembling of low-temperature-cofired ceramics for MEMS and MST applications. *Materials chemistry and physics*, 89(1):72–79, 2005. 21

[34] L. Halbo and P. Ohlckers. *Electronic Components, Packaging and Production*. Book, ISBN 82-992193-2-9. University of Oslo Press, Finland, December 1997. 21

[35] K. G. Ewsuk, C. B. DiAntonio, F. Uribe, and S. L. Monroe. Materials and Process Control Technology for LTCC Microelectronics Packaging. In *Conference on Ceramic Interconnect Technology: The Next Generation II*, Denver, USA, April 26-28 2004. 21

[36] M. Descamps, G. Ringuet, D. Leger, and B. Thierry. Tape-casting: relationship between organic constituents and the physical and mechanical properties of tapes. *Journal of the European Ceramic Society*, 15(4), 1995. 21, 61, 208

[37] S.-H. Lee, A. Mohanram, G. L. Messing, and D. J. Green. Constrained Sintering for Dimensional Control in Co-fired Systems. Pennsylvania State University, 2003. 21, 51, 58, 80

[38] A. Mohanram, G. L. Messing, and D. J. Green. Co-firing of Integrated Ceramics: Process Modeling of LTCC Systems. Pennsylvania State University, 2003. 21, 51, 58, 215

[39] A. Mohanram. *Co-Sintering of Integrated Ceramics: Fundamentals, Observations and Design Guidelines*. PhD thesis, Pennsylvania State University, USA, 2005. 21, 51, 58

[40] B. Balluch, W. Smetana, G. Stangl, and X. Wang. Fine structured channel arrays and bridging elements for LTCC-technology applications. In *XXXII International Conference of IMAPS Poland Chapter*, paper A05, Pultusk, Poland, 2008. 22, 36, 79, 208, 209

[41] W. Smetana, B. Balluch, G. Stangl, S. Lüftl, and S. Seidler. Processing procedures for the realization of fine structured channel arrays and bridging elements by LTCC-Technology. *Microelectronics Reliability*, 49(6):592–599, 2009. 22, 36, 79, 208, 209

[42] M. R. Haskard, M. A. Macdonald, and G. Pilkington. CAHL – computer aided hybrid layout software. *Microelectronics Journal*, 25(5):323–334, 1994. 30

[43] DURST CAD/CONSULTING GmbH. HYDE Hybrid Design Software. Hohenzollernstrasse 2, D-71088 Holzgerlingen, Germany, http://www.durst.de, 2010. 31

[44] F. Seigneur, Y. Fournier, T. Maeder, P. Ryser, and J. Jacot. Hermetic package for optical MEMS. In *Int'l Conference on Ceramic Interconnect and Ceramic Microsystems Technologies (CICMT)*, pages 627–633, Munich, Germany, 2008. 31

[45] F. Seigneur, Y. Fournier, T. Maeder, P. Ryser, and J. Jacot. Hermetic package for optical MEMS. *Journal of Microelectronics and Electronic Packaging*, 6(1):32–37, 2009. 31, 32, 70, 71, 204, 243

[46] F. Seigneur. *Encapsulation hermétique pour systèmes hydro- et thermo-sensibles*. PhD thesis, #4348, EPFL, Lausanne, Switzerland, 2009. 31, 32, 45, 70, 71, 204

[47] Scrantom Inc. Low Temperature Cofired Ceramic - Design Guidelines. Technical report, Scrantom Inc., 3545A Cadillac Ave., Costa Mesa, CA 92626, USA, 2004. 33

[48] H. Birol, T. Maeder, C. Jacq, and P. Ryser. Effects of firing conditions on thick-film PTC thermistor characteristics in LTCC technology. In *Conference on Ceramic Interconnect Technology: The Next Generation II*, pages 106–109, Denver, USA, April 26-28 2004. 33

[49] H. Birol, T. Maeder, I. Nadzeyka, M. Boers, and P. Ryser. Fabrication of a Millinewton Force Sensor Using Low Temperature Co-fired Ceramic (LTCC) Technology. *Sensors and Actuators A: Physical*, 134:334–338, 2007. 34, 101, 106, 224, 225

[50] E. Horváth. Low temperature co-fired ceramics technology based on thick-film technology. Internal article, Department of Electronics Technology, Budapest University of Technology and Economics, Hungary, 2008. 34, 37, 209

[51] K. Law. Pyrolyzable backing tape for singulation of ceramic components. Technical disclosure, Motorola Inc., 30 March 2001. 35

[52] LS Laser Systems GmbH. LS9000 trimming laser. Gollierstrasse 70, D-80339 Munich, Germany, http://www.ls-laser-systems.com, 2010. 36, 173

[53] S. Vionnet Menot. *Low firing temperature thick-film piezoresistive composites*. PhD thesis, #3290, EPFL, Lausanne, Switzerland, 2005. 37

[54] Aurel Automation. Stencil and screen printing machines (among which our Aurel 900T). Via Foro dei Tigli, 4 47015 Modigliana (FC), Italy, www.aurelautomation.com, 2010. 37

[55] ASYS (formerly EKRA). Stencil and screen printing machines (among which Ekra models). ASYS Automatisierungssysteme GmbH, Benzstrasse 10, 89160 Dornstadt, Germany, http://www.asys.de/asys-gmbh/, 2010. 37

[56] M. Richtarsic and J. Thornton. Characterization and Optimization of LTCC for High Density Large Area MCM's. In *Int'l Conference on Multichip Modules and High Density Packaging*, 1998. 37

[57] S. Giudice. Dispositif d'alignement de précision pour feuilles de LTCC [Precision alignment device for LTCC tapes]. Master project, EPFL-STI-IMT-LPM, Lausanne, Switzerland, 2008. 39

[58] ATV Technologie GmbH. PEO-601 and SRO-702 firing ovens. Johann-Sebastian-Bach-Str. 38, D-85591 Vaterstetten/Munich, Germany, www.atv-tech.com, 2010. 40, 41, 43, 63, 64, 163, 217, 218

[59] SierraTherm. Furnaces for thick-film technology. 200 Westridge Drive, Watsonville, CA 95076 USA, http://www.sierratherm.com, 2010. 42

[60] J. Müller, J. Pohlner, D. Schwanke, G. Reppe, H. Thust, and R. Perrone. Development and Evaluation of Hermetic Ceramic Microwave Packages for Space Applications. In *1st Int'l Conference on Ceramic Interconnect and Ceramic Microsystems Technologies (CICMT)*, Baltimore, USA, 2005. 45

[61] F. Seigneur, Y. Fournier, T. Maeder, and J. Jacot. Laser soldering of LTCC hermetic packages with minimal thermal impact. In *16th IMAPS European Microelectronics and Packaging Conference (EMPC)*, pages 526–530, Oulu, Finland, June 2007. 45

[62] A. Salette. Fluidic and thermal interface in LTCC for a satellite micropropulsion. Master project, EPFL-STI-IMT-LPM/LMTS, Lausanne, Switzerland & INP Grenoble, France, June 20 2008. 45, 204

[63] N. Craquelin. Régulateur de débit en LTCC pour applications médicales [Flow regulator in LTCC for medical applications]. Master project, EPFL-STI-IMT-LPM, Lausanne, Switzerland, 2008. 45

[64] T. Zerna and K. J. Wolter. X-ray and Ultrasonic Microscopy – Non-destructive Test Methods for Reliability Relevant Phenomenon in Electronics Packaging. In *XXX International Conference of IMAPS Poland Chapter*, Krakow, Poland, 2006. 46

[65] M. Oppermann, A. Striegler, K. J. Wolter, and T. Zerna. New methods of non-destructive evaluation for advanced packages. In *XXXII International Conference of IMAPS Poland Chapter*, volume I01, Pultusk, Poland, 2008. 46

[66] Y. Fournier. Analysis of some defective ITER-MAG LTCC coils with X-ray scanner. Internal report, EPFL-STI-IMT-LPM, Lausanne, Switzerland, May 08 2009. 47

[67] D. Testa, M. Toussaint, R. Chavan, J. Guterl, J. Lister, J.-M. Moret, A. Perez, F. Sanchez, B. Schaller, G. Tonetti, Y. Fournier, T. Maeder, A. Encheva, G. Vayakis, C. Walker, H. Carfantan, A. Le Luyer, P. Moreau, and S. Peruzzo. Baseline system design and prototyping for the ITER high-frequency magnetic diagnostic set. *IEEE Transactions on Plasma Science*, 2009. 47, 204

[68] D. Testa, M. Toussaint, R. Chavan, J. Guterl, J. Lister, J.-M. Moret, A. Perez, F. Sanchez, B. Schaller, G. Tonetti, Y. Fournier, T. Maeder, A. Encheva, G. Vayakis, C. Walker, H. Carfantan, A. Le Luyer, P. Moreau, and S. Peruzzo. The magnetic diagnostic set for ITER. *IEEE Transactions on Plasma Science*, 38(3):284–294, 2010. 47, 204

[69] Y. Fournier, L.-S. Bieri, T. Maeder, and P. Ryser. Influence of lamination parameters on LTCC shrinkage under unconstrained sintering. In *4th IMAPS European Microelectronics and Packaging Symposium (EMPS)*, pages 165–170, Terme Catež, Slovenia, May 22-24 2006. 51

[70] V. Sunappan, A. Periannan, C. K. Meng, and W. C. Khuen. Process issues and characterization of LTCC substrates. In *Electronic Components and Technology Conference ECTC*, Las Vegas, USA, June 1-4 2004. 51, 58, 59, 215

[71] M. Hintz, H. Thust, A. Albrecht, and R. Tschernev. Advanced LTCC Processes Using Pressure Assisted Sintering (PAS). In *SMTA Pan Pacific Conference*, Hawaii, USA, 2004. 52, 80

[72] M. Hintz, H. Thust, and E. Polzer. Generic Investigation on 0-Shrinkage processed LTCC. In *IMAPS Nordic 2002*, Stockholm, Sweden, 2002. 53, 80

[73] A. Roosen and K. Schindler. Cold Low Pressure Lamination of Ceramic Green Tapes. In *1st Int'l Conference on Ceramic Interconnect and Ceramic Microsystems Technologies (CICMT)*, Baltimore, USA, 2005. 54, 81, 82

[74] M. A. Piwonski and A. Roosen. Low Pressure Lamination of Ceramic Green Tapes by Gluing at Room Temperature. *J. of the European Ceramic Society*, 19:263–270, 1999. 54, 81

[75] R. Coccioli. Design and Optimization of a Broadband Surface Mount Package. Presentation given by Inphi at Converge Workshop, Oct. 18, 2005. 54, 68, 151

[76] Y. Fournier. Results of first tested series of LTCC fluidic platforms. Internal report (20041208 ergebnisse erste reihe yf.doc), EPFL-STI-IMT-LPM, Lausanne, Switzerland, 2004. 58

[77] Y. Fournier. Results of special purpose LTCC fluidic platforms. Internal report (20050131 ergebnisse von reihe mandat-spezielles ltcc platten yf.doc), EPFL-STI-IMT-LPM, Lausanne, Switzerland, 2005. 58

[78] F. Lautzenhiser, E. Amaya, P. Barnwell, and J. Wood. Microwave module design with HeraLock™ HL2000 LTCC. In *IMAPS Deutschland Konferenz*, München, Germany, 2002. 58, 69

[79] J.-M. Fürbringer. Design of Experiments. Lecture of the Institute of Production and Robotique, EPFL, Lausanne, Switzerland, 2005. 60

[80] M. Rauscher and A. Roosen. Interpretation of the influence of LTCC green tape characteristics on shrinkage behavior. In *3rd Int'l Conference on Ceramic Interconnect and Ceramic Microsystems Technologies (CICMT)*, Denver, USA, 2007. 61

[81] A. Roosen, D. Pohle, and M. Wagner. Characterization of the Shrinkage Behavior of Pure, Screen Printed Thick Film Pastes and LTCC Green Tapes. In *Conference on Ceramic Interconnect Technology: The Next Generation II*, volume WP4, Denver, USA, April 26-28 2004. 69, 215

[82] T. Thelemann, H. Thust, and M. Hintz. Using LTCC for microsystems. *Microelectronics International*, 19(3):19–23, 2002. 75

[83] M. D. Pleskach, P. B. Koeneman, B. R. Smith, C. M. Newton, and C. A. Gamlen. Electro-fluidic device and interconnect and related methods, Patent US 2005/0068726 A1, 2003. 75

[84] K. Malecha and L. J. Golonka. Microchannel Fabrication Process in LTCC Ceramics. In *XXXI International Conference of IMAPS Poland Chapter*, pages 261–264, Krasiczyn, Poland, Sept. 23-26 2007. 75, 87, 99

[85] K. Malecha, D. Jurków, and L. J. Golonka. Comparison of solvent and sacrificial volume-material-based lamination processes of low-temperature co-fired ceramics tapes. *Journal of Micromechanics and Microengineering*, 19(6):065022, 2009. 75, 82, 86, 87, 88, 99

[86] H. Thust, M. Hintz, and A. Albrecht. Advanced LTCC processes using Pressure Assisted Sintering. In *Conference on Ceramic Interconnect Technology: The Next Generation II*, Denver, USA, April 26-28 2004. 80

[87] A. Roosen. Materials Process and Manufacturing: Current and Future Directions. In *1st Int'l Conference on Ceramic Interconnect and Ceramic Microsystems Technologies (CICMT)*, Baltimore, USA, 2005. 81, 215

[88] D. Couto, L. Schwegler, and A. Roosen. Cold Low Pressure Lamination of Metallized Ceramic Green Tapes. In *Conference on Ceramic Interconnect Technology: The Next Generation II*, Denver, USA, April 26-28 2004. 81, 89, 201

[89] A. Roosen, T. Schulte, M. Sibert, and S. Zollner. Ceramic green body, method of manufacturing a green body of this type and a method of manufacturing a ceramic body using the green body, Patent US 2004/0011453 A1, 2004. 82

[90] A. Roosen, A. Schroder, and S. Zollner. Method for joining ceramic green bodies using transfer tape and conversion of bonded green body into a ceramic body, Patent US 7,318,874 B2, 2008. 82

[91] N. Suppakarn, H. Ishida, and J. D. Cawley. Roles of Poly(propylene glycol) during Solvent-Based Lamination of Ceramic Green Tapes. *Journal of the American Ceramic Society*, 84(2):289–294, 2001. 83

[92] Z. M. Da Rocha, N. Ibanez Garcia, N. A. De Oliveira, J. Do Rosario Matos, and M. R. Gongora Rubio. Low Temperature and Pressure Laminations of LTCC Tapes for Meso-Systems. In *Conference on Ceramic Interconnect Technology: The Next Generation II*, pages 205–210, Denver, USA, April 26-28 2004. 83, 84

[93] A. Baker, M. Lanagan, E. Semouchkina, G. Semouchkin, and T. Kerr. Miniaturization of LTCC Devices by Using Mixed Dielectric Substrates. In *3rd Int'l Conference on Ceramic Interconnect and Ceramic Microsystems Technologies (CICMT)*, paper TP31, Denver, USA, 2007. 83

[94] T. Maeder, C. Jacq, Y. Fournier, and P. Ryser. Formulation and processing of screen-printing vehicles for sacrificial layers on thick-film and LTCC substrates. In *XXXII International Conference of IMAPS Poland Chapter*, paper B16, Pultusk, Poland, 2008. 84, 125, 133, 135

[95] D. Jurków and L. J. Golonka. Cold chemical lamination - new bonding method of green tapes. In *XXXII International Conference of IMAPS Poland Chapter*, paper G08, Pultusk, Poland, 2008. 86

[96] D. Jurków and L. Golonka. Novel cold chemical lamination bonding technique – A simple LTCC thermistor-based flow sensor. *Journal of the European Ceramic Society*, 29(10):1971–1976, July 2009. 86, 87

[97] D. Jurków, K. Malecha, and L. Golonka. Three Element Gas Flow Sensor Integrated with Low Temperature Cofired Ceramic (LTCC) Module. In *16th International Conference "Mixed Design of Integrated Circuits and Systems", MIXDES*, Lódz, Poland, June 25-27 2009. 86, 148

[98] K. Malecha and L. J. Golonka. Three-Dimensional Structuration of Zero-Shrinkage LTCC Ceramics for Microfluidic Applications. In *XXXII International Conference of IMAPS Poland Chapter*, volume G09, Pultusk, Poland, 2008. 87

[99] K. Malecha and L. J. Golonka. Three-dimensional structuration of zero-shrinkage LTCC ceramics for microfluidic applications. *Microelectronics Reliability*, 49(6):585–591, 2009. 87, 99

[100] E. Horváth and G. Harsányi. Realizing fluidic microchannel in low temperature co-fired ceramic substrate. Internal article, Department of Electronics Technology, Budapest University of Technology and Economics, Hungary, 2009. 87

[101] N. Serra, T. Maeder, C. Jacq, Y. Fournier, and P. Ryser. Screen-printed polymer-based microfluidic and micromechanical devices based on evaporable compounds. In *17th IMAPS European Microelectronics & Packaging Conference (EMPC)*, paper 16-S3-8, Rimini, Italy, June 2009. 88, 99

[102] DuPont. *DuPont GreenTape 951 A2/AT/AX MSDS datasheet*, 2005. 89, 201

[103] A. Dhaliwal and J. Hay. The characterization of polyvinyl butyral by thermal analysis. *Thermochimica Acta*, 391(1-2):245–255, 2002. 89, 201

[104] K. M. Nowak, H. J. Baker, and D. R. Hall. Cold processing of green state LTCC with a CO2 laser. *Applied Physics A*, 84(3):267–270, 2006. 89, 201, 209

[105] Y. Fournier, S. Wiedmer, T. Maeder, and P. Ryser. Capacitive micro force sensors manufactured with mineral sacrificial layers. In *16th IMAPS European Microelectronics and Packaging Conference (EMPC)*, pages 298–303, Oulu, Finland, June 2007. 91

[106] Y. Fournier, O. Triverio, T. Maeder, and P. Ryser. LTCC free-standing structures with mineral sacrificial paste. In *Int'l Conference on Ceramic Interconnect and Ceramic Microsystems Technologies (CICMT)*, pages 11–18, paper TA12, Munich, Germany, 2008. 91

[107] K. Peterson, S. Rohde, T. Turner, R. Stokes, A. Casias, and S. Spie. Novel structures in ceramic interconnect technology. In *Ceramic Interconnect Technology: Next Generation*, volume 5231 of *Proceedings of the Society of Photo-Optical Instrumentation Engineers (SPIE)*, pages 223–228. Bellingham, USA, 2003. 92, 101

[108] K. A. Peterson, K. D. Patel, C. K. Ho, S. B. Rohde, C. D. Nordquist, C. A. Walker, B. D. Wroblewski, and M. Okandan. Novel microsystem applications with new techniques in low-temperature co-fired ceramics. *International Journal of Applied Ceramic Technology 2 (5)*, pages 345–363, 2005. 92, 93, 101, 103, 104, 151

[109] K. A. Peterson, K. D. Patel, C. K. Ho, S. B. Rohde, C. D. Nordquist, C. A. Walker, B. D. Wroblewski, and M. Okandan. Novel microsystem applications with new techniques in low-temperature co-fired ceramics. In *1st Int'l Conference on Ceramic Interconnect and Ceramic Microsystems Technologies (CICMT)*, Baltimore, USA, 2005. 92, 101, 104, 151, 152

[110] H. Birol, T. Maeder, C. Jacq, G. Corradini, R. Passerini, Y. Fournier, S. Strässler, and P. Ryser. Fabrication of LTCC Micro-fluidic Devices Using Sacrificial Carbon Layers. In *1st Int'l Conference on Ceramic Interconnect and Ceramic Microsystems Technologies (CICMT)*, pages 59–66, Baltimore, USA, 2005. 92, 96, 100, 101, 102, 229

[111] H. Birol, T. Maeder, C. Jacq, G. Corradini, Y. Fournier, I. Saglini, S. Straessler, and P. Ryser. Structuration of micro-fluidic devices based on low temperature co-fired ceramic (LTCC) technology. In *15th IMAPS European Microelectronics and Packaging Conference (EMPC)*, pages 243–247, paper S9.04, Bruges, Belgium, 2005. 92

[112] H. Birol, T. Maeder, and P. Ryser. Preparation and application of minerals-based sacrificial pastes for fabrication of LTCC structures. In *4th IMAPS European Microelectronics and Packaging Symposium (EMPS)*, pages 57–60, Terme Catež, Slovenia, 2006. 92, 106, 107, 114, 139, 143

[113] H. Birol, T. Maeder, and P. Ryser. Application of graphite-based sacrificial layers for fabrication of LTCC (low temperature co-fired ceramic) membranes and micro-channels. *Journal of Micromechanics and Microengineering*, 17:50–60, 2007. 92, 93, 100, 121, 153

[114] S. Wiedmer. Capteur low-cost de très basses forces [Low-cost sensor for very low forces]. Semester project, EPFL-STI-IMT-LPM, Lausanne, Switzerland, Feb. 20 2007. 92, 109, 117, 133, 227

[115] O. Triverio. Capteur bio-inspiré pour la mesure de vitesse sur des micro-avions [Bio-inspired sensor for speed measurement on micro-airplanes]. Semester project, EPFL-STI-IMT-LPM, Lausanne, Switzerland, Dec. 20 2007. 93, 176

[116] E. Horváth and G. Harsányi. Microchannel fabrication in low temperature co-fired ceramic. Internal article, Department of Electronics Technology, Budapest University of Technology and Economics, Hungary, 2009. 93

[117] C. B. Sippola and C. H. Ahn. A ceramic sealed cavity with screen printed ceramic diaphragm. In *Conference on Ceramic Interconnect Technology: The Next Generation II*, paper WA41, Denver, USA, April 26-28 2004. 97

[118] C. B. Sippola and C. H. Ahn. A thick film screen-printed ceramic capacitive pressure microsensor for high temperature applications. *Journal of Micromechanics and Microengineering*, 16(5):1086, 2006. 97

[119] K. A. Peterson, S. B. Rohde, C. A. Walker, K. D. Patel, T. S. Turner, and C. D. Nordquist. Microsystem Integration with New Techniques in LTCC. In *Conference on Ceramic Interconnect Technology: The Next Generation II*, Denver, USA, April 26-28 2004. 98, 101

[120] D. G. Plumlee, Y. Morales, B. Cheek, A. J. Paris, H. A. Ackler, W. B. Knowlton, and A. J. Moll. Pressure Sensors built in Low Temperature Co-Fired Ceramic Materials. In *IMAPS Advanced Technology Workshop on Packaging of MEMS and Related Micro Integrated Nano Systems*, Denver, USA, Sept. 6-8 2002. 98

[121] D. J. Miehls, F. J. Martin, R. G. Pond, and P. S. Fleischner. Method of fabricating a multilayer electrical circuit structure, Patent US 5,249,355, 1993. 98

[122] P. Espinoza Vallejos, J. H. Zhong, M. Gongora Rubio, L. Sola Laguna, and J. J. Santiago Aviles. Meso (intermediate)-scale electromechanical systems for the measurement and control of sagging in LTCC structures. In S. Brown, J. Gilbert, H. Guckel, R. Howe, G. Johnson, P. Krulevitch, and C. Muhlstein, editors, *Microelectromechanical Structures for Materials Research*, volume 518 of *Materials Research Society Symposium Proceedings*, pages 73–79. Materials Research Society, Warrendale, 1998. 98

[123] W. K. Jones, Y. Q. Liu, and M. C. Gao. Micro heat pipes in low temperature cofire ceramic (LTCC) substrates. *IEEE Transactions on Components and Packaging Technologies*, 26(1):110–115, Mar. 2003. 98

[124] W. K. Jones, S. Kappagantula, and J. Wang. Micro Channel Fabrication in LTCC Substrate. In *1st Int'l Conference on Ceramic Interconnect and Ceramic Microsystems Technologies (CICMT)*, Baltimore, USA, 2005. 98

[125] J. D. Cawley, A. H. Heuer, and W. S. Newman. Method for constructing three dimensional bodies from laminations, Patent US 5,779,833, 1998. 98

[126] E. A. Trickett and R. C. Assmus. Ceramic monolithic structure having an internal cavity contained therein and a method of preparing the same, Patent US 4,833,000, May 1989. 98

[127] J. H. Alexander. Method of making ceramic article with cavity using LTCC tape, Ferro Corporation, Patent US 5,601,673, 1997. 98, 242

[128] J. W. Burdon, R. Huang, D. Wilcox, and N. Naclerio. Method for fabricating a multilayered structure and the structures formed by the method, Patent US 6,592,696 B1, 2003. 98

[129] H. Birol, T. Maeder, C. Jacq, and P. Ryser. 3-D structuration of LTCC for Sensor Micro-fluidic Applications. In *IMAPS European Microelectronics and Packaging Symposium (EMPS)*, pages 366–371, Prague, Czech Republic, 2004. 98, 100

[130] S. Pranonsatit and S. Lucyszyn. Self-assembled screen-printed microwave inductors. *Electronics Letters*, 41(23):1287–1288, Nov. 2005. 100

[131] TFT Thick Film Technologies. Application Notes: Nanocarbon Tape (TCS-CARB-1). Formerly Harmonics Inc., 3101 111th Street SW Suite R, Everett, WA 98204, USA, http://thickfilmtech.com, 2009. 101, 103, 215

[132] T. Maeder, Y. Fournier, S. Wiedmer, H. Birol, C. Jacq, and P. Ryser. 3D structuration of LTCC / thick-film sensors and fluidic devices. In *3rd Int'l Conference on Ceramic Interconnect and Ceramic Microsystems Technologies (CICMT)*, paper THA13, Denver, USA, 2007. 102, 103

[133] R. Backreedy, J. M. Jones, M. Pourkashanian, and A. Williams. A study of the reaction of oxygen with graphite : Model chemistry. *Faraday Discussions - The Royal Society of Chemistry*, 119:385–394, 2001. 102

[134] G. Stecher and H. Zimmermann. Electrical thick-film, free-standing, self-supporting structure, and method of its manufacture, particularly for sensors used with internal combustion engines, Robert Bosch GmbH, Patent US 4,410,872, 1983. 102, 103

[135] G. Stecher, K. Spitzenberger, and K. Müller. Pressure sensor, Robert Bosch GmbH, Patent US 4'382'247, 1983. 102

[136] G. Stecher. Free supporting structures in thickfilm technology: a substrate integrated pressure sensor. In *6th European Microelectronics Conference (ISHM)*, pages 421–427, Bournemouth, UK, June 3-5 1987. 102

[137] D. A. Vermilyea. Dissolution of MgO and Mg(OH)2 in aqueous solutions. *Journal of the Electrochemical Society*, 116(9):1179–1183, 1969. 104

[138] T. Kotani, T. Nakanishi, and K. Nomura. Fabrication of a new pyroelectric infrared-sensor using MgO surface micromachining. *Japanese Journal of Applied Physics Part 1*, 32(12B):6297–6300, Dec. 1993. 105, 135

[139] C. Lucat, P. Ginet, and F. Ménil. New sacrificial layer based screen-printing process for free-standing thick-films applied to MEMS. In *3rd Int'l Conference on Ceramic Interconnect and Ceramic Microsystems Technologies (CICMT)*, paper WP13, Denver, USA, 2007. 105, 121, 135

[140] C. Lucat, P. Ginet, C. Castille, H. Debéda, and F. Ménil. Devices based on free standing thick-films made with a new sacrificial layer process. In *XXXI International Conference of IMAPS Poland Chapter*, pages 457–460, Krasiczyn, Poland, Sept. 23-26 2007. 105

[141] P. Ginet, C. Lucat, F. Ménil, and J.-L. Battaglia. Modelling and Characterization of Screen-Printed Metallic Electrothermal Microactuators. In *3rd Int'l Conference on Ceramic Interconnect and Ceramic Microsystems Technologies (CICMT)*, paper WP14, Denver, USA, 2007. 105, 106

[142] C. Lucat, F. Ménil, H. Debéda Hickel, and P. Ginet. Production of multilayer microcomponents by the sacrificial thick layer method, CNRS France, Patent WO 2007/077397, 2007. 105

[143] P. Ginet. *Conception et élaboration de microstructures en technologie hybride couche épaisse pour des applications MEMS*. PhD thesis, #3529, Université Bordeaux I, Bordeaux, France, Dec. 13 2007. 105, 106

[144] P. Ginet, C. Lucat, P. Tardy, F. Ménil, J.-L. Battaglia, and C. Pradère. Thermomechanical Characterization of a Screen-printed Thermal Actuator. In *XXXI International Conference of IMAPS Poland Chapter*, pages 461–464, Krasiczyn, Poland, Sept. 23-26 2007. 105

[145] C.-L. Lo, J.-G. Duh, B.-S. Chiou, and W.-H. Lee. Low-temperature sintering and microwave dielectric properties of anorthite-based glass-ceramics. *Journal of the American Ceramic Society*, 85(9):2230–2235, Sept. 2002. 106

[146] T. Maeder, C. Jacq, Y. Fournier, W. Hraiz, and P. Ryser. Structuration of zero-shrinkage LTCC using mineral sacrificial materials. In *17th IMAPS European Microelectronics and Packaging Conference (EMPC)*, paper 16-S3-10, Rimini, Italy, June 2009. 107, 108, 133, 138, 141

[147] T. Rabe, W. A. Schiller, T. Hochheimer, C. Modes, and A. Kipka. Zero shrinkage of LTCC by self-constrained sintering. *International Journal of Applied Ceramic Technology*, 2(5):374–382, 2005. 107, 108, 138

[148] T. Rabe, W. A. Schiller, T. Hochheimer, C. Modes, and A. Kipka. Zero shrinkage of LTCC by self-constrained sintering. In *1st Int'l Conference on Ceramic Interconnect and Ceramic Microsystems Technologies (CICMT)*, Baltimore, USA, 2005. 107, 108, 138

[149] A. Kipka, C. Modes, F. Gora, and M. Deckelmann. Zero Shrinkage LTCC. In *XXXII International Conference of IMAPS Poland Chapter*, paper I10, Pultusk, Poland, 2008. 107, 138, 242

[150] H. Birol, T. Maeder, and P. Ryser. Materials compatibility issues in LTCC technology and their effects on structural and electrical properties. In *1st Int'l Conference on Ceramic Interconnect and Ceramic Microsystems Technologies (CICMT)*, pages 300–309, 2005. 109

[151] T. Maeder. Electrostatic cantilever resonator - calculations. Internal report, HITCLES project, EPFL-STI-IMT-LPM, Lausanne, Switzerland, May 26 2005. 109

[152] Kyocera. *Characteristics of Kyocera technical ceramics (datasheet)*, 2004. 113, 151

[153] P. Becker and P. Held. Crystal growth and basic characterisation of the bismuth borate Bi2B8O15. *Crystal Research and Technology*, 36(12):1353–1356, 2001. 120, 124

[154] J.-C. Zufferey, A. Klaptocz, A. Beyeler, J.-D. Nicoud, and D. Floreano. A 10-gram Vision-based Flying Robot. *Advanced Robotics*, 21(14):1671–1684, 2007. 121, 176

[155] Y. Iguchi, T. Narushima, and C. Izumi. Calorimetric study on hydration of CaO-based oxides. *Journal of Alloys and Compounds*, 321(2):276–281, 2001. 130

[156] T. Maeder, C. Jacq, Y. Fournier, W. Hraiz, and P. Ryser. Structuration of thin bridge and cantilever structures in thick-film technology using mineral sacrificial materials. In *5th IMAPS / ACerS Int'l Conference on Ceramic Interconnect and Ceramic Microsystems Technologies (CICMT)*, pages 175–182, paper WA24, Denver, USA, 2009. 134, 136, 137

[157] H. Yu, Q. Chen, and Z. Jin. *Thermodynamic assessment of the CaO-B2O3 system*, volume 23 of *Calphad*. Elsevier, 1999. 135

[158] R. E. Eitel and W. Zhang. Biostability of LTCC materials for microfluidics and biomedical devices. In *Int'l Conference on Ceramic Interconnect and Ceramic Microsystems Technologies (CICMT)*, pages 198–201, paper WA23, Munich, Germany, 2008. 140, 202, 207

[159] Y. Fournier, G. Boutinard Rouelle, N. Craquelin, T. Maeder, and P. Ryser. SMD pressure and flow sensor for compressed air in LTCC technology with integrated electronics. In *Eurosensors XXIII*, pages 1471–1474, Lausanne, Switzerland, Sept. 2009. 145

[160] J.-B. Coma. Caractérisation d'un capteur industriel d'air comprimé [Characterization of an industrial compressed air sensor]. Master project, EPFL-STI-IMT-LPM, Lausanne, Switzerland, Jan 15 2010. 145

[161] D. Güleryüz and W. Smetana. Mass Flow Sensor Realized in LTCC-Technology. In *XXIX International Conference of IMAPS Poland*, pages 373–376, Koszalin, Poland, 2005. 148

[162] Z. Magonski, B. Dziurdzia, and S. Nowak. Fabrication of Micro-Fluidic Devices with Fodel Dielectric. In *XXIX International Conference of IMAPS Poland*, pages 369–372, Koszalin, Poland, 2005. 148, 212

[163] M. Santo Zarnik and D. Belavic. Design Study for a Thick-Film Piezoelectric Actuator in an LTCC Structure. In *6th. Int'l Conf. on Thermal, Mechanical and Multiphysics Simulation and Experiments in Micro-Electronics and Micro-Systems, EuroSimE*, Berlin, Germany, 2005. 148, 206, 207

[164] M. Santo Zarnik, K. P. Friedel, A. Wymyslowski, and D. Belavic. A Procedure for Validating the Finite Element Model of a Piezoresistive Ceramic Pressure Sensor. *IEEE Transactions on Components and Packaging Technologies*, 27(4), 2004. 149

[165] M. Santo Zarnik, D. Belavic, and S. Macek. Thick-Film Piezoceramic Structures for Miniaturised Sensors and Actuators: Experimental and Numerical Analyses. In *XXXI International Conference of IMAPS*, Krasiczyn, Poland, Sept. 23-26 2007. 149, 207

[166] D. Belavic, M. Santo Zarnik, M. Hrovat, M. Jerlah, and S. Macek. Three-Dimensional Structuration of Zero-Shrinkage LTCC Ceramics for Microfluidic Applications. In *XXXII International Conference of IMAPS Poland Chapter*, paper A07, Pultusk, Poland, 2008. 149

[167] U. Partsch, S. Gebhardt, D. Arndt, H. Georgi, H. Neubert, D. Fleischer, and M. Gruchow. LTCC-Based Sensors for Mechanical Quantities. In *16th IMAPS European Microelectronics and Packaging Conference (EMPC)*, Oulu, Finland, June 2007. 149

[168] T. Maeder, B. Afra, Y. Fournier, N. Johner, and P. Ryser. LTCC ultra high isostatic pressure sensors. In *16th IMAPS European Microelectronics and Packaging Conference (EMPC)*, pages 375–380, Oulu, Finland, June 2007. 149, 204

[169] F. Bechtold. Innovative Integrationslösungen für Sensoren mit LTCC. *Sensor Magazin*, 16:5, 2008. 149

[170] M. R. Gongora Rubio. Non-Packaging Applications of LTCC Technology. Conference in Micro-Electro-Mechanical Systems, Panamerican Advanced Studies Institute, San Carlos de Barchiloche, Argentina, June 21-30 2004. 149, 150, 154, 206, 208

[171] Z. M. Da Rocha, M. A. C. Ferreira, N. Ibanez Garcia, A. C. Seabra, J. Alonso, and M. R. Gongora Rubio. Construction and Evaluation of Miniaturized Photometer Device for Phosphate Ion Determination Using LTCC Continuous Flow Systems. In *Int'l Conference on Ceramic Interconnect and Ceramic Microsystems Technologies (CICMT)*, Munich, Germany, 2008. 150

[172] T. Pisarkiewicz, A. Sutor, P. Potempa, W. Maziarz, H. Thust, and T. Thelemann. Microsensor based on low temperature cofired ceramics and gas-sensitive thin film. *Thin Solid Films*, 436(1):84–89, 2003. 151

[173] J. Kita, F. Rettig, R. Moos, K.-H. Drüe, and H. Thust. Hot-Plate Gas Sensors - are Ceramics Better? In *1st Int'l Conference on Ceramic Interconnect and Ceramic Microsystems Technologies (CICMT)*, Baltimore, USA, 2005. 151, 204

[174] T. Maeder, N. Dumontier, T. Haller, Y. Fournier, F. Seigneur, and P. Ryser. LTCC active oxygen getter module for hermetic packaging applications. In *Int'l Conference on Ceramic Interconnect and Ceramic Microsystems Technologies (CICMT)*, Munich, Germany, 2008. 151, 152, 204

[175] W. Smetana, M. Unger, and W. Gschohsmann. A New Concept of a Humidity Sensor Realized in LTCC-Technology. In *4th IMAPS European Microelectronics and Packaging Symposium (EMPS)*, pages 67–72, Terme Catež, Slovenia, May 22-24 2006. 152, 153

[176] T. Maeder, N. Dumontier, C. Jacq, G. Corradini, and P. Ryser. LTCC gas viscosity sensor. IMAPS Deutschland Tagung, Munich, Germany, Oct. 8-9 2007. 153, 204

[177] R. Bauer, L. Rebenklau, M. Luniak, and K.-J. W. T. Dresden). Mikrotechnische Applikationen mit der Dickfilmtechnik [Microtechnique Applications with Thick-film Technology]. Presentation at Deutschen ISHM Konferenz, München, Germany, 1998. 154

[178] S. Kaminski, L. Rebenklau, J. Uhlemann, and K. J. Wolter. Mixer with Microchannels in LTCC Technology. In *XXX International Conference of IMAPS Poland Chapter*, Krakow, Poland, 2006. 154, 181

[179] K. Malecha, D. Pijanowska, L. Golonka, and W. Torbicz. LTCC enzymatic microreactor. In *3rd Int'l Conference on Ceramic Interconnect and Ceramic Microsystems Technologies (CICMT)*, paper WA25, Denver, USA, 2007. 154

[180] M. R. Gongora Rubio, M. R. d. Cunha, and C. K. Saul. LTCC Microfluidic Diode. In *Int'l Conference on Ceramic Interconnect and Ceramic Microsystems Technologies (CICMT)*, Munich, Germany, 2008. 154

[181] Y. Fournier, R. Willigens, T. Maeder, and P. Ryser. Integrated LTCC micro-fluidic modules – an SMT flow sensor. In *15th IMAPS European Microelectronics and Packaging Conference (EMPC)*, Bruges, Belgium, paper P2.06, 577-581, 2005. 155, 181, 182

[182] Y. Fournier, A. Barras, G. Boutinard Rouelle, T. Maeder, and P. Ryser. SMD pressure and flow sensors for industrial compressed air in LTCC technology. In *17th IMAPS European Microelectronics and Packaging Conference (EMPC)*, paper 17-S3-8, Rimini, Italy, June 2009. 156, 232

[183] ZMD. Signal-conditioning electronics for industrial and automotive applications. Dresden, Germany, http://www.zmdi.com/, 2010. 156, 160, 233

[184] D. L. Kellis, A. J. Moll, and D. G. Plumlee. Effects of silver paste application on embedded channels in low temperature co-fired ceramics. *Journal of Microelectronics and Electronic Packaging*, 6(1):54–58, 2009. 165

[185] H. Birol, T. Maeder, and P. Ryser. Low Temperature Co-fired Ceramic (LTCC) Technology: General Processing Aspects and Fabrication of 3-D Structures for Micro-fluidic Devices. In *Sintering '05*, pages 216–219, paper 3b6, Grenoble, France, 2005. 165

[186] P.-A. Thivolle. Capteur thermique bio-inspiré pour la mesure de vitesse sur des micro-avions [Bio-inspired thermal sensor for speed measurement on micro-airplanes]. Semester project, EPFL-STI-IMT-LPM, Lausanne, Switzerland, Dec 20 2007. 177, 187, 188, 189, 190

[187] J. Gerrard. The wakes of cylindrical bluff bodies at low Reynolds number. *Philosophical Transactions for the Royal Society of London. Series A, Mathematical and Physical Sciences*, 288(1354):351–382, 1978. 179

[188] T. Maeder. Integrated calorimetric microreactor in low-temperature cofired ceramic (LTCC) technology. Swiss Society for Thermal Analysis & Calorimetry, 08 June 2006. 181, 184

[189] J. Thakur, R. Pratap, Y. Fournier, T. Maeder, and P. Ryser. Realization of a Solid-Propellant based Microthruster using Low Temperature Co-fired Ceramics. *Journal of Sensors & Transducers*, 117(6):29–40, June 25 2010. 191, 192, 193, 194, 195, 204

[190] M. Mach and J. Müller. 3D-Fluidic Cooling Structures in LTCC. In *16th IMAPS European Microelectronics and Packaging Conference (EMPC)*, Oulu, Finland, June 2007. 204

[191] H. Kishi, Y. Mizuno, and H. Chazono. Base-Metal Electrode-Multilayer Ceramic Capacitors: Past, Present and Future Perspectives. *Jpn. J. Appl. Phys.*, 42(2003):1–15, 2002. 205

[192] J. Bernard, D. Belavic, M. S. Zarnik, M. Hrovat, and M. Kosec. The development of the thick film piezoelectric actuator on LTCC substrate. In *4th IMAPS European Microelectronics and Packaging Symposium (EMPS)*, Terme Catež, Slovenia, May 22-24 2006. 207

[193] S. Gebhardt, L. Seffner, F. Schlenkrich, and A. Schönecker. PZT thick films for sensor and actuator applications. *Journal of the European Ceramic Society*, 27(13-15):4177–4180, 2007. 207

[194] L. J. Golonka, M. Buczek, M. Hrovat, D. Belavic, A. Dziedzic, H. Roguszczak, and T. Zawada. Properties of PZT thick films made on LTCC. *Microelectronics International*, 22(2):13–16, 2005. 207

[195] M. Hrovat, J. Holc, S. Drnovsek, D. Belavic, J. Cilensek, and M. Kosec. PZT thick films on LTCC substrates with an interposed alumina barrier layer. *Journal of the European Ceramic Society*, 26(6):897–900, 2006. 207

[196] M. Santo Zarnik and D. Belavic. A Feasibility Study for a Thick-Film PZT Bending-Mode Actuator. In *XXIX International Conference of IMAPS*, Koszalin, Poland, Sept. 19-21 2005. 207

[197] M. Santo Zarnik, D. Belavic, and S. Macek. Simulation and experimental testing of a thick-film PZT bending actuator. In *4th IMAPS European Microelectronics and Packaging Symposium - (EMPS)*, Terme Catež, Slovenia, May 22-24 2006. 207

[198] J. A. Lewis. Binder removal from ceramics. *Annual Reviews of Materials Science*, (27):147–174, 1997. 208

[199] R. K. Yamamoto, M. R. Gongora Rubio, M. R. d. Cunha, R. S. Pessoa, and H. S. Maciel. Mixed LTCC and LTTT Technology for Microplasma Generator Fabrication. In *Int'l Conference on Ceramic Interconnect and Ceramic Microsystems Technologies (CICMT)*, Munich, Germany, 2008. 208, 210, 211, 212, 213, 214, 215

[200] R. K. Yamamoto, M. R. Gongora Rubio, M. R. d. Cunha, R. S. Pessoa, and H. S. Maciel. Mixed LTCC and LTTT Technology for Microplasma Generator Fabrication. *Journal of microelectronics and electronic packaging*, 6(2):101–107, 2009. 208, 209, 212, 213, 215

[201] R. Gorges, S. Meyer, and G. Kreisel. Photocatalysis in microreactors. *Journal of Photochemistry and Photobiology A: Chemistry*, 167:95–99, 2004. 209

[202] D. Jurków, K. Malecha, L. Golonka, G. Hagen, P. Petkov, J. Stiernstedt, and M. Cristea. Laser pattering of green ceramic tapes for 3D structures. In *XXXIII International Conference of IMAPS Poland Chapter - CPMT IEEE*, pages 167–170, Gliwice–Pszczyna, Poland, 22 Sept. 2009. 209

[203] W. K. C. Yung and J. Zhu. Studies on laser ablation of low temperature co-fired ceramics (LTCC). *Microelectronics International*, 24(3):27–33, Oct. 9 2007. 209

[204] J. Zhu and W. K. C. Yung. Studies on laser ablation of low temperature co-fired ceramics (LTCC). *The International Journal of Advanced Manufacturing Technology*, 42(7-8):696–702, 2008. 209

[205] K. M. Nowak, H. J. Baker, and D. R. Hall. A model for "cold" laser ablation of green state ceramic materials. *Applied Physics A*, 91(2):341–348, 2008. 210

[206] M. Kittila, J. Hagberg, E. Jakku, and S. Leppavuori. Direct gravure printing (DGP) method for printing fine-line electrical circuits on ceramics. *IEEE Transactions on Electronics Packaging Manufacturing*, 27(2):109–114, 2004. 210

[207] R. J. Bacher, Y. L. Wang, M. A. Skurski, J. C. Crumpton, and K. M. Nair. Next Generation Ceramic Multilayer Systems. Internal article, Dupont iTechnologies, Microcircuit Materials, 14 Alexander Drive, Research Triangle Park, NC 27709, Durham, USA, 2001. 211

[208] R. Perrone, H. Bartsch de Torres, M. Hoffmann, M. Mach, and J. Müller. Miniaturized Embossed Low Resistance Fine Line Coils in LTCC. *Journal of microelectronics and electronic packaging*, 6(1):42–48, 2009. 212

[209] APTA Advanced Packaging Technology of America. LTTT Transfer Tapes, http://www.aptagroup.com/pptconv/index.htm, 2010. 212

[210] ESL Electro Science Laboratories. Ceramic tape systems. 416 East Church Rd., King of Prussia, PA 19406-2625, USA, http://www.electroscience.com/, 2010. 212, 242

[211] J. Kita, F. Rettig, and R. Moos. Integration of Fired Ceramics on LTCC Structures – Feasibility Study. In *4th IMAPS European Microelectronics and Packaging Symposium (EMPS)*, Terme Catež, Slovenia, May 22-24 2006. 214

[212] M. Wagner, A. Roosen, A. Stiegelschmitt, D. Schwanke, and F. Bechtold. In-situ Shrinkage Measurements of LTCC Multilayers by Means of an Optical Dilatometer. *Key Engineering Materials*, 206-213:1281–1284, 2002. 215

[213] EoPlex Technologies. HVPF Technology. Redwood City, CA, USA, http://www.eoplex.com/, 2010. 216

[214] C. S. Taylor, P. Cherkas, H. Hampton, J. J. Frantzen, B. O. Shah, W. B. Tiffany, L. Nanis, P. Booker, A. Salahieh, and R. Hansen. "Spatial forming" – A three dimensional printing process© - EoPlex. Technical report, Advanced Cardiovascular Systems, Inc., Santa Clara, California, USA, 2005. 216

[215] A. L. Chait. High-Volume Print Forming, HVPF™ – A New Method for Manufacturing Large Volumes of Complex Metal-Ceramic and Hybrid Components. Technical report, EoPlex, 2006. 216

[216] J. E. Blendell, J. S. Wallace, M. R. Locatelli, and B. J. Hockey. Sintering Behavior of Low Temperature Co-fired Ceramics. *ANN*, Materials for Wireless Communication:35, 2001. 220

[217] T. Maeder, V. Fahrny, S. Stauss, G. Corradini, and P. Ryser. Design and characterisation of low-cost thick-film piezoresistive force sensors for the 100 mN to 100 N range. In *XXIX International Conference of IMAPS Poland*, pages 429–434, Koszalin, Poland, 2005. 222

[218] L. Dovat, O. Lambercy, R. Gassert, T. Maeder, T. Milner, T. C. Leong, and E. Burdet. HandCARE: a cable-actuated rehabilitation system to train hand function after stroke. *IEEE Transactions on Neural Systems and Rehabilitation Engineering*, 16(6):582–591, 2008. 222

[219] K. H. Suphan. Fadenspannungssensor in Dickschichttechnik. Presentation at Deutsches IMAPS-Seminar, Göppingen, Germany, 2006. 223

[220] T. Maeder, H. Birol, C. Jacq, and P. Ryser. Strength of ceramic substrates for piezoresistive thick-film sensor applications. In *IMAPS European Microelectronics and Packaging Symposium (EMPS)*, pages 272–276, Prague, Czech Republic, 2004. 223

[221] H. Birol, M. Boers, T. Maeder, G. Corradini, and P. Ryser. Design and processing of low-range piezoresistive LTCC force sensors. In *XXIX International Conference of IMAPS*, pages 385–388, Koszalin, Poland, 2005. 223

[222] H. Birol, M. Boers, T. Maeder, G. Corradini, and P. Ryser. Design and processing of low-range piezoresistive LTCC force sensors, 2005. 223

[223] T. Maeder, C. Jacq, H. Birol, and P. Ryser. High-strength ceramic substrates for thick-film sensor applications. In *14th IMAPS European Microelectronics and Packaging Conference (EMPC)*, pages 133–137, Friedrichshafen, Germany, 2003. 223

[224] T. Maeder and D. Genoud. Solder assembly of cantilever bar force or displacement sensors. In *Sensor 2001*, Nürnberg, Germany, 2001. 223

[225] T. Maeder and P. Ryser. Effet des interconnexions brasées sur le signal de capteurs de force réalisés en technologie des couches épaisses. In *12e Forum de l'Interconnexion et du Packaging Microelectronique, IMAPS*, pages 37–43, Versailles, France, 2002. 223

[226] N. Craquelin, T. Maeder, Y. Fournier, and P. Ryser. Low-cost LTCC-based sensors for low force ranges. In *Eurosensors XXIII*, pages 899–902, Lausanne, Switzerland, Sept. 2009. 224, 225

[227] A. Barras. Brasure sans plomb hermétique de composants fluidiques – Capteur de pression SMD en LTCC [Hermetic lead-free soldering of fluidic components - SMD pressure sensor in LTCC]. Semester project, EPFL-STI-IMT-LPM, Lausanne, Switzerland, Dec. 18 2008. 232

[228] O. Thommen. Etude d'alternatives pour l'ajustement de capteurs [Study of alternatives for sensors trimming]. Semester project, EPFL-STI-IMT-LPM, Lausanne, Switzerland, Feb. 2007. 233

[229] G. Boutinard Rouelle. Capteur intégré de débit, température et pression en LTCC [Integrated flow, temperature and pressure sensor in LTCC]. Semester project, EPFL-STI-IMT-LPM, Lausanne, Switzerland, May 28 2009. 236

[230] M. Monneraye. Les encres sérigraphiables en microélectronique hybride: les matériaux et leur comportement. *Acta Electronica*, 21(4):263–281, 1978. 240

[231] T. Garino and M. Rodriguez. The Effect of Atmosphere on the Interdiffusion of Silver and Palladium. *Journal of the American Ceramics Society*, 1999. 240

[232] Y. Wang, G. Zhang, and J. Ma. Research of LTCC/Cu, Ag multilayer substrate in microelectronic packaging. *Mat. Science and Engineering B*, 94(1):48–53, 2002. 240

[233] A. Dziedzic, L. J. Golonka, J. Kozlowski, B. W. Licznerski, and K. Nitsch. Thick-film resistive temperature sensors. *Measurement Science and Technology*, 8(1):78–85, 1997. 240

[234] M. Hrovat and D. Belavic. Temperature sensors made by combinations of some standard thick film materials. *Journal of materials science letters*, 19(8), 2000. 240

[235] D. Jurków, K. Malecha, and L. J. Golonka. Investigation of LTCC Thermistor Properties. In *XXXII International Conference of IMAPS Poland Chapter*, paper G07, Pultusk, Poland, 2008. 240

[236] DuPont Microcircuit Materials. LTCC & Thick-film technologies. DuPont (U.K.) Limited, MicroCircuit Materials, 2010. 245, 246

Index

Yannick FOURNIER
Microengineer

Ch. du Stand 19c
CH – 1024 Ecublens VD
+41 76 538 09 41
yannick.fournier@a3.epfl.ch

Born on 10 April 1980
Swiss citizen
Single

EDUCATION

2004 – 2010	**Ecole Polytechnique Fédérale de Lausanne (EPFL) – PhD thesis** Doctor in science, microsystems packaging
2003 – 2004 (6 months)	**Carnegie Mellon University, Pittsburgh (PA, USA) – Master thesis in Robotics** Integration of a vision feature recognition algorithm into a smart camera
2001 – 2004	**Ecole Polytechnique Fédérale de Lausanne (EPFL) – Master in Microengineering** Orientation in Manufacturing and Robotics
1995 – 2000	**Engineering School of Geneva (EIG) HES-SO –** Bachelor in Microengineering

PROFESSIONAL EXPERIENCES

2004 – 2010	**EPFL – Doctoral thesis on micro-fluidic applications with ceramics** Presentation of scientific articles at 8 various international conferences Direction of 13 scientific student projects on Master level Execution of 7 research/industrial mandates for space, mechanics, physics domains Responsible for safety, equipment and supply of a clean room production facility IT administrator (40 people)
	Engineering for artistic exhibitions – Japan, China, France, Switzerland Creation of autonomous robotized zeppelins for museums Partnership with the EPFL Laboratory of Intelligent Systems
2004 (1.5 month)	**CERN – Feasibility study of an inspection robot** Conclusion of the technical infeasibility of an autonomous mobile robot in the ATLAS detector of the LHC due to radiations and magnetic fields
2002 – 2003 (9 months)	**EPFL – Design of a vacuum mechanical table for a screen printer** Hired by the lab for realization; machine still in use today
2000 (4 months)	**Parker Lucifer SA (Geneva) – Bachelor thesis in automation** Improvement of the precision of an electropneumatic regulator
1999 (2 months)	**ABB Sécheron SA (Geneva) – Engineer internship** Design of a telescopic tool for manufacturing of high-power transformers

LANGUAGES

French	Mother tongue
English	Fluent (C2); 6 months in the USA
German	Good (C1); regularly practiced at work and at military service.

Continuing Education

2008 – 2009	**Accounting and Finance**, EPFL Career Center
2007 – 2009	Various seminaries on **safety, risk analysis,** and **health at work** (EPFL + UniNE) Harsh environment workshop, CSEM Neuchâtel
2004 – 2009	Finite-elements modelisation softwares: ANSYS, Comsol Multiphysics Optical imaging instruments: X-ray 3D scanner, scanning electron microscope
2004	**McKinsey & Company DIVE workshop, Lugano (CH)** Business-oriented introduction to consulting and solving complex cases
2004	**ESA-Snecma Moteurs, space propulsion workshop, Vernon (F)** Introduction to Ariane's rocket engines and analysis of failed launches

Honors and Awards

2007	EPFL Human Ressources Reward for exceptional work (lab safety)
2001	Prize of the *Services Industriels de Genève* (SIG) Prize of the *Société Suisse des Ingénieurs et des Architectes* (SIA) Prize of the *Association des Anciens Élèves du Technicum de Genève* (ATG)
1995	Prize of Mathematics *Alice Treuthardt*

Scientific Contributions

Publication of **6 scientific articles** in the field of Electronics Packaging and Sensors as main author, and contribution to 15 publications and 1 patent as second author; list in appendix.

Presentation of my research work to large audience (>200 attendees) at **8 international conferences**.

Computer Skills

Design	Mechanics: Pro/ENGINEER Electronics: HYDE, Altium, PSpice, ORCAD
Programmation	C/C++, Assembly, Java, ADA, Matlab/Simulink, LabView
Office	MS Office, Photoshop, webdesign, LyX/LaTeX

Parallel Activities

Aeronautics	**Private pilot** (2006) with night extension **EPFL's aeronautical association, *AéroPoly*** **Co-founder, vice-president and treasurer (2007 – 2009)** 135 members; organization of various events and conferences
Robotics	**Co-organizer of EPFL's flying robots contests** (2004 – 2007) Participation to the EPFL's autonomous wheeled robotic contest (2000)
Photography	Weddings, travels
Nautical sports	Motor and sailing driving licenses; water-skiing
Running	Competition at national level

Publications

As first author

Peer-reviewed journal article

Y. Fournier, T. Maeder, G. Boutinard Rouelle, A. Barras, N. Craquelin, and P. Ryser. *Integrated LTCC pressure / flow / temperature multisensor for compressed air diagnostics.* Submitted to Sensors in 2010.

Conference proceedings

Y. Fournier, G. Boutinard Rouelle, N. Craquelin, T. Maeder, and P. Ryser. *SMD pressure and flow sensor for compressed air in LTCC technology with integrated electronics.* In Procedia Chemistry - Proceedings of Eurosensors XXIII, volume 1, pages 1471-1474, Lausanne, Switzerland, 2009.

Y. Fournier, A. Barras, G. Boutinard Rouelle, T. Maeder, and P. Ryser. *SMD pressure and flow sensors for industrial compressed air in LTCC technology.* In Proceedings, 17th IMAPS European Microelectronics & Packaging Conference (EMPC), paper 17-S3-8, Rimini, Italy, 2009.

Y. Fournier, O. Triverio, T. Maeder, and P. Ryser. *LTCC free-standing structures with mineral sacrificial paste.* In Proceedings, Int'l Conference on Ceramic Interconnect and Ceramic Microsystems Technologies, pages 11-18 (TA12), Munich, Germany, 2008.

Y. Fournier, F. Seigneur, T. Maeder, and J. Jacot. *Assembly of microvalves actuated by PZT bender.* In Proceedings, Int'l Conference on Electroceramics (ICE2007), Arusha, Tanzania, July 31-Aug. 3, 2007.

Y. Fournier, S. Wiedmer, T. Maeder, and P. Ryser. *Capacitive micro force sensors manufactured with mineral sacrificial layers.* In Proceedings, 16th IMAPS European Microelectronics & Packaging Conference (EMPC), pages 298-303, Oulu, Finland, 2007.

Y. Fournier, L. Bieri, T. Maeder, and P. Ryser. *Influence of lamination parameters on LTCC shrinkage under unconstrained sintering.* In Proceedings, 4th IMAPS European Microelectronics and Packaging Symposium (EMPS), pages 165-170, Terme Čatež, Slovenia, 2006.

Y. Fournier, R. Willigens, T. Maeder, and P. Ryser. *Integrated LTCC micro-fluidic modules - an SMT flow sensor.* In Proceedings, 15th IMAPS European Microelectronics and Packaging Conference (EMPC), pages 577-581 (P2.06), Brugge, Belgium, 2005.

Presentation

Y. Fournier. *How to manufacture 3D circuits for microtechnique applications? With LTCC! - Introduction for engineers*, EPFL-LPM, Switzerland, 4 Sept. 2006, PPT/PDF files available on http://lpm.epfl.ch/ltcc.

As secondary author

Peer-reviewed journal articles

J. Thakur, R. Pratap, **Y. Fournier**, T. Maeder, P. Ryser. *Realization of a Solid-Propellant based Microthruster using Low Temperature Co-fired Ceramics*. Sensors & Transducers, 117(6):29-40, 2010.

D. Testa, M. Toussaint, R. Chavan, J. Guterl, J. Lister, J.-M. Moret, A. Perez, F. Sanchez, B. Schaller, G. Tonetti, **Y. Fournier**, T. Maeder, A. Encheva, G. Vayakis, C. Walker, H. Carfantan, A. Le-Luyer, P. Moreau, and S. Peruzzo. *The magnetic diagnostic set for ITER.* IEEE Transactions on Plasma Science, 38(3):284-294, 2010.

D. Testa, M. Toussaint, R. Chavan, J. Guterl, J. Lister, J.-M. Moret, A. Perez, F. Sanchez, B. Schaller, G. Tonetti, **Y. Fournier**, T. Maeder, A. Encheva, G. Vayakis, C. Walker, H. Carfantan, A. Le-Luyer, P. Moreau, and S. Peruzzo. *Baseline system design and prototyping for the ITER high-frequency magnetic diagnostic set.* IEEE Transactions on Plasma Science, 2009.

F. Seigneur, **Y. Fournier**, T. Maeder, P. Ryser, and J. Jacot. *Hermetic package for optical MEMS.* Journal of Microelectronics and Electronic Packaging, 6(1):32-37, 2009.

Conference proceedings

N. Craquelin, T. Maeder, **Y. Fournier**, and P. Ryser. *Low-cost LTCC-based sensors for low force ranges.* In Procedia Chemistry - Proceedings of Eurosensors XXIII, volume 1, pages 899-902, Lausanne, Switzerland, 2009.

T. Maeder, C. Jacq, **Y. Fournier**, W. Hraiz, and P. Ryser. *Structuration of thin bridge and cantilever structures in thick-film technology using mineral sacrificial materials.* In Proceedings, 5th IMAPS / ACerS Int'l Conference on Ceramic Interconnect and Ceramic Microsystems Technologies (CICMT), pages 175-182 (WA24), Denver, USA, 2009.

N. Serra, T. Maeder, C. Jacq, **Y. Fournier**, and P. Ryser. *Screen-printed polymer-based microfluidic and micromechanical devices based on evaporable compounds.* In Proceedings, 17th IMAPS European Microelectronics & Packaging Conference (EMPC), paper 16-S3-8, Rimini, Italy, 2009.

T. Maeder, C. Jacq, **Y. Fournier**, W. Hraiz, and P. Ryser. *Structuration of zero-shrinkage LTCC using mineral sacrificial materials.* In Proceedings, 17th IMAPS European Microelectronics & Packaging Conference (EMPC), paper 16-S3-10, Rimini, Italy, 2009.

T. Maeder, C. Jacq, **Y. Fournier**, and P. Ryser. *Formulation and processing of screen-printing vehicles for sacrificial layers on thick-film and LTCC substrates.* In Proceedings, XXXII International Conference of IMAPS Poland Chapter, paper B16, Pultusk, Poland, 2008.

F. Seigneur, **Y. Fournier**, T. Maeder, P. Ryser, and J. Jacot. *Hermetic package for optical MEMS.* In Proceedings, Ceramic Interconnect and Ceramic Microsystems Technologies (CICMT), pages 627-633, Munich, Germany, 2008.

T. Maeder, N. Dumontier, T. Haller, **Y. Fournier**, F. Seigneur, and P. Ryser. *LTCC active oxygen getter module for hermetic packaging applications.* In Proceedings, Int'l Conference on Ceramic Interconnect and Ceramic Microsystems Technologies (CICMT), Munich, Germany, 2008.

F. Seigneur, **Y. Fournier**, T. Maeder, and J. Jacot. *Laser soldering of LTCC hermetic packages with minimal thermal impact.* In Proceedings, 16th IMAPS European Microelectronics & Packaging Conference (EMPC), pages 526-530, Oulu, Finland, 2007.

T. Maeder, **Y. Fournier**, S. Wiedmer, H. Birol, C. Jacq, and P. Ryser. *3D structuration of LTCC / thick-film sensors and fluidic devices.* In Proceedings, 3rd Int'l Conference on Ceramic Interconnect and Ceramic Microsystems Technologies (CICMT), paper THA13, Denver, USA, 2007.

T. Maeder, B. Afra, **Y. Fournier**, N. Johner, and P. Ryser. *LTCC ultra high isostatic pressure sensors.* In Proceedings, 16th IMAPS European Microelectronics & Packaging Conference (EMPC), pages 375-380, Oulu, Finland, 2007.

H. Birol, T. Maeder, C. Jacq, G. Corradini, R. Passerini, **Y. Fournier**, S. Strässler, and P. Ryser. *Fabrication of LTCC Micro-fluidic Devices Using Sacrificial Carbon Layers.* In Proceedings, 1st Int'l Conference on Ceramic Interconnect and Ceramic Microsystems Technologies (CICMT), pages 59-66, Denver, USA, 2005.

H. Birol, T. Maeder, C. Jacq, G. Corradini, **Y. Fournier**, I. Saglini, S. Straessler, and P. Ryser. *Structuration of micro-fluidic devices based on low temperature co-fired ceramic (LTCC) technology.* In Proceedings, 15th IMAPS European Microelectronics and Packaging Conference (EMPC), pages 243-247 (S9.04), Bruges, Belgium, 2005.

Patent

N.F.Y. Durand, **Y. Fournier** and T. Lasser, *"Nanofluidic biosensor and its use for rapid measurement of biomolecular interactions in solution and methods"*, International Patent Application, PCT/01824/09, 2009.